

# **Triazole-Based Radiopeptidomimetics: Novel Neurotensin (8-13) Analogues with Increased Metabolic Stability**

**Inauguraldissertation**

Zur Erlangung der Würde eines Doktors der Philosophie

vorgelegt

der Philosophisch-Naturwissenschaftlichen Fakultät  
der Universität Basel



von

**Alba Mascarin**

aus Basel, Schweiz

Basel 2015

Originaldokument gespeichert auf dem Dokumentenserver der Universität Basel  
**edoc.unibas.ch**

Dieses Werk ist unter dem Vertrag „Creative Commons Namensnennung-Keine kommerzielle Nutzung-Keine Bearbeitung 3.0 Schweiz“ (CC BY-NC-ND 3.0 CH) lizenziert. Die vollständige Lizenz kann unter [creativecommons.org/licenses/by-nc-nd/3.0/ch/](https://creativecommons.org/licenses/by-nc-nd/3.0/ch/) eingesehen werden.

**Genehmigt von der Philosophisch-Naturwissenschaftlichen Fakultät**

**auf Antrag von**

Prof. Dr. Edwin Constable

Prof. Dr. Thomas Mindt

Prof. Dr. Helma Wennemers

Basel, den 19. Mai 2015

---

Prof. Dr. Jörg Schibler (Dekan)

**Für Brigitte und Marco  
In Dankbarkeit gewidmet**



---

## Danksagung

Ich bedanke mich herzlichst bei folgenden Personen:

- Prof. Thomas Mindt für die Betreuung meiner Dissertation, die interessante Aufgabenstellung und für die Möglichkeit an äusserst lehrreichen Weiterbildungen teilzunehmen.
- Prof. Edwin Constable für die Übernahme der Funktion des Fakultätsvertreters.
- Prof. Helma Wennemers für die Übernahme des Korreferats.
- Prof. Catherine Housecroft für die Übernahme der Funktion als Vorsitzende.

Ich möchte mich bei Dr. Ibai Valverde besonders dafür bedanken, dass er mich mit seinem Wissen und seiner Tatkraft unterstützt und mir alles beigebracht hat, was ich für die Durchführung dieser Arbeit gebraucht habe. Gracias!

Ein grosses Dankeschön geht an Sandra Vomstein, für ihre Hilfe und ihre Unterstützung bei Zell- und Tierversuchen. Bei Rudolf von Wartburg bedanke ich mich ebenfalls für seine Hilfe bei Tierversuchen. Dr. Andreas Baumann danke ich für die Einführung in radiochemische Arbeitstechniken. Bei Lisa McDougall und Dr. Guillaume Nicolas bedanke ich mich für ihre Hilfe bei der Aufnahme und Bearbeitung von SPECT/CT Bildern. Danke an Dr. Heiko Gsellinger, der mir bei der Messung und Auswertung schwieriger NMR Spektren immer behilflich war. Bei Christophe Daepfen bedanke ich mich für seine Hilfe bei der Messung der spezifischen Drehwinkel.

Für finanzielle Unterstützung bedanke ich mich bei dem Schweizerischen Nationalfond, für die Finanzierung meiner Forschungsarbeit und bei der Schweizer Gesellschaft für Radiopharmazie/Radiopharmazeutische Chemie, für die Vergabe von Reisestipendien.

Bei allen Mitgliedern der Forschungsgruppe Mindt bedanke ich mich für die gute Zusammenarbeit. Ein ganz grosses Dankeschön geht an das Labor-Team: besonders Daniela, Sandra, Nadia, Pia, und Rada, dafür dass sie immer behilflich waren und für ein gutes Arbeitsklima gesorgt haben. Ich werde die kleinen Pausen bei euch vermissen!

Danke auch an die Arbeitsgruppe von Prof. Edwin Constable und Prof. Catherine Housecroft, dafür dass ich an ihren Forschungssitzungen und Weihnachtsfeiern dabei sein durfte.

Herzlichen Dank an Kevin Guex, Jörg Duschmale, Chaim Howald, Brigitte Zogg und Martin Kopp, dafür dass sie mir bei den Korrekturen dieser Arbeit geholfen haben und sehr viel Zeit und Sorgfalt investiert haben.

Ich möchte mich bei meiner Familie bedanken, Brigitte, Marco und Dario, dafür dass sie mich immer unterstützt haben und mir gute Ratschläge mit auf den Weg gegeben haben.

Meine Freunde: Elena, Miri, Kevin, Sarah, Laura, Constanze, Karo, Christiane und Chaim, die immer für mich da waren und mit denen ich in diesen vier Jahren so viele schöne Momente erlebt durfte. Martin, danke dass du immer an mich glaubst.

---

Parts of this thesis have been published and presented at national and international congresses.

## Publications

1,2,3-Triazole Stabilized Neurotensin-Based Radiopeptidomimetics for Improved Tumour Targeting, Mascarin, A., Valverde, I.E., Vomstein S., Mindt T.L., *Bioconjugate Chemistry*, **2015**, Published Online 5. September 2015

Probing the Backbone Function of Tumor Targeting Peptides by an Amide-to-Triazole Substitution Strategy, Valverde, I.E., Vomstein, S. Fischer, C., Mascarin, A., Mindt, T. L., *Journal of Medicinal Chemistry*, **2015**, 58 (18), 7475–7484

Effect of a spacer moiety on radiometal labelled Neurotensin derivatives, Mascarin, A., Valverde, I.E., Mindt T.L., *Radiochimia Acta*, **2013**, 101, 733.

## Oral Presentations

,1,2,3-Triazol-basierende Radiopeptidomimetika'; A. Mascarin, I.E. Valverde, T.L. Mindt; *21. Jahrestagung der Arbeitsgemeinschaft Radiochemie/Radiopharmazie*, **2012**, Pamhagen, Austria.

,Untersuchungen zum Einfluss verschiedener Spacer auf Neurotensin-basierender Radiopharmazeutika für das Tumor-Targeting'; A. Mascarin, I.E. Valverde, T.L. Mindt; *20. Jahrestagung der Arbeitsgemeinschaft Radiochemie/Radiopharmazie*, **2013**, Bad Honeff, Germany.

## Poster

Poster Walk: ,Stabilized Neurotensin-Based Radiopeptidomimetics by Click-Chemistry'; A. Mascarin, I.E. Valverde, T.L. Mindt; *Annual Conference of the European Association of Nuclear Medicine*, **2014**, Göteborg, Sweden.

Poster Walk: ,1,2,3-Triazole containing Neurotensin-based Radiopeptidomimetics'; A. Mascarin, I.E. Valverde, T.L. Mindt; *Swiss Congress of Radiology (SGNM)*, **2014**, Montreux, Switzerland.

,1,2,3- Triazole containing Neurotensin-based Radiopeptidomimetics'; A. Mascarin, I.E. Valverde, T.L. Mindt; *Annual Research Meeting of the Department of Pharmaceutical Sciences*, **2014**, Basel, Switzerland.

,Effect of different spacers on Neurotensin-based radiotracers' A. Mascarin, I.E. Valverde, T.L. Mindt; *Annual Research Meeting of the Department of Pharmaceutical Sciences*, **2013**, Basel, Switzerland.

,Effect of different spacers on Neurotensin-based radiotracers'; A. Mascarin, I.E. Valverde, T.L. Mindt; *Swiss Chemical Society Fall Meeting*, **2012**, Lausanne, Switzerland

---

### Summary

Neurotensin (NT) is a regulatory peptide with a nanomolar affinity towards NT receptors, which are overexpressed by different types clinically relevant tumours (e.g. Ewing' sarcoma, breast, colon and exocrine pancreatic cancer).<sup>[1-3]</sup> Regulatory peptides have been shown to be suitable vectors for the specific delivery of radioactivity to tumours for diagnostic and therapeutic applications in nuclear medicine.<sup>[4-5]</sup> Therefore, the binding sequence of Neurotensin, NT (8-13), is a promising vector for the development of peptidic radiotracers for tumour imaging and therapy. A potential drawback of this peptide vector is its instability *in vivo* as the result of rapid degradation by proteases. It has been shown that stabilization of a peptide against proteases can lead to an increased tumour uptake. However, classical peptide backbone modifications (e.g., *N*-methylation or reduction of the amide bond) were only partially successful in providing stabilized NT-analogues with improved tumour-targeting properties.<sup>[6-7]</sup> It has been suggested that 1,4-disubstituted 1,2,3-triazoles might represent suitable *trans*-amide bond bioisosters, which are resistant to proteases.<sup>[8]</sup> To study the effect of 1,4-disubstituted 1,2,3-triazoles on NT (8-13) as amide bond mimics, we performed a 'triazole scan' of the amino acid sequence by which every backbone amide bond of the NT (8-13) sequence is substituted with a 1,4-disubstituted 1,2,3-triazole. We herein wish to report the synthesis and biological evaluation of a series of novel, radiolabelled peptidomimetics of NT (8-13) with promising tumour-targeting properties.

The peptide conjugates were synthesized on solid support by a combination of Fmoc-based solid phase peptide synthesis, diazo-transfer reaction and the Cu(I) catalysed azide-alkyne cycloaddition (CuAAC). The required  $\alpha$ -amino alkynes for the CuAAC were successfully synthesized from the corresponding  $\alpha$ -amino acids and their enantiomeric purity was verified. The peptides were then elongated *N*-terminally with a PEG<sub>4</sub>-spacer and conjugated to a DOTA-chelator. After HPLC-purification, the compounds were labelled with [<sup>177</sup>Lu]LuCl<sub>3</sub> in high radiochemical yields and purities and evaluated *in vitro*. The *in vitro* evaluation included quantification of the internalisation of the peptide conjugates into NTR1 expressing HT-29 cells (colon adenocarcinoma) and determination of their receptor affinity and specificity. Additionally, measurements of the lipophilicity of the conjugates (log D) and their metabolic stability in human blood serum were performed. The NT (8-13) analogues with the most promising properties *in vitro* were further evaluated *in vivo* with nude mice bearing HT-29 xenografts.

The focus of the first part of this thesis was on the investigation of the pharmacological influence of a spacer on a radiometallated DOTA-functionalized NT (8-13) sequence. A NT (8-13)-based peptide conjugate without a spacer to separate the chelator from the tumour-targeting peptide was compared side-by-side with two NT (8-13) peptide conjugates, each having a different spacer, one hydrophilic (tetraethylenglycol, PEG<sub>4</sub>) and one lipophilic (6-aminohexanoic acid, Ahx). The compound with the PEG<sub>4</sub>-spacer exhibited the best properties *in vitro* and was thus selected as reference compound and starting point for future peptide conjugates.

A 'triazole scan' of NT (8-13) yielded several triazole backbone-modified NT (8-13) analogues with interesting properties. It was found that a triazole modification was only tolerated between the *N*-terminal PEG<sub>4</sub> spacer and Arg<sup>8</sup> and in the position between Arg<sup>8</sup> and Arg<sup>9</sup>. Substitution of these bonds yielded two single-triazole containing compounds as well as one bis-triazole analogue with nanomolar affinities towards



## Summary

---

NTR1 and moderately improved metabolic stabilities (1<sup>st</sup> generation of triazole-containing NT (8-13) peptidomimetics). The central and C-terminal regions of NT (8-13) were not modifiable with a triazole without a complete loss of receptor affinity towards NTR1. These observations are in agreement with the results of other reported modification strategies for NT (8-13) (e.g. reduction of amide bonds or the use of  $\beta$ -homo amino acids).<sup>[9-10]</sup>

Further enhancement of the metabolic stability of the peptidomimetics of the first generation was achieved by the substitution of Ile<sup>12</sup> of NT (8-13) with a Tle<sup>12</sup>. The triazole insertion was only introduced at the previously identified positions which tolerate the modification. The obtained compounds (2<sup>nd</sup> generation of triazole-containing NT (8-13) analogues) were evaluated *in vitro* and compared side-by-side to the reference compound DOTA-PEG<sub>4</sub>-[Tle<sup>12</sup>]NT (8-13). Our investigations revealed that the Ile<sup>12</sup> to Tle<sup>12</sup> residue switch led to a substantial improvement of the metabolic stability of the compounds, however a significant loss of receptor affinity was observed. Only DOTA-PEG<sub>4</sub>-[Arg<sup>8</sup>- $\Psi$ Tz-Arg<sup>9</sup>][Tle<sup>12</sup>]NT (8-13) maintained a nanomolar affinity towards NTR1.

The compounds with the most promising properties *in vitro* (retained nanomolar NTR1 affinity and improved metabolic stability) were selected for biodistribution studies in nude mice bearing HT-29 xenografts and compared side-by-side with the corresponding reference compounds of the first and second generation. The NT (8-13) analogues with a 1,4-disubstituted 1,2,3-triazole between Arg<sup>8</sup> and Arg<sup>9</sup> exhibited a 2-fold tumour uptake, in comparison to the reference compounds. Favourable fast blood clearance and a high tumour to organs ratio was observed for all the evaluated radiolabelled triazole-peptidomimetics. Compared to literature data we can report exceptionally good tumour to background ratios in general, especially for the tumour to kidney ratio. A high tumour to background ratio is beneficial for the potential application of peptidic radiopharmaceuticals as imaging or therapeutic agents. In general, no or little correlation between the *in vitro* behaviour (metabolic stability or receptor binding affinity) and the uptake of the conjugates in the HT-29 tumour *in vivo* could be observed, which demonstrates the necessity of preclinical evaluations of novel radiotracers.

In summary, we report the first 'triazole scan' of the binding sequence of NT (8-13) and the synthesis and biological evaluation of novel radiolabelled triazole-peptidomimetics. The synthesis of the 1,2,3-triazole-containing peptide conjugates (including CuAAC and diazo-transfer reaction) is fully compatible with solid phase synthesis and thus generally applicable to other regulators peptides of interest for medical applications. The substitution of amide bonds with 1,4-disubstituted 1,2,3-triazoles provided NT (8-13) peptidomimetics with improved tumour-targeting properties. The NT (8-13) analogues described in this thesis represent interesting candidates for the development of novel tumour-targeting probes with applications in nuclear medicine.

---

## Table of Contents

**SUMMARY ..... IV**

**ABBREVIATIONS ..... X**

**1. INTRODUCTION..... 1**

1.1 CANCER..... 1

1.2 NUCLEAR MEDICINE ..... 3

1.2.1 General Introduction..... 3

1.2.2 Radioactive Decay ..... 3

1.2.3 Radiobiology..... 4

1.3 IMAGING METHODS ..... 6

1.4 RADIOPHARMACEUTICALS ..... 8

1.4.1 General Introduction..... 8

1.4.2 Clinically Relevant Radionuclides ..... 10

1.4.2.1 Lutetium-177 ..... 12

1.4.3 Radiometal-Labelled Targeted Radiopharmaceuticals ..... 13

1.4.4 Radiometal Labelled Peptide-Based Radiopharmaceuticals for the Treatment of Tumours ... 15

1.4.5 Chelators for Peptide-Based Radiopharmaceuticals..... 17

1.4.5.1 Chelators for Technetium..... 17

1.4.5.2 Chelators for M<sup>3+</sup> Radiometals..... 18

1.5 NEUROTENSIN ..... 21

1.5.1 General Introduction..... 21

1.5.2 The Neurotensin Receptor Family..... 22

1.5.3 Development of Neurotensin Analogues..... 23

1.5.3.1 Structure-Activity Relationship Studies of NT (8-13) ..... 24

1.5.3.2 Influence of Chelator, the Radionuclide and the Spacer ..... 27

1.5.3.2.1 Influence of the Chelator ..... 28

1.5.3.2.2 Influence of the Radionuclide ..... 29

1.5.3.2.3 Influence of the Spacer ..... 29

1.5.4 State of the Art in the Development of Stabilized NT (8-13)-Based Radiotracers..... 30

1.6 PEPTIDOMIMETICS ..... 32

1.6.1 General Introduction..... 32

## Table of Contents

---

1.6.2	Triazoles as Amide Bond Isosters for Peptides .....	34
1.6.3	The Chemistry of 1,4-Disubstituted 1,2,3-Triazoles .....	36
1.6.4	Preparation of $\alpha$ -Azido Acids .....	38
1.6.5	Synthesis of Chiral $\alpha$ -Amino Alkynes.....	41
<b>2.</b>	<b>OBJECTIVES .....</b>	<b>45</b>
<b>3.</b>	<b>RESULTS AND DISCUSSION.....</b>	<b>49</b>
3.1	IDENTIFICATION OF A SUITABLE SPACER .....	49
3.1.1	Synthesis of NT (8-13) Analogues AM-NT 1-3. ....	50
3.1.2	Biological Investigation of Peptide Conjugates [ $^{177}\text{Lu}$ ]-AM-NT 1-3 .....	52
3.1.3	Discussion of the <i>In Vitro</i> Evaluation of [ $^{177}\text{Lu}$ ]-AM-NT 1-3.....	56
3.2	'TRIAZOLE SCAN' OF NT (8-13) .....	58
3.2.1	Synthesis of Precursors .....	59
3.2.1.1	Synthesis of $\alpha$ -Azido Acids .....	59
3.2.1.2	Synthesis of $\alpha$ -Amino Alkynes.....	60
3.2.1.2.1	Synthesis of $\alpha$ -Amino Alkynes without a Functional Group in the Side-Chain .....	61
3.2.1.2.2	Synthesis of Fmoc-PEG <sub>4</sub> -alkyne 29f.....	63
3.2.1.2.3	Synthesis of $\alpha$ -Amino Alkynes with a Functional Group in the Side-chain .....	63
3.2.1.2.4	Determination of the Enantiomeric Purity of $\alpha$ -Amino Alkynes.....	66
3.2.2	Synthesis of the First Generation of Triazole-Containing NT (8-13) Analogues.....	70
3.2.3	Biological Investigation of Peptide Conjugates [ $^{177}\text{Lu}$ ]-AM-NT 4-10 .....	73
3.2.4	Discussion of the <i>In Vitro</i> Investigation of [ $^{177}\text{Lu}$ ]-AM-NT 4-10.....	76
3.3	SYNTHESIS AND BIOLOGICAL EVALUATION OF A SECOND GENERATION OF STABILIZED TRIAZOLE-CONTAINING NT (8-13) ANALOGUES .....	79
3.3.1	Identification of a Suitable Amino Acid Substitution for NT (8-13) Analogues.....	79
3.3.1.1	Biological Investigation of [ $^{177}\text{Lu}$ ]-AM-NT 11-14. ....	80
3.3.1.2	Discussion of the <i>In Vitro</i> Evaluation of [ $^{177}\text{Lu}$ ]-AM-NT 11-14.....	82
3.3.2	Synthesis of the Second Generation of Triazole-Containing NT (8-13) Analogues.....	84
3.3.2.1	Biological Investigation of the Second Generation of Triazole-Containing NT (8-13) Analogues .....	85
3.3.2.2	Discussion of the <i>In Vitro</i> Evaluation of [ $^{177}\text{Lu}$ ]-AM-NT 15-17.....	87
3.4	<i>IN VIVO</i> EVALUATION .....	89
3.4.1	<i>In Vivo</i> Imaging .....	97
3.4.2	Discussion of the <i>In Vivo</i> Evaluation.....	98
<b>4.</b>	<b>CONCLUSION AND OUTLOOK .....</b>	<b>101</b>
<b>5.</b>	<b>EXPERIMENTAL PROCEDURES .....</b>	<b>109</b>

## Table of Contents

---

5.1	INSTRUMENTS AND CHEMICALS .....	109
5.2	ORGANIC SYNTHESIS.....	111
5.2.1	General Procedures.....	111
5.3	SYNTHESIS OF PEPTIDES .....	133
5.3.1	General Procedures.....	133
5.3.3	Synthesis of Peptide Conjugates .....	135
5.4	RADIOLABELLING .....	152
5.5	<i>IN VITRO</i> EVALUATION .....	153
5.6	<i>IN VIVO</i> EVALUATION .....	155
<b>6.</b>	<b>APPENDIX .....</b>	<b>157</b>
6.1	NMR SPECTRA.....	157
6.3	MS DATA.....	176
6.5	PEPTIDES .....	182
6.5.1	Analytical UV-chromatograms .....	182
6.5.2	$\gamma$ -HPLC Chromatograms.....	188
6.5.3	MS Data .....	194
6.7	BIODISTRIBUTION DATA .....	210
<b>7.</b>	<b>BIBLIOGRAPHY .....</b>	<b>217</b>



## Abbreviations

%	percentage	equiv	equivalent
°C	degree Celsius	ESI	electrospray ionization
μ	micro	eV	electron volt
<sup>18</sup> F	[ <sup>18</sup> F]fluorobenzoyl	FDG	fluorodesoxyglucose
Å	ångström	Fmoc	9-fluorenylmethoxycarbonyl
AA	amino acid	G	giga
Ac	acetyl	GLP	glucagon-like peptide
Ahx	aminohexanoic acid	GPCR	G protein coupled receptor
Ala	alanine	HAMA	human anti-mouse antibody
aq	aqueous	HATU	1-Bis(dimethylamino) methylene]-1H-1,2,3-triazolo[4,5-b]pyridinium 3-oxid hexafluorophosphate
Arg	arginine	HDAC	histone deacetylase
BBN	bombesin	HMBC	heteronuclear multiple bond correlation
BFCA	bifunctional chelating agent	HMQC	heteronuclear multiple quantum correlation
Boc	<i>tert</i> -butoxycarbonyl	HOBt	1-Hydroxybenzotriazole
Bq	Becquerel	HPLC	high-performance liquid chromatography
br	broad (spectral)	HSA	Human serum albumin
calcd	calculated	HT-29	colon carcinoma cells
CCK	cholecystokinin B	Hz	hertz
CD	circular dichroism	i.e.	id est
CD20	B-lymphocyte antigen	IC <sub>50</sub>	half maximal inhibitory concentration
Cha	cyclohexylalanine	ID/g	injected dose per gram
Ci	curie	Ile	isoleucine
CNS	central nervous system	<i>J</i>	coupling constant
COSY	correlation spectroscopy	k	kilo
CT	computer tomogram	K <sub>D</sub>	dissociation constant
CuAAC	copper catalysed alkyne azide cycloaddition	L	litre
d	doublet	LET	linear energy transfer
D <sub>2</sub>	dopamine receptors	Leu	leucine
dd	doublet of doublets	Ln	lanthanide
DIBAL-H	diisobutylaluminium hydride	Log D	water/octanol distribution coefficient
DIPEA	diisopropylethylamine	M	molarity
DMEM	Dulbecco's modified eagle medium	m	milli; meter; multiplet (spectral)
DMF	dimethylformamide	m/z	mass-to-charge ratio
DMSO	dimethyl sulfoxide	MAbs	monoclonal antibodies
DNA	deoxyribonucleic acid	MC1R	melanocortin 1 receptor
DOTA	1,4,7,10-tetraazacyclododecane-1,4,7,10-tetraacetic acid	MDS	multiple damage site
DOTAGA	1,4,7,10-tetraazacyclododecane-4,7,10-triacetic acid-1-[2-glutaric acid]	Me	methyl
DOTATATE	DOTA-(Tyr <sup>3</sup> )-octreotate	MeOH	methanol
DOTATOC	DOTA-(Phe <sup>1</sup> )-(Tyr <sup>3</sup> )-octreotide	min	minute
DSB	double-strain breaks	MRI	magnetic resonance imaging
DTPA	diethylene triamine pentaacetic acid	MS	mass spectroscopy
e.g.	exempli gratia	MW	molecular weight
EC	electron capture		
EDTA	ethylenediaminetetracetic acid		
X			

## Abbreviations

---

n	nano	s	singlet (spectral); second
n	neutron	s.c.	subcutaneously
n.a.	not applicable	SAR	structure-activity relationship
n.d.	not determined	SPECT	single photon emitting computed tomography
n.o.	not observed	SPPS	solid phase peptide synthesis
nat	natural	SSB	single-strain breaks
NET	neuroendocrine tumour	sst	somatostatin
NODAGA	1,4,7-triazacyclononane, 1-glutaric acid-4,7-acetic acid	t	triplet
NOESY	nuclear Overhauser effect spectroscopy	$t_{1/2}$	half-life
NPY	neuropeptide Y	<sup>t</sup> Bu	<i>tert</i> -Butyl
NT	Neurotensin	td	triplet of doublet
NTR	Neurotensin receptor	TFA	trifluoroacetic acid
p	pico	theor.	theoretical
p.i.	post injection	TIS	triisopropylsilane
Pbf	pentamethyl-2,3-dihydrobenzofuran-5-sulfonyl	TLC	thin layer chromatography
PBS	phosphate buffered saline	Tle	<i>tert</i> -leucine
PEG	polyethylenglycol	TOF-MS	time of flight mass spectroscopy
PET	positron emission tomography	$t_R$	retention time
Pmc	2,2,5,7,8-pentamethylchroman-6-sulfonyl	TRH	thyrotropin releasing hormone
ppm	parts per million	Tyr	tyrosine
Pro	proline	UV	ultraviolet
PRRT	peptide receptor radionuclide therapy	VIP	vasoactive intestinal peptide
PS	polystyrene	CXCR	chemokine receptor
q	quartet	VPAC	vasoactive intestinal peptide receptor
RIL	radioimmunolocalization	vs.	versus
RIT	radioimmunotherapy	$\alpha$	alpha
RP	reversed phase	$[\alpha]_D$	observed optical rotation in degrees
rpm	revolutions per minute	$\beta$	beta
RT	room temperature	$\delta$	chemical shift in parts per million
RuAAC	ruthenium catalysed alkyne azide cycloaddition	$\gamma$	gamma
		v	neutrino





# 1. Introduction

## 1.1 Cancer

*“Cancer is the uncontrolled growth and spread of cells. It can affect almost any part of the body. The growths often invade surrounding tissue and can metastasize to distant sites. Many cancers can be prevented by avoiding exposure to common risk factors, such as tobacco smoke. In addition, a significant proportion of cancers can be cured, by surgery, radiotherapy or chemotherapy, especially if they are detected early.”*

### Definition of cancer of the World Health Organisation

Cancer is one of the leading causes of death worldwide. 14 million new cases are diagnosed every year and 8.2 million cancer related deaths in the year 2012 alone corroborate that statement.<sup>[11]</sup> This number is expected to increase by 70% in the next two decades. In 2012, cancer was responsible for 14.7% of deaths worldwide, only preceded by cardiovascular diseases, with 31.4%. The number of deaths by cancer has increased since 2002 (**Table 1**). Among men, the most common cancer types are lung, prostate, colorectal, stomach and liver cancer, whereas among women it is breast, colorectal, lung, cervix and stomach cancer.<sup>[12]</sup>

**Table 1:** The three most common causes of death worldwide, in 2012 and 2002.<sup>[12]</sup>

Cause of Death	2012 (%)	2002 (%)
Infectious and parasitic diseases	11.5	16.8
Cardiovascular diseases	31.4	28.2
Malignant tumours	14.7	12.1

Cancer is the consequence of a failure of the mechanisms responsible for the growth and proliferation of cells. This failure can be caused by a genetic change due to the exposure to environmental factors such as chemicals, hormones and viruses or the choice of an unhealthy lifestyle (obesity, low fruit and vegetables intake, lack of physical activity, abuse of alcohol and tobacco or the practice of unsafe sex),<sup>[13]</sup> but also due to erroneous gene functions. There are three types of genes which can cause cancer: proto-oncogenes, tumour suppressor genes and caretaker genes. Among these, proto-oncogenes can promote the

excessive growth of cells, which can lead to the formation of malignant tumours. Tumour-suppressor genes normally restrain the cell growth, but once deactivated an abnormal cell division can take place. Finally, caretaker genes are responsible for the integrity of the genome. If these caretaker genes are deactivated, the cell genome can undergo new mutations at an increased rate, which can affect the cell growth and therefore, cause cancer.<sup>[14]</sup>

Given the high incidence of cancer among the global population, it is not a surprise that it has become one of the main subjects of worldwide pharmaceutical research efforts. These have provided healthcare with diagnostic tools such as tissue sampling (biopsy), blood tests, endoscopy, surgical exploration and imaging, as well as therapeutic approaches including surgery, chemotherapy, hormone therapy, immunotherapy, gene therapy and radiotherapy.<sup>[15]</sup> However, because of the large diversity of different tumours and cancer types, medicine is becoming increasingly personalized and consequently there is an ever growing need for the development of new diagnostic tools and efficient therapeutic methods.

This work will be focused on radionuclide supported imaging and radioendotherapy. These are important tools in the diagnosis (imaging) and treatment of diverse types of cancer, as these techniques are non-invasive, highly sensitive and specific.

## 1.2 Nuclear Medicine

### 1.2.1 General Introduction

Nuclear Medicine, a medical speciality which uses the properties of unsealed, radioactive material for diagnostic and therapeutic purposes, allows in a non-invasive manner to examine abnormalities in the human body with high precision and sensitivity. The first clinical application of a radionuclide was described in 1936 by John H. Lawrence, who used  $^{32}\text{P}$  to treat leukaemia. Important breakthroughs include the discovery of  $^{99\text{m}}\text{Tc}$ , the 'work horse' of nuclear medicine, in 1938, the development of the first cameras for nuclear imaging in the sixties, of the first gamma-camera in 1958 by Hal O. Anger and the first SPECT-camera (single photon emission computed tomography) in 1963 by David E. Kuhl and Roy Q. Edwards as well as 15 years later the introduction of PET technology (positron emission tomography). Since then, the development of new radiopharmaceuticals has been constantly ongoing<sup>[16]</sup>

### 1.2.2 Radioactive Decay

Nuclear medicine exploits the ability of some nuclei to emit ionizing radiation. There are three types of radiation,  $\alpha$ -emission,  $\beta$ -emission and  $\gamma$ -emission. They are all distinct because of their range of action, their energy and the nature of the emission.

During an  $\alpha$ -decay a helium atom is released from the nucleus of an atom. As a consequence, the mass of the mother nuclide is reduced by two protons and two neutrons. Because of the charge and the high mass of the He-atom, the range of action of an  $\alpha$ -emitter is low, with a penetration range of less than 100  $\mu\text{m}$  in normal tissue. Because  $\alpha$ -emission has a high LET (linear energy transfer; energy transferred by path length) it is used for therapeutic purposes.

There are two types of  $\beta$ -decay:  $\beta^-$ - and  $\beta^+$ -radiation. On the one hand, neutron-rich nuclei one neutron can be converted into a proton and an electron ( $\beta^-$ -particle). This  $\beta^-$ -particle carries part of the released kinetic energy, whereas the rest of the energy is converted into a mass- and charge-free neutrino  $\nu$ .  $\beta^-$ -radiation has a deeper penetration range than  $\alpha$ -radiation, a lower LET, and can also be used for therapeutic applications. On the other hand, proton-rich nuclei can emit a positive charged electron (positron  $\beta^+$ ). After the emission, the

positron collides with an electron (annihilation), emitting two electromagnetic beams of 511 keV each, with an exact angle of 180 °C. This type of radiation is used in PET technology.

In a proton rich nucleus, EC (electron capture) can also take place. During this process, a proton captures an electron, resulting in the formation of a neutron and while radiation in form of X-rays or low energy electrons (Auger electrons) is emitted. Whereas the electrons emitted during a  $\beta^-$ -decay are the result of the decay of a nucleus, the Auger electrons originate after a relaxing event in the K- or L-shell of the atom. Auger electrons can be employed for therapeutic purposes. Thereby, the short range of Auger electron-emitting radionuclides requires their close proximity to the cell nucleus of the targeted tissue.<sup>[16-17]</sup>

The third type of radiation is  $\gamma$ -radiation, an electromagnetic radiation, which is emitted after a previous  $\alpha$ ,  $\beta^-$ ,  $\beta^+$  or EC decay or from metastable radionuclides. Because of its long range of action, this type of radiation is detectable with cameras located outside the patient's body.  $\gamma$ -Radiation has a lower LET than  $\alpha$ - and  $\beta^-$ -radiation, causing less damage to the exposed tissue and is therefore exclusively used as a diagnostic tool.<sup>[16-17]</sup>

### 1.2.3 Radiobiology

When applied as a radiopharmaceutical, the target of ionizing radiation is the DNA of the cancer cells. Direct ionization of DNA can cause lesions like single-strand breaks (SSB), double-strand breaks (DSB), multiple damaged sites (MDS) and cross-links of DNA-bases. These lesions can also be caused by the interaction of the DNA with free radicals, mostly hydroxyl radical originated in water (indirect ionization). Additionally, cells can be irradiated by neighbouring cells, containing a source of radiation ('cross-fire').<sup>[18]</sup>

The first cellular response to the ionizing radiation is a delay of the cell division rate. The cell division delay depends on the cell cycle, as not all phases of the cell cycle are equally sensitive to radiation. After cell irradiation and DNA damage, several genes are activated to repair the DNA damage. If the repair of DNA is successful, the cell cycle is continued as normal. On the contrary, if the damages are irreparable, the cells undergo programmed cell death or apoptosis. DSB and MDS are examples for severe DNA-damages, difficult to repair. It has been reported that cells that are adjacent to irradiated cells but have not been irradiated themselves also show increased mutation rates and decreased survival rates ('bystander effect').<sup>[18]</sup>

The type and the severity of the DNA-lesions depend on the type and energy of the radiation.  $\alpha$ -particles and Auger electrons have high ionization densities and can cause more damage to the DNA than  $\beta^-$ -particles (low ionisation density). However, as the range of action of particles and Auger electrons is short, a homogeneous distribution of the radiolabelled pharmaceutical in the targeted tissue is important for an efficient therapy.<sup>[18]</sup>

### 1.3 Imaging Methods

The essential advantage of nuclear imaging methods over other imaging modalities like CT (computed tomography) and MRI (magnetic resonance imaging) is their sensitivity. Whereas the strength of CT and MRI is the high spatial resolution of morphological information, nuclear imaging provides information about biochemical functions at a cellular level. Due to the high sensitivity of these methods, only a low concentration ( $10^{-12}$  M) of the administered radiopharmaceutical agent is required for imaging.<sup>[19]</sup> Undesired interactions between the examined molecular process and the imaging agent are thereby avoided. For comparison, the concentration of contrast agents used in CT and MRI is in the range of  $10^{-2}$ - $10^{-6}$  M. In diagnostic nuclear medicine, two types of imaging methods are used, SPECT (single photon emission computed tomography) imaging and PET (positron emission tomography) imaging.

$\gamma$ -radiation is detected with a gamma-camera. This type of camera contains a detector, an amplifier, an analogue digital converter and a computer to evaluate the measured data. **Figure 1** shows a schematic representation of the detector of a gamma-camera. The detector consists of a round or rectangular NaI(Tl) crystal as a scintillator, covered with photomultipliers, which converts the radiation particles into light. Additionally, a collimator is built in. A collimator improves the spatial resolution of the imaging by only permitting vertical radiation to pass through and producing a parallel beam of radiation. While there are different types of collimators (e.g. pin hole, converging and diverging collimators), parallel-hole collimators are the most common.<sup>[16-17]</sup>

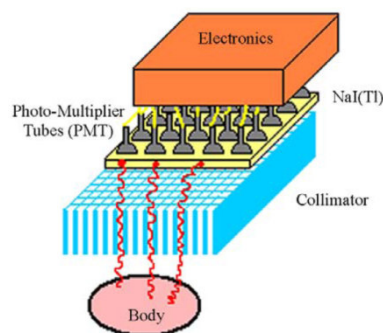


**Figure 1:** Schematic representation of the detector of a gamma-camera.<sup>[20]</sup>

A gamma-camera with one detector is only able to produce two-dimensional images. In order to address this issue, the SPECT-camera (single photon emission computer tomography) was developed in 1963, five years after the first gamma-camera. A SPECT camera

possesses one or more gamma-camera heads and rotates around the patient. In doing so, it is able to provide three-dimensional information about the location of the emitting nuclide at an image resolution of 8-20 mm.

A PET-camera is used for the detection of  $\beta^+$ -radiation (positrons). PET technology is more precise and sensitive than SPECT technology. The principle behind PET is the annihilation event after the  $\beta^+$ -decay, which produces two 511 keV gamma photons in opposite directions (**Figure 2**). The simultaneous detection of two photons in opposite directions (coincidence measurement) allows determining the location of the annihilation event with an accuracy of 3-10 mm. This provides the basis for the higher spatial resolution of PET in comparison with SPECT.<sup>[16-17]</sup>

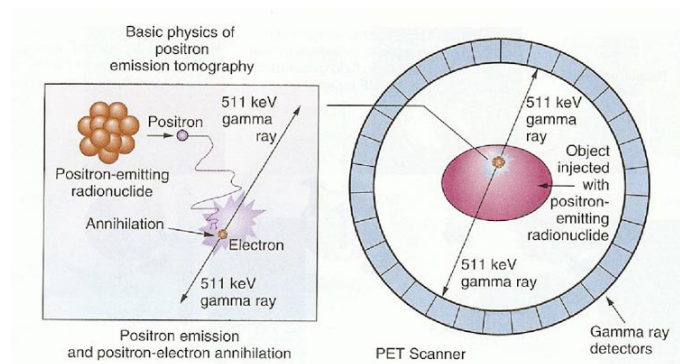


**Figure 2:** Principle of PET technology.<sup>[21]</sup>

Today, SPECT and PET are often combined with other imaging techniques like CT and more recently, with MRI ('hybrid imaging'). CT and MRI are able to provide the morphological information with high resolution ( $< 1$  mm), whereas SPECT and PET give information of the physiological and molecular aspect of the disease.<sup>[22]</sup> This so called hybrid or bimodal imaging techniques help to accurately localize lesions, tumours or malfunctions, and are a useful tool for the optimized and personalized treatments of diseases.

## 1.4 Radiopharmaceuticals

### 1.4.1 General Introduction

A radiopharmaceutical is a radionuclide-containing molecule with a diagnostic or therapeutic application in nuclear medicine. There are large numbers of radiopharmaceuticals able to target a manifold of biological functions or processes in the body. A radiopharmaceutical should accumulate specifically in the target organ or system, and show a fast clearance in the rest of the body, in order to guarantee a high quality of imaging and as little therapeutic side-effects as possible. Radiopharmaceuticals can be categorized in terms of their way of accumulation: those which accumulate by their chemical or physical properties and those with a specific molecular target.

The majority of the radiopharmaceuticals follow an unspecific accumulation pathway through passive diffusion, ionic transport or adsorption effects. Examples for diagnostic radiopharmaceuticals with an unspecific accumulation in the body are the [ $^{15}\text{O}$ ]- $\text{H}_2\text{O}$  (determination of blood flow) or [ $^{14}\text{N}$ ]- $\text{NH}_3$  (heart perfusion). [ $^{99\text{m}}\text{Tc}$ ]-labelled phosphonates (e.g. methylenediphosphonate or dicarboxyphosphonate) are used for bone scintigraphies. As the selectivity of these radiopharmaceuticals is often insufficient, they frequently have to be applied directly on the lesion.<sup>[16]</sup>

The second type of radiopharmaceuticals is distinguished by their specific accumulation in a particular system or organ. The target of such a radiopharmaceutical can be a metabolic system, an antigen, a receptor or a cell membrane.

The labelling of the radiopharmaceutical can be performed with non-metallic or metallic radionuclides. Non-metallic radionuclides are bound covalently to the molecule. Examples of radiopharmaceuticals labelled with non-metallic isotopes are [ $^{18}\text{F}$ ]FDG (imaging of tumours with high glucose metabolism), [*S*-methyl- $^{11}\text{C}$ ]Methionine (detection of cancers through amino acid transport systems) or [ $^{11}\text{C}$ ]Choline (marker for cell membranes). Examples for radiometal-labelled targeted radiopharmaceuticals are [ $^{111}\text{In}$ ]Zevalin, a radiolabelled anti-CD20 antibody developed for the treatment of Non-Hodgkin lymphomas and DOTA-TOC, a somatostatin analogue that, in combination with different radionuclides (e.g.  $^{68}\text{Ga}$ ,  $^{90}\text{Y}$ ,  $^{177}\text{Lu}$ ), is used for the diagnosis and treatment of neuroendocrine tumours.<sup>[16-17, 23]</sup> We are especially interested in the development of targeted radiopharmaceuticals labelled with a metallic radionuclide (chapter 1.4.3).



Each labelling strategy has its advantages and drawbacks. Due to their small atomic size, the introduction of non-metallic radionuclides like  $^{18}\text{F}$  or  $^{11}\text{C}$  does usually not dramatically alter the structure and properties of a molecular ligand, whereas labelling with metallic isotopes require the introduction of a chelator that can modify the biological properties of the molecule to label. However, labelling with non-metallic isotopes is often done in harsh reaction conditions, whereas chelation can be done in mild conditions compatible with delicate biomolecules such as peptides and antibodies. In addition, the fact that some chelators, such as DOTA, can host a wide variety of radiometals with different emissions makes them very attractive for both diagnostic as well as therapeutic applications, depending on the radiometal used (theranostics).

The clinically relevant radionuclides for diagnostic and therapeutic applications are described in chapter 1.4.2.

### 1.4.2 Clinically Relevant Radionuclides

The radionuclides for a specific application are selected depending on the type of radiation they emit, their half-life and their energy range.

As mentioned above, for diagnostic purposes,  $\gamma$ - or  $\beta^+$ -emitting radionuclides are required, due to the long range and low radiation energy of these kinds of radiation. Furthermore, the isotopes ideally have a short half-life, in the range of one to three hours (**Table 2**). The daughter nuclides resulting after the decay additionally should be non-toxic and non-radioactive.

**Table 2:** Selection of diagnostic radionuclides and their physical properties.

Nuclide	$t_{1/2}$	Radiation Type (MeV)	Particle max. Range	Application
$^{11}\text{C}^{[16]}$	20.4 min	$\beta^+$ (0.511)	0.1- 0.5 mm	PET
$^{13}\text{N}^{[17]}$	10 min	$\beta^+$ (0.511)	0.1- 0.5 mm	PET
$^{15}\text{O}^{[16]}$	2.0 min	$\beta^+$ (0.511)	0.1- 0.5 mm	PET
$^{18}\text{F}^{[16]}$	110 min	$\beta^+$ (0.511)	0.1- 0.5 mm	PET
$^{64}\text{Cu}^{[24]}$	13 h	$\beta^+$ (0.511)	0.1- 0.5 mm	PET
		$\beta^-$ (0.579)	0.1- 0.3 mm	Therapy
$^{67}\text{Ga}^{[17]}$	78.3 h	EC (0.093, 0.185, 0.3)	0.1- 0.3 mm	SPECT
$^{68}\text{Ga}^{[17]}$	67.6 min	$\beta^+$ (0.511)	< 1 $\mu\text{m}$	PET
$^{99\text{m}}\text{Tc}^{[16]}$	6.0 h	$\gamma$ (0.141)	-	SPECT
$^{111}\text{In}^{[16]}$	67 h	EC (0.171, 0.245)	< 1 $\mu\text{m}$	SPECT
$^{123}\text{I}^{[16]}$	13.2 h	EC (0.160)	< 1 $\mu\text{m}$	SPECT

In contrast, radionuclides emitting  $\alpha$ - or  $\beta^-$ -radiation or Auger electrons are suitable for therapy (**Table 3**). Long-lived isotopes are preferred in order to increase the radiation dose in the targeted tissue (e.g. tumours). It has been determined that a range between 6 hours and 7 days is ideal for therapeutic purposes.<sup>[25]</sup> Longer half-lives would have a negative impact on the patient due to excessive radiation exposure.<sup>[26]</sup> The maximal radiation dose applicable to a patient is limited by dose-limiting organs, e.g. the bone marrow, the kidneys and the gonads, which are particularly sensitive to radioactivity.

**Table 3:** Physical properties of a selection of radionuclides used in therapy.

Nuclide	$t_{1/2}$	Radiation Type (MeV)	Particle max. Range
$^{32}\text{P}^{[27]}$	14.3 d	$\beta^-$ (1.71)	8.7 mm
$^{67}\text{Cu}^{[27]}$	2.6 d	$\beta^-$ (0.54) $\gamma$ (0.185)	2.2 mm
$^{80\text{m}}\text{Br}^{[28]}$	4.4 h	Auger	< 10 nm
$^{90}\text{Y}^{[27]}$	2.7 d	$\beta^-$ (2.28)	12.0 mm
$^{105}\text{Rh}^{[27]}$	1.5 d	$\beta^-$ (0.57) $\gamma$ (0.320)	2.4 mm
$^{111}\text{Ag}^{[29]}$	7.5 d	$\beta^-$ (1.03) $\gamma$ (0.342)	4.8 mm
$^{125}\text{I}^{[28]}$	60.0 d	Auger	10 nm
$^{131}\text{I}^{[27]}$	8.0 d	$\beta^-$ (0.6) $\gamma$ (0.364)	2.4 mm
$^{149}\text{Pm}$	2.2 d	$\beta^-$ (1.07) $\gamma$ (0.289)	5.0 mm
$^{142}\text{Pr}^{[27]}$	19.1 h	$\beta^-$ (2.16)	11.3 mm
$^{153}\text{Sm}^{[16]}$	2.0 d	$\beta^-$ (0.8) $\gamma$ (0.103)	3.0 mm
$^{169}\text{Er}^{[27]}$	9.5 d	$\beta^-$ (0.34)	1 mm
$^{177}\text{Lu}^{[30]}$	6.7 d	$\beta^-$ (0.497) $\gamma$ (0.208)	2.3 mm
$^{186}\text{Re}^{[27]}$	3.8 d	$\beta^-$ (1.08) $\gamma$ (0.131)	5.0 mm
$^{188}\text{Re}^{[27]}$	17.0 h	$\beta^-$ (2.13) $\gamma$ (0.155)	11.0 mm
$^{198}\text{Au}^{[27]}$	2.7 d	$\beta^-$ (0.96) $\gamma$ (0.411)	4.4 mm
$^{211}\text{At}^{[31]}$	7.2 h	$\alpha$ (6.8)	65 $\mu\text{m}$
$^{212}\text{Bi}^{[31]}$	1.0 h	$\alpha$ (7.8)	70 $\mu\text{m}$

Therapeutic radionuclides which additionally emit  $\gamma$ -radiation can be used in ‘theranostics’. Examples of such theranostic radionuclides ( $^{177}\text{Lu}$  or  $^{186}\text{Re}$ ) are shown in **Table 3**. This new medical field combines diagnosis and therapy, using this type of radionuclides or by using the same radiopharmaceutical radiolabelled with different radionuclides for diagnosis and therapy.

### 1.4.2.1 Lutetium-177

In this context,  $^{177}\text{Lu}$ , the isotope used for the experiments in this work is an isotope of particular interest.  $^{177}\text{Lu}$  is considered a very attractive radionuclide for PRRT (peptide receptor radionuclide therapy) due to its long half-life and a tissue penetration depth of the radiation of approximately 2.3 mm (**Table 3**). These are ideal characteristics for the treatment of small tumours and metastasis. Additionally, the simultaneous emission of  $\gamma$ -radiation offers the possibility to monitor the state of the disease by concurrent imaging of the lesions on a gamma-camera (theranostics).

$^{177}\text{Lu}$  decays to the stable isotope  $^{177}\text{Hf}$ . The simplified decay scheme of  $^{177}\text{Lu}$  is shown **Figure 3**.

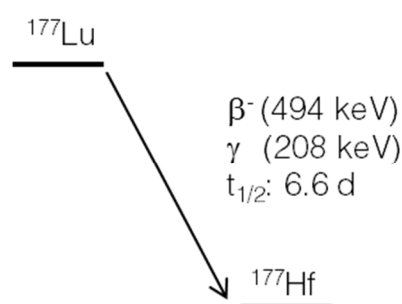


**Figure 3:** Simplified decay scheme for  $^{177}\text{Lu}$ .

$^{177}\text{Lu}$  can be produced in a nuclear reactor *via* direct or indirect methods. On the one hand, during the so called direct nuclear reaction, a neutron is captured by  $^{176}\text{Lu}$  to afford  $^{177}\text{Lu}$ . The main disadvantage of this method is the generation of  $^{177\text{m}}\text{Lu}$  ( $t_{1/2}$ : 160 d) as an undesired, inseparable side-product. The long half-life of this radioisotope represents a drawback for medical applications, in terms of radiation protection as well as for the management of the resulting radioactive waste. On the other hand, the indirect method provides highly pure  $^{177}\text{Lu}$ .  $^{176}\text{Yb}$  is irradiated with neutrons and in the subsequent neutron capture,  $^{177}\text{Yb}$  is produced, which then decays to  $^{177}\text{Lu}$  *via*  $\beta^-$ -decay.<sup>[32]</sup> Despite an additional purification step (removal of  $^{177}\text{Yb}$ ), the major advantage of the indirect method is the generation of impurity free  $^{177}\text{Lu}$  (also called carrier-free or non-carrier added) with high specific activity. The nuclear reactions of the direct and indirect method of  $^{177}\text{Lu}$  production are shown in **Figure 4**.

Direct method:  $^{176}\text{Lu}(n,\gamma)^{177}\text{Lu}$

Indirect method:  $^{176}\text{Yb}(n,\gamma)^{177}\text{Yb} \rightarrow ^{177}\text{Lu}$

**Figure 4:** Nuclear reactions for the production of  $^{177}\text{Lu}$ .

### 1.4.3 Radiometal-Labelled Targeted Radiopharmaceuticals

The general structure of a radiometal-labelled targeted radiopharmaceutical is shown in **Figure 5** and contains a vector (V) with a specific target (R) in the body, often a spacer (S), a radionuclide (M) and a chelator (C). Each of the components of a radiometal-based radiopharmaceutical can have an influence on the binding properties and the pharmacological behaviour of the molecule. <sup>[16-17]</sup>

The vector, which is responsible for reaching the target in the body, can be a biomolecule (peptide or antibody) with the necessary chemical, biological and pharmacokinetic properties, whereas the target in the body can be an antigen, a cell membrane, a transport system or a receptor. <sup>[16-17]</sup>

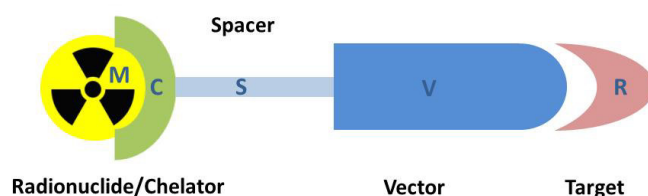


**Figure 5:** Schematic representation of a radiometal labelled targeted radiopharmaceutical and its specific interaction with a molecular target.

The spacer (S), not always necessary, is used as a link between the tracer and the chelate. <sup>[16, 33]</sup> The function of the chelator (C) is the connection of the radiometal to the vector. A metal-chelator complex must be thermodynamically and kinetically stable in order to avoid decomposition under physiological conditions. Most chelators can easily be functionalized into BFCAs (bifunctional chelating agents), in order to conjugate them to the desired biomolecule. There are two types of chelators, linear and macrocyclic. Linear chelators are based on the structure of diethylenetriaminepentaacetic acid (DTPA) and are known for their favourable coordination kinetics and radiolabelling efficacy. Their ability to

quantitatively bind to a radiometal in a short amount of time (~15 min) at room temperature is important for the labelling of heat sensitive molecules (e.g. antibodies) or when working with short lived isotopes.<sup>[34]</sup> Unfortunately, however, only a few radiometals form thermodynamically stable complexes with acyclic chelators. Therefore, macrocyclic chelators are preferentially used for the labelling with radiometals. Macrocyclic chelators have a similar thermodynamic stability as linear chelators, but they are more kinetically inert. They present pre-organized binding sites, so less entropic loss is encountered and the complexation is thermodynamically more favourable (macrocyclic effect). An disadvantage of the macrocycles is that the labelling conditions often require heating (60-100 °C) and longer reaction times (30-90 min), making them unsuitable for the labelling of heat-sensitive molecules.<sup>[34]</sup>

The development of radiometal labelled specific targeted radiopharmaceuticals, also called “magic bullets”, commenced in the 1970s, when the first radiolabelled monoclonal antibody was tested *in vivo* in rats with human choriocarcinoma xenografts.<sup>[35]</sup> Rapidly, RIL (radioimmunolocalization imaging) and RIT (radioimmunotherapy) became the subject of a high number of research projects and publications. Although some of those radiolabelled antibodies reached clinical trials and have become commercially available,<sup>[36]</sup> they never fully succeeded and did not have a substantial clinical impact as the first radiolabelled MAb (monoclonal antibodies) faced various problems:

- 1) A low specific activity of the injected MABs. The radiation delivered to the tumour was small, although the antibodies had long circulation times.
- 2) The radiolabelled MABs showed a high bone marrow toxicity due to the long circulation times.
- 3) Formation of HAMA (human anti-mouse antibodies) was observed, with an impact on the administration limit.<sup>[37]</sup>

Some of these problems faced by MABs have subsequently been solved, for example the formation of HAMA has been reduced by the development of human or chimeric antibodies and the long circulation time has been reduced by the use of antibody fragments.<sup>[38]</sup>

In the 1980s the first stabilized somatostatin analogues were developed and since then it has become clear that the use of regulatory peptides as radiolabelled carriers offer some advantages over antibodies. Due to their small size (8-20 amino acids), they have good tissue permeability and therefore rapid access to the tumour site. In contrary to antibodies, peptides can be synthesized and modified using simple organic chemistry methods and their production costs are lower. Additionally, labelling with different radionuclides, metallic and non-metallic, is easily achievable. They usually exhibit high affinities (nanomolar range) to

receptors overexpressed by tumours, possess no antigenicity and show rapid blood clearance. A drawback of regulatory peptides is their rapid degradation by peptidases, an issue which can be addressed by chemical modification of the structure of the peptides.<sup>[5]</sup>

For all the reasons listed above, we are particularly interested in developing receptor-targeting, peptide-based radiopharmaceuticals for the imaging and treatment of tumours. They will be extensively described in chapter 1.4.4.

### **1.4.4 Radiometal Labelled Peptide-Based Radiopharmaceuticals for the Treatment of Tumours**

Regulatory peptides are peptides naturally present in the human body, where they play modulatory roles in different parts of the body like the brain, the gastrointestinal tract or in the endocrine, vascular or lymphoid system. The use of these naturally-occurring peptides as therapeutic and diagnostic agents may seem odd because of their presence and role in many physiological systems. Yet, it has been shown that numerous tumours overexpress the receptors of these peptides.<sup>[5]</sup> These receptors belong, in the majority of cases, to the family of G-protein-coupled receptor (GPCR).<sup>[39]</sup> Since the development of <sup>123</sup>I-labelled tyr-3-octreotide, the first somatostatin analogue for the localization of neuroendocrine tumours,<sup>[40]</sup> a large number of other regulatory peptides and their receptors have been investigated preclinically and clinically for the development of targeted radiopharmaceuticals for molecular imaging and peptide receptor radionuclide therapy (PRRT) (**Table 4**).

The most investigated family of regulatory peptides are the derivatives of the somatotropin release-inhibiting factor (SRIF), also known as Somatostatin, which bind with high affinity to the family of Somatostatin (sst) receptors. Due to the overexpression of sst receptors (particularly sst receptor subtype 2) in neuroendocrine tumours (NET), several stabilized somatostatin analogues are currently being used in the clinic for the diagnosis and therapy of NET. An example of a somatostatin analogue is <sup>111</sup>In-DTPA-octreotide (Octreoscan®), originally developed for the diagnosis of neuroendocrine tumours. Residue modifications and a change in the chelator of DTPA-octreotide led to the discovery of DOTATOC and DOTATATE, two radiopharmaceuticals with dramatically improved targeting properties thanks to their high selectivity towards Somatostatin receptor subtype 2.<sup>[41-43]</sup>

**Table 4:** Interesting receptors for molecular imaging and PRRT and their corresponding peptide-ligands.

Target Receptor	Peptide	Tumour Type	Clinical Status
Somatostatin receptors (sst1-sst5) <sup>[41, 44-45]</sup>	Somatostatin	Neuroendocrine tumours, gastroenteropancreatic tumours, non- Hodgkins's lymphoma, small lung cancer	Clinical application
Gastrin-releasing peptide receptor (GRPR/BB2) <sup>[41, 45-46]</sup>	Bombesin	Prostate, breast, pancreas, gastric, small cell lung carcinoma, colorectal cancer	Studies in patients
Cholecystokinin B/ gastrin <sup>[41, 45, 47]</sup>	CCK/gastrin	Medullary thyroid cancer, small lung cancer, gastrointestinal stromal cancer, stromal ovarian cancer, astrocytomas	Studies in patients
Glucagon-like peptide-1 Receptor (GLP-1) <sup>[41, 45, 48]</sup>	Exendin	Insulinomas, gastrinomas, paragangliomas, medullary thyroid carcinomas	Studies in patients
$\alpha_v\beta_3$ -integrin <sup>[41, 45, 49]</sup>	RGD	Brain, lung, ovary, breast, skin	Studies in Patients
Neurotensin receptor (NTR1) <sup>[41, 45, 50]</sup>	Neurotensin	Small lung cancer, Ewing's sarcoma, breast, colon, exocrine pancreas, prostate	Studies in patients
Melanocortin 1 receptor (MC1R) <sup>[41, 45, 51]</sup>	$\alpha$ -MSH	Melanomas	Studies in patients
Neuropeptide 1 receptor (Y-1) <sup>[41, 45, 48]</sup>	NPY	Breast, prostate cancer	Preclinical studies
Vasoactive intestinal peptide (VPAC1) <sup>[41, 45, 52]</sup>	VIP	Breast, ovary, prostate, bladder, colon, oesophagus, brain	
Luteinizing hormone- releasing hormone (LHRH- R) <sup>[41, 53]</sup>	LHRH	Prostate, breast, endometrial and ovarian carcinomas	Studies in patients
Neurokinin 1 receptor (NK-1) <sup>[41]</sup>	Substance P	Glioblastoma, astrocytoma, medullary thyroid carcinoma, breast, blood vessels	Studies in patients
Chemokine receptor 4 (CXCR4) <sup>[41]</sup>	CXCT4	Lymphatic system, ling, breast, prostate	Preclinical studies

The subject of this thesis is the synthesis of new Neurotensin analogues. Neurotensin and its stabilized analogues described in literature will be extensively described in detail in chapter 1.5.

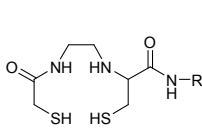
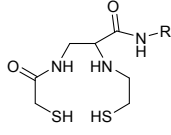
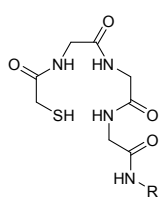
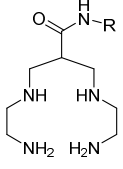
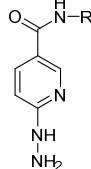
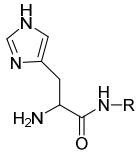
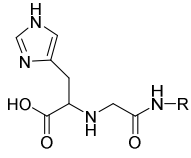
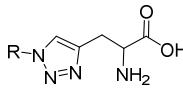


## 1.4.5 Chelators for Peptide-Based Radiopharmaceuticals

### 1.4.5.1 Chelators for Technetium

$^{99m}\text{Tc}$  is a radiometal of particular interest for nuclear medicine. 80% of the radiopharmaceuticals are  $^{99m}\text{Tc}$ -based. Favourable physical properties like a half-life of 6.02 h and energy of radiation of 141 keV, combined with economic aspects such as price and good availability are the reasons for the extensive use of this radionuclide.  $^{99m}\text{Tc}$  is readily available from a  $^{99}\text{Mo}/^{99m}\text{Tc}$ -generator, from where  $^{99m}\text{Tc}$  is eluted as  $^{99m}\text{TcO}_4^-$  in a sterile saline solution. Most of the commercial radiopharmaceutical agents consist of  $^{99m}\text{Tc}$ -complexes with the oxidation states +V, but also +I, +III and +IV. As the oxidation state of  $^{99m}\text{Tc}$  in  $^{99m}\text{TcO}_4^-$  is +VII, it needs to be reduced with reducing agents like  $\text{Na}_2\text{S}_2\text{O}_4$  and  $\text{SnCl}_2$  to obtain the desired oxidation state. This reduction takes place in presence of the ligand needed for the complexation. As mentioned in chapter 1.4.1, bifunctional chelating agents (BFCAs) are used for the labelling of a peptide. A selection of BFCAs suitable for the labelling of  $^{99m}\text{Tc}$  is shown in **Table 5**.  $^{99m}\text{Tc}$  forms mainly penta- or hexa-coordinated complexes with either a  $\text{TcO}^{3+}$  or a  $\text{TcO}^{2+}$  core.<sup>[41]</sup> For complexation of some of the ligands, one or more co-ligands, (donors like amines, hydroxyls or carboxylates), are needed for the completion of the coordination sphere. Another approach for the labelling with  $^{99m}\text{Tc}$  is the use of the  $^{99m}\text{Tc}(\text{CO})_3(\text{H}_2\text{O})_3$  ( $^{99m}\text{Tc}$ -tricarbonyl core), where the metallic ion contains three tightly coordinated CO ligands and three water molecules, the latter of which can be readily replaced by mono-, bi- and tri-dentate ligand systems.<sup>[54]</sup>

**Table 5:** Selection of commonly used BFCAs for the labelling of peptides with  $^{99m}\text{Tc}$ . [41, 55]

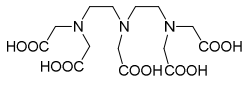
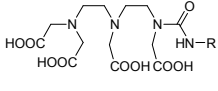
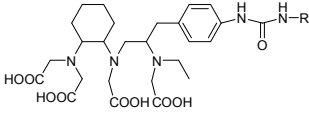
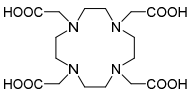
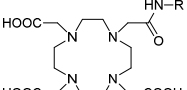
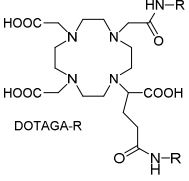
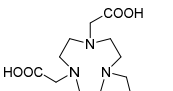
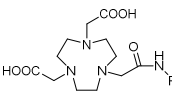
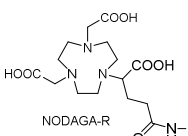
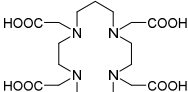
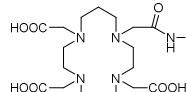
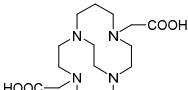
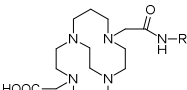
$^{99m}\text{Tc}$ -core	Bifunctional Chelators		
$^{99m}\text{TcO}^{3+}$ or $^{99m}\text{TcO}_2^+$	 $\text{N}_2\text{S}_2\text{-R}$	 $\text{N}_2\text{S}_2\text{-R}$	 $\text{N}_3\text{S-R}$
	 $\text{N}_4\text{-R}$	 $\text{HYNIC-R}$	
$^{99m}\text{Tc}(\text{CO})_3(\text{H}_2\text{O})_3^+$	 $\text{His-R}$	 $(\text{N}^{\text{H}}\text{His})\text{Ac-R}$	 'Click-to-chelate'

### 1.4.5.2 Chelators for $\text{M}^{3+}$ Radiometals

Besides  $^{99m}\text{Tc}$ , there are a large number of other clinically relevant radionuclides, including  $^{111}\text{In}$ ,  $^{90}\text{Y}$ ,  $^{177}\text{Lu}$ ,  $^{68}\text{Ga}$  and  $^{64}\text{Cu}$ . The most important aspect of these radionuclides is the thermodynamic stability *in vivo* of the resulting complexes and their kinetic inertness under physiological conditions. The radiometal-chelator complex needs to be stable, in order to avoid competition with other chelators present in the body. Transchelation, the loss of the radiometal to a complexation agent naturally present in the body, like ferritin (metal storage) or transferrin and lactoferrin (metal transport), can lead to an uptake of radioactive material in non-targeted organs. This undesired accumulation of radioactivity can lead to a high background radiation, which compromises the quality of the imaging as well as to a high radiation exposure of non-targeted tissue.<sup>[56]</sup>

Most of these radionuclides, with the exception of  $^{64}\text{Cu}$ , form  $\text{M}^{3+}$  cations in aqueous solutions at physiological pH.  $^{64}\text{Cu}$  forms  $\text{M}^{2+}$  cations. All these radiometals are hard Lewis acids and therefore form stable complexes with chelators containing hard Lewis bases like carboxylates, amines, phosphonates or hydroxamates groups. A selection of chelators and their corresponding BFAs are shown in **Table 6**.

**Table 6:**  $M^{2+/3+}$  radiometals and their corresponding chelators and BFCAs.<sup>[41]</sup>

Radiometal	Chelators	Bifunctional Chelators	
$^{111}\text{In}$	 DTPA	 DTPA-R	 SCN-CHX-ADTPA-R
$^{111}\text{In}$ $^{86/90}\text{Y}$ $^{177}\text{Lu}$ $^{67/68}\text{Ga}$	 DOTA	 DOTA-R	 DOTAGA-R
$^{67/68}\text{Ga}$	 NOTA	 NOTA-R	 NODAGA-R
$^{111}\text{In}$ $^{64/67}\text{Cu}$	 TETA	 TETA-R	
$^{64/67}\text{Cu}$	 CB-TE2A	 CB-TE2A-R	

The most commonly used of these macrocyclic chelators is DOTA (1,4,7,10-tetraazacyclododecane-1,4,7,10-tetraacetic acid), which is applied for the labelling of  $^{111}\text{In}$ ,  $^{90}\text{Y}$ ,  $^{177}\text{Lu}$ ,  $^{213}\text{Bi}$  and  $^{68}\text{Ga}$ .<sup>[41]</sup> The hexadentate, chelator, NOTA (1,4,7-triazacyclononane-1,4,7-triacetic acid) one of the first chelators investigated, is used for the labelling of isotopes with a smaller ionic radius, like  $^{68}\text{Ga}$ , because of its small cavity size. The *in vivo* stability and kinetic inertness of the complex of  $^{68}\text{Ga}$  with NOTA is superior to the one with DOTA, but due to differences in the physical properties (charge), the latter is still preferred for the labelling of some vectors. NOTA is also suitable for the labelling of  $^{64}\text{Cu}$ .<sup>[34]</sup>

In some of the DOTA- and NOTA-based bifunctional chelating agents, one of the carboxylic acid arms of the macrocycle functionalized to an amide carbonyl group for bioconjugation. The amide carbonyl group is still able to coordinate the radionuclide, but weakly. To address this issue, DOTAGA and NODAGA have been developed, where an additional sidechain is used for the bioconjugation to the vector, retaining full denticity of the original chelator (**Table 6**).<sup>[34]</sup>

Stable complexation of  $^{64}\text{Cu}$  is especially challenging as there are many copper chelating proteins (e.g. ceruloplasmin superoxide dismutase, metallothionein, copper transporters and chaperones) that potentially can displace the copper ion from the chelator.<sup>[57]</sup> Also, Cu(I) is known for its disproportionation *in vivo* into Cu(II) and Cu(0). As a consequence, classical cyclen- and cyclam-based macrocycles such as DOTA and TETA (1,4,8,11-tetraazacyclotetradecane-1,4,8,11-tetraacetic acid), a chelator which has been exclusively investigated for the labelling of  $^{64}\text{Cu}$ , show signs of *in vivo* instability. For this reason new chelators with superior *in vivo* and kinetic stability, like NOTA and CB-TE2A have been developed. CB-TE2A is a crossbridged TETA-derivative and due to its superior stability *in vivo*, it has become one of the most used chelators for  $^{64}\text{Cu}$ .<sup>[34]</sup>

As this work includes the complexation of  $^{177}\text{Lu}$  with DOTA, special attention is given to this radionuclide. The chemistry of  $^{177}\text{Lu}$  is similar to other lanthanide radiometals. The mechanism of complexation of lanthanides with DOTA is still unclear. In 2004 Moreau *et al.*<sup>[58]</sup> suggested that the complexation takes place in three steps. In the first step the  $\text{Ln}^{3+}$  metal is coordinated by the four carboxylate groups of DOTA, but the metal is still located in the plane above the cavity and is still coordinated to four  $\text{H}_2\text{O}$  molecules (**1, Figure 6**). Step two includes the formation of two  $\text{Ln}^{3+}$ -N bonds (**2, Figure 6**). During the last step, the metal is introduced into the cavity and the final two  $\text{Ln}^{3+}$ -N bonds are formed (**3, Figure 6**). The final coordination number is 9, as one position is still occupied by a  $\text{H}_2\text{O}$  molecule. This coordination mode seems to be typical for lanthanide metals, also for  $^{177}\text{Lu}$ . A crystal structure of a  $\text{Lu}^{3+}$ -bound DOTA conforming this coordination geometry has been published by Bombiere and his co-workers in 1996.<sup>[59]</sup>

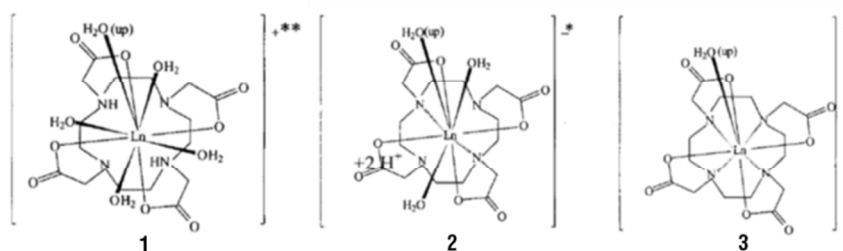


**Figure 6:** The three intermediate complexation steps of the complexation of a  $\text{Ln}^{3+}$  metal with DOTA.<sup>[58]</sup>

## 1.5 Neurotensin

### 1.5.1 General Introduction

Neurotensin (NT) is a regulatory peptide localized in the peripheral tissues of mammals, mainly in the gastrointestinal tract. It was first isolated from bovine hypothalamic in 1973 by Carraway.<sup>[60]</sup> In 1976 it was isolated in bovine intestines as well as, in the same concentration, from bovine brain.<sup>[61]</sup> NT has also been isolated in canine, porcine and human gut.<sup>[62]</sup> NT is a tridecapeptide, with the sequence H-pGlu<sup>1</sup>-Leu<sup>2</sup>-Tyr<sup>3</sup>-Glu<sup>4</sup>-Asn<sup>5</sup>-Lys<sup>6</sup>-Pro<sup>7</sup>-Arg<sup>8</sup>-Arg<sup>9</sup>-Pro<sup>10</sup>-Tyr<sup>11</sup>-Ile<sup>12</sup>-Leu<sup>13</sup>-OH.<sup>[63]</sup> The minimal binding sequence of NT is the N-terminal hexapeptide NT (8-13), Arg<sup>8</sup>-Arg<sup>9</sup>-Pro<sup>10</sup>-Tyr<sup>11</sup>-Ile<sup>12</sup>-Leu<sup>13</sup>-OH.<sup>[64]</sup> Both NT and NT (8-13) have a nanomolar affinity towards NTR1 (Neurotensin receptor 1). There are four subtypes of Neurotensin receptors, NTR1, NTR2, NTR3, and NTR4. The NTR family will be described in detail in chapter 1.5.2.

Neurotensin has an extended role in many physiologic and pathologic processes. For example, in the gastrointestinal system, it reduces the gastric mobility and has a protective effect on gastrointestinal tissues.<sup>[65]</sup> Another example is in the central nervous system (CNS), where Neurotensin acts as a neurotransmitter and as a neuromodulator. It plays a central role in the modulation of the dopamine signalling, inhibiting the D<sub>2</sub>-receptors, which results in an increase of dopamine release.<sup>[66]</sup> The dopamine system is involved in CNS disorders like Parkinson's disease, schizophrenia or drug abuse,<sup>[67-68]</sup> which makes Neurotensin a candidate for the drug development for such disorders. The involvement of the NT receptor NTR2 in pain modulation has been described in literature.<sup>[67, 69]</sup>

In addition to these physiological roles, Neurotensin and its receptors are also suspected to participate in cancer growth. There are several studies describing the role of Neurotensin in the endocrine, autocrine and paracrine growth stimulation in pancreatic, colorectal, breast, lung, and prostate cancer.<sup>[70]</sup> The exact mechanism of how NT receptor activation works as a cell growth factor remains unclear, although several pathways have been proposed.<sup>[71-72]</sup> For example, Oleszewski *et al.* demonstrated that Neurotensin induces intra- and intercellular acidification in pancreatic carcinoma. Acidosis (accumulation of lactic acid in the extracellular space) due to tumour hypoxia is often observed in solid tumours and promotes the specific selection of malignant phenotypes and therefore the growth of the tumour.<sup>[73]</sup>

## 1.5.2 The Neurotensin Receptor Family

The NT receptor family consists of four subtypes; NTR1, NTR2, NTR3 and NTR4. NTR1 and NTR2 belong to the family of G-protein-coupled receptors, with seven trans-membrane helices, whereas NTR3 is identical to the gp5/sortilin receptor and NTR4 is a yeast sorting receptor SorLA (sortilin related receptor). Since NTR4 was only recently isolated from the brain of bullfrogs in 2005, little is known about it to date.<sup>[74]</sup>

Within the NT receptor family, the most important receptor subtype for medical applications (e.g. tumour targeting) is NTR1. It binds its ligands NT and NT (8-13) with an affinity in the subnanomolar range. NTR1 is expressed in the brain of rats and humans.<sup>[75-76]</sup> Additionally, it is specifically overexpressed on the cell membrane of numerous tumours such as ductal pancreatic adenocarcinoma,<sup>[1]</sup> Ewing's sarcoma,<sup>[2]</sup> prostate,<sup>[77]</sup> colon,<sup>[78]</sup> small cell lung,<sup>[79]</sup> and breast cancer.<sup>[3]</sup> Thus, NTR1 is an appealing potential target for receptor-mediated molecular imaging and therapy. The human NTR1 is a 418 amino acid protein sharing 84% homology with the rat receptor. In 2012, White *et al.* published the first crystal structure of the NT-bound receptor NTR1 (rat).<sup>[80]</sup>

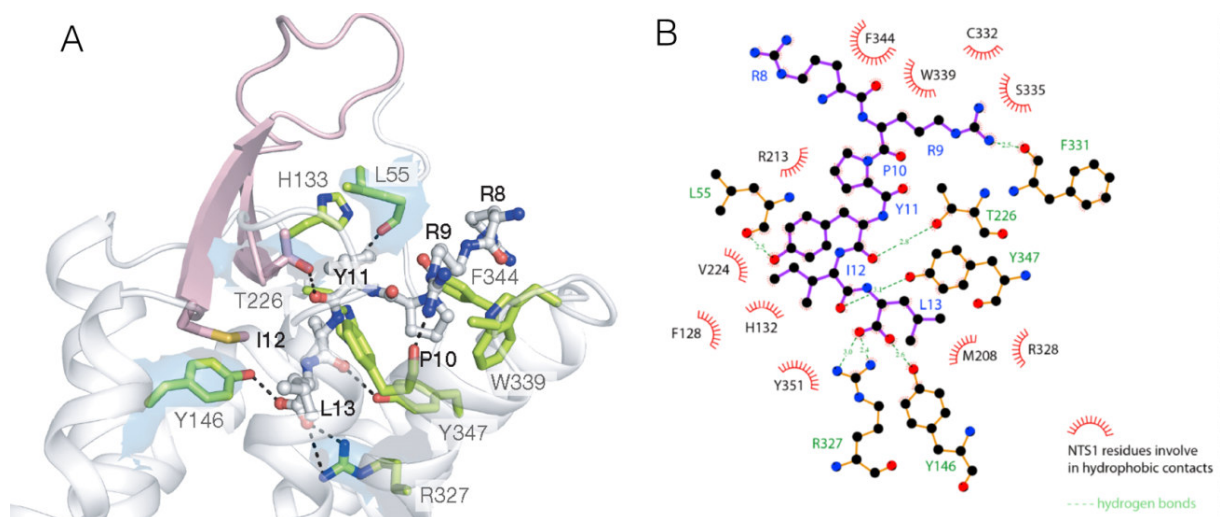


**Figure 7:** A) The NTR1 agonist binding pocket. B) Schematic drawing of NT (8-13) binding pocket.<sup>[80]</sup>

White and his co-workers found interesting data about the binding of NT (8-13) to the binding pocket of the rat receptor. Overall, the peptide agonist binds to the rat NTR1 in an extended conformation, which is nearly perpendicular to the membrane plane, with the C-terminus oriented towards the receptor core. As shown in **Figure 7**, the C-terminal COOH group forms hydrogen bonds to Tyr146 and Arg327 of the receptor, which suggests that this COOH group

is essential for the binding of NT (8-13) to the receptor. Additionally, the carbonyl groups of the amide bonds between Ile<sup>12</sup>-Leu<sup>13</sup> and Tyr<sup>11</sup>-Ile<sup>12</sup> form hydrogen bonds to Tyr347 and Thr226, respectively and the sidechains of Tyr<sup>11</sup> and Arg<sup>10</sup> form additional hydrogen bonds to the binding pocket. This information is crucial for the development of new Neurotensin analogues because it provides insight on the type and the position of modifications which may be tolerated in Neurotensin.

Of less importance is NTR2, which is localized mostly in the brains of mammals, especially in the olfactory system, the cerebral and cerebellar cortices and the hippocampus.<sup>[81]</sup> NT and NT (8-13) have a lower affinity (nanomolar) to NTR2 than to NTR1.<sup>[81-82]</sup> NTR2, however, can be selectively blocked by the NT antagonist SR48692 (a small organic molecule known to inhibit cell proliferation in small cell lung cancer) and it has a physiological role in pain modulation.<sup>[83]</sup>

### 1.5.3 Development of Neurotensin Analogues

Neurotensin has appealing properties for its use in the development of a peptide-based radiopharmaceutical for targeting NTR1-positive tumours. Despite these promising characteristics (high affinity towards NTR1, low molecular weight) like many regulatory peptides, it suffers from a low metabolic stability.

The low metabolic stability of Neurotensin and of its minimal binding sequence NT (8-13) has been subject to investigation since the isolation of the peptide. The main cleavage sites were found to be at the Arg<sup>8</sup>-Arg<sup>9</sup>, Pro<sup>10</sup>-Tyr<sup>11</sup> and Tyr<sup>11</sup>-Ile<sup>12</sup> bonds. The Arg<sup>8</sup>-Arg<sup>9</sup> bond is readily cleaved by the metalloendopeptidase 24.15. The Pro<sup>10</sup>-Tyr<sup>11</sup> bond is susceptible to the metalloendopeptidase 24.16 and to a neutral endopeptidase. This latter endopeptidase, together with the angiotensin converting enzyme is also responsible for the degradation of the Tyr<sup>11</sup>-Ile<sup>12</sup> bond (**Figure 8**).<sup>[84-85]</sup>

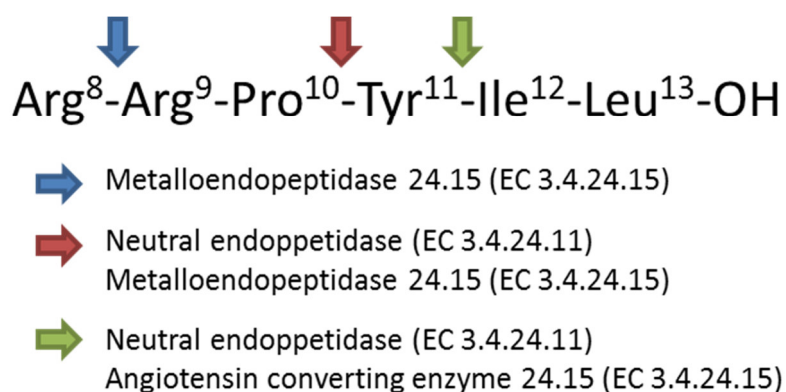


**Figure 8:** Schematic representation of Neurotensin (8-13) and its cleavage sites.

The stabilization of the NT (8-13) sequence has been a major topic of Neurotensin research in the past years. Classical peptide stabilization approaches like carbonyl reduction,<sup>[9]</sup> *N*-methylation of amide bonds,<sup>[6]</sup> amino acid substitution,<sup>[6, 86]</sup> and formation of multimeric analogues were only partially successful in providing stabilized NT-analogues with improved tumour-targeting properties.<sup>[87]</sup> To determine which amino acids are responsible for the biological behaviour of NT (8-13), several structure-activity relationship studies (SAR studies) of NT (8-13) have been described in literature. A detailed discussion about the results of these studies follows in chapter 1.5.3.1. Additionally, the influence of the chelator, the radionuclide and the spacer on NT (8-13) on its receptor binding affinity will be discussed in chapter 1.5.3.2.

### 1.5.3.1 Structure-Activity Relationship Studies of NT (8-13)

In 1991, Lugin *et al.* published the systematic replacement of each of the five NT (8-13) amide bonds by reduced amide bonds.<sup>[9]</sup> These analogues, as well as NT (8-13) and [Lys<sup>8/9</sup>]NT (8-13) were tested for their receptor binding affinity (IC<sub>50</sub>) and their metabolic stability in rat brain homogenates. It was found that the reduction of amide bonds between residues Arg<sup>9</sup>-Pro<sup>10</sup>, Pro<sup>10</sup>-Tyr<sup>11</sup>, Tyr<sup>11</sup>-Ile<sup>12</sup> and Ile<sup>12</sup>-Leu<sup>13</sup> bonds led to a loss of affinity. Only the Arg<sup>8</sup>-Arg<sup>9</sup> bond could be reduced without showing a dramatic loss of affinity toward its receptor. In addition, it was observed that the compounds H-[Ψ8,9] and H-[Ψ9,10] showed a significantly higher metabolic stability than the other analogues (**Table 7**).



**Table 7:** Reduced amide bond analogues of NT (8-13).<sup>[9]</sup>

	Structure	IC <sub>50</sub> (nM) <sup>a</sup>	Stability <sup>b</sup> (% after 1 h)
NT (8-13)	H-Arg-Arg-Pro-Tyr-Ile-Leu	0.14 ± 0.015	~ 20
H-[Lys <sup>8-9</sup> ]NT (8-13)	H-Lys-Lys-Pro-Tyr-Ile-Leu	0.16 ± 0.005	-
H[Ψ <sup>8,9</sup> ]	H-Lys <b>Ψ(CH<sub>2</sub>NH)</b> Lys-Pro-Tyr-Ile-Leu	0.15 ± 0.02	~ 80
H[Ψ <sup>9,10</sup> ]	H-Arg-Lys <b>Ψ(CH<sub>2</sub>NH)</b> Pro-Tyr-Ile-Leu	473 ± 72	~ 90
H[Ψ <sup>10,11</sup> ]	H-Arg-Arg-Pro <b>Ψ(CH<sub>2</sub>NH)</b> Tyr-Ile-Leu	27.5 ± 5.0	~ 18
H[Ψ <sup>11,12</sup> ]	H-Arg-Arg-Pro-Tyr <b>Ψ(CH<sub>2</sub>NH)</b> Ile-Leu	477 ± 113	~ 10
H[Ψ <sup>12,13</sup> ]	H-Arg-Arg-Pro-Tyr-Ile <b>Ψ(CH<sub>2</sub>NH)</b> Leu	283 ± 63	~ 22

<sup>a</sup> IC<sub>50</sub> values were measured in new-born mouse brain homogenates. <sup>b</sup> Stabilities were measured in rat brain homogenates.

Henry *et al.* published a complete ‘Alanine scan’ of the NT (8-13) sequence in 1993.<sup>[88]</sup> Tyr<sup>11</sup> and C-terminal Leu<sup>13</sup> were described as the most critical positions for a side-chain modification since their substitution with an Ala residue led to a significant erosion of the binding affinity towards NTR1. Although also necessary for the binding, Arg<sup>8</sup> and Pro<sup>10</sup> were found to be the least critical residues. The peptides of the Ala-screening and their relative receptor binding affinities in comparison to NT (8-13) are shown in **Table 8**.

**Table 8:** Ala-substituted analogues of NT (8-13) and their relative receptor binding affinities.

	Structure	K <sub>i</sub> /1.8 x10 <sup>-11</sup> M
NT (8-13)	Arg-Arg-Pro-Tyr-Ile-Leu	1
[Ala <sup>8</sup> ]NT (8-13)	<b>Ala</b> -Arg-Pro-Tyr-Ile-Leu	14
[Ala <sup>9</sup> ]NT (8-13)	Arg- <b>Ala</b> -Pro-Tyr-Ile-Leu	120
[Ala <sup>10</sup> ]NT (8-13)	Arg-Arg- <b>Ala</b> -Tyr-Ile-Leu	50
[Ala <sup>11</sup> ]NT (8-13)	Arg-Arg-Pro- <b>Ala</b> -Ile-Leu	6100
[Ala <sup>12</sup> ]NT (8-13)	Arg-Arg-Pro-Tyr- <b>Ala</b> -Leu	250
[Ala <sup>13</sup> ]NT (8-13)	Arg-Arg-Pro-Tyr-Ile- <b>Ala</b>	11000

In an extensive study of the binding site of the NTR1 receptor, the group of Richelson<sup>[89]</sup> synthesized a series of amino acid substituted NT (8-13) analogues. They were able to successfully substitute Arg<sup>8</sup> and Arg<sup>9</sup> with Lys. Tyr<sup>11</sup> could also be substituted, but only with an amino acid with an aromatic side-chain. As illustrated in **Table 9**, a loss of receptor affinity was observed when changing from an aromatic sidechain (Phe) to a non-aromatic sidechain (Cha; cyclohexylalanine).

**Table 9:** NT (8-13) analogues with amino acid substitutions in position 8, 9 and 11 and their receptor binding affinities.<sup>[89]</sup>

	Structure	K <sub>D</sub> (nM)
NT (8-13)	Arg-Arg-Pro-Tyr-Ile-Leu-OH	0.14 ± 0.01
[Lys <sup>8</sup> ]NT (8-13)	<b>Lys</b> -Arg-Pro-Tyr-Ile-Leu-OH	0.25 ± 0.02
[Lys <sup>9</sup> ]NT (8-13)	Arg- <b>Lys</b> -Pro-Tyr-Ile-Leu-OH	1.69 ± 0.08
[Lys <sup>8-9</sup> ]NT (8-13)	<b>Lys-Lys</b> -Pro-Tyr-Ile-Leu-OH	1.0 ± 0.2
[Trp <sup>11</sup> ]NT (8-13)	Arg-Arg-Pro- <b>Trp</b> -Ile-Leu-OH	3.2 ± 0.3
[Phe <sup>11</sup> ]NT (8-13)	Arg-Arg-Pro- <b>Phe</b> -Ile-Leu-OH	3.4 ± 0.2
[Cha <sup>11</sup> ]NT (8-13)	Arg-Arg-Pro- <b>Cha</b> -Ile-Leu-OH	700 ± 100

In 2008, the group of Gmeiner performed a complete 'β-homo amino acid scan' (**Table 10**).<sup>[10]</sup> It was observed that the introduction of β-homo-amino acids in the NT (8-13) sequence led to new analogues with high affinities towards NTR1 receptor as well as the NTR2 receptor. Interestingly, the modification of the Ile<sup>12</sup> position led to a loss of affinity for NTR1, but the affinity to NTR2 was preserved. With this observation, the group of Gmeiner was able to develop several NTR2 specific NT (8-13) analogues, applicable for example to pain therapy.<sup>[90-91]</sup> Gmeiner continued the studies on β-homo amino acid-substituted NT (8-13) analogues in collaboration with Seebach, Reubi, Prante, and Rougeot, developing double β-homo amino acid substituted analogues with high affinities towards NTR1 and NTR2.<sup>[10, 92-93]</sup>

**Table 10:** Structures and receptor binding affinities of the β-homo amino acid-containing NT (8-13) analogues.

	Structure	K <sub>i</sub> (nM)	
		NTR1	NTR2
NT (8-13)	Arg-Arg-Pro-Tyr-Ile-Leu	0.23 ± 0.04	1.2 ± 0.2
[β-hArg <sup>8</sup> ]NT (8-13)	<b>β-hArg</b> -Arg-Pro-Tyr-Ile-Leu-OH	0.130 ± 0.005	0.6 ± 0.1
[β-hArg <sup>9</sup> ]NT (8-13)	Arg- <b>β-hArg</b> -Pro-Tyr-Ile-Leu-OH	2.3 ± 1.0	16 ± 2
[β-hPro <sup>10</sup> ]NT (8-13)	Lys-Lys- <b>β-hPro</b> -Tyr-Ile-Leu-OH	47 ± 11	210 ± 46
[β-hTyr <sup>11</sup> ]NT (8-13)	Arg-Arg-Pro- <b>β-hTyr</b> -Ile-Leu-OH	8.4 ± 0.3	44 ± 30
[β-hIle <sup>12</sup> ]NT (8-13)	Arg-Arg-Pro-Tyr- <b>β-hIle</b> -Leu-OH	250 ± 26	5.4 ± 1.0
[β-hLeu <sup>13</sup> ]NT (8-13)	Arg-Arg-Pro-Tyr-Ile- <b>β-hLeu</b> -OH	8.4 ± 1.9	25 ± 0

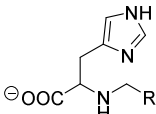
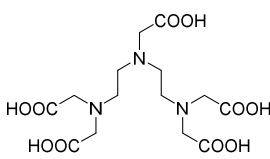
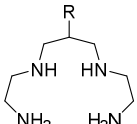
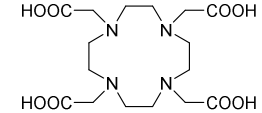
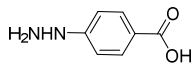
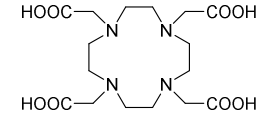
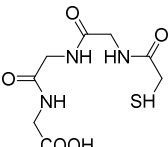
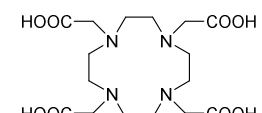
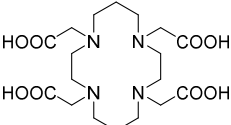
The main conclusion after revision of the SAR studies performed on NT (8-13) is that the position 12 of the NT (8-13) sequence (Ile<sup>12</sup>) is the most critical to modify. Introduction of a backbone modification on this position or its substitution with an amino acid without side chains led to an abolishment of the receptor affinity towards NTR1 of the NT (8-13)

analogue. The other positions in NT (8-13) are less critical and can be modified without a dramatic loss of affinity.

### 1.5.3.2 Influence of Chelator, the Radionuclide and the Spacer

The functionalization of a peptide with a chelator and a spacer and the subsequent labelling with a radiometal represents a chemical modification in the structure of the peptide. It is therefore not surprising that these elements can have a substantial influence on the pharmacological properties (e.g. receptor binding affinity, metabolic stability or lipophilicity) of a peptide-based radiopharmaceutical.<sup>[94-95]</sup>

**Table 11:** Metallic radionuclides reported for the labelling of NT analogues and their corresponding chelators.

Radionuclide	Chelator	Radionuclide	Chelator
	$(N^{\alpha}\text{-His})\text{Ac}$ <sup>[84, 96-98]</sup> 		$\text{DTPA}$ <sup>[99-100]</sup> 
$^{99m}\text{Tc}$	$\text{N}_4$ <sup>[101]</sup> 	$^{111}\text{In}$	
	$\text{HYNIC}$ <sup>[103]</sup> 	$^{90}\text{Y}$	$\text{DOTA}$ <sup>[102]</sup> 
	$\text{MAG}_3$ <sup>[103]</sup> 	$^{68}\text{Ga}$	$\text{DOTA}$ <sup>[93, 102, 104]</sup> 
$^{64}\text{Cu}$	$\text{TETA}$ 		

Neurotensin analogues have been labelled with a variety of different radionuclides and have consequently been conjugated to many different chelators. In **Table 11** the most commonly used radiometals for NT analogues are shown with their corresponding chelators. NT analogues have also been labelled with  $^{18}\text{F}$ , using 4( $^{18}\text{F}$ )Fluorobenzoyl or  $^{18}\text{F}$ -FDG as acylation agents.<sup>[105-106]</sup>

### 1.5.3.2.1 Influence of the Chelator

The influence of the chelator on the binding properties of NT (8-13) analogues has not been investigated systematically. Nonetheless, some information on the influence of combining a chelator to NT (8-13) can be obtained from literature data. Some examples are given in **Table 12**. Entries **1** and **2** show two examples of NT (8-13) analogues with and without a chelator. In both cases, the introduction of a chelator to a NT (8-13) analogue led to a loss in receptor affinity of a factor 10. The group of Gruaz-Gruyon selected two of the NT (8-13) analogues described by the group of Schubiger, NT-VI and NT-XI, and labelled them with  $^{111}\text{In}$ , using DTPA as a chelator. In this case, no significant change in binding affinity towards NTR1 could be observed between ( $\text{N}^{\alpha}$ -His)Ac and DTPA as a chelator (entries **3** and **4**, **Table 12**).

**Table 12:** Comparison of receptor binding affinities between pairs of peptide conjugates with different chelators.

		Structure	IC <sub>50</sub> (nM)
<b>1</b>	NT (8-13) <sup>[100]</sup>	Arg-Arg-Pro-Tyr-Ile-Leu-OH	1.6
	DTPA-NT (8-13) <sup>[100]</sup>	<b>DTPA</b> -Arg-Arg-Pro-Tyr-Ile-Leu-OH	21.7
<b>2</b>	[ <sup>nat</sup> F]Glc-NT4 <sup>[106]</sup>	[ <sup>nat</sup> F]Glc-Tz-Lys-Lys-Pro-Tyr-Tle-Leu	16 <sup>a</sup>
	[ <sup>nat</sup> Ga]-DOTA-NT4 <sup>[104]</sup>	[ <sup>nat</sup> Ga]- <b>DOTA</b> -Lys-Lys-Pro-Tyr-Tle-Leu	180 <sup>a</sup>
<b>3</b>	NT-VI <sup>[84]</sup>	<b>(N<sup>α</sup>-His)Ac</b> -Lys ψ(CH <sub>2</sub> NH)Arg-Pro-Tyr-Ile-Leu-OH	23
	DTPA -NT-VI <sup>[100]</sup>	<b>DTPA</b> -Lys ψ(CH <sub>2</sub> NH)Arg-Pro-Tyr-Ile-Leu-OH	14.7
<b>4</b>	NT-XI <sup>[6]</sup>	<b>(N<sup>α</sup>-His)Ac</b> -Lys ψ(CH <sub>2</sub> NH)Arg-Pro-Tyr-Tle-Leu-OH	158
	DTPA -NT-XI <sup>[100]</sup>	<b>DTPA</b> -Lys ψ(CH <sub>2</sub> NH)Arg-Pro-Tyr-Tle-Leu-OH	101

<sup>a</sup> Values are K<sub>i</sub> (nM) values.

### 1.5.3.2.2 Influence of the Radionuclide

The influence of the radionuclide on the receptor binding properties of a regulatory peptide is well documented.<sup>[107]</sup> For example, the group of Prante observed a difference on receptor affinity of a DOTA-NT (8-13) analogue with and without gallium (entry **1**, **Table 13**).<sup>[104]</sup> In another example, Alshoukr *et al.* studied the receptor affinities of an NT (8-13) analogue labelled with different metals, (entry **2**, **Table 13**) and observed a higher receptor affinity towards NTR1 when labelling with <sup>nat</sup>Y rather than with <sup>nat</sup>In or <sup>nat</sup>Ga.<sup>[102]</sup> The inhibition experiments (IC<sub>50</sub>) were performed with cold metals (i.e. non-radioactive isotopes). The behaviour of the corresponding radiometal is very similar, and therefore it can be concluded that the choice of the radiometal can have the same influence on the receptor binding affinity of a radiopeptide.

**Table 13:** Influence of the radionuclide on the receptor binding affinity of NT (8-13) analogues.

	Structure	IC <sub>50</sub> (nM)
<b>1</b> <sup>[104]</sup>	DOTA-Lys-Lys-Pro-Tyr-Tle-Leu	2300 <sup>a</sup>
	[ <sup>nat</sup> Ga]-DOTA-Lys-Lys-Pro-Tyr-Tle-Leu	180 <sup>a</sup>
	[ <sup>nat</sup> In]-DOTA-Pro(N-CH <sub>3</sub> )Arg-Arg-Pro-Tyr-Tle-Leu-OH	15
<b>2</b> <sup>[102]</sup>	[ <sup>nat</sup> Ga]-DOTA-Pro(N-CH <sub>3</sub> )Arg-Arg-Pro-Tyr-Tle-Leu-OH	14
	[ <sup>nat</sup> Y]-DOTA-Pro(N-CH <sub>3</sub> )Arg-Arg-Pro-Tyr-Tle-Leu-OH	5.6

<sup>a</sup> Values are K<sub>i</sub> (nM) values.

The labelling of Neurotensin with <sup>177</sup>Lu only has been published only once. The group of Gruia synthesized [<sup>177</sup>Lu]-DOTA-NT (for structure see chapter 1.5.1) and [<sup>177</sup>Lu]-DOTA-SR48692 (for structure see chapter 1.6.1) and compared their therapeutic efficacy *in vivo* in murine Rs-1 hepatoma.<sup>[108]</sup> The usage of <sup>177</sup>Lu is well documented for other radiopeptides,<sup>[109]</sup> and it has been applied for clinical purposes (DOTATOC).<sup>[110]</sup>

### 1.5.3.2.3 Influence of the Spacer

A spacer is used as a link between the tracer and the chelate. The influence of the spacer on a radiopeptide conjugate has been investigated for other regulatory peptides like Bombesin and it has been determined that the right choice of spacer is important for the pharmacological behaviour of a radiopeptide.<sup>[94-95]</sup> For Neurotensin, no systematic study of the influence of spacers has been published to date, but there is some evidence in the literature that a spacer strongly influences the biological properties of a NT analogue. As an

example, Alshoukr *et al.* published a comparison of peptides modified with an Ahx-spacer (6-aminohexanoic acid).<sup>[100]</sup> The results of this study are summarized in **Table 14**. Entry **1** shows the difference between DTPA-NT-VI and DTPA-Ahx-NT-VI, whereas entry **2** shows the difference between DTPA-NT-XI and DTPA-Ahx-NT-XI. The introduction of the Ahx-spacer into DTPA-NT VI and DTPA-NT-XI led to a loss of receptor affinity towards NTR1 of the radiolabelled peptide conjugates. These results suggest that 6-aminohexanoic acid is not the spacer of choice for these conjugates. However, other more favourable spacers could be identified, that lead to conjugates with favourable properties. Therefore, the first part of this thesis includes the evaluation of different spacers for NT (8-13) optimising the pharmacological properties of NT (8-13) derivatives.<sup>[33]</sup>

**Table 14:** Influence of an Ahx spacer on the binding affinities of NT (8-13) analogues.

		Structure	IC <sub>50</sub> (nM)
<b>1</b>	DTPA -NT-VI <sup>[100]</sup>	DTPA-Lys $\Psi$ (CH <sub>2</sub> NH)Arg-Pro-Tyr-Ile-Leu-OH	14.7
	DTPA -Ahx-NT-VI <sup>[100]</sup>	DTPA-Ahx-Lys $\Psi$ (CH <sub>2</sub> NH)Arg-Pro-Tyr-Ile-Leu-OH	132
<b>2</b>	DTPA-NT-XI <sup>[100]</sup>	DTPA-Lys $\Psi$ (CH <sub>2</sub> NH)Arg-Pro-Tyr-Tle-Leu-OH	101
	In-DTPA-Ahx-NT-XI <sup>[100]</sup>	DTPA-Ahx-Lys $\Psi$ (CH <sub>2</sub> NH)Arg-Pro-Tyr-Tle-Leu-OH	626

#### 1.5.4 State of the Art in the Development of Stabilized NT (8-13)-Based Radiotracers

From the amide bond screening,<sup>[9]</sup> the ‘Ala scan’<sup>[88]</sup> and the ‘ $\beta$ -homo amino acid scan’,<sup>[10]</sup> described in chapter 1.5.3.1, it can be concluded that Ile<sup>12</sup> is an important cleavage site of the NT (8-13) sequence, however this position is difficult to modify with backbone modifications or amino acid substitutions. The substitution of Ile<sup>12</sup> with Tle<sup>12</sup> (*tert*-leucine) has been described numerous times in literature.<sup>[86, 105]</sup> Bergmann *et al.*<sup>[105]</sup> reported the substitution of Ile<sup>12</sup> with Tle<sup>12</sup> in 2002 (entry **1**, **Table 15**). The same year these results were confirmed by the groups of Schubiger and Bläuenstein (entries **2** and **3**, **Table 15**) and a year later by the group of De Jong (entry **4**, **Table 15**). All the groups observed a retained receptor affinity towards NTR1. Additionally, the metabolic degradation in serum of the Tle<sup>12</sup>-containing analogues was substantially decreased. Based on these observations, it can be concluded that a substitution of Ile<sup>12</sup> with Tle<sup>12</sup> appears to be beneficial for the stabilization of NT (8-13) and a good alternative to backbone modifications.

**Table 15:** Structure, receptor binding affinities and serum stabilities of [ $^{125}$ I]NT analogues.

	Structure	IC <sub>50</sub> (nM) <sup>a</sup>	Stability (t <sub>1/2</sub> )
1	[ <sup>nat</sup> FB]-Arg(CH <sub>2</sub> NH)Arg- Pro-Tyr-Ile-Leu-OH <sup>[105]</sup>	0.4	7% after 5 min <sup>c</sup>
	[ <sup>nat</sup> FB]-Arg(CH <sub>2</sub> NH)Arg- Pro-Tyr- <b>Tle</b> -Leu-OH <sup>[105]</sup>	0.3	Stable over 480 min <sup>c</sup>
2	[ <sup>99m</sup> Tc]-(N <sup>α</sup> -His)Ac-Arg-Arg-Pro-Tyr-Ile-Leu-OH <sup>[84]</sup>	0.3 <sup>b</sup>	5.6 min <sup>d</sup>
	[ <sup>99m</sup> Tc]-(N <sup>α</sup> -His)Ac-Arg-Arg-Pro-Tyr- <b>Tle</b> -Leu-OH <sup>[6]</sup>	0.2 <sup>b</sup>	4 h <sup>d</sup>
3	[ <sup>99m</sup> Tc]-(N <sup>α</sup> -His)Ac-Lys $\Psi$ (CH <sub>2</sub> NH)Arg-Pro-Tyr-Ile-Leu-OH <sup>[84]</sup>	0.5 <sup>b</sup>	8 min <sup>d</sup>
	[ <sup>99m</sup> Tc]-(N <sup>α</sup> -His)Ac-Lys $\Psi$ (CH <sub>2</sub> NH)Arg-Pro-Tyr- <b>Tle</b> -Leu-OH <sup>[6]</sup>	0.5 <sup>b</sup>	21 d <sup>d</sup>
4	DTPA-DLys-Pro-Phe(4-Gu)-Pro-Tyr-Ile-Leu-OH <sup>[86]</sup>	0.5	14.1 <sup>e</sup>
	DTPA-DLys-Pro-Phe(4-Gu)-Pro-Tyr- <b>Tle</b> -Leu-OH <sup>[86]</sup>	24.6	72.0 <sup>e</sup>

<sup>a</sup> IC<sub>50</sub> values were measured for the unlabelled peptide conjugates (competition assay with [ $^{125}$ I]NT). <sup>b</sup> K<sub>D</sub> values. <sup>c</sup> Stabilities were measured in rat plasma. <sup>d</sup> Half-life measured in human serum at 37 °C. <sup>e</sup> Percentage of intact peptide after 24h incubation in serum at 37 °C.

Probably the most successful development of metabolically stable, high affinity NT (8-13) analogues was performed by the groups of Schubiger, Bläuenstein, and Tourwé by using a combination of both backbone and residue modifications (**Table 16**).<sup>[6, 84, 96, 98, 111]</sup>

**Table 16:** Structures of <sup>99m</sup>Tc-labelled NT (8-13) analogues with their binding affinities and stabilities.

	Structures	K <sub>D</sub> (nM)	t <sub>1/2</sub> <sup>b</sup>
NT-II <sup>[84]</sup>	[ <sup>99m</sup> Tc]-( <b>N<sup>α</sup>-His</b> )Ac-Arg-Arg-Pro-Tyr-Ile-Leu-OH	0.3	5.6 min
NT-VI <sup>[84]</sup>	[ <sup>99m</sup> Tc]-( <b>N<sup>α</sup>-His</b> )Ac-Lys $\Psi$ (CH <sub>2</sub> NH)Arg-Pro-Tyr-Ile-Leu-OH	0.5	8 min
NT-XI <sup>[6]</sup>	[ <sup>99m</sup> Tc]-( <b>N<sup>α</sup>-His</b> )Ac-Lys $\Psi$ (CH <sub>2</sub> NH)Arg-Pro-Tyr- <b>Tle</b> -Leu-OH	0.5	21 d
NT-XII <sup>[98]</sup>	[ <sup>99m</sup> Tc]-( <b>N<sup>α</sup>-His</b> )Ac-Arg( <b>N-CH<sub>3</sub></b> )Arg-Pro-Ty- <b>Tle</b> -Leu-OH	2.0	21 d
NT-XVIII <sup>[98]</sup>	[ <sup>99m</sup> Tc]-( <b>N<sup>α</sup>-His</b> )Ac-Lys(shikimic)-Arg( <b>N-CH<sub>3</sub></b> )Arg-Pro-Tyr- <b>Tle</b> -Leu-OH	4.5	21 d
NT-XIX <sup>[112]</sup>	[ <sup>99m</sup> Tc]-( <b>N<sup>α</sup>-His</b> )Ac-Arg( <b>N-CH<sub>3</sub></b> )Arg-Pro- <b>Dmt-Tle</b> -Leu-OH	15	28 d

One of the first analogues, NT VI, was designed with an Arg<sup>8</sup> to Lys<sup>8</sup> switch and a reduced amide Lys<sup>8</sup>-Arg<sup>9</sup> bond. This modification resulted in a peptide conjugate with retained receptor affinity, but also low serum stability. The metabolic stability was then increased by the substitution of Ile<sup>12</sup> with Tle<sup>12</sup> giving peptide conjugate NT-XI. <sup>99m</sup>Tc-NT-XI was evaluated in four patients with ductal pancreatic adenocarcinomas in an initial clinical study.<sup>[7]</sup> Although a specific uptake in the patients' tumours was obtained, unfortunately, a high non-specific kidney uptake was also observed. For this reason, peptide conjugates NT-XII, NT-XVIII and NT-XIX, with methylated Arg<sup>8</sup>-Arg<sup>9</sup> bonds, were designed to reduce the kidney uptake. While this goal was achieved for NT-XIII and NT XVIII, the tumour uptake was also decreased.<sup>[98]</sup> NT-XI has been the only NT analogue evaluated in patients so far.<sup>[7]</sup> Thus, there is a need of new stabilization techniques which offer new stabilized NT (8-13) analogues with retained binding affinities towards NTR1 and improved tumour-targeting properties.

## 1.6 Peptidomimetics

### 1.6.1 General Introduction

A peptidomimetic is a compound designed to mimic a natural peptide in its biological functions. Peptidomimetics are used when certain characteristics of the original sequence need to be improved, for example, to overcome issues of metabolic instability or poor bioavailability. Also receptor affinity or receptor subtype selectivity can be substantially improved.<sup>[113]</sup>

Peptidomimetics are classified as type I, II or III peptidomimetics. Type I peptidomimetic are peptide backbone mimetics, also called structural mimetics. These structures mimic the local conformation of the amide bond *via* amide bond isosters or amino acid surrogates. All the examples of NT (8-13) analogues described in chapter 1.5 are examples for this type of peptidomimetics. **Figure 9** shows the structure of the original NT (8-13) sequence together with an example of type I peptidomimetic.<sup>[114]</sup>

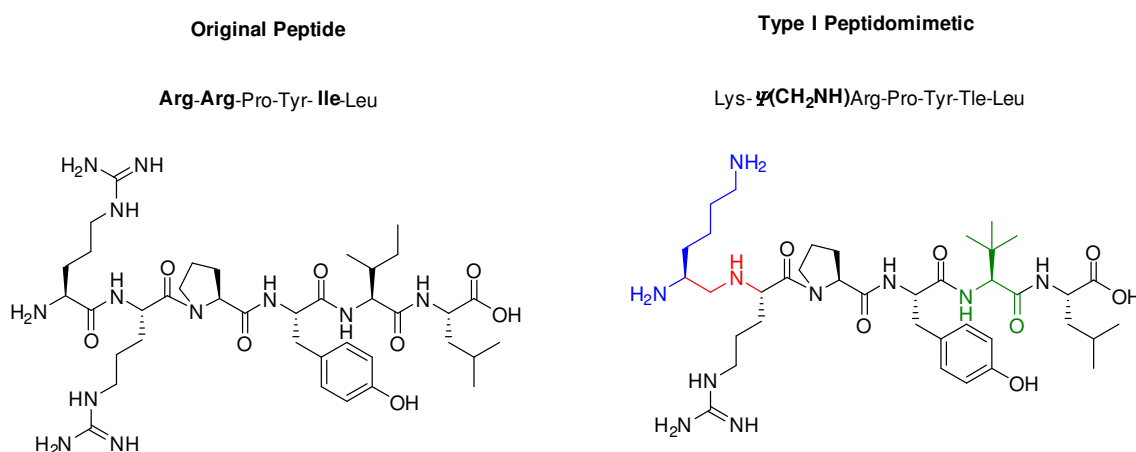


**Figure 9:** Example of type I peptidomimetics of NT (8-13).

Type II peptidomimetics, also called functional mimetics, are non-peptidic molecules with the ability to bind to the desired receptor. They do not fully mimic the structure of the original peptide but instead mimic its interactions with the binding pocket of the receptor, thus leading to a biological response.<sup>[114]</sup> Neurotensin antagonist SR48692 is an example of a type II peptidomimetic (**Figure 10**).<sup>[115]</sup>



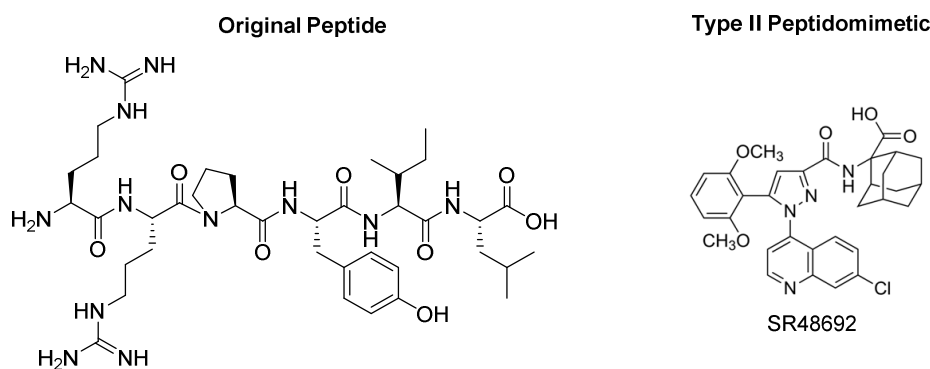


**Figure 10:** Example of a type II peptidomimetic.

Finally, type III peptidomimetics are scaffold-based peptides. This means that all the necessary functionalities of the original peptide needed for binding, are present on a non-peptidic scaffold. <sup>[114, 116-117]</sup> An elegant example is the thyrotropin releasing hormone (TRH) mimetic (**Figure 11**), where the peptidic backbone is replaced by a cyclohexane scaffold containing all the necessary functionalities for binding. <sup>[118]</sup>

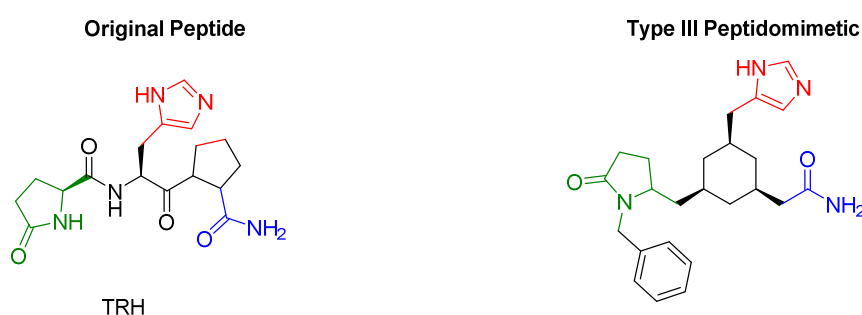


**Figure 11:** Example of a type III peptidomimetic.

Type I peptidomimetics are the most interesting for us as we are interested in peptide bond isosters for the development of radiolabelled peptides with improved tumour-targeting properties. This type of type I peptidomimetics includes two types of modifications: backbone modifications and amino acid substitutions. Backbone alterations include modifications like *N*-methylation, <sup>[6]</sup> amide bond reduction, <sup>[9]</sup> bond extension by introduction of  $\beta$ -amino acids, <sup>[92]</sup> or isosteric replacements. Isosteric replacements can include the replacement of the  $\alpha$ -carbon of an amino acid by nitrogen (azapeptides), <sup>[119]</sup> or substitution of the nitrogen of the amide functionality by a heteroatom such as oxygen (depsipeptide) <sup>[120]</sup> or sulphur (thiodepsipeptides). <sup>[120-121]</sup> Also, small heterocyclic structures like triazoles, thiazoles or oxazoles can act as amide bond isosters. <sup>[122-124]</sup>

The purpose of this thesis is the generation of radiolabelled peptidomimetics with a 1,4-1,2,3-disubstituted triazole as amide bond bioisosters. For this reason, 1,2,3-triazoles, in their function as amide bond mimics, will be described in detail in chapter 1.6.2.

## 1.6.2 Triazoles as Amide Bond Isosters for Peptides

1,2,3-Triazoles are an interesting class of heterocycles in peptide and medicinal chemistry. Examples of small molecule drugs containing 1,2,3-triazoles are tazobactam, a  $\beta$ -lactamase inhibitor or cephalosporin-derivatives, a class of orally active antibiotics.<sup>[125-127]</sup> 1,2,3-Triazoles have found applications in bioconjugation,<sup>[106, 128]</sup> as amino acid mimics (e.g. mimicking histidine),<sup>[129]</sup> in side chain modifications,<sup>[130]</sup> and have also been described as amide bond surrogates<sup>[131]</sup>.

1,4-Disubstituted 1,2,3-triazoles and amide bonds have similar properties in terms of planarity, their strong dipole moment and similar H-bonding properties.<sup>[132-134]</sup> The focus of this work is on 1,4-disubstituted triazoles, but both 1,4-disubstituted 1,2,3-triazoles and 1,5-disubstituted 1,2,3-triazoles have been proposed as amide bond mimics. As shown in **Figure 12**, 1,4-disubstituted 1,2,3-triazoles are considered as *trans*-amide bond isosters and are exclusively accessible by CuAAC (copper catalysed azide-alkyne cyclization), whereas 1,5-disubstituted 1,2,3-triazoles are *cis*-amide bond isosters and can be selectively synthesized *via* RuAAC (ruthenium catalysed azide-alkyne cyclization).<sup>[132]</sup>

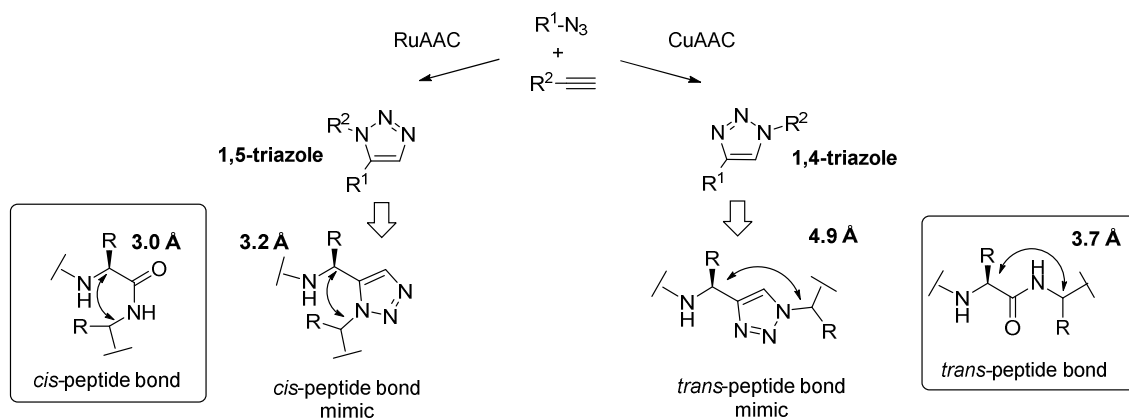


**Figure 12:** Comparison of 1,4- and 1,5-substituted triazoles as *trans*- and *cis*-amide bond mimics.<sup>[132]</sup>

One of the first examples of a triazole-containing peptidomimetic was the synthesis of an analogue of Cyclo[Pro-Val-Pro-Tyr], a tyrosinase inhibitor isolated from *L. helveticus*. It is worth mentioning that several attempts of synthesising the cyclic tetrapeptide by classical

macrolactamisation methods were unsuccessful and cyclization could only be achieved through the use of CuAAC. Several analogues of these peptides, containing one or several triazoles as amide bond surrogates (e.g. Cyclo-[Pro-Val-(triazole)-Pro-Tyr]) were successfully synthesized *via* CuAAC, with full retention of their function as tyrosinase inhibitors.<sup>[135]</sup> In 2009, Horne *et al.* published triazole-containing analogues of apidicin, a cyclic tetrapeptide acting as an inhibitor for HDAC (histone deacetylase). Interestingly, in this case the triazole-containing analogue developed a different receptor subspecificity than the original peptide.<sup>[136]</sup> Davis *et al.* reported a triazole-containing analogue of sansalvamide A, a cyclic peptide functioning as an inhibitor of heat shock protein 90, with an additional cytotoxic effect on several cancer cell lines. Again, the triazole-containing peptidomimetic fully retained the cytotoxicity against the tested cell lines.<sup>[137]</sup>

Another attractive feature of the use of triazoles as amide bond isosters is their stability towards enzymatic degradation. Our group was the first to report a systematic replacement of amide bonds by 1,4-disubstituted 1,2,3-triazoles in a short, linear, biologically active peptide.<sup>[138]</sup> The main goal of the project was the improvement of the tumour-targeting properties of a DOTA functionalized derivative of [Nle<sup>14</sup>]BBN (7-14) through the stabilization of the peptide moiety. [Nle<sup>14</sup>]BBN (7-14) is an analogue of the regulatory peptide Bombesin with high affinity towards the gastrin releasing peptide receptor, overexpressed in tumours like prostate or breast cancer.<sup>[46]</sup> The systematic replacement of each amide bond by 1,2,3-triazoles in the peptide sequence (termed ‘triazole scan’) led to the identification of a series of radio-peptidomimetic with retained nanomolar receptor affinity and an up-to-fivefold improved serum stability (**Figure 13**). Compound **5** exhibited a 2-fold *in vivo* uptake in the tumour when compared to the unmodified [Nle<sup>14</sup>]BBN (7-14) sequence, probably as the result of its prolonged blood circulation time *in vivo*. The *in vitro* properties of the triazole-analogues of ‘triazole scan’ of BBN were superior to that of other reported peptide bond substitution strategies.<sup>[138-139]</sup>

Compound	Structure <sup>[a]</sup>	half-life [hrs] <sup>[b]</sup>	% uptake after 4 h <sup>[c][e]</sup>	K <sub>D</sub> <sup>[e][f]</sup> [nM]
1 (reference)	[ <sup>177</sup> Lu]DOTA-PEG <sub>4</sub> -Gln-Trp-Ala-Val-Gly-His-Leu-Nle-NH <sub>2</sub>	5	27.7	2.0 ± 0.6
2	[ <sup>177</sup> Lu]DOTA-PEG <sub>4</sub> -Gln-Trp-Ala-Val-Gly-His-Leu-Nleψ[Tz]-H	6	29.1	3.0 ± 0.5
3	[ <sup>177</sup> Lu]DOTA-PEG <sub>4</sub> -Gln-Trp-Ala-Val-Gly-His-Leuψ[Tz]Nle-NH <sub>2</sub>	60	0.2	n.d.
4	[ <sup>177</sup> Lu]DOTA-PEG <sub>4</sub> -Gln-Trp-Ala-Val-Gly-Hisψ[Tz]Leu-Nle-NH <sub>2</sub>	>100	n.o. <sup>[d]</sup>	n.d.
5	[ <sup>177</sup> Lu]DOTA-PEG <sub>4</sub> -Gln-Trp-Ala-Val-Glyψ[Tz]His-Leu-Nle-NH <sub>2</sub>	17	28.3	3.1 ± 1.0
6	[ <sup>177</sup> Lu]DOTA-PEG <sub>4</sub> -Gln-Trp-Ala-Valψ[Tz]Gly-His-Leu-Nle-NH <sub>2</sub>	25	8.4	48.6 ± 11.5
7	[ <sup>177</sup> Lu]DOTA-PEG <sub>4</sub> -Gln-Trp-Alaψ[Tz]Val-Gly-His-Leu-Nle-NH <sub>2</sub>	16	24.5	5.9 ± 1.8
8	[ <sup>177</sup> Lu]DOTA-PEG <sub>4</sub> -Gln-Trpψ[Tz]Ala-Val-Gly-His-Leu-Nle-NH <sub>2</sub>	8	n.o. <sup>[d]</sup>	n.d.
9	[ <sup>177</sup> Lu]DOTA-PEG <sub>4</sub> -Glnψ[Tz]Trp-Ala-Val-Gly-His-Leu-Nle-NH <sub>2</sub>	14	n.o. <sup>[d]</sup>	n.d.
10	[ <sup>177</sup> Lu]DOTA-PEG <sub>4</sub> ψ[Tz]Gln-Trp-Ala-Val-Gly-His-Leu-Nle-NH <sub>2</sub>	5	0.5	n.d.

[a] ψ[Tz] represents the replacement of an amide bond by a 1,4-disubstituted [1,2,3]-triazole; [b] determined in blood serum at 37 °C; [c] specific surface-bound and internalized ratio in % of administered dose normalized to 10<sup>6</sup> cells; [d] n.o.: not observed; no specific binding or internalization was detected at a peptide concentration of 2.5 pmol/well; [e] all the values are means of at least two experiments performed in triplicates; [f] determined by receptor saturation binding assay; n.d.: not determined.

**Figure 13:** New stabilized triazole-containing [Nle<sup>14</sup>]BBN-analogues with half-life in serum, cell internalisation and K<sub>D</sub> data in PC3 cells.<sup>[138]</sup>

This thesis represents an extension to 'triazole scan' methodology to NT (8-13). The peptidomimetics described contain 1,4-disubstituted 1,2,3-triazoles in their sequences. The 1,2,3-triazoles were prepared on solid-phase by combination on Fmoc solid phase peptide chemistry, diazo-transfer and CuAAC. In the following chapters, details of the CuAAC synthesis (chapter 1.6.3) and of the synthesis of chiral azido acids (chapter 1.6.4) and chiral  $\alpha$ -amino alkynes building blocks (chapter 1.6.5) will be described.

### 1.6.3 The Chemistry of 1,4-Disubstituted 1,2,3-Triazoles

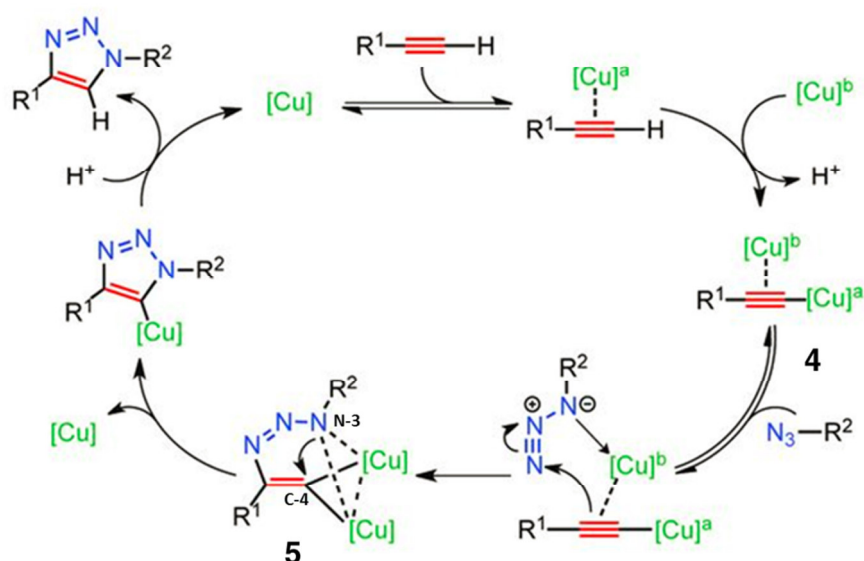
The great advantage of 1,4-disubstituted 1,2,3-triazoles is their straightforward synthesis. They can be readily synthesized with high efficiency from terminal alkynes and azides *via* the CuAAC reaction.<sup>[140-141]</sup> The chemospecificity and efficiency of the reaction, paired with the fact that alkynes and azides are relatively inert in the absence of copper (I), makes the CuAAC a very attractive reaction in all fields of chemistry, particularly for bioconjugation applications.

The Huisgen dipolar cycloaddition of alkynes and azides was discovered by Rolf Huisgen in the early 1960s.<sup>[142-143]</sup> However, the Huisgen dipolar cycloaddition requires elevated temperatures and usually results in a mixture of the 1,4- and 1,5-regioisomers. In 2002, the groups of Meldal<sup>[140]</sup> and Sharpless<sup>[141]</sup> simultaneously discovered the catalytic effect of Cu(I) on the Huisgen dipolar cycloaddition (CuAAC). The CuAAC reaction belongs to a class of reactions termed 'click chemistry', a terminology popularised by Sharpless and his co-workers since 1999.<sup>[144-145]</sup> As stated by Sharpless 'Click chemistry' reactions must be '*modular, wide in scope, give very high yields, generate only inoffensive by-products that can be removed by nonchromatographic methods and be stereospecific (but not necessarily enantioselective)*'.<sup>[145]</sup> CuAAC fulfils the majority of these criteria. The starting materials, alkynes and azides, are readily available, easy to install, relatively chemically inert and extremely stable under standard conditions. The reaction yields exclusively 1,4-disubstituted 1,2,3-triazoles and can be performed in a wide variety of solvents (e.g. DMF, DMSO, <sup>t</sup>BuOH or H<sub>2</sub>O). Additionally, elevated temperatures are not required during the reaction and it is mostly unaffected by steric factors.<sup>[146]</sup>

The Cu(I) source for the catalysis can be provided by Cu(II)-salts (e.g. copper(II)sulphate pentahydrate), which are then reduced *in situ* to Cu(I) with a reducing agent (e.g. sodium ascorbate). Alternatively, Cu(I) can be introduced directly to the reaction in form of Cu(I)-salts (e.g. CuBr) or Cu(I)-complexes (e.g. tetrakis(acetonitrile)copper(I) hexafluorophosphate).<sup>[147]</sup> Since Cu(I) is unstable in aqueous solutions and has a tendency to disproportionate into

Cu(0) and Cu(II), stabilizing ligands were soon developed after the initial description of the reaction. From a series of polytriazole-based ligands, TBTA (*tris*[1-benzyl-1H-1,2,3-triazol-4-yl)methyl]amine) turned out to be the most effective one in most cases.<sup>[148]</sup> In aprotic solvents, the most common bases applied in this reaction are Hünig's base or NEt<sub>3</sub>.<sup>[147]</sup>

The mechanism of the CuAAC is not yet fully understood. In 2013, Fokin performed crossover experiments with a <sup>63</sup>Cu-enriched catalyst. This study gave evidence that the CuAAC mechanism involves a dinuclear copper intermediate. The presence of this dinuclear copper intermediate was verified with TOF-MS. The proposed catalytic model for the CuAAC with two copper atoms is shown in **Scheme 1**.



**Scheme 1:** Catalytic cycle of the CuAAC reaction proposed by Fokin.<sup>[149]</sup>

It is hypothesised that in the first step of the reaction, the alkyne undergoes a  $\pi$ -complex with the Cu-catalyst. The  $\pi$ -complexation with the Cu-catalyst lowers the pK<sub>a</sub> of the alkyne and a deprotonation of the alkyne occurs (in organic solvents a proton acceptor is required) and a Cu-acetylide is formed.<sup>[150]</sup> In the following step, the Cu-acetylide undergoes a  $\pi$ -complexation with a second molecule of the Cu-catalyst, forming intermediate **4**. The azide then coordinates to the dinuclear Cu-acetylide complex resulting in its activation towards nucleophilic attack. The N-3 of the azide can then attack the C-4 of the alkyne and a dinuclear Cu-triazole complex **5** is formed. Protonation of the triazole, followed by the release of the catalyst closes the catalytic cycle.<sup>[146, 150-151]</sup>

### 1.6.4 Preparation of $\alpha$ -Azido Acids

Organic azides are energy-rich substances with a wide scope of applications, from medicinal chemistry (e.g. as protecting group for amines) to the development of explosive agents. Since the discovery of the CuAAC<sup>[140, 152]</sup> and the Staudinger ligation,<sup>[153]</sup> azides have regained the attention of the organic chemistry community. Azides can be synthesized in different ways. One method is the introduction of a  $N_3$ -group *via* nucleophilic substitution of a halogen or sulfonate precursor by an azide anion. The complication of this method is the inversion of the chiral centre during the reaction when the leaving group is attached to a chiral centre. Another method is the introduction of a  $N_2$ -group to a primary amine, also called diazo-transfer. Diazo-transfer a very popular method and best suited for the synthesis of  $\alpha$ -azido acids. Older methods include the diazotisation of a hydrazine and the cleavage of triazenes.<sup>[154]</sup> Reaction examples of each of these methods to generate azides are shown in **Figure 14**.

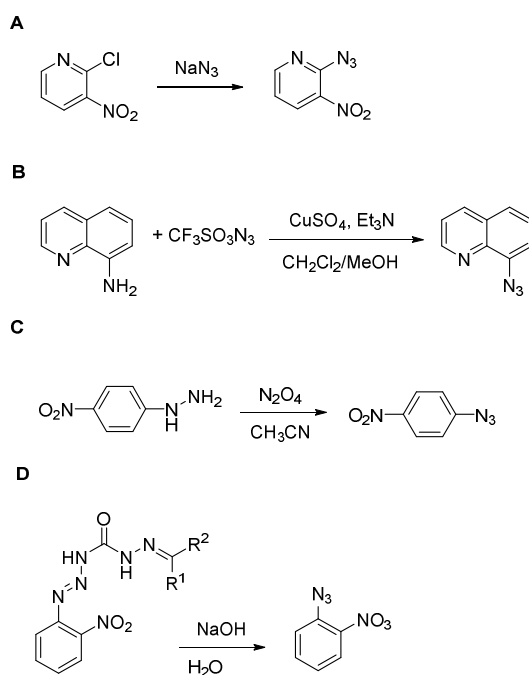
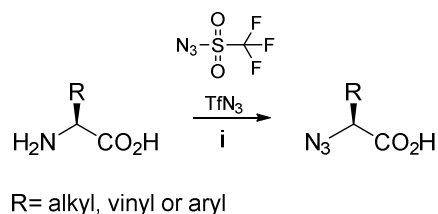


**Figure 14:** Examples of reactions for the preparation of azides. A) Substitution *via*  $S_NAr$ -reaction.<sup>[155]</sup> B) Diazo-transfer.<sup>[156]</sup> C) Diazotisation.<sup>[157]</sup> D) Cleavage of triazenes.<sup>[158]</sup>

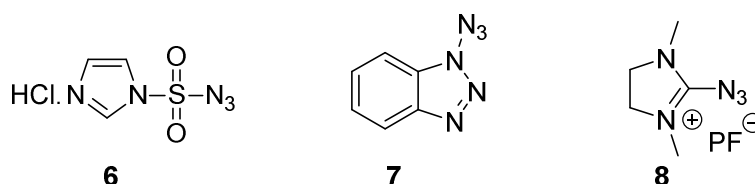
The diazo-transfer reaction is the method of choice for the introduction of an azide into a molecule when racemization, epimerization or the inversion of a chiral centre are to be avoided. One of the most efficient diazo transfer reagents for the preparation of organic

azides from primary amines is trifluoromethanesulfonyl azide ( $\text{TfN}_3$ ), introduced by Cavender and Shiner in 1972.<sup>[159]</sup> The diazo-transfer reaction gained new attention in 1996, when Wang and co-workers discovered that the addition of substoichiometric amounts of metallic ions such as  $\text{Cu(II)}$  and  $\text{Zn(II)}$  salts, greatly increases the yields and the kinetics of the reaction.<sup>[160]</sup> However,  $\text{TfN}_3$  is reported to be explosive and having a poor shelf-life. For this reason it is generated *in situ* by the reaction of  $\text{Tf}_2\text{O}$  with  $\text{NaN}_3$  (**Scheme 2**).



**Scheme 2:** Diazo-transfer reaction by Wong: i)  $\text{TfN}_3$ ,  $\text{CuSO}_4$ ,  $\text{K}_2\text{CO}_3$ ,  $\text{H}_2\text{O}$ ,  $\text{MeOH}$ ,  $\text{CH}_2\text{Cl}_2$ .

As an alternative to the explosive  $\text{TfN}_3$ , Goddard-Borger and Stick published in 2007 the synthesis of imidazole-1-sulfonyl azide hydrochloride (**6**) (**Scheme 3**), an efficient and shelf-stable diazo-transfer reagent in crystalline form.<sup>[161]</sup> Unlike  $\text{TfN}_3$ , the imidazolylsulfonylazide is soluble in a wide range of solvents such as methanol or DMF and can easily be used for solid phase diazo-transfer, even in the absence of a metal catalyst.<sup>[162]</sup> Further alternatives of  $\text{TfN}_3$  include benzotriazol-1-yl-sulfonyl azide (**7**), developed in 2010 by the group of Steel,<sup>[163]</sup> (**Scheme 3**) as well as 2-azido-1,3-dimethylimidazolium hexafluorophosphate (**8**), reported in 2011 by the group of Okauchi.<sup>[164]</sup> Today imidazole-1-sulfonyl azide hydrochloride (**6**) has been established as the standard diazo-transfer reagent, as reagents (**7**) and (**8**) have been developed recently and there is still a lack of synthetic reports confirming their efficacy.



**Scheme 3:** Selection of diazo-transfer reagents: imidazole-1-sulfonyl azide hydrochloride (**6**), benzotriazol-1-yl-sulfonyl azide (**7**) and 2-azido-1,3-dimethylimidazolium hexafluorophosphate (**8**).



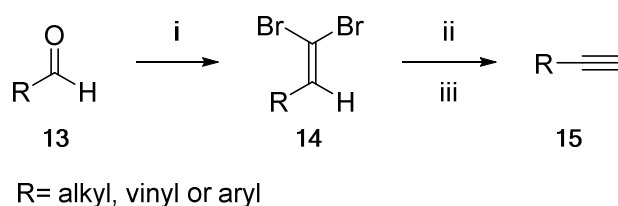


### 1.6.5 Synthesis of Chiral $\alpha$ -Amino Alkynes

Terminal alkynes are widely used in organic chemistry, e.g. as substrates for the Sonogashira cross-coupling reaction,<sup>[168]</sup> the Grubbs olefin metathesis<sup>[169]</sup> or the synthesis of triazoles *via* CuAAC or RuAAC.

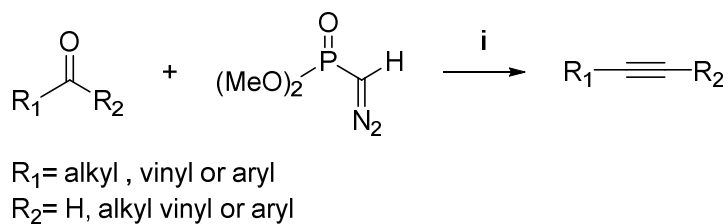
For the synthesis of 1,4-disubstituted 1,2,3-triazoles as amide bond mimics in peptides chiral  $\alpha$ -amino alkynes are needed. The easiest way to date for the synthesis of these compounds is starting from amino acid derivatives. Three reactions can be used: Corey-Fuchs reaction, Seyferth-Gilbert rearrangement or Colvin rearrangement. The starting materials for all three reactions are  $\alpha$ -amino aldehydes, easily accessible from amino acids by a simple reduction.

Historically, the Corey-Fuchs procedure was the first example.<sup>[170]</sup> In this reaction, somewhat reminiscent of the Wittig reaction, an aldehyde **13** is converted into a dibromoolefin **14**, which then upon treatment with *n*-butyllithium and aqueous workup results in a terminal alkyne **15** (**Scheme 6**).



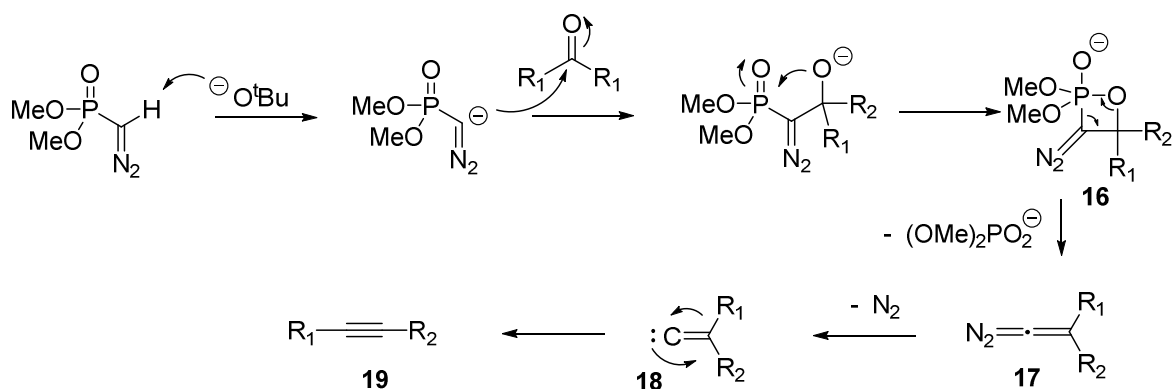
**Scheme 6:** Corey-Fuchs synthetic route to terminal alkynes: i) PPH<sub>3</sub>, CBr<sub>4</sub>; ii) BuLi, iii) H<sub>2</sub>O.

However, this procedure is not universal because the reaction conditions are not fully compatible with all amino acids, especially those bearing functional groups in their side chain. One disadvantage of the Corey-Fuchs method is the possible racemization of the  $\alpha$ -amino aldehyde due to the use of a strong base (BuLi). Other procedures such as the Seyferth-Gilbert homologation can be performed under much milder conditions. The Seyferth-Gilbert homologation converts aldehydes or ketones into terminal alkynes using dimethyldiazomethylphosphonate (**Scheme 7**).



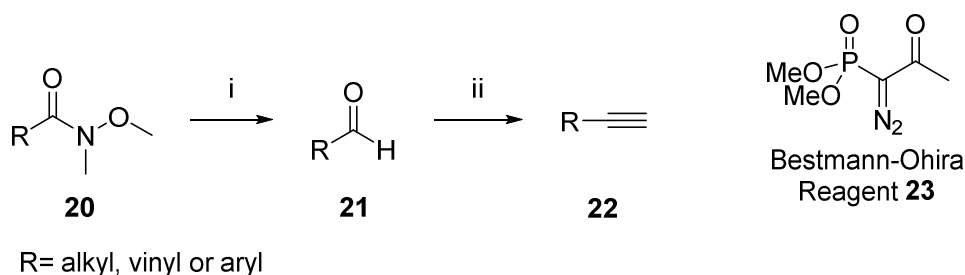
**Scheme 7:** Seyferth-Gilbert homologation: i) *t*-BuOK, THF, -78 °C.

The mechanism of the Seyferth-Gilbert homologation is shown in **Scheme 8**. After the nucleophilic attack of the deprotonated dimethyldiazomethylphosphonate on the carbonyl of the aldehyde or ketone, an oxophosphetane **16** is formed. A subsequent cyclo-elimination yields the diazo-intermediate **17**. Alkyne **19** is formed after elimination of  $N_2$  and rearrangement of the formed carbene **18**.



**Scheme 8:** Mechanism of the Seyferth-Gilbert homologation.

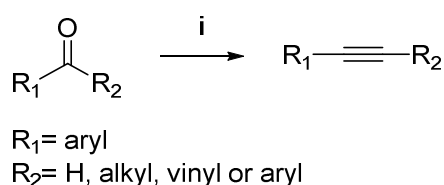
All the reactions described above require strictly anhydrous conditions, as well as the use of strong bases, which restricts the application to delicate substrates. The use of the Bestmann-Ohira modification of the Seyferth-Gilbert approach allows the synthesis of the desired products under mild conditions, without the use of strong bases.<sup>[171]</sup> In 2004, Dickson *et al.*, published a one-pot approach using the Bestmann-Ohira reagent to obtain terminal alkynes.<sup>[172]</sup> A Weinreb amide **20** is reduced with DIBAL-H to an aldehyde **21** which is then converted to an alkyne **22** using the Bestmann-Ohira reagent **23**. The mechanism is similar to the Seyferth-Gilbert homologation (**Scheme 9**). The advantage of this approach is, in comparison to others, that the isolation of the aldehyde, which is prone to racemization, is not required.



**Scheme 9:** One-pot approach for the synthesis of terminal alkynes: i) DIBAL-H,  $\text{CH}_2\text{Cl}_2$ ,  $-78\text{ }^\circ\text{C}$ ; ii) Bestmann-Ohira reagent, MeOH,  $\text{K}_2\text{CO}_3$ , RT.

This reaction is applicable to a wide scope of substrates. We are especially interested in amino acids as substrates, as they are easily transformed into Weinreb amides and therefore this method is perfectly suitable for the preparation of  $\alpha$ -amino alkynes. The only drawback is the poor compatibility of  $\text{K}_2\text{CO}_3$  with base-labile protecting groups like Fmoc. This issue can be solved, however, by the re-installation of the Fmoc-protecting group after the synthesis of the terminal alkyne.

Finally, the Colvin rearrangement is an alternative to the above-described strategies (**Scheme 10**).<sup>[173]</sup> During this reaction, an aldehyde or a ketone reacts with trimethylsilyldiazomethane to afford an alkyne. The Colvin rearrangement follows a similar mechanism as the Seyferth-Gilbert homologation, but it requires lower temperatures and the use of a strong base.<sup>[174-176]</sup>



**Scheme 10:** Colvin rearrangement: i)  $\text{TMSC}(\text{Li})\text{N}_2$ .



## 2. Objectives

The development of tools for early diagnosis and efficient therapy is the key to a personalized treatment of cancer. Towards this goal, within nuclear medicine, targeting radiopeptides have a high potential for the imaging and treatment of tumours, because of their high sensitivity and low side-effects. Neurotensin in general and its binding sequence NT (8-13) (Arg<sup>8</sup>-Arg<sup>9</sup>-Pro<sup>10</sup>-Tyr<sup>11</sup>-Ile<sup>12</sup>-Leu<sup>13</sup>) in particular, are ideal candidates for the development of new targeted radiopharmaceuticals. NT (8-13) has a high affinity and specificity towards NTR1, a receptor which is overexpressed by colon, breast, pancreas and small cell lung cancer.<sup>[1-2, 77-79]</sup> However, the challenge associated with the use Neurotensin as a tumour-targeting vector is its rapid degradation by peptidases and proteases *in vivo*.<sup>[84]</sup> Because of the poor metabolic stability, a radiolabelled NT (8-13)-based conjugate is more often than not degraded before reaching the targeted tissue (tumour). Thus, an increased tumour uptake is expected to be achievable by stabilization of the NT (8-13) sequence against proteolysis.

Several strategies for the stabilization of radiolabelled peptides have more or less successfully been applied to NT (8-13), such as reduction or methylation of amide bonds,<sup>[6, 9]</sup> amino acid substitution,<sup>[6, 86]</sup> or multimerisation.<sup>[87, 177]</sup> However, only one compound has so far reached a phase I clinical trial.<sup>[7]</sup> Thus, there is a need for new stabilization techniques which provide new metabolically stable NT (8-13) analogues with improved tumour-targeting properties.

The aim of this project is the identification of radiolabelled NT (8-13) derivatives with improved properties for tumour targeting. This includes the systematic replacement of backbone amide bonds within the NT (8-13) sequence with 1,4-disubstituted triazoles 1,2,3-triazoles ('triazoles scan'). 1,4-disubstituted triazoles are known amide bond bioisosteres, whose incorporation into peptides can lead to proteolysis-resistant peptidomimetics, as the triazole moiety cannot be degraded by peptidases. This novel stabilisation strategy has already been successfully applied to the binding sequence of the peptide bombesin.<sup>[138]</sup>

The presented thesis is divided into four main parts:

- 1) In a first step the influence of a spacer between the peptidic part and the chelator within the structure of DOTA-substituted NT (8-3) analogues is investigated with the aim of improving the tumour-targeting properties of this kind of radiopharmaceuticals. In doing so, a NT (8-13)-based peptide conjugate, in which the chelator is directly attached to the binding sequence will be compared side-by-side with two NT (8-13) peptide conjugates, each having a different spacer, one hydrophilic

(tetraethylenglycol, PEG<sub>4</sub>) and one lipophilic (6-aminohexanoic acid, Ahx). After preparation of the peptide conjugates on solid phase, the three DOTA-X-NT (8-13) analogues (X: no spacer, PEG<sub>4</sub> or Ahx) are radiolabelled with [<sup>177</sup>Lu]LuCl<sub>3</sub> and evaluated *in vitro*. The *in vitro* evaluation includes quantification of the internalisation of the peptide conjugates into NTR1 expressing HT-29 cells (colon adenocarcinoma) and determination of the receptor affinities and specificities. Additionally, measurements of the lipophilicity of the conjugates (log D) and their metabolic stability in human serum are performed. The spacer with the best biological properties in these studies will be used for the 'triazole scan' work described below.

- 2) In the second part of this thesis describes the synthesis and biological evaluation of the peptide conjugates of the 'triazole scan'. Every backbone amide bond within the NT (8-13) sequence but the Arg<sup>9</sup>-Pro<sup>10</sup> position will be substituted, one at the time, with a triazole, yielding six different triazole backbone-modified NT (8-13) analogues. If more than one amide bond can be substituted with a triazole without loss of receptor binding affinity, conjugates with multiple triazoles will also be synthesized and evaluated. All the peptides are attached *N*-terminally to a DOTA chelator *via* the optimal spacer identified in the first part of this thesis. After labelling with [<sup>177</sup>Lu]LuCl<sub>3</sub>, a full *in vitro* evaluation (see part 1) is performed. The incorporation of the triazole moieties into the peptides is achieved *via* solid phase copper (I) azide-alkyne cycloaddition (CuAAC) on solid support. The azide functionality is incorporated *N*-terminally into the peptide directly on solid phase, whereas the  $\alpha$ -amino alkynes are synthesized in solution and fully characterized.
- 3) In the third part of the thesis, the investigation of a second generation of NT (8-13) triazole-peptides will be described. In this second generation of triazole-modified NT (8-13) analogues, amino acid substitutions within the NT (8-13) sequence will be examined as a means for further improvement of its metabolic stability in addition to the backbone modification (see part 2). More precisely, Ile<sup>12</sup> will be substituted with Tle<sup>12</sup>, as this modification has been described in literature to have a positive effect on the metabolic stability of a NT (8-13) analogue.<sup>[6, 84, 86, 105]</sup> After the synthesis of the triazole-containing [Tle<sup>12</sup>]-NT (8-13) analogues, a full biological evaluation (see part 1), is performed.
- 4) The final part of this work describes the *in vivo* evaluation of the triazole backbone-modified, <sup>177</sup>Lu-labelled DOTA/NT (8-13) conjugates identified in parts 1-3 of this thesis. The *in vivo* evaluation includes biodistribution experiments in a mouse model

with an implanted NTR1 expressing HT-29 tumour xenograft. Based on the results of these biodistribution studies, *in vivo* SPECT-imaging will be performed with selected compounds.

A schematic representation of the work described in this thesis is shown in **Figure 15**:

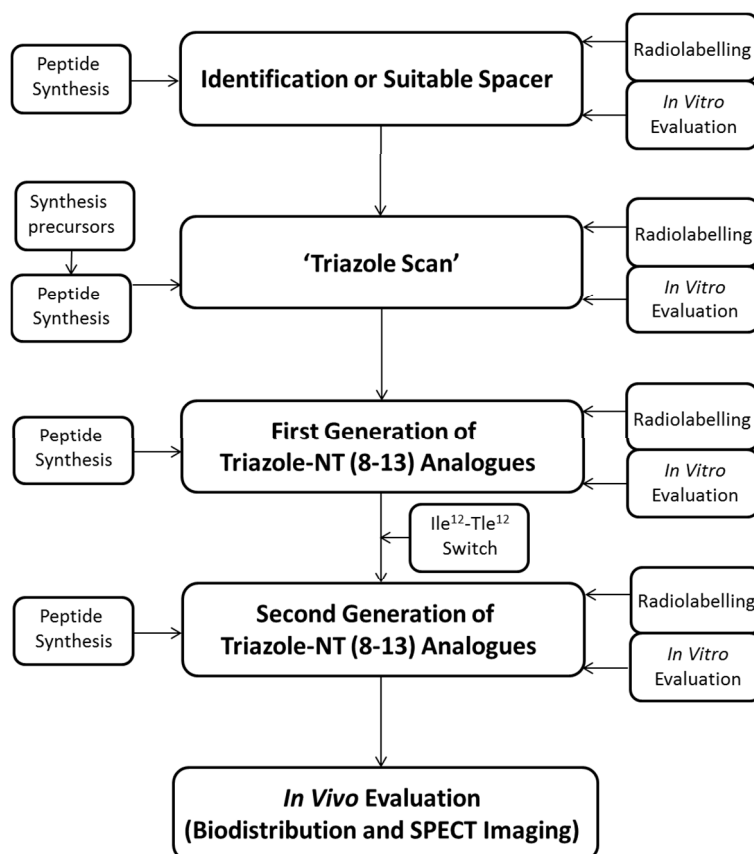


**Figure 15:** Schematic representation of this study.





### 3. Results and Discussion

#### 3.1 Identification of a Suitable Spacer

The nature of a spacer moiety between a tumour-targeting vector (e.g. peptide) and a radiometal chelate (see chapter 1.5.3.2) is known to influence potentially the pharmacological properties of a radiometal-peptide conjugate. For example, the lipophilicity of a spacer moiety, or its absence, can change the properties of radiolabelled tracers.<sup>[94, 100, 178-181]</sup> Because no systematic evaluation of the effect of spacers has yet been described for radiometallated NT (8-13) analogues, we set out to investigate three different conjugates. In addition to a derivative without a spacer, two conjugates bearing different uncharged spacers, 6-aminohexanoic acid (Ahx) and tetraethylglycol (PEG<sub>4</sub>) were examined. Both have been used successfully in radiometal-peptide conjugates and differ with respect to their lipophilicity.<sup>[94, 100, 182-183]</sup> All three conjugates were functionalized with the universal macrocyclic chelator 1,4,7,10-tetrazacyclododecane-1,4,7,10-tetraacetic acid (DOTA) and labelled with [<sup>177</sup>Lu]LuCl<sub>3</sub>. <sup>177</sup>Lu is a radiometal with a half-life of 6.9 days with β- and γ-radiation and is therefore suitable for both diagnostic and therapeutic applications (see chapter 1.4.2.1). The structures of the NT (8-13) analogues **AM-NT 1** (without a spacer), **AM-NT 2** (PEG<sub>4</sub>-spacer) and **AM-NT 3** (Ahx-spacer) are shown in **Figure 16**.

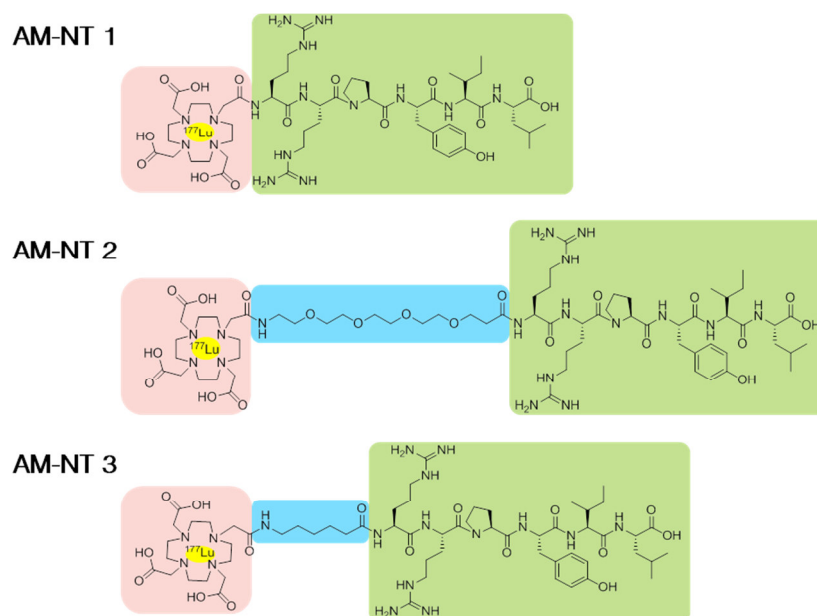
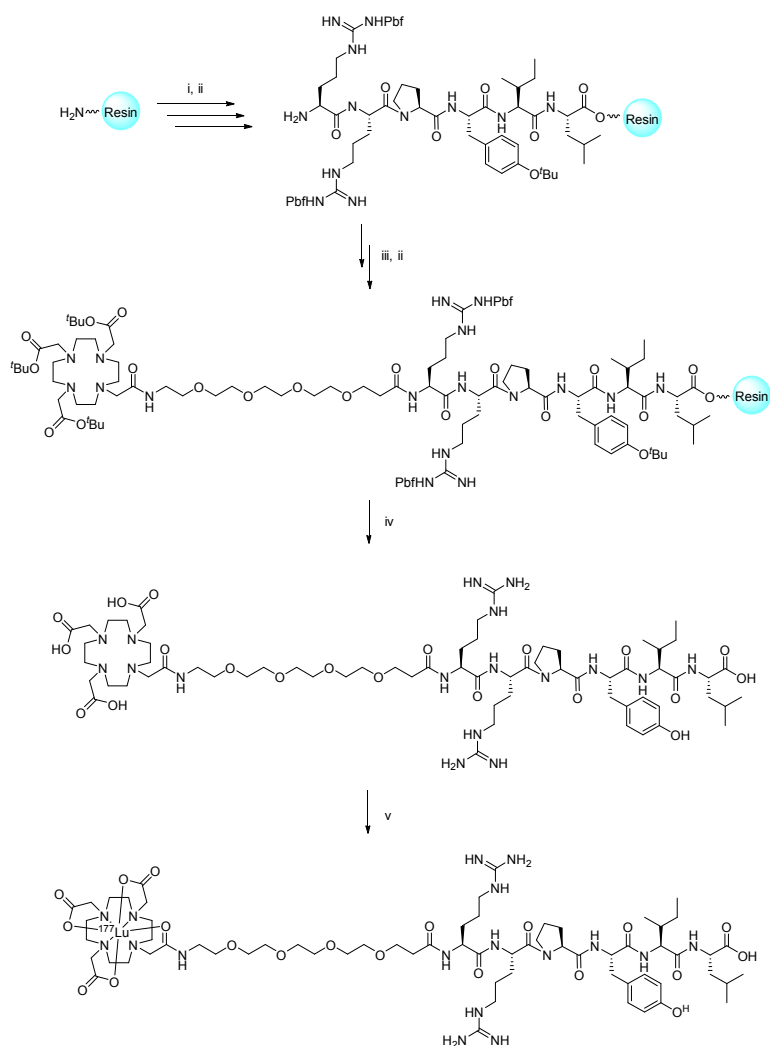


**Figure 16:** Structures of radiolabelled NT (8-13) conjugates [<sup>177</sup>Lu]-AM-NT 1-3.

### 3.1.1 Synthesis of NT (8-13) Analogues AM-NT 1-3

The three peptides (**AM-NT 1-3**) were synthesised manually on solid support (Fmoc-L-Leu-PEG-PS resin), using standard Fmoc peptide chemistry (**Scheme 11**). Amino acids (Fmoc-Ile-OH, Fmoc-Tyr(<sup>t</sup>Bu)-OH, Fmoc-Pro-OH and Fmoc-Arg(Pbf)-OH), were coupled in DMF (dimethylformamide), using HATU (1-[Bis(dimethylamino)methylene]-1H-1,2,3-triazolo[4,5-b]pyridinium 3-oxid hexafluorophosphate) as a coupling reagent and Hünig's base as a base. After the coupling, a Kaiser test was performed to verify the completion of the amide bond formation.



**Scheme 11:** Example of the synthesis and radiolabelling of a NT (8-13)-based peptide conjugate (**AM-NT 2**). i) Fmoc-AA-OH, HATU, Hünig's base, DMF, 2 h, RT; ii) 20% piperidine in DMF, 10 min, RT; iii) Fmoc-PEG<sub>4</sub>-CO<sub>2</sub>H or DOTA-(*tris*-<sup>t</sup>Bu)<sub>3</sub>, HATU, Hünig's base, DMF, 2 h, RT; iv) TFA/H<sub>2</sub>O/PhOH/*Pr*<sub>3</sub>SiH, 6 h, RT; v) [<sup>177</sup>Lu]LuCl<sub>3</sub>, ammonium acetate buffer (pH 4.5), 30 min, 100 °C.

After completion of the amino acid sequence, the *N*-terminal Fmoc-protecting group was cleaved using 20% piperidine in DMF as reagent. The spacer and the chelator were installed using the same coupling conditions as for the coupling of amino acids, with Fmoc-PEG<sub>4</sub>-CO<sub>2</sub>H or DOTA-(*tris*-*t*Bu)<sub>3</sub>. Finally, the complete peptide conjugates were cleaved off the solid support under acidic conditions, purified *via* preparative HPLC and recovered by lyophilisation. The obtained compounds were characterized by means of analytical HPLC as well as high-resolution electron spray mass spectrometry (ESI-HRMS). All three conjugates were obtained in satisfactory yields and with high purity. **Table 17** shows the structures of **AM-NT 1-3** and their analytical data.

**Table 17:** Structures of peptide conjugates **AM-NT 1-3** and their analytical data.

	Structure	MW (g/mol)	ESI-HRMS [M+2H] <sup>2+</sup>	Yield (%)	Purity (%)
<b>AM-NT 1</b>	DOTA-Arg-Arg-Pro-Tyr-Ile-Leu	1202.68	602.36	70	> 98
<b>AM-NT 2</b>	DOTA-PEG <sub>4</sub> -Arg-Arg-Pro-Tyr-Ile-Leu	1449.82	725.92	2	> 98
<b>AM-NT 3</b>	DOTA- <b>Ahx</b> -Arg-Arg-Pro-Tyr-Ile-Leu	1315.76	439.59 <sup>a</sup>	3	> 98

<sup>a</sup>[M+3H]<sup>3+</sup>.

Subsequently, the DOTA-substituted peptide conjugates were labelled with [<sup>177</sup>Lu]LuCl<sub>3</sub> in a buffered solution (ammonium acetate buffer, pH 5.0) at elevated temperature (30 min, 100 °C). After labelling, the radiochemical yields and purities were determined by  $\gamma$ -HPLC (**Table 18**). Due to the presence of the chelator, the peptide conjugates were handled only with plastic spoons or pipettes, in order to avoid contamination with other metals. The labellings were reproducible and failed only occasionally, likely because of the presence of metal impurities despite the precautions taken. High radiochemical purities and radiochemical yields were achieved. The structures of the radiolabelled peptide conjugates [<sup>177</sup>Lu]-**AM-NT 1-3** and their radiochemical yields are shown in **Table 18**.

**Table 18:** Radiolabelled peptide conjugates [<sup>177</sup>Lu]-**AM-NT 1-3** and radiolabelling yields and purities achieved.

	Structure	Radiochemical Yield (%)	Radiochemical Purity (%)
<b>[<sup>177</sup>Lu]-AM-NT 1</b>	[ <sup>177</sup> Lu]-DOTA-Arg-Arg-Pro-Tyr-Ile-Leu		
<b>[<sup>177</sup>Lu]-AM-NT 2</b>	[ <sup>177</sup> Lu]-DOTA-PEG <sub>4</sub> -Arg-Arg-Pro-Tyr-Ile-Leu	> 95	> 98
<b>[<sup>177</sup>Lu]-AM-NT 3</b>	[ <sup>177</sup> Lu]-DOTA- <b>Ahx</b> -Arg-Arg-Pro-Tyr-Ile-Leu		

The specific activities (radioactivity per unit of mass of the compounds) of the radiolabelled peptide conjugates were chosen depending on the type of experiment planned. For cell internalisation and receptor binding affinity experiments, a low specific activity was sufficient (~ 6 MBq/nmol), whereas for serum stabilities and *in vivo* experiments a higher specific

activity was required (~ 21 MBq/nmol). Further details are described in the experimental section of this work.

### 3.1.2 Biological Investigation of Peptide Conjugates [<sup>177</sup>Lu]-AM-NT 1-3

A full investigation of the physico-chemical and biological properties (internalisation in HT-29 cells, binding affinity and specificity towards NTR1, lipophilicity and metabolic stability) of the peptide conjugates [<sup>177</sup>Lu]-AM-NT 1-3 was performed. The results of these experiments are summarized in the **Table 19**.

**Table 19:** Summary of physico-chemical and biological properties of [<sup>177</sup>Lu]-AM-NT 1-3.

	Internalisation after 4 h (%)	K <sub>D</sub> (nM)	B <sub>max</sub> (nM)	Log D	Stability t <sub>1/2</sub> (min)
[ <sup>177</sup> Lu]-AM-NT 1	3.0 ± 0.2	14.9 ± 0.7	0.5	-2.5	6.1
[ <sup>177</sup> Lu]-AM-NT 2	7.3 ± 0.4	3.8 ± 0.9	0.4	-2.6	39.4
[ <sup>177</sup> Lu]-AM-NT 3	5.6 ± 0.4	3.4 ± 1.5	0.3	-2.3	10.0

The cell internalisation properties of [<sup>177</sup>Lu]-AM-NT 1-3 were investigated using NTR1-expressing HT-29 cells (human colon adenocarcinoma). HT-29 cells were seeded out the day prior to the experiment in six-well plates. On the day of the experiment, each radiolabelled conjugate was administered to the cells and was incubated in cell culture medium for 30, 60, 120 and 240 min. The medium was then removed and the cells were washed with PBS (free fraction). The peptide conjugate bound to the receptor was then released by washing with acidic glycine-NaCl buffer at pH 2.8 (bound fraction). Finally, the radiolabelled conjugate internalized in the cells was recovered by incubation with 1 M NaOH aqueous solution (internalized fraction). The different fractions were then measured on a gamma-counter. Blocking experiments to confirm the specificity of the cell internalisation were performed as a control in each experiment, by the addition of a 1000-fold excess of NT (8-13) to the cells. The non-specific uptake was always less than 0.3% of the total peptide conjugate incubated. The receptor bound fraction was always negligible (0.1-0.5% of total peptide conjugate incubated). Specific internalisation kinetics (total cell internalisation minus non-specific cell internalisation) are shown in **Figure 17** for the examined compounds [<sup>177</sup>Lu]-AM-NT 1-3.

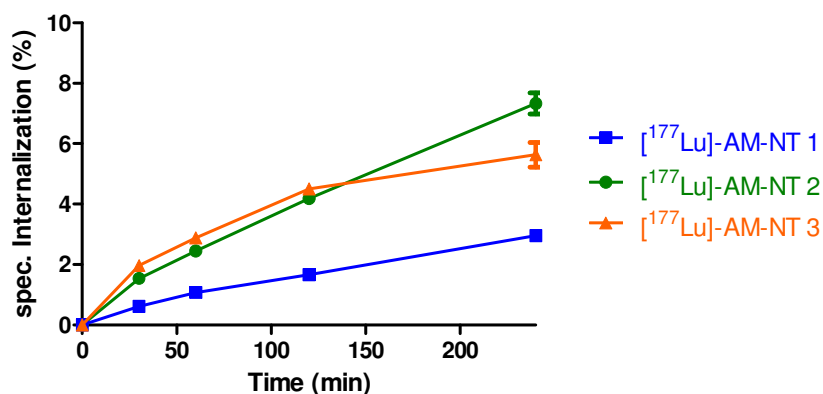


**Figure 17:** Cell internalisation results of [<sup>177</sup>Lu]-AM-NT 1-3.

The introduction of the PEG<sub>4</sub>-spacer led to the peptide conjugate with the highest internalisation rate, [<sup>177</sup>Lu]-AM-NT 2, followed by [<sup>177</sup>Lu]-AM-NT 3, the analogue with the Ahx-spacer and [<sup>177</sup>Lu]-AM-NT 1, without any spacer. The observed internalisation rates are in the range of values described in literature for related radiometallated NT derivatives.<sup>[98]</sup>

To determine the receptor affinity of the three radiolabelled conjugates towards NTR1, receptor saturation experiments were performed, resulting in  $K_D$  values measured in nM. The seeded cells were treated with each of the radiolabelled peptide conjugates in various concentrations (0.1-200 nM) and incubated in cell culture medium (1 h at 37 °C). After incubation, the medium was removed and the cells were washed. These fractions represent the free fraction. The bound fraction was obtained by lysis of the cells with 1 M NaOH. Blocking experiments to confirm binding specificity were performed by addition of a 1000-fold excess of NT (8-13) to the cells. The different fractions were measured with a gamma counter. The specific bound fraction was calculated as the result of the total bound fraction minus the non-specific bound fraction. After non-linear regression of the saturation curve, the  $K_D$  and  $B_{max}$  values were calculated.  $K_D$  is, as an indication of receptor affinity, the equilibrium dissociation constant between the peptide conjugate and the receptor and  $B_{max}$  is the maximum number of binding sites per 1 million cells. The saturation curves of [<sup>177</sup>Lu]-AM-NT 1-3 are shown in **Figure 18**:

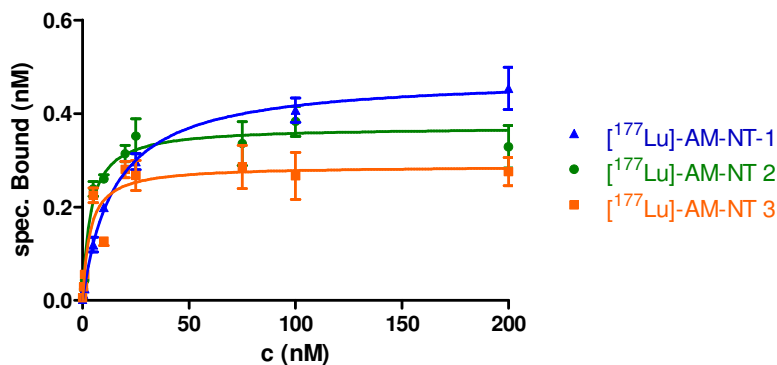


**Figure 18:** Results of receptor saturation experiments of [<sup>177</sup>Lu]-AM-NT 1-3.

The three peptide derivatives exhibited a high affinity towards the NTR1 receptor, in the low nanomolar range. However, the conjugates functionalized with a spacer moiety, [<sup>177</sup>Lu]-AM-NT 2 and [<sup>177</sup>Lu]-AM-NT 3, exhibited more favourable  $K_D$  values than the analogue without the spacer, [<sup>177</sup>Lu]-AM-NT 1. With a  $K_D$  value of  $14.9 \pm 0.7$  nM, the latter had almost a five times lower affinity to the NTR1 receptor than [<sup>177</sup>Lu]-AM-NT 2 and [<sup>177</sup>Lu]-AM-NT 3 with  $K_D$  values of  $3.8 \pm 0.9$  and  $3.4 \pm 1.5$  nM, respectively.

As the nature of the spacer can influence the lipophilicity of the peptide conjugates, log D values were also determined. Log D is the logarithm of the distribution coefficient of a molecule between in *n*-octanol and PBS (pH 7.4). Each radiolabelled peptide conjugate was added to a mixture of *n*-octanol/PBS (1:1), the mixture was shaken vigorously and then centrifuged. Then, samples of the *n*-octanol phase and of the PBS phase were withdrawn and analysed in a gamma counter. The lipophilicity of the three NT (8-13) analogues appeared not to be affected by the spacer. The peptide conjugates displayed log D values between -2.3 and -2.6, demonstrating an overall hydrophilic character of the peptide conjugates.

Finally, the serum stabilities of [<sup>177</sup>Lu]-AM-NT 1-3 were evaluated. Fresh human serum (not older than a month; conserved at -20 °C) from healthy donors was used. The radiolabelled peptide conjugates were added to the serum and incubated at 37 °C. The incubation times were chosen based on preliminary experiments. At different time points, aliquots of serum were taken and the serum proteins were precipitated with ethanol. After several centrifugation and washing steps, the supernatant was diluted with H<sub>2</sub>O and analysed by  $\gamma$ -HPLC. The final dilution with H<sub>2</sub>O turned out to be very important, otherwise, co-elution of the radiolabelled metabolites and the intact peptide conjugate was observed in the HPLC chromatogram. In **Figure 19**, two HPLC profiles of the same sample, one without dilution with water (**A**) and one with dilution with water (**B**) are shown.

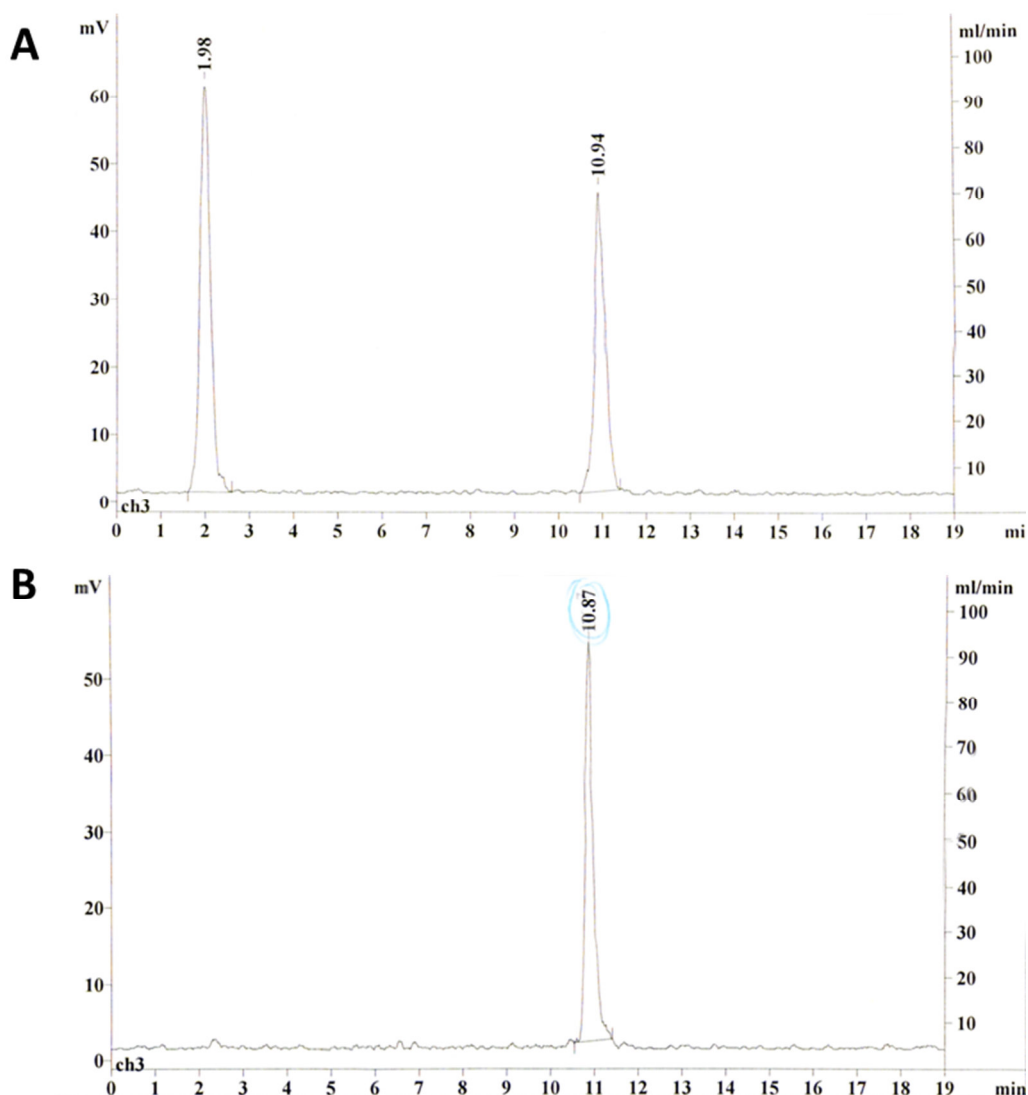


**Figure 19:** **A:**  $\gamma$ -HPLC track of  $[^{177}\text{Lu}]\text{-AM-NT 2}$  in serum, 5 min incubation, without dilution in water. **B:**  $\gamma$ -HPLC track of  $[^{177}\text{Lu}]\text{-AM-NT 2}$  in serum, 5 min incubation, with dilution in water.

$[^{177}\text{Lu}]\text{-AM-NT 1-3}$  degraded rapidly in human serum. The half-lives of  $[^{177}\text{Lu}]\text{-AM-NT 1-3}$  were calculated from the data shown in **Figure 20**, fitting the degradation curve with the equation  $A(t) = \exp(-\lambda t)$  ( $t_{1/2} = \ln 2 / \lambda$ ). The spacer-free compound showed a half-life of ca. 6 min, compound  $[^{177}\text{Lu}]\text{-AM-NT 3}$ , with the Ahx-spacer, displayed slightly more stable with a half-life of 10 min and  $[^{177}\text{Lu}]\text{-AM-NT 2}$ , with the  $\text{PEG}_4$ -spacer, was the most stable conjugate with a half-life of almost 40 min. Conjugate  $[^{177}\text{Lu}]\text{-AM-NT 1}$  was completely degraded after 30 min and  $[^{177}\text{Lu}]\text{-AM-NT 3}$  after 1 h. However, peptide conjugate  $[^{177}\text{Lu}]\text{-AM-NT 2}$  was not degraded completely until 4 h of incubation.

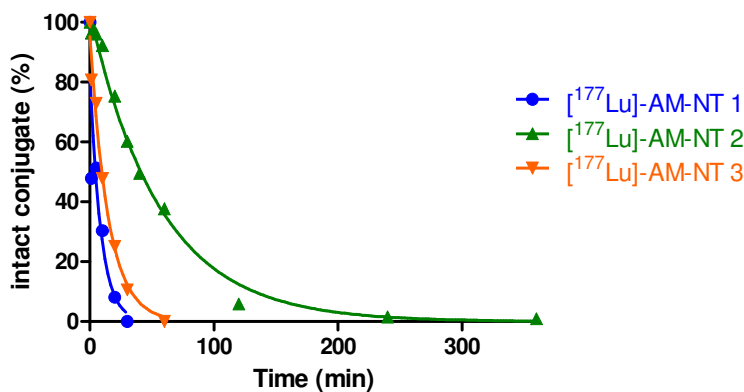


Figure 20: Serum stabilities of [<sup>177</sup>Lu]-AM-NT 1, [<sup>177</sup>Lu]-AM-NT 2 and [<sup>177</sup>Lu]-AM-NT 3.

### 3.1.3 Discussion of the *In Vitro* Evaluation of [<sup>177</sup>Lu]-AM-NT 1-3

The presence of a spacer moiety in DOTA-NT (8-13) seems to be favourable, as both [<sup>177</sup>Lu]-AM-NT 2 and [<sup>177</sup>Lu]-AM-NT 3 displayed higher internalisation rates and binding affinities towards NTR1 than the spacer-free parent compound [<sup>177</sup>Lu]-AM-NT 1. The observed receptor binding affinities are comparable to the values described in literature for related radiometallated NT derivatives.<sup>[84]</sup>

Interestingly, the lipophilicity of the peptide conjugates seemed neither affected by the presence or absence of a spacer nor by its chemical composition. We can hypothesize that this is due to the intrinsic hydrophilicity of the peptide sequence and the presence of the large-sized hydrophilic metal complex. They all exhibited a hydrophilic character, a favourable characteristic for a radiometal-labelled peptide conjugate as the likelihood of an unspecific liver-accumulation *in vivo* due to hepatobiliary excretion is reduced.

Whereas the receptor binding properties were unaffected by the nature of the spacer (PEG<sub>4</sub> or Ahx), the serum stability experiments revealed the superiority of the PEG<sub>4</sub>-spacer in terms of metabolic stability. Thus, compared to the analogue without a spacer, the introduction of a PEG<sub>4</sub>-spacer into the NT (8-13) conjugate was not only beneficial in terms of cell internalisation and an improved K<sub>D</sub>, but also increased substantially (by a factor 6) its metabolic stability.

However, a literature survey suggested that the achieved stabilization of the NT (8-13) peptide conjugate by employing a spacer may not yet be sufficient for clinical applications. Thus, further stabilization of NT (8-13) by chemical modifications is the subject of the main



project of this thesis, for which [<sup>177</sup>Lu]-**AM-NT 2** served as both a starting point and reference compound in terms of biological activity and metabolic stability.

### 3.2 'Triazole Scan' of NT (8-13)

After the identification of PEG<sub>4</sub> as the most suitable spacer for DOTA-NT (8-13) conjugates, a series of triazole-containing NT (8-13) analogues were synthesized and evaluated biologically. **Figure 21** shows all the positions that allow for the introduction of a 1,4-disubstituted 1,2,3-triazole as an amide bond mimic. The position Arg<sup>9</sup>-Pro<sup>10</sup> could not be modified because the secondary amine of the proline does not allow the introduction of an azide functionality. After identification of the amide bonds of NT (8-13) that can be replaced with a triazole without inducing a significant loss of the biological properties, conjugates with multiple triazoles were synthesized and evaluated. The synthesis of the building blocks and peptide conjugates as well as the challenges encountered during this work are discussed in detail in chapters 3.2.1, 3.2.2 and 3.2.3.

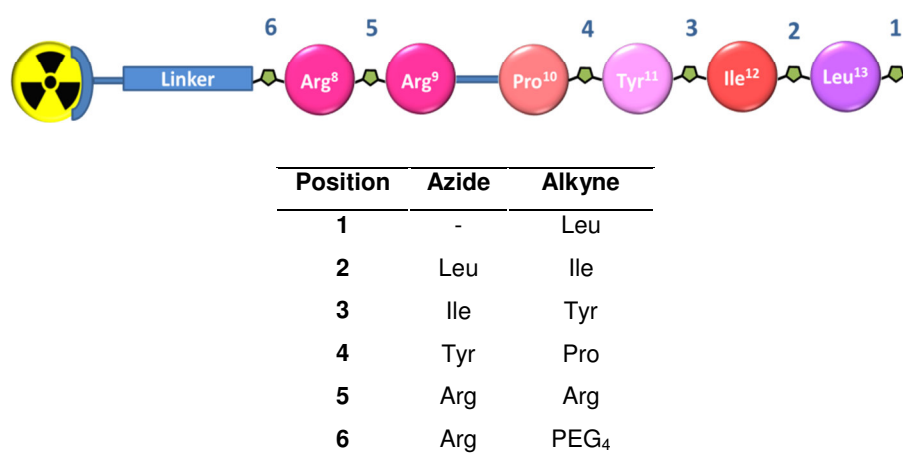
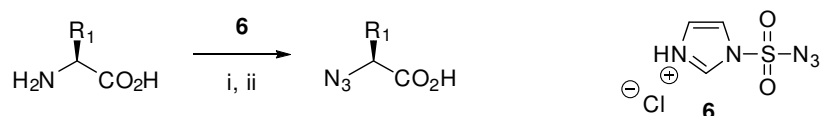


**Figure 21:** Schematic representation of [<sup>177</sup>Lu]-DOTA-PEG<sub>4</sub>-NT (8-13) and all modifiable positions and a summary of the needed azide and alkyne building blocks.

### 3.2.1 Synthesis of Precursors

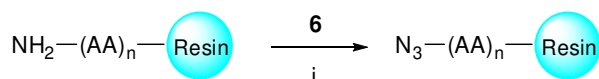
#### 3.2.1.1 Synthesis of $\alpha$ -Azido Acids

The synthesis of the azides was originally planned to be performed in solution, by introducing an azide into commercially available amino acids *via* a diazo transfer reaction. The diazo transfer reagent required for this transformation, imidazole-1-sulfonyl azide hydrochloride (**6**), was synthesized following the protocol first described by Goddard-Borger and Stick.<sup>[184]</sup> The  $\alpha$ -azido acids were then synthesized then according to the **Scheme 12**.



**Scheme 12:** General synthesis approach for  $\alpha$ -azido acids: i) imidazole-1-sulfonyl azide hydrochloride (**6**),  $\text{K}_2\text{CO}_3$ ,  $\text{CuSO}_4$ , MeOH, RT, 12 h.

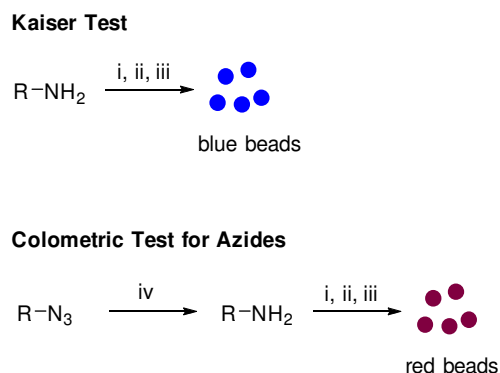
The benefit of this synthetic strategy lies on the retention of the chirality of the amino acid, the chemospecificity of the conversion and the mild reaction conditions. Despite these advantages, the use of this synthetic strategy failed to provide  $\text{N}_3\text{-Tyr}(\text{tBu})\text{-OH}$ . During these investigations, a paper by Löwik and co-workers was published which describes the feasibility of a diazo-transfer reaction on solid support. This prompted us to abandon solution phase synthesis and instead, perform the diazo-transfer reaction directly on solid support.<sup>[162]</sup> The preparation of  $\alpha$ -azido peptides on solid phase does not require the presence of a metal catalyst (**Scheme 13**).



**Scheme 13:** Schematic representation of the synthesis of azides on solid phase. i) imidazole-1-sulfonyl azide hydrochloride (**6**), Hünig's base, 1 h, RT.

The solid phase synthesis of azides was very efficient and saved time and resources. The presence of the azides on the resin was confirmed after each synthesis with a colorimetric

test developed by Punna and Finn.<sup>[185]</sup> This test uses the Staudinger reaction to reduce the azides to amines, which can then be detected with the Kaiser test. Blue coloured beads reveal the presence of free amines when using the classical Kaiser test. Reddish coloured beads confirm the presence of azides on the solid phase (**Scheme 14**). In order to obtain a reliable result, the phosphine-solution was applied first to the resin beads and heated and then the Kaiser test was performed.



**Scheme 14:** Schematic representation of the Kaiser test and the colorimetric test for azides. i) KCN in aq. pyridine; ii) Ninhydrin in ethanol; iii) Phenol in ethanol; iv) PPH<sub>3</sub> in ethanol, H<sub>2</sub>O.

### 3.2.1.2 Synthesis of $\alpha$ -Amino Alkynes

The required  $\alpha$ -amino alkynes were synthesized by reduction of the corresponding Weinreb amide to an aldehyde, followed by a Seyferth-Gilbert homologation. The use of a mild base such as potassium carbonate or potassium *tert*-butoxide is necessary for the Seyferth-Gilbert homologation. However, the presence of such reagents also leads to partial or complete cleavage of the Fmoc protective group. Thus, two different synthetic strategies were developed.  $\alpha$ -amino alkynes without acid-labile protective groups in their side-chains (isoleucine, proline and leucine) were synthesized starting from Boc-protected amino acids whereas  $\alpha$ -amino alkynes with functional groups in the side chain (arginine and tyrosine) were synthesized from Fmoc-protected amino acids. Both strategies are explained in detail in chapters 3.2.1.2.1 and 3.2.1.2.3.

Due to the formation of a substituted  $\alpha$ -amino aldehyde intermediate, which is prone to racemization, the enantiomeric purity of the alkyne building blocks had to be verified in each case. This will be described in chapter 3.2.1.2.4. The structures of the alkynes used for the

synthesis of the triazole containing NT (8-13) analogues are summarized in **Table 20**, together with the obtained yields and their enantiomeric intactness.

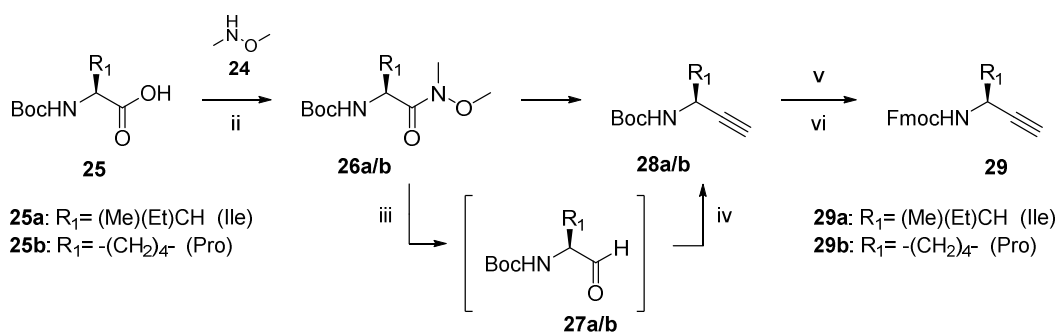
**Table 20:** Structures of  $\alpha$ -amino alkynes **29a-f** with the corresponding yields and enantiomeric purities.

	Structure	Yield (%)	Enantiomeric Purity
<b>29a</b> <sup>[186]</sup>		84	No racemization observed
<b>29b</b> <sup>[187]</sup>		95	No racemization observed
<b>29c</b>		51	No racemization observed
<b>29d</b>		22	No racemization observed
<b>29e</b> <sup>[188]</sup>		87	No racemization observed
<b>29f</b> <sup>[138]</sup>		50	n.a.

### 3.2.1.2.1 Synthesis of $\alpha$ -Amino Alkynes without a Functional Group in the Side-Chain

For the synthesis of Fmoc-Ile-alkyne **29a** and Fmoc-Pro-alkyne **29b**, Boc-protected starting materials were chosen. Fmoc-Leu-alkyne **29e** has previously been described.<sup>[131]</sup>

**Scheme 15** shows the synthetic pathway from amino acid starting materials **25** to the desired alkynes **29**. The Boc-protected amino acids **25** were converted into Weinreb amides **26** by the coupling of *N,O*-dimethylhydroxylamine **24**. The Weinreb amides **26** were reduced with DIBAL-H to the aldehydes **27**, which was then transformed *in situ* to Boc-alkyne **28** via Seyferth-Gilbert homologation using the Bestmann-Ohira reagent **23**. Finally, the Boc-protecting group was removed under acidic conditions and a Fmoc-protecting group was installed instead, giving alkynes **29a** and **29b**.



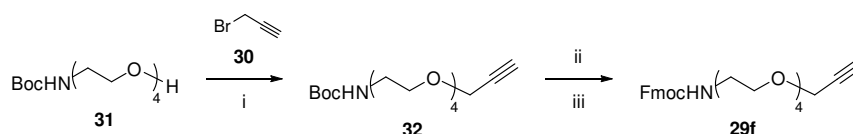
**Scheme 15:** Synthetic pathway to  $\alpha$ -amino alkynes without functional groups on the side-chain. i) BOP, Hünig's base, CH<sub>2</sub>Cl<sub>2</sub>, 15 min, RT; ii) *N,O*-dimethylhydroxylamine **24**, 15 h, RT; iii) DIBAL-H in toluene, CH<sub>2</sub>Cl<sub>2</sub>, 2 h, -78 °C; iv) Bestmann-Ohira reagent **23**, K<sub>2</sub>CO<sub>3</sub>, anhydrous MeOH, 15 h, 0 °C to RT; v) 30% TFA in CH<sub>2</sub>Cl<sub>2</sub>, 30 min, RT; vi) Fmoc-OSu, BOP, Hünig's base, 2 h, RT.

The conversion of Boc-Ile-OH **25a** and Boc-Pro-OH **25b** into their corresponding Weinreb amides **29a** and **29b** yielded pure products in high yields after flash chromatography. High yields in the subsequent reduction to the aldehydes **27a** and **27b** could be obtained when the reaction was carried out under anhydrous conditions, using fresh DIBAL-H in toluene. Completion of the reduction step was monitored through the use of an aldehyde-specific TLC-staining reagent (e.g. 2,4-dinitrophenylhydrazine). If the conversion to the aldehyde was not complete after 1 h, another equivalent DIBAL-H was added. After full consumption of the Weinreb amide, the reaction was allowed to warm up from -78 to 0 °C, before addition of the base. The addition of the base often resulted in the formation of a gel, depending on the ratio of DIBAL-H and the solvents used. This gel hindered the stirring of the reaction solution and had to be dispersed by ultrasonication and dilution with anhydrous solvents (MeOH/CH<sub>2</sub>Cl<sub>2</sub>), prior to the homologation. The addition of the Bestmann-Ohira reagent **23** was performed at 0 °C, and the reaction mixture was allowed to warm up to room temperature overnight. To our surprise, reagent **23** could not be stored over long periods of time and underwent slow degradation, even upon storage under inert atmosphere at -20 °C. This unexpected degradation of the reagent **23** could be observed by TLC and might have been the cause for the low yields of the resulting alkynes observed at the beginning of the project.

Both Fmoc-Ile-alkyne **29a** and Fmoc-Pro-alkyne **29b** were obtained in crystalline form, in high purities and moderate overall yields. Their enantiomeric purities were determined indirectly *via* the formation of pseudodipeptides by coupling with Fmoc-protected alanine, followed by NMR analysis of the diastereomeric purity of products obtained. No racemization was observed (see chapter 3.2.1.2.4).

### 3.2.1.2.2 Synthesis of Fmoc-PEG<sub>4</sub>-alkyne **29f**

A different approach was used for the synthesis of Fmoc-PEG<sub>4</sub>-alkyne **29f**. The alkyne functionality was introduced into commercial Boc-PEG<sub>4</sub>-CO<sub>2</sub>H **31** via nucleophilic substitution using propargylbromide (**30**) (**Scheme 16**). Fmoc-PEG<sub>4</sub>-alkyne **29f** was obtained in moderate yield and high purity.

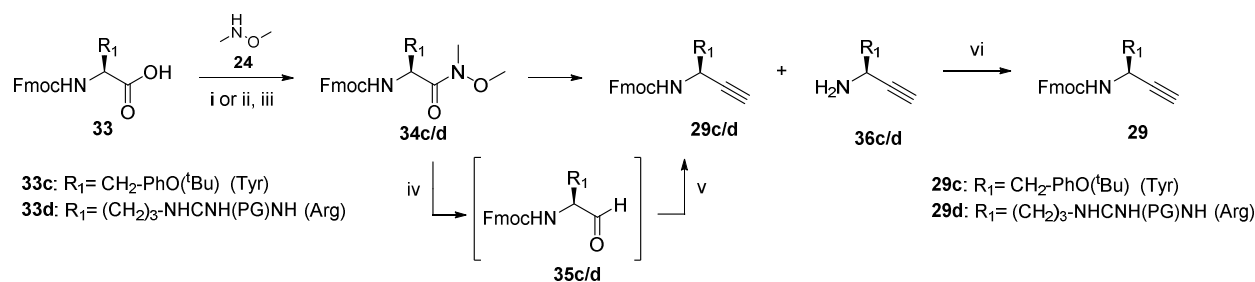


**Scheme 16:** Synthetic route to Fmoc-PEG<sub>4</sub>-alkyne **29f**. i) Propargylbromide **30**, NaH, THF, 12 h, RT; ii) 30% TFA in CH<sub>2</sub>Cl<sub>2</sub>, 30 min, RT; iii) Fmoc-OSu, Hünig's base, 2 h, RT.

### 3.2.1.2.3 Synthesis of $\alpha$ -Amino Alkynes with a Functional Group in the Side-chain

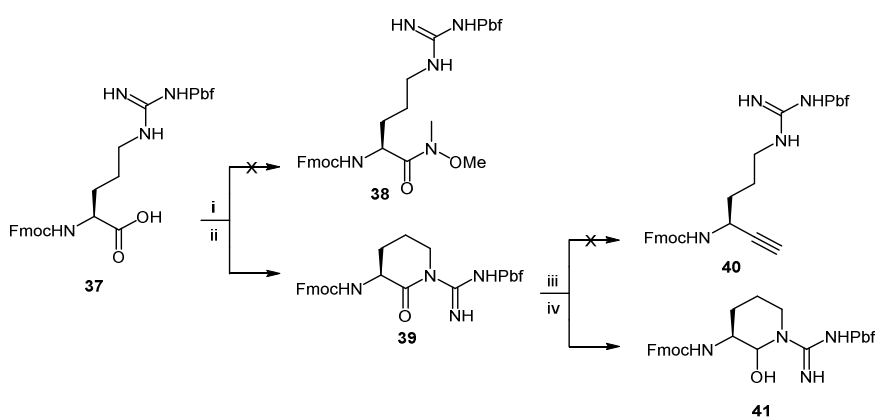
For the synthesis of the amino acid derived  $\alpha$ -amino alkynes with functional groups in the side-chain, Fmoc-protected amino acids were used as starting materials. Under the basic reaction conditions of the Seyferth-Gilbert homologation, a partial deprotection of the Fmoc-group can take place. As a consequence, a mixture of Fmoc-protected and deprotected products is obtained (**Scheme 17**). This complication can be resolved by treatment of the crude reaction mixture with Fmoc-OSu, a simple procedure to obtain only the desired Fmoc-protected  $\alpha$ -amino alkyne product. Fmoc-Tyr(<sup>t</sup>Bu)-alkyne **29c** was obtained in high purity and moderate yields.

## Results and Discussion



**Scheme 17:** Synthetic pathway to  $\alpha$ -amino alkynes with functional groups in the side-chain. i) BOP, Hünig's base, CH<sub>2</sub>Cl<sub>2</sub>, 15 min, RT; ii) HOBt, EDC, *N*-methylmorpholine, 15 min, 0 °C; iii) *N,O*-dimethylhydroxylamine **24**, 15 h, RT; iv) DIBAL-H in toluene, CH<sub>2</sub>Cl<sub>2</sub>, 2 h, -78 °C; v) Bestmann-Ohira reagent **23**, K<sub>2</sub>CO<sub>3</sub>, MeOH, 15 h, RT; vi) Fmoc-OSu, Hünig's base, 2 h, RT.

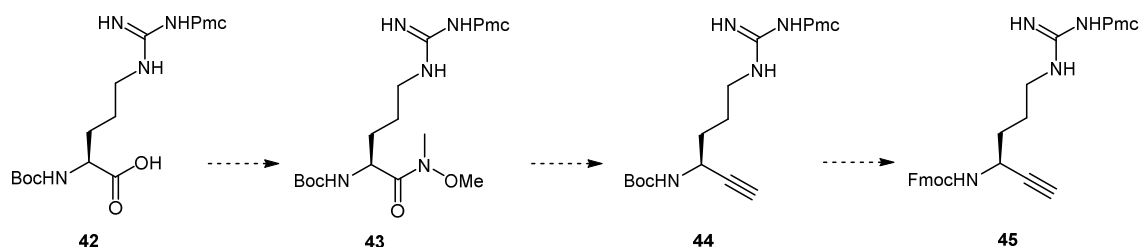
The synthesis of the alkyne-derivative of arginine proved to be challenging. Following the procedure described above for Fmoc-Tyr(<sup>t</sup>Bu)-alkyne **29c** (Scheme 17) lactam **39** was obtained instead of the desired Weinreb amide **38**. The formation of the cyclic side-product **39** is most likely due to an intramolecular cyclization of the guanidine group of **37** once the carboxylic acid is activated towards nucleophilic attack under the reaction conditions. Attempted direct reduction of lactam **39** with DIBAL-H and treatment with the Bestmann-Ohira reagent **23** did not afford alkyne **40**, but hemi-aminal **41**, a side-product which obviously did not react further to afford alkyne **40** (Scheme 18). Similar observations have been made by Ho and Ngu.<sup>[189]</sup> They reported the formation of a cyclic hemi-aminal when reducing an Mrt-protected arginine-S-benzyl thioester to the corresponding aldehyde.



**Scheme 18:** Synthesis of hemi-aminal **41**. i) BOP, Hünig's base, CH<sub>2</sub>Cl<sub>2</sub>, 15 min, RT; ii) *N,O*-dimethylhydroxylamine **24**, 15 h, RT; iii) DIBAL-H in toluene, CH<sub>2</sub>Cl<sub>2</sub>, 2 h, -78 °C; iv) Bestmann-Ohira reagent **23**, K<sub>2</sub>CO<sub>3</sub>, MeOH, 15 h, RT.



In a further attempt to obtain the desired alkyne derivative of arginine, we employed Boc-Arg(Pmc)-OH **42** as starting material. The synthetic pathway was identical as for Fmoc-Ile-alkyne **29a** and Fmoc-Pro-alkyne **29b** (Scheme 19).



**Scheme 19:** Proposed synthetic pathway to obtain Fmoc-Arg(Pmc)-alkyne **45**.

Because conversion of Boc-Arg(Pmc)-OH **42** to the Weinreb amide **43** under standard reaction conditions was unsuccessful, we studied the use of different bases and coupling reagents (Table 21). Only the combination of HATU and Hünig's base afforded Weinreb amide **43**, however only in low yield, while the corresponding lactam side-product was still the major product of the reaction. All other examined reaction conditions gave only the lactam.

Unfortunately, the exposure of Boc-Arg(Pmc)-N(Me)OMe **43** to the Seyferth-Gilbert homologation reaction conditions did not result in detectable amounts of the desired alkyne **44**. This could be again the result of the formation of a hemi-aminal product as in the case of Pbf-protected Arg-derivative **41**.

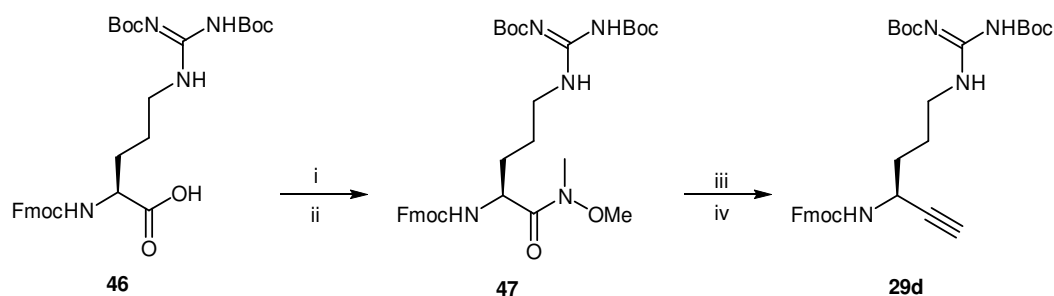
**Table 21:** Optimization of the reaction conditions for the synthesis of Boc-Arg(Pmc)-N(Me)OMe.

	Coupling Reagent	Base	Reaction Time	Temperature	Observations
Boc-Arg(Pmc)-OH	BOP	Hünig's base	14 h	RT	100% lactam
Boc-Arg(Pmc)-OH	BOP	NEt <sub>3</sub>	14 h	RT	100% lactam
Boc-Arg(Pmc)-OH	PyBOP	Hünig's base	14 h	RT	100% lactam
Boc-Arg(Pmc)-OH	HATU	Hünig's base	14 h	RT	15% Weinreb amide 85% lactam

We thus resorted to an alternative approach for the preparation of arginine-alkyne **29d** (Scheme 20). In 2011, Burgess reported the successful homologation of Boc-Arg(Boc)<sub>2</sub>-OH.<sup>[117]</sup> The double protected guanidine side-chain of arginine is presumably less prone to reactions with electrophiles (e.g. in an intramolecular fashion), due to steric and electronic effects.

Thus, we studied the use of Fmoc-Arg(Boc)<sub>2</sub>-OH **46** as a substrate for the synthesis of alkyne **29d**. Weinreb amide **47** was synthesized from Fmoc-Arg(Boc)<sub>2</sub>-OH **46**, following the protocols from Burgess and co-workers.<sup>[117]</sup> HOBt and EDC were used as coupling reagents and *N*-methylmorpholine as base. The Weinreb amide **27** was formed with in a satisfying yield of approx. 40%. The formation of the corresponding lactam was still observed but only as a minor side-product.

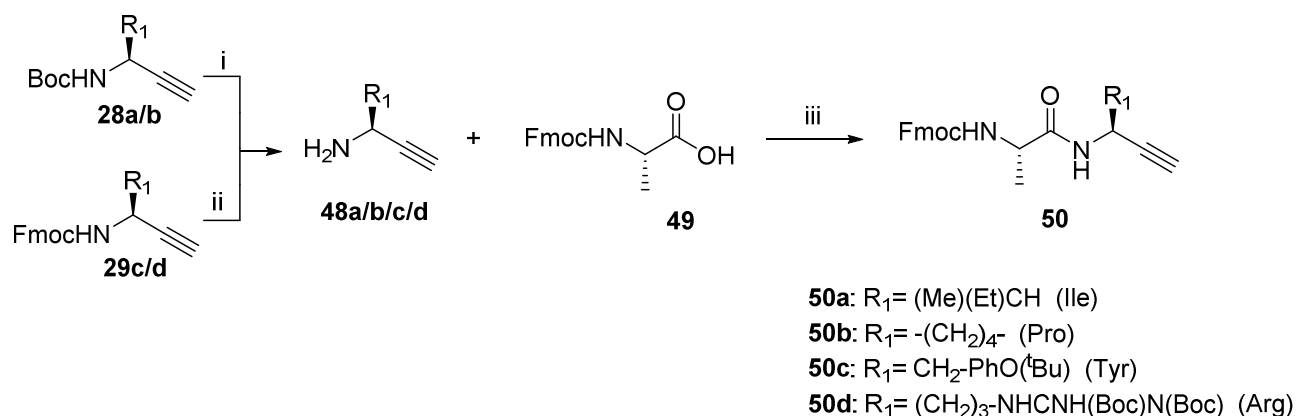
The reduction of the Weinreb amide **47** to the corresponding aldehyde and the subsequent homologation reaction proceeded straightforwardly, providing finally arginine derivative **29d**. The desired compound was obtained as a colourless crystalline substance, in high purity and in sufficient amounts for the synthesis of the corresponding triazole-containing NT (8-13) analogues.



**Scheme 20:** Synthesis of Fmoc-Arg(Boc)<sub>2</sub>-alkyne **29d**. i) HOBt, EDC, CH<sub>2</sub>Cl<sub>2</sub>, 0 °C, 15 min; ii) *N*-methylmorpholine, *N,O*-dimethylhydroxylamine **24**, RT, 15 h; iii) DIBAL-H in toluene, CH<sub>2</sub>Cl<sub>2</sub>, -78 °C, 2 h; iv) Bestmann-Ohira reagent **23**, K<sub>2</sub>CO<sub>3</sub>, MeOH, RT, 15 h.

#### 3.2.1.2.4 Determination of the Enantiomeric Purity of $\alpha$ -Amino Alkynes

The enantiomeric purity of  $\alpha$ -amino alkynes was determined by coupling with Fmoc-Ala-OH and the determination of the diastereomeric purity of the resulting pseudodipeptides by NMR (<sup>1</sup>H- and <sup>13</sup>C-NMR). **Scheme 21** shows the synthesis for the Ala-dipeptidoids **50**. The Fmoc- or Boc-protected alkynes (**28** or **29**) were used as substrates. After cleavage of the Fmoc- or Boc-protecting groups of the amine functional group, respectively, the unprotected  $\alpha$ -amino alkyne **48** was coupled to Fmoc-Ala-OH **49**, using BOP and Hünig's base. The products were then analysed with NMR spectroscopy.



**Scheme 21:** Synthesis of Ala-dipeptides **50a-d**: i) 20% TFA in CH<sub>2</sub>Cl<sub>2</sub>, RT, 30 min; ii) 20% piperidine in DMF, RT, 1 h; iii) BOP; Hünig's base; CH<sub>2</sub>Cl<sub>2</sub>, RT, 2 h.

The desired compounds **50a-d** were obtained in a straightforward manner in moderate to good yields after flash chromatography (**Table 22**).

**Table 22:** Structures of dipeptides **50a-d** with corresponding yields.

	Structure	Yield (%)	Diastereomeric Excess
<b>50a</b>		90	> 98
<b>50b</b>		30	> 98
<b>50c</b>		65	> 98
<b>50d</b>		65	> 98

Racemization of the amino acid during the synthesis of a  $\alpha$ -amino alkyne would result in the presence of diastereomers that can be distinguished by NMR. In particular, doubling of the <sup>1</sup>H-NMR signals of the H $\alpha$  of the alkyne and of H $\alpha'$  of the alanine, the terminal alkyne proton and the methyl group of the Alanine was expected.<sup>[138]</sup>

In none of the cases reported herein was a doubling of the  $^1\text{H-NMR}$  signals of the dipeptides observed. Therefore it can be concluded, that no racemization occurred during the synthesis of the  $\alpha$ -amino alkynes **29a-d**, under the conditions described. This is in agreement with data previously reported by us and others,<sup>[172]</sup> which reports no sign of racemization during the homologation of several amino acids (Nle, Leu, Gly, Val, Ala, Trp and Gln), with the exception of histidine.<sup>[131]</sup> **Figure 22** shows the NMR spectra of Fmoc-Ala-Ile-alkyne **50a**, Fmoc-Ala-Tyr(<sup>t</sup>Bu)-alkyne **50c** and Fmoc-Ala-Arg(Boc)<sub>2</sub>-alkyne **50d** and the corresponding H $\alpha$  of the  $\alpha$ -amino alkyne and alkyne signals.

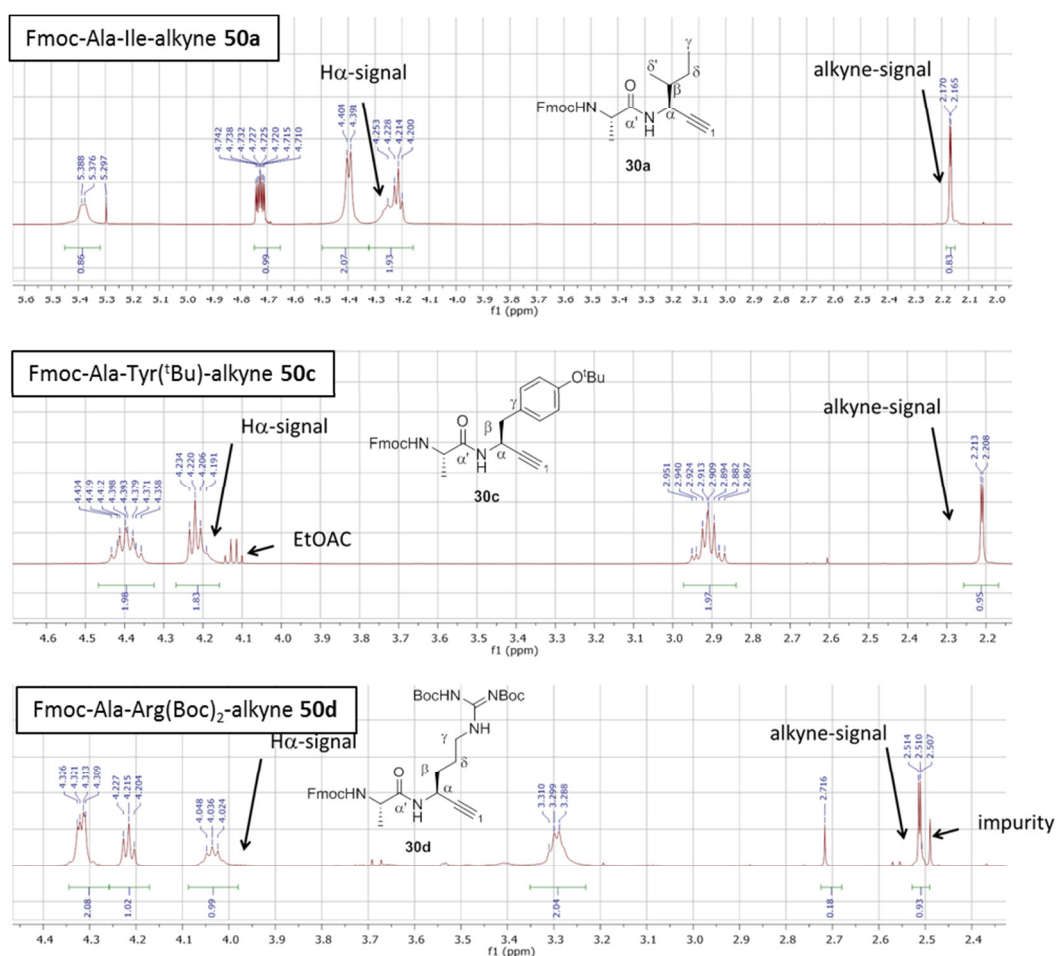


**Figure 22:** NMR spectra of Fmoc-Ala-Ile-alkyne **50a**, Fmoc-Ala-Tyr(<sup>t</sup>Bu)-alkyne **50c** and Fmoc-Ala-Arg(Boc)<sub>2</sub>-alkyne **50d**, showing H $\alpha$  and alkyne signals.

Proline occurs naturally as a mixture of *trans*- and a *cis*-conformers around a Xaa-Pro amide bond (Xaa: amino acid). This was also observed in the NMR spectrum of the dipeptide Fmoc-Ala-Pro-alkyne **50b**, where the H $\alpha_{cis}$  and the H $\alpha_{trans}$  are both visible, in a ratio of 0.4 to 0.6, which is in agreement with literature data.<sup>[190]</sup> The signal of the alkyne was not doubled,

but for  $H_{\alpha}$ , both *cis*- and *trans*-signals were visible (**Figure 23**). In case of a racemization a set of four signals for the  $H_{\alpha}$  of the  $\alpha$ -amino alkyne would be expected. This was not the case and thus, also in this case, it can be concluded that no racemization has occurred during the synthesis of Fmoc-Pro-alkyne **29b**.

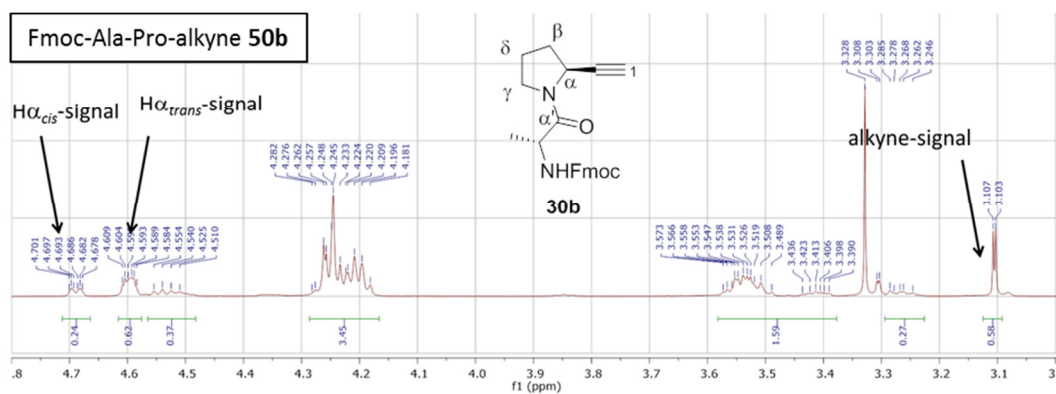


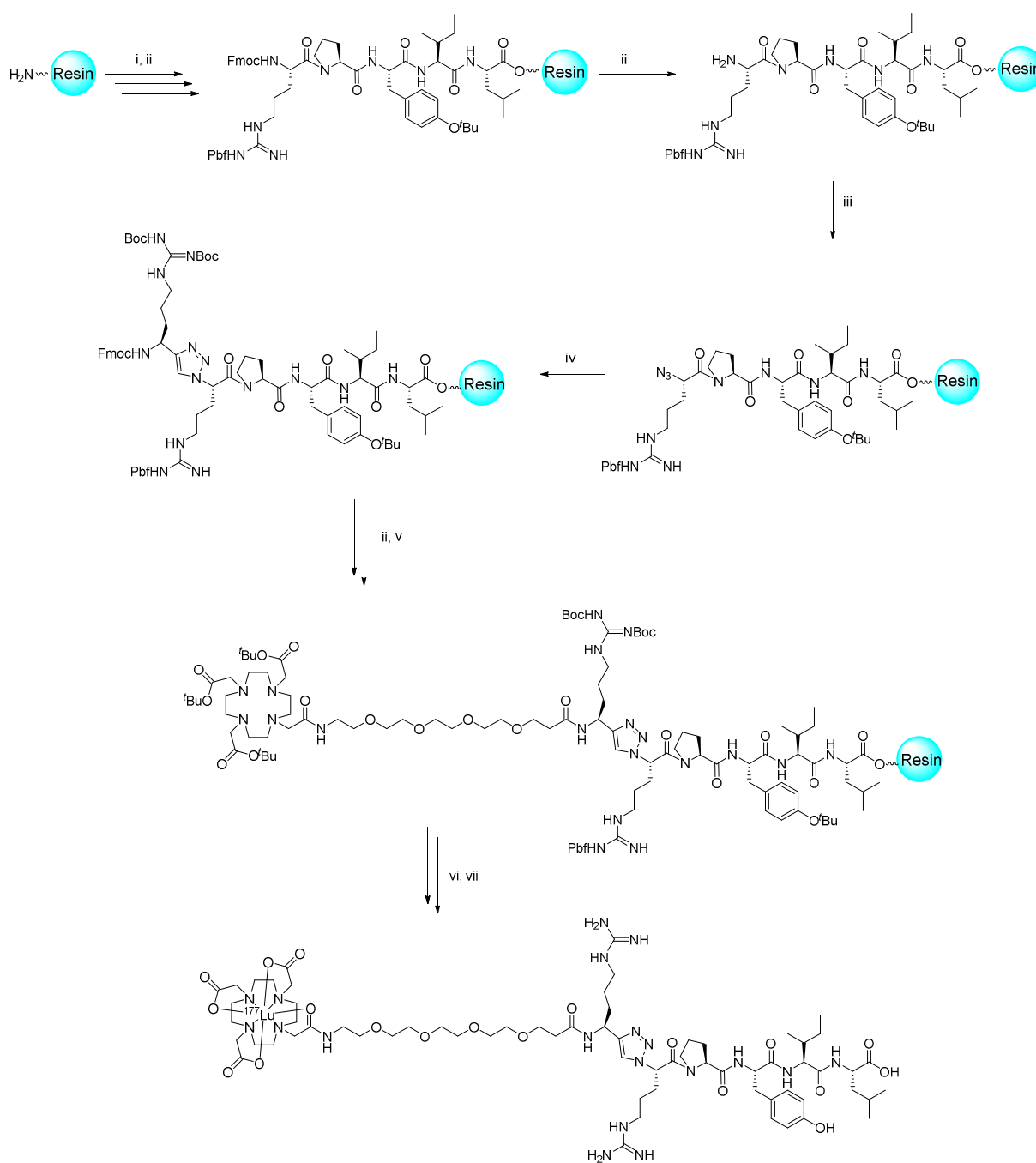
**Figure 23:** NMR spectrum of Fmoc-Ala-Pro-alkyne **50d**, showing  $H_{\alpha}$  and alkyne signals.

### 3.2.2 Synthesis of the First Generation of Triazole-Containing NT (8-13) Analogues

The substitution of each amide bond, one at the time, of DOTA-PEG<sub>4</sub>-NT (8-13) conjugates with a triazole yielded six conjugates (**AM-NT 4-9**) bearing a single backbone modification. After identification of the amide bonds of NT (8-13) that can be replaced with a triazole without the loss of biological activity, a conjugate with multiple triazoles (**AM-NT 10**) was also prepared and evaluated (**Table 23**).

The peptide conjugates **AM-NT 4-10** were synthesized manually on solid phase *via* classical Fmoc-chemistry till the position of the triazole (see chapter 3.1.1). An example of the synthesis of a triazole-containing peptide conjugate is shown in **Scheme 22**. In order to introduce the triazole in the peptide backbone, the corresponding amino acid was deprotected with 20% piperidine in DMF and the resulting *N*-terminal amine was converted into an azide *via* a diazo-transfer reaction. The presence of the azides on the resin was confirmed with the colorimetric test for azides described in chapter 3.2.1.1. The triazole was obtained *via* copper catalysed azide alkyne cycloaddition (CuAAC) under anhydrous conditions. The corresponding  $\alpha$ -amino alkyne, the copper (I) source ( $[(\text{CH}_3\text{CN})_4\text{Cu}]\text{PF}_6$ ), the copper (I) ligand TBTA and the proton acceptor (Hünig's base) were dissolved in DMF and added to the resin. After 12-16 h of vigorous stirring, the resin was extensively washed with a solution of 0.5% diethyldithiocarbamate in DMF to remove the copper (I) from the resin. Colorimetric azide test were performed to verify the completion of the reaction. If the azide test was positive (red beads) the CuAAC reaction was repeated. After the cycloaddition, the amino acid sequence was completed by standard Fmoc peptide chemistry. After attachment of the spacer and the chelator, the peptide conjugates were cleaved and purified *via* HPLC (see chapter 3.1.1).

## Results and Discussion



**Scheme 22:** Solid phase synthesis of a triazole-containing NT (8-13)-based peptide conjugate (**AM-NT 8**). i) Fmoc-AA-OH, HATU, Hünig's base, DMF, 2 h, RT. ii) 20% piperidine in DMF, 10 min, RT. iii) imidazole-1-sulfonyl azide hydrochloride **1**, Hünig's base, DMF, 1 h, RT; iv) Fmoc-alkynes **7a-d**,  $[\text{Cu}(\text{CH}_3\text{CN})_4]\text{PF}_6$ , Hünig's base, DMF, 12 h, RT; v) Fmoc-PEG<sub>4</sub>-OH or DOTA-(*tris*-<sup>t</sup>Bu), HATU, Hünig's base, DMF, 2 h, RT; vi) TFA/H<sub>2</sub>O/PhOH/*i*Pr<sub>3</sub>SiH, 6 h, RT. vii) [<sup>177</sup>Lu]LuCl<sub>3</sub>, ammonium acetate buffer (pH 4.5), 30 min, 100 °C.

Conjugate **AM-NT 4**, with a C-terminal triazole, was synthesized on a different resin. The synthesis of peptide conjugate **AM-NT 4**, was performed on a Fmoc-protected Rink Amide MBHA LL resin. The resin was deprotected with 20% piperidine in DMF and the resulting free amine was converted into an azide *via* diazo transfer reaction. The CuAAC reaction to

introduce the triazole, followed by the coupling of the remaining amino acids, the spacer and the chelator DOTA was performed according to the protocol described in **Scheme 22**. Cleavage and purification of **AM-NT 4** was performed as described in chapter 3.1.1.

Peptide conjugates **AM-NT 4-10** were obtained as highly pure compounds (verified by HPLC) and their mass was verified by ESI-HRMS (**Table 23**).

**Table 23:** Summary of the peptide conjugates from the 'triazole scan' and their analytical information.

	Structure	MW (g/mol)	ESI-HRMS [M+2H <sup>+</sup> ] <sup>2+</sup>	Yield (%)	Purity (%)
<b>AM-NT 2</b> (1 <sup>st</sup> G Reference) <sup>a</sup>	DOTA-PEG <sub>4</sub> -Arg-Arg-Pro-Tyr-Ile-Leu	1449.82	725.92	2	> 99
<b>AM-NT 4</b>	DOTA-PEG <sub>4</sub> -Arg-Arg-Pro-Tyr-Ile-Leu- <b>ψ</b> [Tz]-H	1472.85	492.28 <sup>b</sup>	11	> 99
<b>AM-NT 5</b>	DOTA-PEG <sub>4</sub> -Arg-Arg-Pro-Tyr-Ile- <b>ψ</b> [Tz]-Leu	1473.83	738.92 <sup>c</sup>	5	> 99
<b>AM-NT 6</b>	DOTA-PEG <sub>4</sub> -Arg-Arg-Pro-Tyr- <b>ψ</b> [Tz]-Ile-Leu	1473.83	737.92	32	> 99
<b>AM-NT 7</b>	DOTA-PEG <sub>4</sub> -Arg-Arg-Pro- <b>ψ</b> [Tz]-Tyr-Ile-Leu	1473.83	737.92	27	> 98
<b>AM-NT 8</b>	DOTA-PEG <sub>4</sub> -Arg- <b>ψ</b> [Tz]-Arg-Pro-Tyr-Ile-Leu	1473.83	737.92	14	> 99
<b>AM-NT 9</b>	DOTA-PEG <sub>4</sub> - <b>ψ</b> [Tz]-Arg-Arg-Pro-Tyr-Ile-Leu	1459.81	730.92	5	> 98
<b>AM-NT 10</b>	DOTA-PEG <sub>4</sub> - <b>ψ</b> [Tz]-Arg- <b>ψ</b> [Tz]-Arg-Pro-Tyr-Ile-Leu	1483.83	742.92	2	> 99

<sup>a</sup> 1<sup>st</sup> generation reference <sup>b</sup> [M+3H<sup>+</sup>]<sup>3+</sup>. <sup>c</sup> ESI-MS, [M+2H<sup>+</sup>]<sup>2+</sup>.

After the successful synthesis and purification of the NT (8-13) analogues, they were labelled with [<sup>177</sup>Lu]LuCl<sub>3</sub>, and their radiochemical purities and yields were determined *via* γ-HPLC (see chapter 3.1.1). **Table 24** shows the radiolabelled structures of [<sup>177</sup>Lu]-**AM-NT 4-10** and their radiochemical yields and purities.

**Table 24:** Radiolabelled peptide conjugates [<sup>177</sup>Lu]-**AM-NT 4-10** and their radiolabelling purities.

	Structure	Radiochemical Yield (%)	Radiochemical Purity (%)
<b>[<sup>177</sup>Lu]-AM-NT 4</b>	[ <sup>177</sup> Lu]-DOTA-PEG <sub>4</sub> -Arg-Arg-Pro-Tyr-Ile-Leu- <b>ψ</b> [Tz]-H		
<b>[<sup>177</sup>Lu]-AM-NT 5</b>	[ <sup>177</sup> Lu]-DOTA-PEG <sub>4</sub> -Arg-Arg-Pro-Tyr-Ile- <b>ψ</b> [Tz]-Leu		
<b>[<sup>177</sup>Lu]-AM-NT 6</b>	[ <sup>177</sup> Lu]-DOTA-PEG <sub>4</sub> -Arg-Arg-Pro-Tyr- <b>ψ</b> [Tz]-Ile-Leu		
<b>[<sup>177</sup>Lu]-AM-NT 7</b>	[ <sup>177</sup> Lu]-DOTA-PEG <sub>4</sub> -Arg-Arg-Pro- <b>ψ</b> [Tz]-Tyr-Ile-Leu	> 95	> 98
<b>[<sup>177</sup>Lu]-AM-NT 8</b>	[ <sup>177</sup> Lu]-DOTA-PEG <sub>4</sub> -Arg- <b>ψ</b> [Tz]-Arg-Pro-Tyr-Ile-Leu		
<b>[<sup>177</sup>Lu]-AM-NT 9</b>	[ <sup>177</sup> Lu]-DOTA-PEG <sub>4</sub> - <b>ψ</b> [Tz]-Arg-Arg-Pro-Tyr-Ile-Leu		
<b>[<sup>177</sup>Lu]-AM-NT 10</b>	[ <sup>177</sup> Lu]-DOTA-PEG <sub>4</sub> - <b>ψ</b> [Tz]-Arg- <b>ψ</b> [Tz]-Arg-Pro-Tyr-Ile-Leu		



### 3.2.3 Biological Investigation of Peptide Conjugates [ $^{177}\text{Lu}$ ]-AM-NT 4-10

The radiolabelled peptidomimetics [ $^{177}\text{Lu}$ ]-AM-NT 4-10 were biologically evaluated and compared side-by-side with reference compound [ $^{177}\text{Lu}$ ]-AM-NT 2 (see chapter 3.1). The cell internalisation in HT-29 cells and the receptor binding affinity and specificity to NTR1 of the compounds were measured. The lipophilicity as well as the stability in blood plasma was determined. For a detailed description of the biological essays see chapter 3.1.2. The results of the biological investigation of peptide conjugates [ $^{177}\text{Lu}$ ]-AM-NT 2-10 are summarized in **Table 25**.

**Table 25:** Summary of biological and physico-chemical properties of [ $^{177}\text{Lu}$ ]-AM-NT 2-10.

	Internalisation after 4 h (%)	$K_D$ (nM)	$B_{\max}$ (nM)	Log D	Stability $t_{1/2}$ (min)
[ $^{177}\text{Lu}$ ]-AM-NT 2 (1 <sup>st</sup> G. reference) <sup>a</sup>	7.3 ± 0.4	3.8 ± 0.9	0.37 ± 0.02	-2.6	39.4
[ $^{177}\text{Lu}$ ]-AM-NT 4	n.o.	n.d.	n.d.	-3.2	69.7
[ $^{177}\text{Lu}$ ]-AM-NT 5	n.o.	n.d.	n.d.	-2.8	72.0
[ $^{177}\text{Lu}$ ]-AM-NT 6	n.o.	n.d.	n.d.	-3.2	164.0
[ $^{177}\text{Lu}$ ]-AM-NT 7	n.o.	n.d.	n.d.	-2.6	13.0
[ $^{177}\text{Lu}$ ]-AM-NT 8	6.4 ± 1.2	8.7 ± 1.7	0.90 ± 0.04	-2.8	64.9
[ $^{177}\text{Lu}$ ]-AM-NT 9	9.4 ± 0.5	4.5 ± 0.8	0.45 ± 0.01	-3.2	46.9
[ $^{177}\text{Lu}$ ]-AM-NT 10	10.8 ± 0.4	4.6 ± 2.3	0.34 ± 0.03	-2.7	17.1

<sup>a</sup> 1<sup>st</sup> generation reference

The four peptide conjugates with a triazole substitution in the C-terminal region of NT (8-13), [ $^{177}\text{Lu}$ ]-AM-NT 4, 5, 6 and 7 did not show a specific cell internalisation into HT-29 cells (**Figure 24**). Less than 0.2% of the peptide conjugates were internalized into the cells after 4 h of incubation.

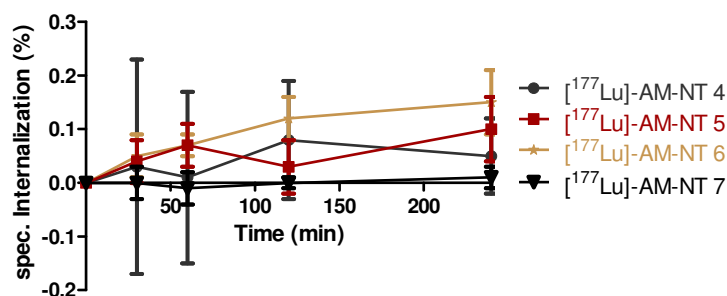


**Figure 24:** Cell internalisation profile of NT (8-13) analogues [ $^{177}\text{Lu}$ ]-AM-NT 4-7.

Peptide conjugates [ $^{177}\text{Lu}$ ]-AM NT 8 and [ $^{177}\text{Lu}$ ]-AM NT 9, with a triazole located between the Arg<sup>8</sup>-Arg<sup>9</sup> bond and between the N-terminal PEG<sub>4</sub> spacer and Arg<sup>8</sup>, showed a similar

internalisation behaviour as the reference compound [ $^{177}\text{Lu}$ ]-AM-NT 2. While the internalized amount of [ $^{177}\text{Lu}$ ]-AM-NT 8 was slightly lower than that of the reference (6.4% vs 7.3%), [ $^{177}\text{Lu}$ ]-AM-NT-9 internalized 9.4%, an even higher amount than the reference [ $^{177}\text{Lu}$ ]-AM-NT 2. [ $^{177}\text{Lu}$ ]-AM-NT 10, the peptide conjugate bearing a double-triazole modification on the Arg<sup>8</sup>-Arg<sup>9</sup> bond and between the *N*-terminal PEG<sub>4</sub> spacer and Arg<sup>8</sup>, both modifications sites of [ $^{177}\text{Lu}$ ]-AM-NT 8 and 9. Indeed, [ $^{177}\text{Lu}$ ]-AM-NT 10 showed the highest internalisation rate into HT-29 cells (10.8%), (Figure 25).

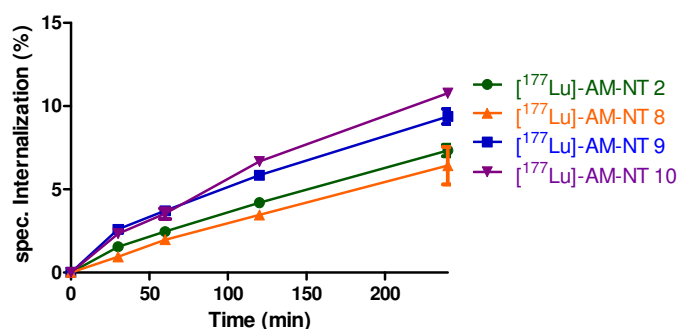


**Figure 25:** Cell internalisation profile of NT (8-13) analogues [ $^{177}\text{Lu}$ ]-AM-NT 8-10, compared to reference compound [ $^{177}\text{Lu}$ ]-AM-NT 2.

The determination of the receptor binding affinities and the receptor specificities of [ $^{177}\text{Lu}$ ]-AM-NT 8-10 was performed as described in chapter 3.1.2. The receptor binding affinities of analogues [ $^{177}\text{Lu}$ ]-AM-NT 3-7 were not determined, as no cell internalisation into HT-29 cells was observed, which indicates an abolished receptor affinity towards NTR1.

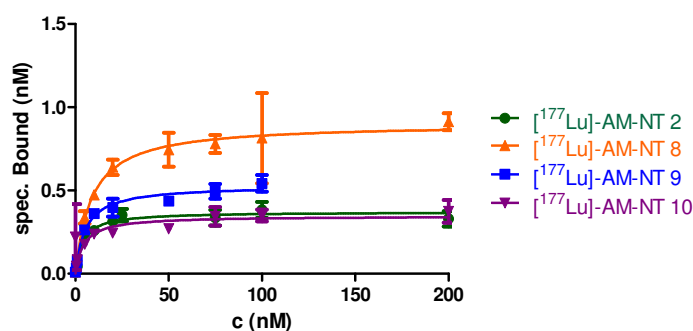


**Figure 26:** Results of receptor saturation experiments of NT (8-13) analogues [ $^{177}\text{Lu}$ ]-AM-NT 8-10, compared to reference compound [ $^{177}\text{Lu}$ ]-AM-NT 2. [ $^{177}\text{Lu}$ ]-AM-NT 9 was measured with one concentration less.

Conjugates [ $^{177}\text{Lu}$ ]-AM-NT 8-10 exhibited a retained high receptor affinity towards the NTR1 receptor. The observed values were similar for the reference peptide conjugate [ $^{177}\text{Lu}$ ]-AM-

**NT 2.** While peptide conjugate [ $^{177}\text{Lu}$ ]-AM-NT **8** exhibited the lowest dissociation constant ( $8.7 \pm 1.7$  nM) of these four compounds, it was still in the nanomolar range. [ $^{177}\text{Lu}$ ]-AM-NT **9** and [ $^{177}\text{Lu}$ ]-AM-NT **10** both had similar  $K_D$  values in comparison with the reference [ $^{177}\text{Lu}$ ]-AM-NT **2**,  $4.5 \pm 0.8$  and  $4.6 \pm 2.6$  nM, respectively (**Figure 26**).

Log D values between -2.6 and -3.2 were observed for of [ $^{177}\text{Lu}$ ]-AM-NT **4-10**. These values are comparable to the value measured for the reference compound of [ $^{177}\text{Lu}$ ]-AM-NT **2** (**Table 25**).

The metabolic stabilities of the radiolabelled peptidomimetics **AM-NT 4-10** were determined in human blood serum, as described in chapter 3.1.2. The conjugate with the Arg<sup>8</sup>-Ψ[Tz]-Arg<sup>9</sup> modification, [ $^{177}\text{Lu}$ ]-AM-NT **8**, showed the most pronounced improvement of stability in comparison with the reference [ $^{177}\text{Lu}$ ]-AM-NT-**2** (**Figure 27**). The half-life was calculated using a one-phase decay equation to fit the degradation curve (see chapter 3.1.2). The calculated half-life for [ $^{177}\text{Lu}$ ]-AM-NT **8** was 64.8 min, whereas for [ $^{177}\text{Lu}$ ]-AM-NT **2** it was 39.4 min. [ $^{177}\text{Lu}$ ]-AM-NT **9**, with a modification between the *N*-terminal PEG<sub>4</sub> spacer and Arg<sup>8</sup>, only exhibited a half-life of 46.9 min. Surprisingly, peptide conjugate [ $^{177}\text{Lu}$ ]-AM-NT **10**, with a double triazole-modification only had a half-life of 17.1 min. After 4 h of incubation in serum, a complete degradation of all the radiolabelled peptidomimetics [ $^{177}\text{Lu}$ ]-AM-NT **8-10** was observed.

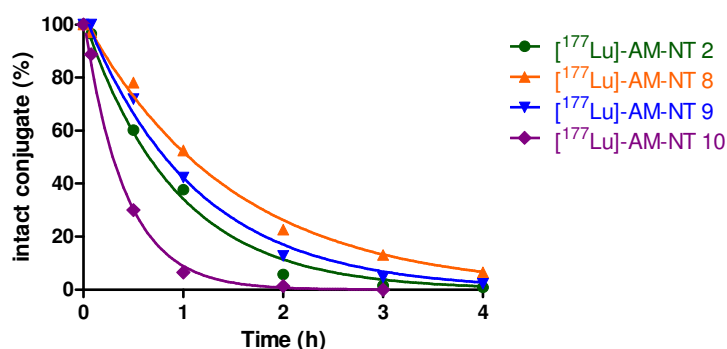


**Figure 27:** Serum stabilities of peptide conjugates [ $^{177}\text{Lu}$ ]-AM-NT **2** and [ $^{177}\text{Lu}$ ]-AM-NT **8-10**.

For the sake of complete data, the serum stabilities of the analogues that did not bind to NTR1, [ $^{177}\text{Lu}$ ]-AM-NT **4-7**, were also measured. Most of these peptide conjugates, with exception of [ $^{177}\text{Lu}$ ]-AM-NT **7**, exhibited an increased serum stability compared to the reference [ $^{177}\text{Lu}$ ]-AM-NT **2** (**Figure 28**). The half-life of [ $^{177}\text{Lu}$ ]-AM-NT **4** was 69.7 min, of [ $^{177}\text{Lu}$ ]-AM-NT **5**, 72.0 min and of [ $^{177}\text{Lu}$ ]-AM-NT **6**, 164.0 min. On the other hand, the half-

life of [ $^{177}\text{Lu}$ ]-AM-NT 7 was only 13.0 min. Among the compounds investigated, only [ $^{177}\text{Lu}$ ]-AM-NT 4-6 were still present in the blood serum (<10%) after 24 h of incubation.

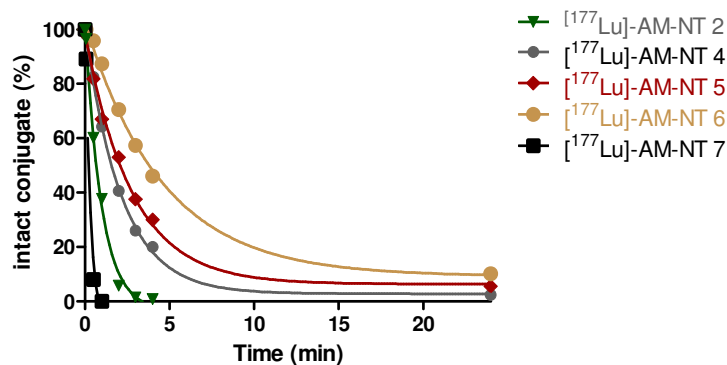


**Figure 28:** Serum stabilities of peptide conjugates [ $^{177}\text{Lu}$ ]-AM-NT 2 and [ $^{177}\text{Lu}$ ]-AM-NT 4-7.

### 3.2.4 Discussion of the *In Vitro* Investigation of [ $^{177}\text{Lu}$ ]-AM-NT 4-10

The first ‘triazole scan’ of NT (8-13) successfully yielded six new triazole-containing NT (8-13) analogues as well as one *bis*-triazole containing peptide conjugate. The hydrophilicity of the compounds was determined *via* log D experiments. Values between 2.6 and 3.2 demonstrated the hydrophilic nature of the peptide conjugate. Cell internalisation studies of the analogues revealed that a triazole-modification was only tolerated between the *N*-terminal PEG<sub>4</sub> spacer and Arg<sup>8</sup> and between the Arg<sup>8</sup> and Arg<sup>9</sup> residues. Compounds [ $^{177}\text{Lu}$ ]-AM-NT 4-7, with triazoles in the other possible positions, did not show any internalisation in HT-29 cells, which led to the conclusion that a triazole backbone modification was not tolerated in the central and *C*-terminal region of NT (8-13). In general, the *C*-terminal region of NT (8-13) has been reported in literature to be sensitive to chemical modifications, including backbone modifications (e.g. reduced amide bonds) as well as amino acid replacements.<sup>[9, 88]</sup> These observations also correlate well with the recently published crystal structure of NT (8-13) bound to the receptor NTR1, which rationalizes the necessity of a *C*-Terminal COOH-group, as this group forms hydrogen bonds to the amino acid residues Arg327 and Tyr146 in the binding pocket of the receptor.<sup>[80]</sup> This explains the loss of receptor affinity of compound [ $^{177}\text{Lu}$ ]-AM-NT 4, as the triazole is not able to engage in the same hydrogen bonds. Also the carbonyl groups of Ile<sup>12</sup> and Tyr<sup>11</sup> form hydrogen bonds to Tyr347 and Thr226 of the binding pocket of the receptor, respectively. This could explain the loss of receptor affinity of compounds [ $^{177}\text{Lu}$ ]-AM-NT 5 and [ $^{177}\text{Lu}$ ]-AM-NT 6.

The modification of the *N*-terminal region of NT (8-13) through amino acid substitutions or backbone engineering is considered less critical for the binding than the modifications on the *C*-terminus.<sup>[9, 88-89]</sup> It has been reported that the *N*-terminal region of NT (8-13) is not inserted entirely into the binding pocket of the NTR1 receptor upon binding.<sup>[80]</sup> This is in accordance with our observations, since [<sup>177</sup>Lu]-AM-NT 8 and [<sup>177</sup>Lu]-AM-NT 9 have been identified as the two compounds of the 'triazole scan' with a retained receptor affinity towards NTR1. The NT (8-13) analogues [<sup>177</sup>Lu]-AM-NT 8, [<sup>177</sup>Lu]-AM-NT 9 and [<sup>177</sup>Lu]-AM-NT 10 all exhibited similar internalisation rates and  $K_D$  values comparable to the reference compound [<sup>177</sup>Lu]-AM-NT 2. The observed values for cell internalisation and receptor affinity are in good agreement with the values described in literature for similar radiometal-labelled conjugates.<sup>[84, 98, 191]</sup> The stabilization gained through the introduction of triazoles was moderate. While the half-lives of [<sup>177</sup>Lu]-AM-NT 8 and 9, both analogues with a single triazole modification, were slightly superior to the half-life of the reference compound [<sup>177</sup>Lu]-AM-NT 2, they still underwent a very fast metabolic degradation. Surprisingly, the introduction of two consecutive triazoles in the NT (8-13) sequence led to a reduced metabolic stability in comparison to the mono-triazole containing peptide conjugates [<sup>177</sup>Lu]-AM-NT 8 and 9. This observation is difficult to explain, as it was expected that the *bis*-triazole compound [<sup>177</sup>Lu]-AM-NT 10 would be highly stabilized. The insertion of two consecutive triazoles into the sequence of NT (8-13) may result in a conformation of the peptide conjugate prone to degradation by the corresponding proteases. This phenomenon should be further investigated, for example with CD (circular dichroism) chromatography, molecular modelling or *in vitro* experiments with the NT (8-13) specific proteases.

Even though the insertion of a triazole into the *C*-terminal region of NT (8-13) led to a diminished receptor affinity of the peptide conjugates [<sup>177</sup>Lu]-AM-NT 4-7, it increased their metabolic stabilities in most cases. This suggests that the introduction of a triazole as an amide bond mimic within the *C*-terminal region is important for stabilization at the expense, however, of an efficient receptor binding. The maximal stabilization was achieved on conjugate [<sup>177</sup>Lu]-AM-NT 6, with a triazole between Tyr<sup>11</sup> and Ile<sup>12</sup>. Several radiolabelled NT (8-13) analogues have been described in literature, where the metabolic stability of the sequence was improved through the substitution of Ile<sup>12</sup> with Tle.<sup>[6, 84, 86, 99, 192]</sup>

The systematic substitution of the amide bonds in NT (8-13) with triazoles led to a first generation of triazole-based NT (8-13) peptidomimetics some of which with a specific receptor affinity towards NTR1. A moderate improvement of the half-life of the reference [<sup>177</sup>Lu]-AM-NT 2 (40 min) was achieved with compounds [<sup>177</sup>Lu]-AM-NT 8 (65 min) and [<sup>177</sup>Lu]-AM-NT 9 (47 min). However, half-lives of up to 20 days are reported for stabilized, radiolabelled NT (8-13) analogues, including the clinically tested NT XI.<sup>[6-7, 112]</sup> Thus, the

metabolic stability of the triazole-substituted NT (8-13) analogues [<sup>177</sup>Lu]-**AM-NT 8** and **9** may not be sufficient for future applications in nuclear imaging and therapy. For this reason, a second generation of triazole-based NT (8-13) peptidomimetics with improved metabolic stabilities was developed and evaluated (chapter 3.3)

### 3.3 Synthesis and Biological Evaluation of a Second Generation of Stabilized Triazole-Containing NT (8-13) Analogues

#### 3.3.1 Identification of a Suitable Amino Acid Substitution for NT (8-13) Analogues

Several NT (8-13) analogues with a modified amino acid sequence have been described in the literature. For example, the exchange of Ile<sup>12</sup> with Tle<sup>12</sup> led to peptide conjugates with improved stabilities.<sup>[6, 86, 96, 105]</sup> Similarly, the replacement of Arg<sup>8</sup> and Arg<sup>9</sup> with Lys has also been reported by several groups, giving rise to several NT (8-13) analogues with promising properties *in vivo*.<sup>[84, 89, 106]</sup> Since such NT (8-13) analogues were reported with different radiometals and chelators, we first set out to investigate which of these modifications in the amino acid sequence of NT (8-13) was suited best for our [<sup>177</sup>Lu]/DOTA system. Thus, we prepared four NT (8-13) analogues, functionalized with DOTA *via* a *N*-terminal PEG<sub>4</sub> spacer and investigated their properties *in vitro*. Again, [<sup>177</sup>Lu]-AM-NT 2 was used as a reference compound for comparison. The peptide conjugates were synthesized, purified and characterized as described in chapter 3.1.1. They were obtained in moderate to good yields and high purities (Table 26).

**Table 26:** Structures and analytical data of AM-NT 2 and AM-NT 11-14.

	Structure	MW (g/mol)	ESI-HRMS [M+2H] <sup>2+</sup>	Yield (%)	Purity (%)
<b>AM-NT 2</b> (1 <sup>st</sup> G. Reference) <sup>a</sup>	DOTA-PEG <sub>4</sub> -Arg-Arg-Pro-Tyr-Ile-Leu	1449.82	725.92	2	> 99
<b>AM-NT 11</b>	DOTA-PEG <sub>4</sub> -Arg-Arg-Pro-Tyr-Tle-Leu	1449.82	725.92	30	> 99
<b>AM-NT 12</b>	DOTA-PEG <sub>4</sub> -Arg-Lys-Pro-Tyr-Tle-Leu	1421.81	711.91	52	> 99
<b>AM-NT 13</b>	DOTA-PEG <sub>4</sub> -Lys-Arg-Pro-Tyr-Tle-Leu	1421.81	711.91	58	> 99
<b>AM-NT 14</b>	DOTA-PEG <sub>4</sub> -Lys-Lys-Pro-Tyr-Tle-Leu	1393.81	697.91	71	> 99

The radiolabelling of the peptide conjugates **AM-NT 11-14** was performed as described in chapter 3.1.1. **Table 27** summarizes the sequences of the radiolabelled conjugates and their radiochemical yields and purities.

**Table 27:** Radiolabelled peptide conjugates [<sup>177</sup>Lu]-AM-NT 11-13 and their radiolabelling yield and purities.

	Structure	Radiochemical Yield (%)	Radiochemical Purity (%)
[ <sup>177</sup> Lu]-AM-NT 11	[ <sup>177</sup> Lu]-DOTA-PEG <sub>4</sub> -Arg-Arg-Pro-Tyr-Tle-Leu	> 95	> 98
[ <sup>177</sup> Lu]-AM-NT 12	[ <sup>177</sup> Lu]-DOTA-PEG <sub>4</sub> -Arg-Lys-Pro-Tyr-Tle-Leu		
[ <sup>177</sup> Lu]-AM-NT 13	[ <sup>177</sup> Lu]-DOTA-PEG <sub>4</sub> -Lys-Arg-Pro-Tyr-Tle-Leu		
[ <sup>177</sup> Lu]-AM-NT 14	[ <sup>177</sup> Lu]-DOTA-PEG <sub>4</sub> -Lys-Lys-Pro-Tyr-Tle-Leu		

### 3.3.1.1 Biological Investigation of [<sup>177</sup>Lu]-AM-NT 11-14.

The radiolabelled peptidomimetics [<sup>177</sup>Lu]-AM-NT 11-14 were biologically evaluated and compared side-by-side with the reference compound [<sup>177</sup>Lu]-AM-NT 2. The cell internalisation in HT-29 cells, the receptor binding affinity and specificity to NTR1 of the compounds were measured, and the lipophilicity as well as the stability in blood serum were determined. For a detailed description of the biological essays, see chapter 3.1.2. The results of these biological investigations of peptide conjugates [<sup>177</sup>Lu]-AM-NT 11-14 are summarized in **Table 28**.

**Table 28:** Biological and physico-chemical properties of [<sup>177</sup>Lu]-AM-NT 2 and [<sup>177</sup>Lu]-AM-NT 11-14.

	Internalisation (%) after 4 h	K <sub>D</sub> (nM)	B <sub>max</sub> (nM)	Log D	Stability % after 4 h
[ <sup>177</sup> Lu]-AM-NT 2 (1 <sup>st</sup> G. Reference) <sup>a</sup>	7.3 ± 0.4	3.8 ± 0.9	0.37 ± 0.02	-2.6	0.9
[ <sup>177</sup> Lu]-AM-NT 11	1.3 ± 0.2	507 ± 114	1.6 ± 0.2	-2.2	70.6
[ <sup>177</sup> Lu]-AM-NT 12	0.23 ± 0.02	>1000	n.d.	-2.1	95.6
[ <sup>177</sup> Lu]-AM-NT 13	0.56 ± 0.02	>1000	n.d.	-2.1	95.7
[ <sup>177</sup> Lu]-AM-NT 14	0.3 ± 0.01	246 ± 44	0.80 ± 0.06	-2.0	91.1

<sup>a</sup> 1<sup>st</sup> generation reference

The internalized fractions of the conjugates [<sup>177</sup>Lu]-AM-NT 11-14 were very small when compared to [<sup>177</sup>Lu]-AM-NT 2 as well as the peptide conjugates of the first generation of triazole-peptidomimetics (see chapter 3.2.3). The highest internalisation rate was observed for peptide conjugate [<sup>177</sup>Lu]-AM-NT 11, with 1.3% cell internalisation after 4 h of incubation. The peptide conjugates in which arginine was substituted with lysine internalized below 1.0% within 4 h of incubation (**Figure 29**).



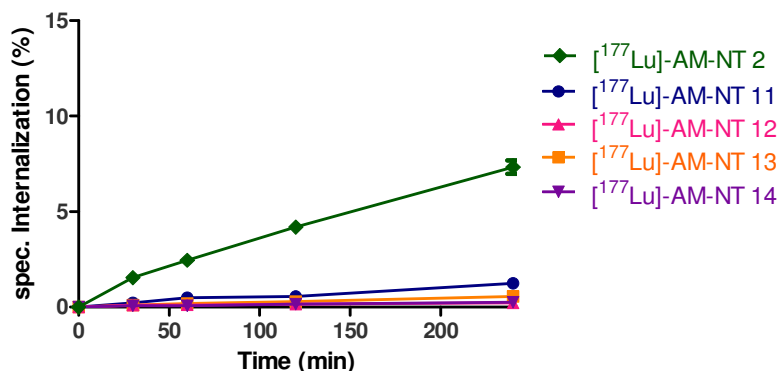


Figure 29: Cell internalisation data of [<sup>177</sup>Lu]-AM-NT 11-14.

Performing  $K_D$  experiments with radiolabelled NT (8-13) peptidomimetics that exhibit such a low receptor affinity represented a challenge. In order to obtain a saturation of the receptors, the concentration of the peptide conjugates was increased up to 800 nM, four times more than in the experimental setup used for the first generation of triazole-peptidomimetics. Even under these conditions, receptor saturation was barely reached. [<sup>177</sup>Lu]-AM-NT 11 exhibited a  $K_D$  value of  $504 \pm 114$  nM and [<sup>177</sup>Lu]-AM-NT 14, a value of  $246 \pm 44$  nM. This means that both peptide conjugates had an receptor affinity towards the NTR 1 which was more than an order of magnitude lower than the receptor affinity of the reference [<sup>177</sup>Lu]-AM-NT 2. Nonetheless, both were still in the nanomolar range. [<sup>177</sup>Lu]-AM-NT 12 and [<sup>177</sup>Lu]-AM-NT 13, the peptide conjugates with Lys residues instead of Arg exhibited  $K_D$  values of over 1000 nM, indicating abolished affinities towards NTR1 (Figure 30).

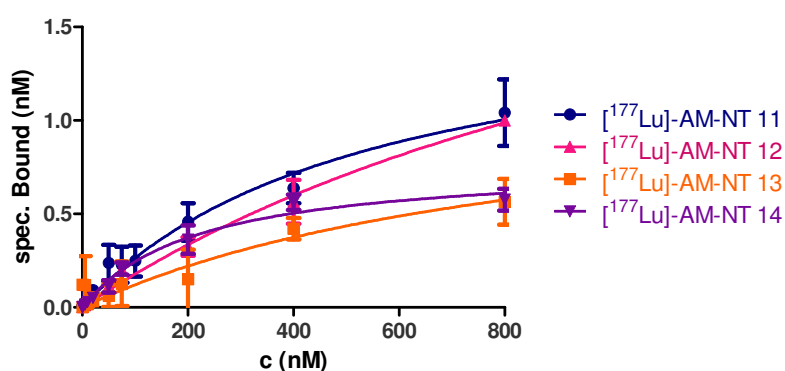
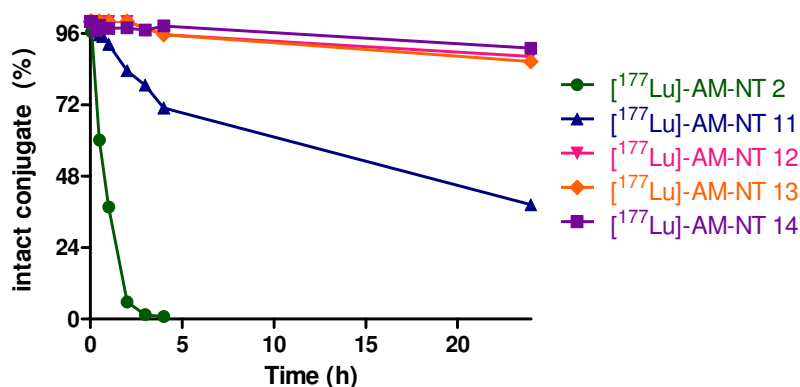


Figure 30: Results of the receptor saturation experiments of [<sup>177</sup>Lu]-AM-NT 11-14.

The log D values of the peptide conjugates [<sup>177</sup>Lu]-AM-NT 11-14 were determined as described in chapter 3.1.2. Very similar values between -2.0 and -2.2 were measured; comparable to the value obtained for the reference [<sup>177</sup>Lu]-AM-NT 2.

Serum stabilities were measured in fresh human serum. [ $^{177}\text{Lu}$ ]-AM-NT 11, with Tle<sup>12</sup> replacing Ile<sup>12</sup>, was considerably less stable than the others, with only ca. 4% intact conjugate after 24 h of incubation. The introduction of lysine as a substitute of Arg<sup>8</sup> and Arg<sup>9</sup> led to a great improvement of the stabilities of the conjugates. Over 90% of the peptide conjugates [ $^{177}\text{Lu}$ ]-AM-NT 12-14 remained intact after 24 h of incubation (**Figure 31**). These conjugates were so stable that no full degradation of the sequence was observed, even after several days of incubation. As a consequence, only an approximation of half-lives was possible. To enable a comparison with other NT (8-13) analogues, the stability of the peptide conjugates was evaluated after 4 h incubation. **Figure 31** shows the degradation of the peptide conjugates up to 24 h of incubation.



**Figure 31:** Serum stabilities of [ $^{177}\text{Lu}$ ]-AM-NT 2 and [ $^{177}\text{Lu}$ ]-AM-NT 11-14.

### 3.3.1.2 Discussion of the *In Vitro* Evaluation of [ $^{177}\text{Lu}$ ]-AM-NT 11-14

Four new NT (8-13) analogues were synthesised and fully evaluated *in vitro*. An Ile<sup>12</sup> to Tle<sup>12</sup> switch was introduced in all four compounds. Additionally two mono-substituted and one di-substituted Lys-derivatives of NT (8-13) were synthesized. A direct comparison of the influence of these amino acid substitutions on NT (8-13) analogues has not yet been reported and is important for future research.

The results of the biological investigation were surprising, as all of the peptide conjugates showed very low internalisations into HT-29 cells. These findings cannot be compared to subject-specific literature, as cell internalisation data of NT (8-13) analogues is seldom published. Detailed internalisation data for NT (8-13) analogues with a Tle<sup>12</sup> substitution was only published by the group of Schubiger.<sup>[98]</sup> The peptide analogues described in this

publication showed 5-10% internalisation into HT-29 cells after 4 h of incubation and a high nanomolar receptor affinity (see chapter 1.5.4). However, these NT (8-13) analogues were labelled with a different chelator and radiometal ( $^{99m}\text{Tc}$ ) and were additionally modified using other stabilization strategies. A direct comparison with [ $^{177}\text{Lu}$ ]-AM-NT 11-14 is therefore not possible.

The  $K_D$  values correlated with the low cell internalisations of these compounds. The data of the receptor saturation assays allows the conclusion that the introduction of a Tle in position 12 of the NT (8-13) sequence led to a loss of receptor affinity towards NTR1, when compared to the reference [ $^{177}\text{Lu}$ ]-AM-NT 2. Furthermore, the introduction of a single lysine in position 8 or 9 resulted in a complete loss of receptor affinity, whereas a double substitution of positions 8 and 9 with lysine provided a compound with somewhat retained receptor affinity. These observations are in contrast to the receptor binding affinity data published for mono- and di-substituted Lys-derivatives of NT (8-13). Mono- and di-substituted Lys derivatives of NT (8-13) are described in literature to have a high receptor affinity towards NTR1. However,  $K_D$  values are only available for  $^{99m}\text{Tc}$ -labelled NT analogues.<sup>[6, 84]</sup> For other cases no saturation binding but ligand competition experiments were performed and only  $K_i$  values derived from  $\text{IC}_{50}$  (ligand competition experiments) are reported.<sup>[85-86, 94, 103]</sup>

The metabolic stabilities were dramatically increased by the amino acid substitutions, especially when a lysine was introduced to the sequence. Peptide conjugate [ $^{177}\text{Lu}$ ]-AM-NT 11, with a single modification, was the least stable of the four tested, but compared to reference compound [ $^{177}\text{Lu}$ ]-AM-NT 2, its stability was substantially improved.

In general, it can be concluded that the introduction of a Tle<sup>12</sup> in the place of Ile<sup>12</sup> led to compounds with great stability, but with a decreased cell internalisation and receptor affinity towards the NTR1 receptor, contrary to what is suggested by literature data.<sup>[6, 86, 98, 104-106, 112]</sup>

The mono-substituted Lys-derivatives of NT (8-13) were not considered further because they did not retain a high receptor affinity towards NTR1, a requirement for the development of tumour-targeting radiopeptides. [ $^{177}\text{Lu}$ ]-AM-NT 11, was chosen for further optimization, because of its cell internalisation properties and its nanomolar receptor affinity towards NTR1.

### 3.3.2 Synthesis of the Second Generation of Triazole-Containing NT (8-13) Analogues

The exchange of Ile with Tle in position 12 of NT (8-13) led to a significant improvement of the metabolic stabilities of NT (8-13) analogues while their receptor affinities as well as their specificities towards the NTR1 receptor were maintained. Based on the lead compound identified in the previous chapter 3.3.1, [<sup>177</sup>Lu]-AM-NT 11, we set out to further optimize the biological characteristics of the peptidic vector. Towards this end, the backbone amide bonds of [<sup>177</sup>Lu]-AM-NT 11 were replaced with 1,4-disubstituted 1,2,3-triazoles at the positions previously identified during the ‘triazole-scan’ of NT (8-13) (chapter 3.2), namely those between the *N*-terminal PEG<sub>4</sub> spacer and Arg<sup>8</sup> and between Arg<sup>8</sup> and Arg<sup>9</sup>. Two mono- and one di-substituted peptide conjugates were synthesized and their biological evaluation was compared side by side to first generation reference [<sup>177</sup>Lu]-AM-NT 2 and second generation reference [<sup>177</sup>Lu]-AM-NT 11.

The synthesis of the peptide conjugates of AM-NT 15-17 was performed as described in chapter 3.2.2. The three conjugates were obtained in moderate yields and in high purities. **Table 29** shows the structures of AM-NT 15-17 and their analytical data.

**Table 29:** Structure and analytical data of AM-NT 2, AM-NT 11 and AM-NT 15-17.

	Structure	MW (g/mol)	ESI-HRMS [M+2H] <sup>2+</sup>	Yield (%)	Purity (%)
<b>AM-NT 2</b> (1 <sup>st</sup> G. Reference) <sup>a</sup>	DOTA-PEG <sub>4</sub> -Arg-Arg-Pro-Tyr-Ile-Leu	1449.82	725.92	2	> 99
<b>AM-NT 11</b> (2 <sup>nd</sup> G. Reference) <sup>b</sup>	DOTA-PEG <sub>4</sub> -Arg-Arg-Pro-Tyr-Tle-Leu	1449.82	725.92	30	> 99
<b>AM-NT 15</b>	DOTA-PEG <sub>4</sub> -Arg- <del>ψ</del> [Tz]-Arg-Pro-Tyr-Tle-Leu	1473.83	737.92	16	> 99
<b>AM-NT 16</b>	DOTA-PEG <sub>4</sub> - <del>ψ</del> [Tz]-Arg-Arg-Pro-Tyr-Tle-Leu	1459.81	730.91	16	> 98
<b>AM-NT 17</b>	DOTA-PEG <sub>4</sub> - <del>ψ</del> [Tz]-Arg- <del>ψ</del> [Tz]-Arg-Pro-Tyr-Tle-Leu	1483.83	742.92	9	> 99

<sup>a</sup> 1<sup>st</sup> generation reference. <sup>b</sup> 2<sup>nd</sup> generation reference.

After the synthesis and purification, the peptide conjugates were successfully labelled with [<sup>177</sup>Lu]LuCl<sub>3</sub>, as described in chapter 3.1.1. **Table 30** shows the structure of the radiolabelled NT (8-13) analogues as well as their radiochemical yields and purities.

**Table 30:** Radiolabelled conjugates [<sup>177</sup>Lu]-AM-NT 2, [<sup>177</sup>Lu]-AM-NT 11 and [<sup>177</sup>Lu]-AM-NT 15-17 and their radiolabelling yields and purities.

	Structure	Radiochemical Yield (%)	Radiochemical Purity (%)
<b>[<sup>177</sup>Lu]-AM-NT 15</b>	[ <sup>177</sup> Lu]-DOTA-PEG <sub>4</sub> -Arg- <del>ψ</del> [Tz]-Arg-Pro-Tyr-Tle-Leu		
<b>[<sup>177</sup>Lu]-AM-NT 16</b>	[ <sup>177</sup> Lu]-DOTA-PEG <sub>4</sub> - <del>ψ</del> [Tz]-Arg-Arg-Pro-Tyr-Tle-Leu	> 95	> 98
<b>[<sup>177</sup>Lu]-AM-NT 17</b>	[ <sup>177</sup> Lu]-DOTA-PEG <sub>4</sub> - <del>ψ</del> [Tz]-Arg- <del>ψ</del> [Tz]-Arg-Pro-Tyr-Tle-Leu		

### 3.3.2.1 Biological Investigation of the Second Generation of Triazole-Containing NT (8-13) Analogues

The results of the evaluation of the biological behaviour as well as the physico-chemical properties of the triazole backbone modified NT (8-13) analogues [ $^{177}\text{Lu}$ ]-AM-NT 15-17 are shown in **Table 31**. For a comparison, the biological data of the first generation reference compound [ $^{177}\text{Lu}$ ]-AM-NT 2 and the second generation reference compound [ $^{177}\text{Lu}$ ]-AM-NT 11 are also listed.

**Table 31:** Biological properties of [ $^{177}\text{Lu}$ ]-AM-NT 2, [ $^{177}\text{Lu}$ ]-AM-NT 11 and [ $^{177}\text{Lu}$ ]-AM-NT 15-17.

Name	Internalisation after 4 h (%)	K <sub>D</sub> (nM)	B <sub>max</sub> (nM)	Log D	Stability % after 4 h
[ $^{177}\text{Lu}$ ]-AM-NT 2 (1 <sup>st</sup> G. Reference) <sup>a</sup>	7.3 ± 0.4	3.8 ± 0.9	0.37 ± 0.02	-2.6	0.9
[ $^{177}\text{Lu}$ ]-AM-NT 11 (2 <sup>nd</sup> G. Reference) <sup>b</sup>	1.3 ± 0.2	507 ± 114	1.6 ± 0.2	-2.2	70.6
[ $^{177}\text{Lu}$ ]-AM-NT 15	2.1 ± 0.1	214 ± 45	n.d.	-2.2	97.7
[ $^{177}\text{Lu}$ ]-AM-NT 16	1.2 ± 0.2	>1000	n.d.	-2.2	94.7
[ $^{177}\text{Lu}$ ]-AM-NT 17	2.19 ± 0.01	>1000	n.d.	-2.3	97.2

<sup>a</sup> 1<sup>st</sup> generation reference. <sup>b</sup> 2<sup>nd</sup> generation reference.

All the peptide conjugates showed a low internalisation profile (1.2-2.2%) when compared to the reference compound of the first generation of triazole-peptide conjugates, [ $^{177}\text{Lu}$ ]-AM-NT 2. The cell internalisation of [ $^{177}\text{Lu}$ ]-AM-NT 15 and [ $^{177}\text{Lu}$ ]-AM-NT 17 into HT-29 cells was around 2.1% within 4 h of incubation, which was twice the internalisation rate of the reference compound of the second generation of triazole-peptides, [ $^{177}\text{Lu}$ ]-AM-NT 11. [ $^{177}\text{Lu}$ ]-AM-NT 16, the conjugate with the triazole modification between the *N*-terminal PEG<sub>4</sub> spacer and Arg<sup>8</sup>, internalized into HT-29 cells to a similar extent as the reference compound [ $^{177}\text{Lu}$ ]-AM-NT 11. [ $^{177}\text{Lu}$ ]-AM-NT 16 has therefore the lowest internalisation profile of the second generation peptide conjugates (**Figure 32**).

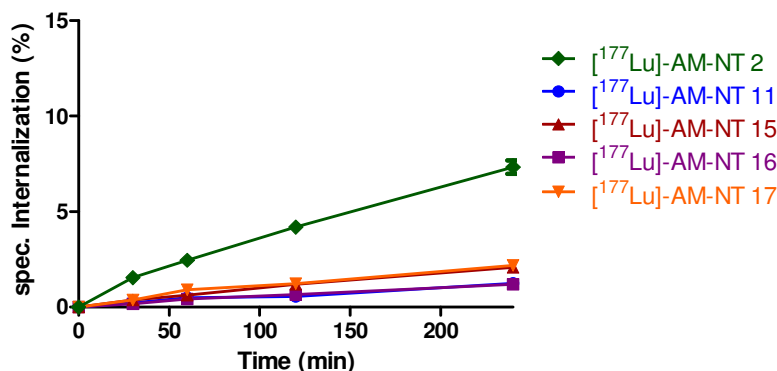


**Figure 32:** Cell internalisation data of [<sup>177</sup>Lu]-AM-NT 2, [<sup>177</sup>Lu]-AM-NT 11 and [<sup>177</sup>Lu]-AM-NT 15-17.

The measurement of the lipophilicity (log D) of the compounds [<sup>177</sup>Lu]-AM-NT 15-17 showed values between -2.2 and -2.3, which suggests the hydrophilic nature of the peptide conjugates [<sup>177</sup>Lu]-AM-NT 15-17. These log D values were comparable to the ones measured for the reference compounds [<sup>177</sup>Lu]-AM-NT 2 and [<sup>177</sup>Lu]-AM-NT 11.

Due to the low internalisation rates of NT (8-13) analogues [<sup>177</sup>Lu]-AM-NT 15-17, the determination of their receptor binding affinities by receptor saturation experiments was once more challenging. No receptor saturation was observed with the experimental conditions described in chapter 3.1.2. The concentration of the peptide conjugates had to be increased up to 800 nM for [<sup>177</sup>Lu]-AM-NT 15 and up to 3200 nM for conjugates [<sup>177</sup>Lu]-AM-NT 16 and [<sup>177</sup>Lu]-AM-NT 17. No receptor saturation was reached even under these extreme conditions and thus, the  $K_D$  values of [<sup>177</sup>Lu]-AM-NT 16 and [<sup>177</sup>Lu]-AM-NT 17 were determined to be outside of the nanomolar range (> 1000 nM). Peptide conjugate [<sup>177</sup>Lu]-AM-NT 15 exhibited a low, but improved receptor binding affinity of  $214 \pm 45$  nM, when compared to reference compound [<sup>177</sup>Lu]-AM-NT 11. The results of the binding saturation experiments for [<sup>177</sup>Lu]-AM-NT 15-17 are shown in **Figure 33**.

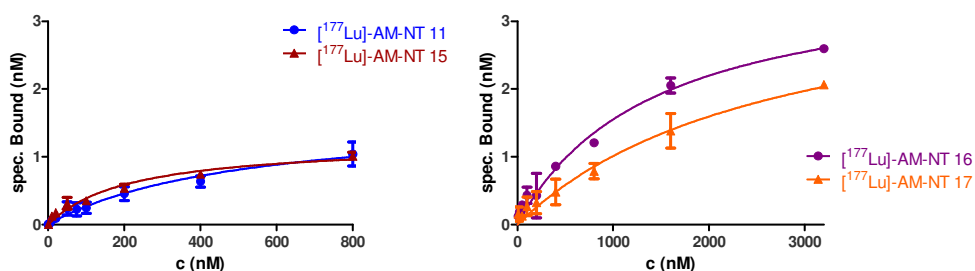


**Figure 33:** Results of the receptor saturation experiments of [<sup>177</sup>Lu]-AM-NT 11 and [<sup>177</sup>Lu]-AM-NT 15-17.

Serum stabilities experiments were performed as described in chapter 3.1.2. As expected, the introduction of an Ile<sup>12</sup> to Tle<sup>12</sup> residue switch had a major impact on the metabolic stabilities of the compounds. Over 90% of the peptide conjugates [<sup>177</sup>Lu]-AM-NT 15-17 were still intact after 4 h of incubation. After 24 h of incubation, over 70% of the peptide conjugates were intact (**Figure 34**). In comparison, the reference compound of the first generation ([<sup>177</sup>Lu]-AM-NT 2) was completely degraded after 4 h of incubation and the reference compound of the second generation ([<sup>177</sup>Lu]-AM-NT 11) was only 38% intact after 24 h of incubation.

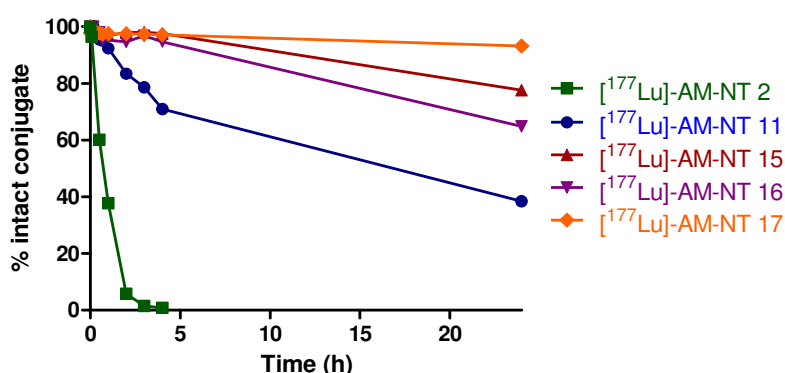


**Figure 34:** Serum stabilities of [<sup>177</sup>Lu]-AM-NT 11 and [<sup>177</sup>Lu]-AM-NT 15-17.

### 3.3.2.2 Discussion of the *In Vitro* Evaluation of [<sup>177</sup>Lu]-AM-NT 15-17

The second generation of triazole-containing NT (8-13) analogues was successfully synthesized and biologically evaluated. The *in vitro* evaluation was compared side by side with the reference compounds of the first generation, [<sup>177</sup>Lu]-AM-NT 2 and of the second generation, [<sup>177</sup>Lu]-AM-NT 11.

The internalisation rates of the three NT (8-13) analogues [<sup>177</sup>Lu]-AM-NT 15-17 were low, in comparison to [<sup>177</sup>Lu]-AM-NT 2, but similar to the reference compound of the second generation, [<sup>177</sup>Lu]-AM-NT 11.

The low internalisation rates of [<sup>177</sup>Lu]-AM-NT 15-17 were confirmed by the receptor saturation experiments. The receptor binding affinity was only preserved for [<sup>177</sup>Lu]-AM-NT 15. Unfortunately, the introduction of *tert*-leucine led to an abolished receptor affinity towards the NTR1 receptor for the triazole-containing peptide conjugates [<sup>177</sup>Lu]-AM-NT 16 and [<sup>177</sup>Lu]-AM-NT 17.

Despite of the loss of affinity, a positive effect of the triazole on the metabolic stability of a NT (8-13) analogue was observed, in addition to the Ile<sup>12</sup> to Tle<sup>12</sup> residue switch. The reference peptide conjugate of the second generation of triazole-peptidomimetics, [<sup>177</sup>Lu]-AM-NT 11, remained 70% stable after 4 h of incubation in serum, whereas [<sup>177</sup>Lu]-AM-NT 15, [<sup>177</sup>Lu]-AM-NT 16, and [<sup>177</sup>Lu]-AM-NT 17 remained stable 97%, 95% and 97%, respectively. After 24 h, only 40% of the peptide conjugates [<sup>177</sup>Lu]-AM-NT 11 was still intact. The conjugates with a single triazole modification ([<sup>177</sup>Lu]-AM-NT 15 and [<sup>177</sup>Lu]-AM-NT 16) remained intact over 65%, whereas the *bis*-triazole analogue ([<sup>177</sup>Lu]-AM-NT 17) remained intact over 93%, suggesting that two triazoles substantially improved the stability of a [Tle<sup>12</sup>]NT (8-13) conjugate. The stabilities measured for these compounds are in good agreement with the stabilities published for [Tle<sup>12</sup>]NT (8-13) analogues, containing additional modifications on the C-terminus, like *N*-methylation.<sup>[100, 111]</sup>

Thus, from the second generation of triazole-modified NT (8-13) analogues, [<sup>177</sup>Lu]-AM-NT 15 was identified as a peptide conjugate with a retained nanomolar affinity towards the NTR1 receptor and further improved metabolic stability.

In summary, the *in vitro* evaluation of several novel <sup>177</sup>Lu-labelled NT (8-13) peptidomimetics provided a set of novel radiolabelled peptide conjugates with promising properties. However, to draw definitive conclusions about the newly identified peptide conjugates, their *in vivo* behaviour needs to be studied. In chapter 3.4, the biodistributions of selected triazole-containing NT (8-13) analogues of the first and the second generation will be discussed.



### 3.4 *In Vivo* Evaluation

The compounds of the first and the second generation of triazole-backbone modified NT (8-13) analogues with a retained receptor affinity towards NTR1 were evaluated *in vivo*. Peptide conjugates [<sup>177</sup>Lu]-AM-NT 2 (reference compound of the 1<sup>st</sup> generation) and [<sup>177</sup>Lu]-AM-NT 11 (reference compound of 2<sup>nd</sup> generation) were also evaluated for comparison (Table 32). Nude Foxn 1nu mice were implanted with a HT-29 xenograft on the right shoulder and the tumour was allowed to grow for 8 days. On the day of the experiment, the mice received the <sup>177</sup>Lu-labelled NT (8-13) analogue (10 pmol, 0.5-0.7 MBq per mouse), *via* tail vein injection. The mice were sacrificed in groups of five, 1 h, 4 h and 24 h post injection. Blocking experiments were performed at 1 h p.i. by co-injection of an excess of NT (1-13) (60 nmol/mouse). After the sacrifice of the mice, their organs were collected and the radioactivity accumulated in the organs was quantified in a gamma-counter. The tissue distribution data is presented as percentage of injected activity per gram of tissue (% ID/g).

**Table 32:** Triazole-backbone modified NT (8-13) analogues and reference compounds evaluated *in vivo*.

Name	Structure
[ <sup>177</sup> Lu]-AM-NT 2 (1 <sup>st</sup> G. reference) <sup>a</sup>	[ <sup>177</sup> Lu]-DOTA-PEG <sub>4</sub> -Arg-Arg-Pro-Tyr-Ile-Leu
[ <sup>177</sup> Lu]-AM-NT 8	[ <sup>177</sup> Lu]-DOTA-PEG <sub>4</sub> -Arg-Ψ[Tz]-Arg-Pro-Tyr-Ile-Leu
[ <sup>177</sup> Lu]-AM-NT 9	[ <sup>177</sup> Lu]-DOTA-PEG <sub>4</sub> -Ψ[Tz]-Arg-Arg-Pro-Tyr-Ile-Leu
[ <sup>177</sup> Lu]-AM-NT 10	[ <sup>177</sup> Lu]-DOTA-PEG <sub>4</sub> -Ψ[Tz]-Arg-Ψ[Tz]-Arg-Pro-Tyr-Ile-Leu
[ <sup>177</sup> Lu]-AM-NT 11 (2 <sup>nd</sup> G reference) <sup>b</sup>	[ <sup>177</sup> Lu]-DOTA-PEG <sub>4</sub> -Arg-Arg-Pro-Tyr-Tle-Leu
[ <sup>177</sup> Lu]-AM-NT 15	[ <sup>177</sup> Lu]-DOTA-PEG <sub>4</sub> -Arg-Ψ[Tz]-Arg-Pro-Tyr-Tle-Leu

<sup>a</sup> 1<sup>st</sup> generation reference. <sup>b</sup> 2<sup>nd</sup> generation reference.

In general, the biodistribution profiles of the radiolabelled NT (8-13) analogues showed an increased accumulation of radioactivity in the NTR1 positive tumour, the intestine, the colon and the kidneys. The uptake in the gastrointestinal tract (NTR1-positive organs) and the tumour could be blocked with an excess of NT (1-13), which means that the uptake was specific and receptor-mediated. The unspecific uptake of radioactivity in the kidneys was the result of renal excretion, a commonly observed feature of radiolabelled peptide conjugates. All peptide conjugates were rapidly distributed in the body and showed a fast blood clearance. The unspecific uptake of the radiotracers in other organs and tissues was almost negligible (<0.3% ID/g). The low uptake in the liver indicated the absence of hepatobiliary excretion of the peptide conjugates and its metabolites. None of the radiolabelled conjugates was able to cross the brain-blood-barrier, as no uptake was observed in the receptor-positive brain.

The highest accumulation of radioactivity in the tumour, kidneys and gastrointestinal tract was observed at 1 h p.i. A washout of radioactivity from the organs at 4 h and 24 h p.i was observed for all the evaluated conjugates. The tumour uptake of the radiolabelled NT (8-13) analogues was generally low (< 2.2% ID/g). These values are in agreement with the *in vivo* data of related radiometallated NT (8-13) analogues described in literature.<sup>[84, 86, 93, 96, 100, 102, 106, 112]</sup> The low NTR1 receptor density on the tumour tissue could explain the low uptake of the radiolabelled conjugate,<sup>[5]</sup> but factors like the receptor affinity and the metabolic stability of the injected peptide conjugate may as well play a role. It should be noted that not only the absolute uptake of the radiotracer in the tumour is important, but also the ratio of uptake in the tumour to other organs. The higher the tumour to tissues ratio, the better is the potential of the investigated radioligand for diagnostic (better imaging quality) and therapeutic applications (dosimetry issues). Also, the radiation sensitive kidneys are usually the dose-limiting organs with respect to peptidic radiopharmaceuticals and thus, particular attention is given in the following to the tumour to kidney ratios.

For the reference compound of the first generation, [<sup>177</sup>Lu]-AM-NT 2, 1.1% of the total injected dose was accumulated in the tumour at 1 h p.i. (**Figure 35**). Almost a third of the activity was washed out of the tumour at 4 h p.i., and at 24 h p.i. only 0.5% ID/g was left. The radioactivity accumulated in the kidneys was in the same range as for the tumour. The washout from the kidney was slower, as after 24 h 0.7% ID/g remained.

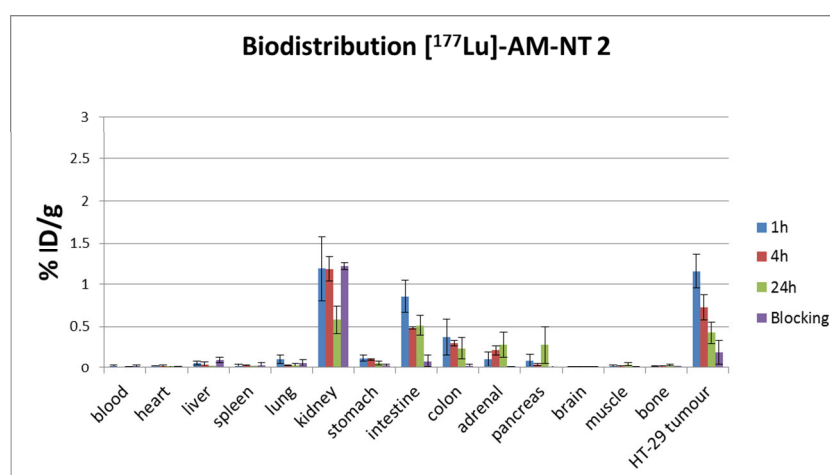


**Figure 35:** Biodistribution profile of analogue [<sup>177</sup>Lu]-AM-NT 2.

Peptide conjugate [<sup>177</sup>Lu]-AM-NT 8, with a single triazole at the Arg<sup>8</sup>-Arg<sup>9</sup> position, showed a tumour uptake of 2.0% ID/g (1 h p.i.), which was twice as much as that for the reference [<sup>177</sup>Lu]-AM-NT 2. The uptake of radioactivity in the kidneys was also slightly increased. This

increase was in the same range as the increase in tumour uptake. At 24 h p.i., 50% of the accumulated radioactivity was washed out of the organs, while 1.0% ID/g remained in the tumour and 1.1% ID/g in the kidneys. The biodistribution of [ $^{177}\text{Lu}$ ]-AM-NT 8 is shown in **Figure 36**.

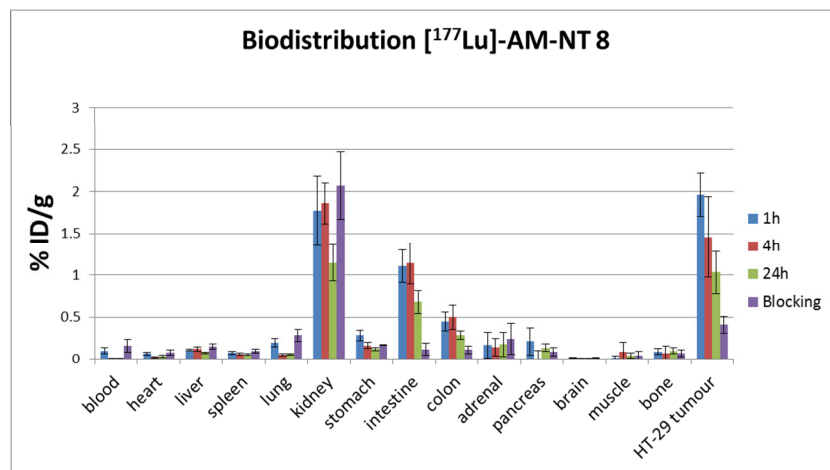


**Figure 36:** Biodistribution profile of analogue [ $^{177}\text{Lu}$ ]-AM-NT 8.

The biodistribution profile of [ $^{177}\text{Lu}$ ]-AM-NT 9 was very interesting because of the low uptake of radioactivity in the receptor-positive gastrointestinal tract and in the kidneys (**Figure 37**). Although the tumour uptake (1.1% ID/g) was only in the range of the reference analogue [ $^{177}\text{Lu}$ ]-AM-NT 2, peptide conjugate [ $^{177}\text{Lu}$ ]-AM-NT 9 exhibited the best tumour to kidney ratio (at 1 h p.i.) of all the compounds tested (**Figure 41**).

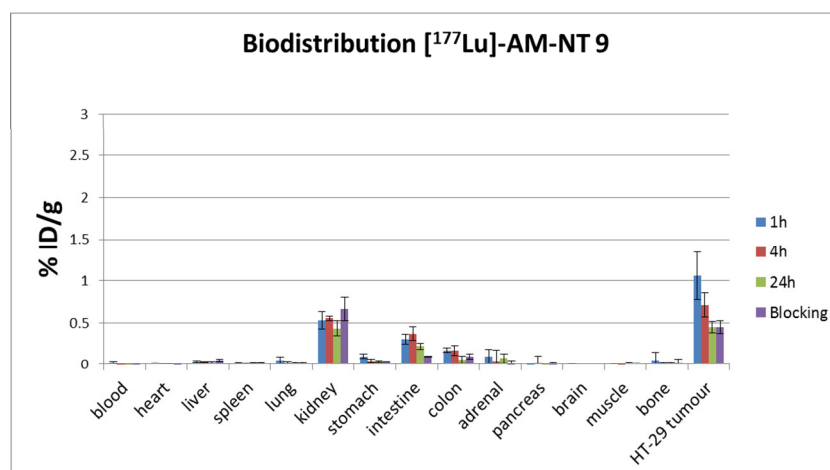


**Figure 37:** Biodistribution profile of analogue [ $^{177}\text{Lu}$ ]-AM-NT 9.

The peptide conjugate with multiple triazoles, [ $^{177}\text{Lu}$ ]-AM-NT 10, exhibited a relatively high tumour uptake of 1.9% ID/g (1 h p.i.), in comparison to reference compound [ $^{177}\text{Lu}$ ]-AM-NT

2. This was, in fact, a surprising result, because the metabolic stability of [ $^{177}\text{Lu}$ ]-AM-NT 10 in human blood serum was quite low. The uptake of radioactivity in the kidneys was the same range as the tumour uptake. After 24 h, approx. 50% of the accumulated radioactivity was washed out of the kidneys, while 0.9% ID/g remained in the tumour and 1.2% ID/g in the kidneys. The biodistribution of [ $^{177}\text{Lu}$ ]-AM-NT 10 is shown in **Figure 38**.

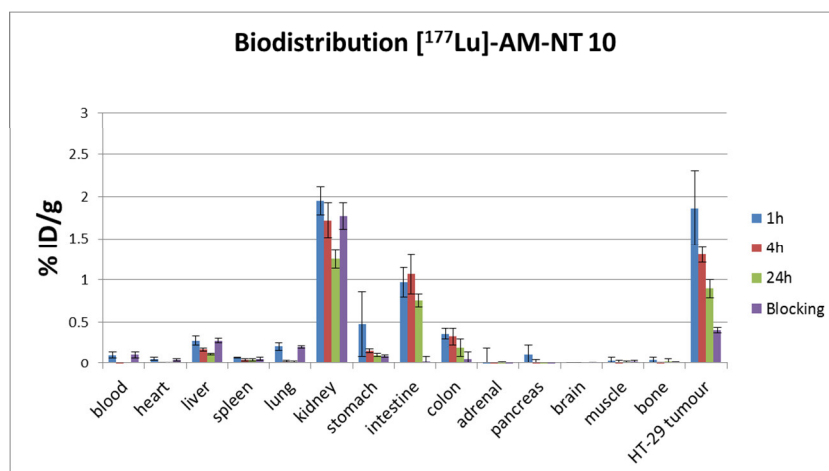


**Figure 38:** Biodistribution profile of analogue [ $^{177}\text{Lu}$ ]-AM-NT 10.

The reference compound of the second generation of triazole-peptidomimetics (with the Ile<sup>12</sup> to Tle<sup>12</sup> residue switch), [ $^{177}\text{Lu}$ ]-AM-NT 11 displayed a similar biodistribution profile as the reference compound of the first generation [ $^{177}\text{Lu}$ ]-AM-NT 2 (**Figure 39**). The highest tumour uptake (1.0% ID/g) was observed 1 h p.i. Washout of the radioactivity was observed over time. In the contrary to the conjugates discussed so far, the kidney uptake was higher than the tumour uptake at all time points.

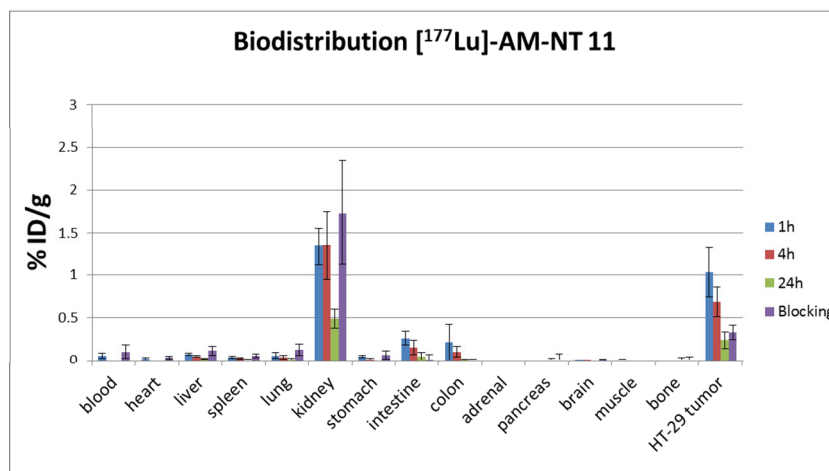


**Figure 39:** Biodistribution profile of analogue [ $^{177}\text{Lu}$ ]-AM-NT 11.

Peptide conjugate [ $^{177}\text{Lu}$ ]-AM-NT 15, a compound of the second generation, with a single triazole at the Arg<sup>8</sup>-Arg<sup>9</sup> position, showed a tumour uptake of 2.3% ID/g at 1 h p.i., which was twice as much as that of the reference of the second generation [ $^{177}\text{Lu}$ ]-AM-NT 11. At 1 h p.i., the peptide conjugate exhibited a good tumour to kidney ratio of 1.4 (Figure 41). However, the radioligand was then rapidly washed out of the tumour (1.0% ID/g at 4 h p.i. and 24 h p.i.), whereas the renal excretion was slower. The biodistribution of [ $^{177}\text{Lu}$ ]-AM-NT 15 is shown in Figure 40.

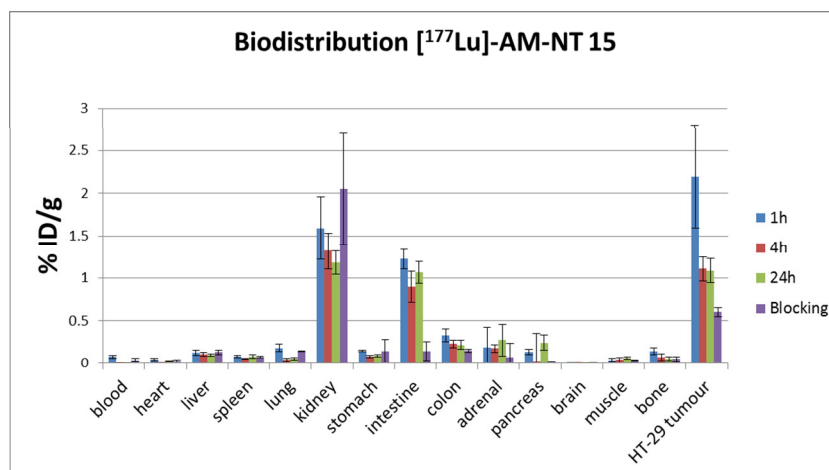


Figure 40: Biodistribution profile of analogue [ $^{177}\text{Lu}$ ]-AM-NT 15.

An accumulation of a peptidic radiotracer in an organ or tissue other than the targeted is, as mentioned before, unfavourable because it decreases the tumour to background ratio, which is important for diagnostics as well as represents an unnecessary radiation dose for a patient, if applied as a therapeutic agent. Figure 41 shows the tumour to kidney ratios of all the evaluated radiolabelled peptide conjugates at every time-point.

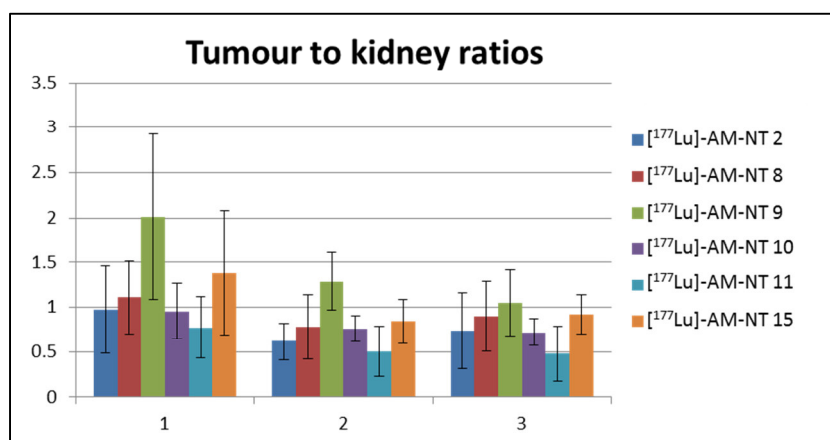
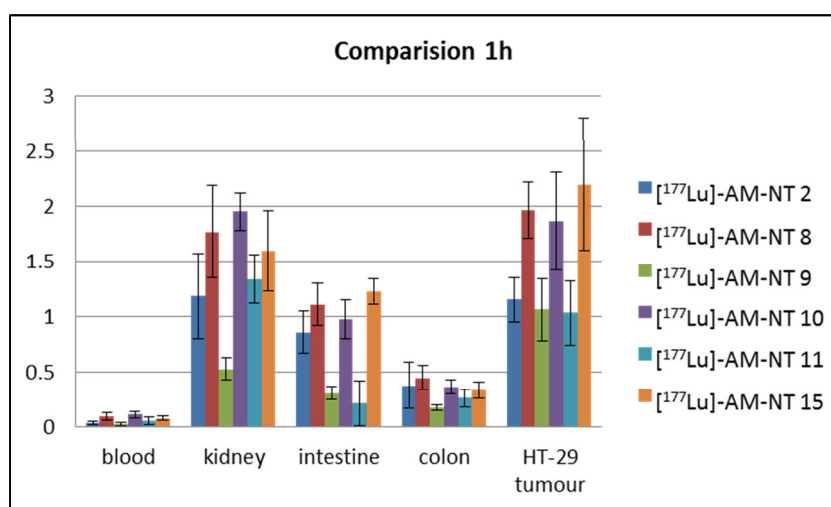


Figure 41: Tumour to kidney ratios at 1, 4 and 24 h p.i. of [ $^{177}\text{Lu}$ ]-AM-NT 2, [ $^{177}\text{Lu}$ ]-AM-NT 8, [ $^{177}\text{Lu}$ ]-AM-NT 9, [ $^{177}\text{Lu}$ ]-AM-NT 10 and [ $^{177}\text{Lu}$ ]-AM-NT 15.

A direct comparison of the uptakes (1, 4, 24 h p.i.) of the evaluated peptide conjugates in the tumour, the intestine and colon (receptor-positive tissues), the kidneys (dose-limiting organs) and the blood (to show blood clearance) are shown in **Figures 42-44**. At 1 h p.i., [<sup>177</sup>Lu]-AM-NT 8, [<sup>177</sup>Lu]-AM-NT 10 and [<sup>177</sup>Lu]-AM-NT 15 exhibited a significantly increased tumour uptake when compared to the unmodified references [<sup>177</sup>Lu]-AM-NT 2 and [<sup>177</sup>Lu]-AM-NT 11. Peptide conjugate [<sup>177</sup>Lu]-AM-NT 9, with a triazole between the *N*-terminal PEG<sub>4</sub> spacer and Arg<sup>8</sup>, exhibited a lower tumour uptake in comparison to the other triazole-containing conjugates, but the best tumour to organs ratio (**Figure 41**), in particular a high tumour to kidney ratio at 1 h p.i (**Figure 41**).



**Figure 42:** Comparison of the biodistribution profiles of [<sup>177</sup>Lu]-AM-NT 2, [<sup>177</sup>Lu]-AM-NT 8, [<sup>177</sup>Lu]-AM-NT 9, [<sup>177</sup>Lu]-AM-NT 10 and [<sup>177</sup>Lu]-AM-NT 15 at 1 h p.i.

At 4 h p.i., [<sup>177</sup>Lu]-AM-NT 8 had the highest tumour uptake, followed by the other Arg<sup>8</sup>-Ψ[Tz]-Arg<sup>9</sup>-containing peptides, [<sup>177</sup>Lu]-AM-NT 10 and [<sup>177</sup>Lu]-AM-NT 15. All three peptidomimetics exhibited similar tumour to kidney ratios. [<sup>177</sup>Lu]-AM-NT 9 still had the best overall tumour to kidney ratio, even though its tumour uptake was reduced to 0.6% ID/g.

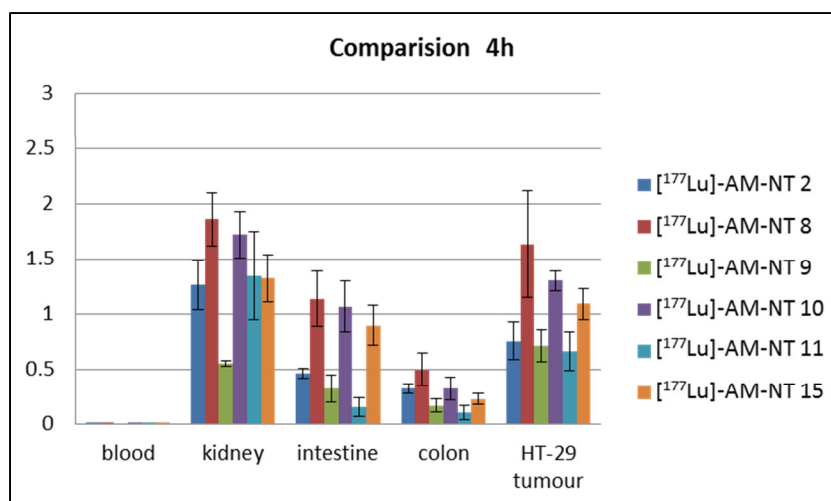


**Figure 43:** Comparison of the biodistribution profiles of [<sup>177</sup>Lu]-AM-NT 2, [<sup>177</sup>Lu]-AM-NT 8, [<sup>177</sup>Lu]-AM-NT 9, [<sup>177</sup>Lu]-AM-NT 10 and [<sup>177</sup>Lu]-AM-NT 15, 4 h p.i.

After 24 h, [<sup>177</sup>Lu]-AM-NT 8 and [<sup>177</sup>Lu]-AM-NT 15 (with Arg<sup>8</sup>-Ψ[Tz]-Arg<sup>9</sup>), had a similar tumour accumulation (**Figure 44**), as well as a comparable tumour to kidney ratio (**Figure 41**). The only difference in the *in vivo* behaviour of the two substances was the higher accumulation of radioactivity of [<sup>177</sup>Lu]-AM-NT 15 in the intestine, which is unfavourable due to high tumour to background ratio. The accumulation of radioactivity of [<sup>177</sup>Lu]-AM-NT 9 in the HT-29 tumour was substantially reduced (under 0.5% ID/g) and the tumour to kidney ratio was then comparable to the one of [<sup>177</sup>Lu]-AM-NT 8 and [<sup>177</sup>Lu]-AM-NT 15. The tumour uptake as well as the tumour to kidney ratio of [<sup>177</sup>Lu]-AM-NT 10 were slightly inferior to the mono-substituted peptide conjugates.

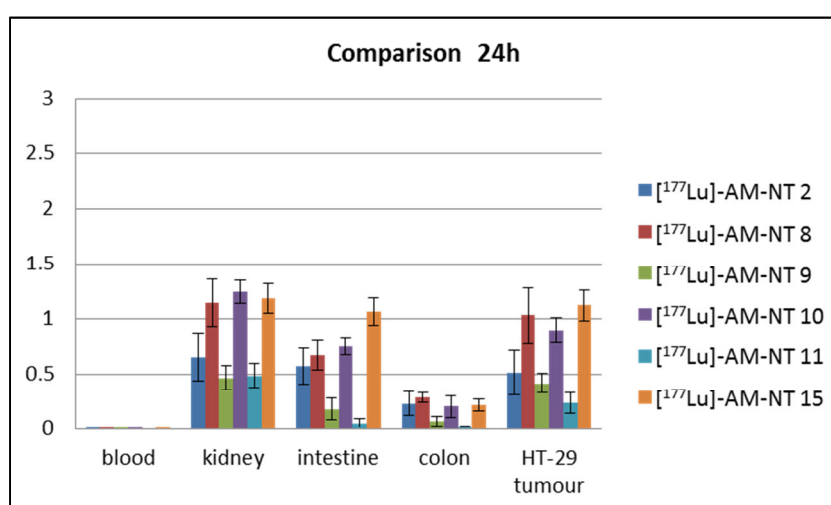


**Figure 44:** Comparison of the biodistribution profiles of [<sup>177</sup>Lu]-AM-NT 2, [<sup>177</sup>Lu]-AM-NT 8, [<sup>177</sup>Lu]-AM-NT 9, [<sup>177</sup>Lu]-AM-NT 10 and [<sup>177</sup>Lu]-AM-NT 15, 24 h p.i.

From the biodistribution data of the radiolabelled NT (8-13) analogues evaluated in this study it can be concluded that a an amide-to-triazole exchange of the Arg<sup>8</sup>-Arg<sup>9</sup> bond led to conjugates with an improved tumour uptake, when compared to reference compounds [<sup>177</sup>Lu]-AM-NT 2 (1<sup>st</sup> generation) and [<sup>177</sup>Lu]-AM-NT 11 (2<sup>nd</sup> generation). However, the Tle<sup>12</sup> substitution did not improve the tumour uptake of the second generation of triazole-peptidomimetics, despite of the increased stability of these conjugates.



### 3.4.1 *In Vivo* Imaging

[<sup>177</sup>Lu]-AM-NT 8 (1<sup>st</sup> generation, Arg<sup>8</sup>-Ψ[Tz]-Arg<sup>9</sup>) and [<sup>177</sup>Lu]-AM-NT 11 (reference 2<sup>nd</sup> generation) were selected to perform first *in vivo* imaging experiments using a small animal SPECT/CT camera. Even though not all compounds of interest could be included in this preliminary imaging study, the obtained images illustrate the potential of NT (8-13)-based radiopeptides for tumour targeting.

For the *in vivo* imaging experiments, the radiolabelled peptide conjugate (60 pmol/mouse, 13 MBq) was injected *via* the tail vein into a mouse with a HT-29 xenograft on the right shoulder. The mouse was then measured 1 h p.i. on a small animal SPECT/CT camera.

In the SPECT/CT-images of [<sup>177</sup>Lu]-AM-NT 11 (A) and [<sup>177</sup>Lu]-AM-NT 8 (B) in **Figure 45**, both the tumour and the kidneys are clearly visible. Little background radiation was observed in the images, confirming the fast clearance of the blood at 1 h p.i. determined in the biodistribution studies of the compounds (**Figure 42**).

From this preliminary *in vivo* imaging study it can be concluded that NT (8-13)-based radiopeptides could represent suitable probes for *in vivo* imaging of NTR1-positive tumours, despite the relatively low uptake of radioactivity in the tumours.

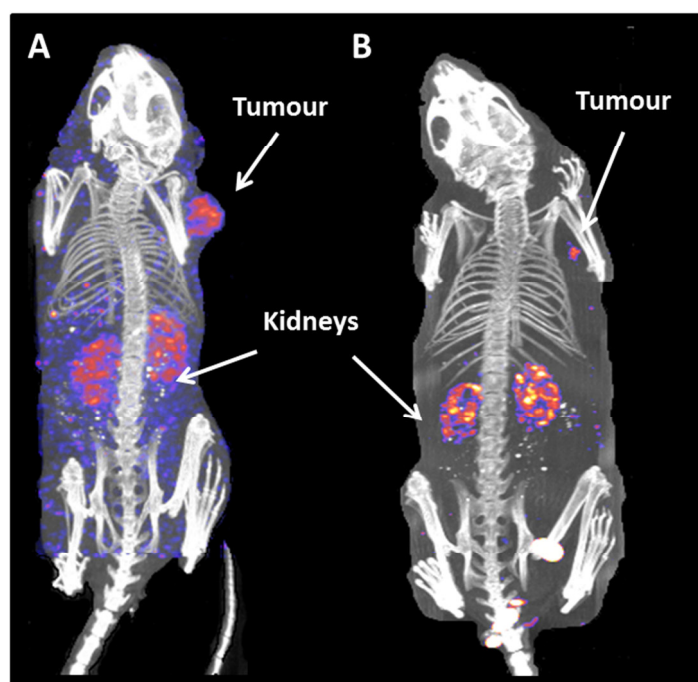


**Figure 45:** *In vivo* imaging. A: [<sup>177</sup>Lu]-AM-NT 11, B: [<sup>177</sup>Lu]-AM-NT 8.

### 3.4.2 Discussion of the *In Vivo* Evaluation

Reference compounds [<sup>177</sup>Lu]-AM-NT 2 (1<sup>st</sup> generation) and [<sup>177</sup>Lu]-AM-NT 11 (2<sup>nd</sup> generation) as well as the triazole-containing conjugates [<sup>177</sup>Lu]-AM-NT 8, [<sup>177</sup>Lu]-AM-NT 9, [<sup>177</sup>Lu]-AM-NT 10, and [<sup>177</sup>Lu]-AM-NT 15, were evaluated *in vivo* because of their retained receptor affinities towards NTR1 and, in most cases, improved serum stabilities. A preliminary *in vivo* SPECT/CT imaging study was performed with [<sup>177</sup>Lu]-AM-NT 8 (Arg<sup>8</sup>-Ψ[Tz]-Arg<sup>9</sup>) and [<sup>177</sup>Lu]-AM-NT 11 (reference 2<sup>nd</sup> generation).

The values of tumour uptake of the evaluated radiopeptides were similar to the values reported in literature, yet they were on the lower end of the range, as uptakes of up to 6.3% ID/g 1 h p.i. have been reported for related radiometallated NT (8-13) analogues.<sup>[98]</sup> On the other hand, all the evaluated radioconjugates had low kidney uptakes, resulting in tumour to kidney ratios above average values published.<sup>[6, 84, 86, 93, 96, 100-102, 104, 106, 112]</sup> The high tumour to background ratio of reference compound [<sup>177</sup>Lu]-AM-NT 11 and [<sup>177</sup>Lu]-AM-NT 8 was confirmed by the results of the preliminary *in vivo* SPECT/CT imaging.

Comparison of the biodistribution profiles of the references of the first and second generation of triazole-peptidomimetics [<sup>177</sup>Lu]-AM-NT 2 (Ile<sup>12</sup>) and [<sup>177</sup>Lu]-AM-NT 11 (Tle<sup>12</sup>) showed no significant difference, despite of their different receptor affinities and stabilities in human serum. A possible reason for these observations could be that the improved stability of [<sup>177</sup>Lu]-AM-NT 11 balances the loss of receptor affinity with respect to [<sup>177</sup>Lu]-AM-NT 2.

Within the first generation of peptide conjugates with triazoles, [<sup>177</sup>Lu]-AM-NT 10, the conjugate with shortest half-life ( $t_{1/2}$ = 17 min) and [<sup>177</sup>Lu]-AM-NT 8 ( $t_{1/2}$ = 65 min) showed twice the tumour uptake of the reference [<sup>177</sup>Lu]-AM-NT 2 ( $t_{1/2}$ = 46 min). Therefore, no correlation between the metabolic stability and the accumulation of the conjugates in the tumours was observed in this study. This may be a consequence of differences between the concentration and types of proteases in human and mouse blood. This issue could be examined by performing serum stabilities studies *in vivo*, an experiment which could not be performed during this thesis. Similarly, no correlation between the  $K_D$  values of the peptide conjugates of the first generation of triazole-peptidomimetics and their tumour uptake *in vivo* was observed. An interesting behaviour was observed with compound [<sup>177</sup>Lu]-AM-NT 9, the conjugate with a triazole-modification situated between the *N*-terminal PEG<sub>4</sub> spacer and the Arg<sup>8</sup> residue. The tumour uptake of the radioconjugate was low, similar to the one of the reference compound [<sup>177</sup>Lu]-AM-NT 2, but the accumulation in the receptor positive organs (intestine and colon) and in the kidney was recognizably reduced. As a consequence, this conjugate exhibited a remarkably promising tumour to background ratio, especially the

tumour to kidney ratio at 1 h p.i. Comparable tumour to kidney ratios have only been observed for a NT (8-13) analogue by the group of Tourwé.<sup>[112]</sup> Despite its low tumour uptake, radiolabelled conjugate [<sup>177</sup>Lu]-AM-NT 9 could be a promising candidate for *in vivo* imaging applications.

Within the second generation of triazole-peptidomimetics, [<sup>177</sup>Lu]-AM-NT 15 (with a Arg<sup>8</sup>-Ψ[Tz]Arg<sup>9</sup>-modification), showed an improved tumour uptake (2-fold) when compared to the reference [<sup>177</sup>Lu]-AM-NT 11. [<sup>177</sup>Lu]-AM-NT 15 exhibited a superior receptor affinity as well as a higher metabolic stability than the reference [<sup>177</sup>Lu]-AM-NT 11.

When comparing the tumour uptakes of [<sup>177</sup>Lu]-AM-NT 8 (1<sup>st</sup> generation, Ile<sup>12</sup>) and [<sup>177</sup>Lu]-AM-NT 15 (2<sup>nd</sup> generation, Tle<sup>12</sup>), both with a 1,4-disubstituted 1,2,3-triazole at the Arg<sup>8</sup>-Arg<sup>9</sup> bond, no significant difference was observed. The metabolic stability of [<sup>177</sup>Lu]-AM-NT 15 was substantially improved when compared to [<sup>177</sup>Lu]-AM-NT 8, but it exhibited a lower receptor binding affinity. However, this was not reflected in the *in vivo* studies. Again, a possible explanation is that the low receptor affinity of [<sup>177</sup>Lu]-AM-NT 15 was compensated by its higher metabolic stability.

The tumour uptake *in vivo* of a radiopeptide can be affected by many different factors including the metabolic stability of the peptide conjugate, the receptor affinity of the conjugate towards the receptor expressed on the tumours or the rate of excretion of the compound. The receptor abundance on the targeted tissue may also play a role. Based on the observations made with the *in vitro* and biodistribution data of the triazole-containing conjugates described, it can be concluded that it is difficult to predict the *in vivo* behaviour of a substance based on *in vitro* data.

In general, we can conclude that the evaluated triazole-containing radiopeptides in this study perform satisfactorily *in vivo*, with tumour uptakes comparable with published biodistribution data of related radiolabelled NT (8-13) analogues. Also, the herein reported new NT (8-13)-based radioconjugates exhibited in general improved tumour to kidney ratios.



## 4. Conclusion and Outlook

The goal of this thesis was the development of metabolically stabilized radiolabelled NT (8-13) analogues with improved tumour-targeting properties. NT (8-13) is the minimal binding sequence of NT and has a high receptor affinity and specificity towards NTR1, a receptor overexpressed by tumours like breast, prostate, small cell lung, pancreatic and colon cancer.<sup>[1-3, 77-79]</sup> NT (8-13) is therefore an interesting candidate for the development of new peptidic tumour-targeting radiotracers with potential applications in nuclear imaging and therapy. The major drawback of NT (8-13) is its low stability in blood. The enhancement of the metabolic stability of NT (8-13) has been studied by different classical peptide stabilization approaches such as *N*-methylation, reductions of the amide bonds or amino acid substitutions.<sup>[6, 9, 86, 112]</sup> However, the success of stabilized NT (8-13) analogues so far reported in preclinical and clinical evaluations has been only moderate. Therefore novel strategies for the optimization of NT (8-13)-derived radiopharmaceuticals are needed.

In this work, the stabilization of the NT (8-13) sequence against proteases was investigated by using 1,4-disubstituted 1,2,3-triazoles as proteolytically stable amide bond mimics and the introduction of an Ile<sup>12</sup> to Tle<sup>12</sup> residue switch. Within this thesis, the first systematic 'triazole scan' of NT (8-13) has been achieved. The structures of the peptide conjugates synthesized and studied are shown in **Table 33** and the results of their biological evaluation in **Table 34**.

The peptide conjugates were synthesized on solid support by a combination of Fmoc-based solid phase peptide synthesis (SPPS), diazo-transfer reaction and the Cu(I) catalysed azide-alkyne cycloaddition (CuAAC). The required  $\alpha$ -amino alkynes for the CuAAC were successfully synthesized from the corresponding  $\alpha$ -amino acids and their enantiomeric purities were verified. The synthesis of the *N*-terminal azido-peptides *via* diazo-transfer reaction and the CuAAC on solid support were highly efficient. The peptides were elongated *N*-terminally with a PEG<sub>4</sub> spacer and conjugated to a DOTA-chelator. After HPLC-purification, the compounds were labelled with [<sup>177</sup>Lu]LuCl<sub>3</sub> in high radiochemical yields and purities.

**Table 33:** Structures of radiolabelled NT (8-13) analogues investigated.

	Structure
[ <sup>177</sup> Lu]-AM-NT 1	[ <sup>177</sup> Lu]-DOTA-Arg-Arg-Pro-Tyr-Ile-Leu
[ <sup>177</sup> Lu]-AM-NT 2 (1 <sup>st</sup> G. Reference) <sup>a</sup>	[ <sup>177</sup> Lu]-DOTA-PEG <sub>4</sub> -Arg-Arg-Pro-Tyr-Ile-Leu
[ <sup>177</sup> Lu]-AM-NT 3	[ <sup>177</sup> Lu]-DOTA-Ahx-Arg-Arg-Pro-Tyr-Ile-Leu
[ <sup>177</sup> Lu]-AM-NT 4	[ <sup>177</sup> Lu]-DOTA-PEG <sub>4</sub> -Arg-Arg-Pro-Tyr-Ile-Leu-Ψ[Tz]-H
[ <sup>177</sup> Lu]-AM-NT 5	[ <sup>177</sup> Lu]-DOTA-PEG <sub>4</sub> -Arg-Arg-Pro-Tyr-Ile-Ψ[Tz]-Leu
[ <sup>177</sup> Lu]-AM-NT 6	[ <sup>177</sup> Lu]-DOTA-PEG <sub>4</sub> -Arg-Arg-Pro-Tyr-Ψ[Tz]-Ile-Leu
[ <sup>177</sup> Lu]-AM-NT 7	[ <sup>177</sup> Lu]-DOTA-PEG <sub>4</sub> -Arg-Arg-Pro-Ψ[Tz]-Tyr-Ile-Leu
[ <sup>177</sup> Lu]-AM-NT 8	[ <sup>177</sup> Lu]-DOTA-PEG <sub>4</sub> -Arg-Ψ[Tz]-Arg-Pro-Tyr-Ile-Leu
[ <sup>177</sup> Lu]-AM-NT 9	[ <sup>177</sup> Lu]-DOTA-PEG <sub>4</sub> -Ψ[Tz]-Arg-Arg-Pro-Tyr-Ile-Leu
[ <sup>177</sup> Lu]-AM-NT 10	[ <sup>177</sup> Lu]-DOTA-PEG <sub>4</sub> -Ψ[Tz]-Arg-Ψ[Tz]-Arg-Pro-Tyr-Ile-Leu
[ <sup>177</sup> Lu]-AM-NT 11 (2 <sup>nd</sup> G. Reference) <sup>b</sup>	[ <sup>177</sup> Lu]-DOTA-PEG <sub>4</sub> -Arg-Arg-Pro-Tyr-Tle-Leu
[ <sup>177</sup> Lu]-AM-NT 12	[ <sup>177</sup> Lu]-DOTA-PEG <sub>4</sub> -Arg-Lys-Pro-Tyr-Tle-Leu
[ <sup>177</sup> Lu]-AM-NT 13	[ <sup>177</sup> Lu]-DOTA-PEG <sub>4</sub> -Lys-Arg-Pro-Tyr-Tle-Leu
[ <sup>177</sup> Lu]-AM-NT 14	[ <sup>177</sup> Lu]-DOTA-PEG <sub>4</sub> -Lys-Lys-Pro-Tyr-Tle-Leu
[ <sup>177</sup> Lu]-AM-NT 15	[ <sup>177</sup> Lu]-DOTA-PEG <sub>4</sub> -Arg-Ψ[Tz]-Arg-Pro-Tyr-Tle -Leu
[ <sup>177</sup> Lu]-AM-NT 16	[ <sup>177</sup> Lu]-DOTA-PEG <sub>4</sub> -Ψ[Tz]-Arg-Arg-Pro-Tyr-Tle -Leu
[ <sup>177</sup> Lu]-AM-NT 17	[ <sup>177</sup> Lu]-DOTA-PEG <sub>4</sub> -Ψ[Tz]-Arg-Ψ[Tz]-Arg-Pro-Tyr-Tle -Leu

<sup>a</sup> 1<sup>st</sup> generation reference. <sup>b</sup> 2<sup>nd</sup> generation reference.

In the first part of the thesis, the influence of a spacer (PEG<sub>4</sub> or Ahx) that separates the NT (8-13) from the chelator DOTA was studied. The insertion of a PEG<sub>4</sub> spacer yielded a peptide conjugate ([<sup>177</sup>Lu]-AM-NT 2) with improved receptor binding properties in comparison to the corresponding conjugate without a spacer or an Ahx-spacer, respectively. Additionally, the PEG<sub>4</sub>-spacer was found to increase the metabolic stability of NT (8-13) by nearly an order of magnitude. [<sup>177</sup>Lu]-AM-NT 2 was subsequently selected as an internal reference compound for the triazole-peptidomimetics discussed below.

In the second part of this thesis, a complete ‘triazole scan’ was performed on the NT (8-13) motif, including the individual substitution of every backbone amide bond (but Arg<sup>9</sup>-Pro<sup>10</sup>) with a 1,4-disubstituted 1,2,3-triazole bioisostere. The use of a triazole as an amide bond mimic was tolerated in two positions of the amino acid sequence of NT (8-13), between the *N*-terminal PEG<sub>4</sub> spacer and Arg<sup>8</sup> and between the Arg<sup>8</sup> and Arg<sup>9</sup> residues. A substitution of both bonds was also possible without losing affinity towards the NTR1 receptor. The stabilities of triazole-containing, radiolabelled NT (8-13) peptidomimetics against proteases were improved by the introduction of the triazoles but not yet to a degree sufficient for clinical applications. The Arg<sup>8</sup>-Ψ[Tz]-Arg<sup>9</sup> and the PEG<sub>4</sub>-Ψ[Tz]-Arg<sup>8</sup> substitution yielded peptide conjugates with up to 1.5-fold increased metabolic stabilities, in comparison to the reference

compound. The Arg<sup>8</sup>-Arg<sup>9</sup> position has been described in literature as one of the main cleavage sites of the peptide, a finding that is supported by the results obtained in this work.<sup>[84]</sup> Surprisingly, the *bis*-triazole peptide conjugate [<sup>177</sup>Lu]-AM-NT 10, in which both previously identified bonds were substituted with a triazole, displayed a loss in metabolic stability. We have currently no explanation for this result but that the consecutive introduction of two triazoles in the amino acid sequence of NT (8-13) may have led to a conformation of the peptide conjugate prone to degradation by peptidases.

The introduction of a triazole in any other position of NT (8-13) led to compounds with an abolished receptor binding affinity towards the NTR1 receptor, however some of these radiopeptides exhibited a remarkably high metabolic stability (improved up to 4-fold), in comparison to the reference compound (e.g. [<sup>177</sup>Lu]-AM-NT 6). These observations are in agreement with the results of other reported peptide stabilization strategies (e.g. the reduction of amide bonds or the employment of β-homo amino acids),<sup>[9-10]</sup> and revealed the necessity to combine our triazole stabilization approach with other methods (e.g. the substitution of Ile<sup>12</sup> with Tle<sup>12</sup>).

**Table 34:** Summary of the biological properties of radiolabelled NT (8-13) analogues.

	Internalisation after 4 h (%)	K <sub>D</sub> (nM)	B <sub>max</sub> (nM)	Log D	Stability after 4 h (%)
[ <sup>177</sup> Lu]-AM-NT 1	3.0 ± 0.2	14.9 ± 0.7	0.5	-2.5	0
[ <sup>177</sup> Lu]-AM-NT 2 (1 <sup>st</sup> G. Reference) <sup>a</sup>	7.3 ± 0.4	3.8 ± 0.9	0.37 ± 0.02	-2.6	0.9
[ <sup>177</sup> Lu]-AM-NT3	5.6 ± 0.4	3.4 ± 1.5	0.3	-2.3	0
[ <sup>177</sup> Lu]-AM-NT 4	n.o.	n.d.	n.d.	-3.2	2.5
[ <sup>177</sup> Lu]-AM-NT 5	n.o.	n.d.	n.d.	-2.8	5.6
[ <sup>177</sup> Lu]-AM-NT 6	n.o.	n.d.	n.d.	-3.2	10.2
[ <sup>177</sup> Lu]-AM-NT 7	n.o.	n.d.	n.d.	-2.6	0
[ <sup>177</sup> Lu]-AM-NT 8	6.4 ± 1.2	8.7 ± 1.7	0.90 ± 0.04	-2.8	6.5
[ <sup>177</sup> Lu]-AM-NT 9	9.4 ± 0.5	4.5 ± 0.8	0.45 ± 0.01	-3.2	2.2
[ <sup>177</sup> Lu]-AM-NT 10	10.8 ± 0.4	4.6 ± 2.3	0.34 ± 0.03	-2.7	0
[ <sup>177</sup> Lu]-AM-NT 11 (2 <sup>nd</sup> G Reference) <sup>b</sup>	1.3 ± 0.2	507 ± 114	1.6 ± 0.2	-2.2	70.6
[ <sup>177</sup> Lu]-AM-NT 12	0.23 ± 0.02	>1000	n.d.	-2.1	95.6
[ <sup>177</sup> Lu]-AM-NT 13	0.56 ± 0.02	>1000	n.d.	-2.1	95.7
[ <sup>177</sup> Lu]-AM-NT 14	0.3 ± 0.01	246 ± 44	0.80 ± 0.06	-2.0	91.1
[ <sup>177</sup> Lu]-AM-NT 15	2.1 ± 0.1	214 ± 45	n.d.	-2.2	97.7
[ <sup>177</sup> Lu]-AM-NT 16	1.2 ± 0.2	>1000	n.d.	-2.2	94.7
[ <sup>177</sup> Lu]-AM-NT 17	2.19 ± 0.01	>1000	n.d.	-2.3	97.2

<sup>a</sup> 1<sup>st</sup> generation reference. <sup>b</sup> 2<sup>nd</sup> generation reference.

In the third part of this work, the use of Tle and Lys as reported substitutes for Ile<sup>12</sup> and Arg<sup>8/9</sup>, within the amino acid sequence of [<sup>177</sup>Lu]-DOTA-PEG<sub>4</sub>-NT (8-13) was investigated to improve further the stability of the peptidic vector. A direct comparison of the influence of these amino

acid substitutions on the pharmacological properties of the NT (8-13) motif has not yet been published. In general, the introduction of Tle<sup>12</sup> led to a significantly reduced cell internalisation as well as receptor binding affinity of the radiolabelled conjugates, but resulted in increased metabolic stability. Similarly, the substitution of one of the Arg residues with Lys led to abolished receptor binding affinities of the radiopeptides, whereas the substitution of both Arg residues with Lys yielded a radiopeptide conjugate with a retained affinity towards NTR1 and improved stability against proteolytic degradation. [<sup>177</sup>Lu]-AM-NT 11, with Tle<sup>12</sup>, was selected as a reference compound for the second generation of triazole-containing peptidomimetics in which the previously identified positions for an amide-to-triazole exchange was investigated.

Triazole-substituted NT (8-13) analogues bearing a Tle<sup>12</sup> exhibited low cell internalisations into NTR1-positive HT-29 cells. All three triazole-peptidomimetics with a Tle<sup>12</sup> substitution showed a significant loss of receptor affinities towards NTR1, with exception of the Arg<sup>8</sup>-Ψ[Tz]-Arg<sup>9</sup>-peptide conjugate. These observations were not completely in agreement with literature data, as the substitution of Ile<sup>12</sup> with Tle<sup>12</sup> is reported to yield NT (8-13) analogues with high receptor affinities towards NTR1.<sup>[6, 104-105]</sup> On the other hand, all the peptide conjugates exhibited a significant improvement of stability when compared to the compounds of the first generation.

Based on their promising properties *in vitro*, three peptide conjugates of the first generation and one of the second generation were selected for a full investigation *in vivo* in a side-by-side comparison with their respective reference compounds. *In vivo* experiments of the radiolabelled NT (8-13) derivatives showed that the Arg<sup>8</sup>-Ψ[Tz]-Arg<sup>9</sup> modification led to the radiolabelled peptidomimetics with the most interesting tumour-targeting properties ([<sup>177</sup>Lu]-AM-NT 8, [<sup>177</sup>Lu]-AM-NT 10 and [<sup>177</sup>Lu]-AM-NT 15). The presence of this modification in the peptide conjugate was responsible for a 2-fold increased accumulation of radioactivity in the HT-29 xenograft of nude mice. The peptide conjugate with the triazole between the *N*-terminal PEG<sub>4</sub> spacer and Arg<sup>8</sup> ([<sup>177</sup>Lu]-AM-NT 9) did not show an improved tumour uptake, but a very promising high tumour to background ratio (Table 35).



**Table 35:** Summary of biodistribution data of the NT (8-13) analogues evaluated *in vivo*

	Tumour uptake (% ID/g)			Tumour to kidney ratio		
	1 h	4 h	24 h	1 h	4 h	24 h
<b>[<sup>177</sup>Lu]-AM-NT 2</b> (1 <sup>st</sup> G. Reference) <sup>a</sup>	1.1 ± 0.2	0.8 ± 0.2	0.5 ± 0.2	1.0 ± 0.5	0.6 ± 0.2	0.7 ± 0.4
<b>[<sup>177</sup>Lu]-AM-NT 8</b>	2.0 ± 0.3	1.6 ± 0.5	1.0 ± 0.3	1.1 ± 0.4	0.8 ± 0.4	0.9 ± 0.4
<b>[<sup>177</sup>Lu]-AM-NT 9</b>	1.0 ± 0.3	0.7 ± 0.1	0.42 ± 0.09	2.0 ± 0.9	1.3 ± 0.3	1.0 ± 0.4
<b>[<sup>177</sup>Lu]-AM-NT 10</b>	1.9 ± 0.4	1.29 ± 0.09	0.9 ± 0.1	1.0 ± 0.3	0.8 ± 0.1	0.7 ± 0.1
<b>[<sup>177</sup>Lu]-AM-NT 11</b> (2 <sup>nd</sup> G. Reference) <sup>b</sup>	1.0 ± 0.3	0.7 ± 0.2	0.2 ± 0.1	0.8 ± 0.3	0.5 ± 0.3	0.5 ± 0.3
<b>[<sup>177</sup>Lu]-AM-NT 15</b>	2.3 ± 0.6	1.1 ± 0.1	1.1 ± 0.1	1.4 ± 0.7	0.8 ± 0.2	0.9 ± 0.2

<sup>a</sup> 1<sup>st</sup> generation reference. <sup>b</sup> 2<sup>nd</sup> generation reference.

In general, it can be concluded that 1,4-disubstituted 1,2,3-triazoles as amide bonds isosters in NT (8-13) led to new radiolabelled peptidomimetics with a nanomolar receptor affinity towards NTR1 and a moderate improvement of the stability against proteases. Substitution of Ile<sup>12</sup> with Tle<sup>12</sup> significantly improved the metabolic stability of the radiopeptides, while a loss of receptor affinity was observed at the same time. Comparison to similar radiopeptides reported in literature was difficult, because of differences in the amino acid sequences, employed spacers, chelators and radiometals or due to different biological assays, (e.g. IC<sub>50</sub> values from ligand competition experiments instead of binding saturation experiments).<sup>[6, 84, 86, 93, 96, 100-102, 104, 106, 112]</sup> The hydrophilicity (log D) of the peptidomimetics was not much affected by the introduction of the triazole, as they all exhibited similar values. The hydrophilic character of the peptide conjugates is a favourable characteristic for a radiometal-labelled peptide conjugate as the likelihood of unspecific accumulation in the liver *in vivo* due to hepatobiliary excretion is reduced and a favourable fast renal clearance is expected. This is beneficial for the application of the radiopeptide conjugates as imaging agents because the background radiation is reduced, which results in higher imaging quality. For therapeutic applications, a high tumour to background ratio is also favourable, as an unnecessary radiation dose to the patient is avoided.

It was observed that the tumour uptake of the radiopeptides evaluated *in vivo* did not correlate with the metabolic stability or the K<sub>D</sub> values determined *in vitro*. A possible explanation could be that the improved metabolic stability of some peptidomimetics balances the loss of receptor binding affinity and vice versa. This would explain that no significant difference in tumour uptake was observed between [<sup>177</sup>Lu]-AM-NT 8 (high receptor affinity, low stability) and [<sup>177</sup>Lu]-AM-NT 15 (low receptor affinity, high stability). This demonstrates that predictions of the *in vivo* behaviour of triazole-substituted NT (8-13) analogues must not be made based on their *in vitro* behaviour and underlines the importance of preclinical *in vivo* experiments.

In summary, we report the first 'triazole scan' of the binding sequence of NT (8-13) and the synthesis and biological evaluation of novel radiolabelled triazole-containing peptidomimetics. The synthesis of the peptide conjugates (including CuAAC and diazo-transfer) was fully compatible with solid phase synthesis. This methodology is likely to find a broad application as a stabilization technique for other peptides of medicinal interest. The substitution of amide bonds with 1,4-disubstituted 1,2,3-triazoles provided NT (8-13) peptidomimetics with improved tumour-targeting properties in comparison to their reference compounds. The tumour uptake of the evaluated triazole-containing radiopeptidomimetics was somewhat low and one has to acknowledge that they are therefore not likely suitable for applications in endoradiotherapy. However, due to their high specificity and good tumour to background ratio, they are interesting candidates for the development of peptidic radiotracers for the molecular imaging of NTR1 positive tumours.

Future research could include further investigations for a better understanding of the *in vivo* behaviour of some of the compounds. Despite seemingly poor internalisation properties and dissociation constants in the high nanomolar range, some of the radiolabelled peptidomimetics performed nevertheless satisfactorily *in vivo*. It would be interesting to characterize the pharmacological properties of these compounds by techniques different to the ones presented in this thesis, (e.g. ligand competition experiments, or studies with other NTR1-expressing cell lines such as WiDr cells or HT-29 and WiDr cell membrane preparations).<sup>[193]</sup> It is known that the metabolic stability of compounds can be different in human and mouse blood plasma due to differences in the expression and concentration of proteases.<sup>[194]</sup> Determination of the metabolic stability of the peptidomimetics in mouse serum *ex vivo* would thus be helpful to understand better why the increased stability did not correlate with the tumour uptakes. In addition, a significant difference can be expected between *in vitro* and *in vivo* experiments since proteases are not only present in the blood but also in organs such as the liver and the kidneys. A detailed *in vivo* imaging study (e.g. at different time points) would help to evaluate the suitability of the radioconjugates as imaging agents.

Especially the *bis*-triazole compound [<sup>177</sup>Lu]-AM-NT 10, which exhibited an improved tumour uptake despite of its lack of metabolic stability, needs to be further evaluated. *In vitro* experiments with different proteases in combination with molecular modelling studies could provide further insights about the cleavage sites important for this specific compound.

Further development of radiolabelled triazole-containing NT (8-13) analogues could include the exploration of other amino acid substitutions for Ile<sup>12</sup> (e.g. <sup>t</sup>BuAla, cyclopentyl-alanine or cyclohexyl-alanine),<sup>[195]</sup> in combination with our amide-to-triazole exchange methodology. Also, the combination of reduced amide bonds with a triazole-modified NT (8-13) analogue

should be evaluated. Combinations of these different techniques could lead to novel triazole-containing NT (8-13) analogues with further improved tumour-targeting properties. Alternatively, Gruaz-Guyon and co-workers have reported that longer fragments of Neurotensin, based on NT (6-13), had higher tumour uptakes.<sup>[100]</sup> Based on literature data, it is likely that an increased size of the tumour-targeting vector enhances the circulation time of the radiopeptide conjugate in the body and thus, its tumour uptake. This offers an additional possibility to improve the tumour-targeting properties of NT-based radiolabelled conjugates.

An alternative to the structural optimization of a peptidic radiopharmaceutical is the co-administration of a protease-inhibitor. In 2014, Nock *et al.* published a new approach for the stabilisation of peptide-based radiopharmaceuticals consisting of the co-administration of the radiotracers with an inhibitor of the metalloprotease NEP 24.10.<sup>[196]</sup> The application of this strategy to three classical radiopeptides resulted in an increased tumour uptake.<sup>[196]</sup> It could be interesting to combine our stabilisation approach with the injection of inhibitors responsible for the degradation of Neurotensin.



## 5. Experimental Procedures

### 5.1 Instruments and Chemicals

All reagents and solvents were purchased from commercial suppliers and were used without further purification. If not mentioned, all the reagents were purchased at Sigma Aldrich (Buchs, Switzerland). Rink amide LL resin, Fmoc-Leu preloaded Novasyn resin, HATU and amino acids were purchased at Novabiochem (Merck Millipore, Darmstadt, Germany) or Bachem (Bubendorf, Switzerland). DOTA (*tris*-<sup>t</sup>Bu) was purchased from Chematech (Dijon, France). 1-(9H-fluoren-9-yl)-3-oxo-2,7,10,13,16-pentaoxa-4-azanonadecan-19-oic acid (Fmoc-PEG<sub>4</sub>-OH) was purchased from PolyPeptide laboratories (Strasbourg, France). Blocking agents NT (8-13) and NT (1-13) were purchased at Bachem (Bubendorf, Switzerland).

[<sup>177</sup>Lu]LuCl<sub>3</sub> in 0.05 M HCl was purchased either from IDB (Baarle-Nassau, Netherlands), ITG (München, Germany) or Perkin Elmer (Boston, USA).

Human colorectal adenocarcinoma (HT-29) cells were obtained from American Type Culture Collection (ATCC, Manassas, USA), Dulbecco's modified Eagle's medium (DMEM, high glucose), containing 10% (v/v) fetal bovine serum (FBS Superior, OXOID, Pratteln, Switzerland), L-glutamine (200 mM), 100 IU mL<sup>-1</sup> penicillin and 100 µg mL<sup>-1</sup> streptomycin.

Animals, female nude Foxn 1nu mice, were purchased either at Charles River (Wilmington, USA) or Harlan (Füllingsdorf, Switzerland).

Analytical and preparative HPLC were carried out with systems from Bischoff Chromatography, equipped with a γ-1010 UV/Vis and an LB509 radioflow detector (Berthold Technologies, Bad Wildbad, Germany), using C18 reversed-phase columns from Macherey Nagel (Oensingen, Switzerland) Nucleodur C18 ISIS, 5 µm, 250 x 4.6 mm for analytics and Nucleodur C18 ISIS, 5 µm, 250 x 16.0 mm for purifications, using 0.1% TFA in H<sub>2</sub>O as solvent A and 0.1% TFA in MeCN as solvent B.

Flash column chromatographies were carried out using Kieselgel C60 as the stationary phase and TLC were performed on precoated silica gel plates (0.25 mm thick, 60F 254, Merck, Germany).

<sup>1</sup>H and <sup>13</sup>C NMR spectra were recorded on Bruker DPX 400, DPX 500 and DPX 600 instruments, at a constant temperature of 25 °C. The corresponding solvent signals were

used as internal standard. Chemical shifts are reported in parts per million (ppm) relative to tetramethylsilane (0.00 ppm). Values of the coupling constant,  $J$ , are given in Hertz (Hz); the following abbreviations are used in the experimental section for the description of  $^1\text{H}$ -NMR spectra: singlet (s), doublet (d), triplet (t), quartet (q), multiplet (m), doublet of doublets (dd), broad singlet (bs),  $\text{C}_\text{q}$  (quaternary carbon),  $\text{C}_\text{t}$  (tertiary carbon) and  $\text{C}_\text{s}$  (secondary carbon). The chemical shifts of complex multiplets are given as the range of their occurrence. Further assignments were achieved by using two-dimensional NMR experiments when appropriate (COSY, NOESY, HMBC, HMQC).

Optical rotations were measured at 20 °C with a Jasco P-2000 Polarimeter. High resolution mass spectrometry measurements were performed by ESI on a maXis 4G (Bruker, Billerica, USA) or by LC-ESI on an LTQ Orbitrap XL mass spectrometer (Thermo Scientific, Waltham, USA). Quantitative  $\gamma$ -counting was performed on a COBRA II auto-gamma system (Model 5003, Packard Instruments, Meriden, USA). Lyophilisation of the peptide conjugates was performed on an Alpha 1-2 LD plus lyophilizer (Christ, Osterode am Harz, Germany).

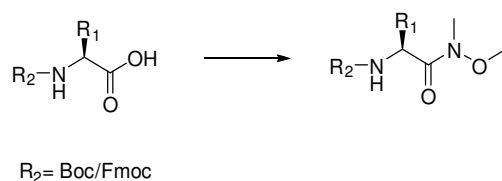
*In vivo* imaging was performed using a NanoSPECT/CT ® Plus *In Vivo* Animal Image scanner (BIOSCAN, Geneva, Switzerland; now Trifoil, Chatsworth, USA). The CT- and SPECT-scans were reconstructed with the software InVivoScope® 1.43 (BIOSCAN) and the reconstruction of the images was performed with the software HiSPECT Version 1.4.1876 (Scivis GmbH, Göttingen, Germany).

LRMS analyses were performed on an ESI Bruker Esquire 3000 plus.

## 5.2 Organic Synthesis

### 5.2.1 General Procedures

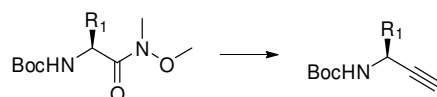
#### General Procedure A: Synthesis of Weinreb Amides<sup>[197]</sup>



The corresponding Fmoc- or Boc-protected amino acid (1 mmol) was dissolved in  $\text{CH}_2\text{Cl}_2$  (0.1 M) and DIPEA (435  $\mu\text{L}$ , 2.5 mmol, 2.5 equiv.) and BOP (442 mg, 1 mmol, 1.0 equiv.) were added. The solution was stirred for 15 min. *N,O*-dimethylhydroxylamine (117 mg, 1.2 mmol, 1.2 equiv.) was added and the reaction was stirred for 12-14 h at RT. The solution was washed with a 0.5 M HCl solution (3 x 50 mL), saturated  $\text{NaHCO}_3$  solution (3 x 5 mL) and NaCl solution (3 x 50 mL). The organic phase was dried over  $\text{MgSO}_4$ , filtered and the solvent was removed *in vacuo*. The corresponding Weinreb amides were purified by silica gel column chromatography.

#### General Procedure B: Synthesis of $\alpha$ -Amino Alkynes<sup>[172]</sup>

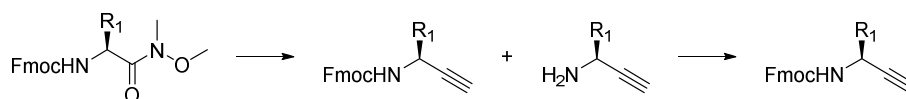
##### B.1 Synthesis of $\alpha$ -Amino Alkynes from Boc-protected Weinreb Amides



Weinreb amide **26** (0.1 mmol) was placed under argon in a flame dried flask and dissolved in anhydrous  $\text{CH}_2\text{Cl}_2$  (0.1 M). The solution was cooled to  $-78\text{ }^\circ\text{C}$  (dry ice/diethyl ether bath). 1 M DIBAL-H in toluene (0.3 mL, 0.3 mmol, 3.0 equiv.) was added slowly. After 1 h of stirring, the reaction was checked for completion by TLC. If the reaction was not finished, 1 M DIBAL-H

in toluene (0.1 mL, 0.1 mmol, 1.0 equiv.) was added and the reaction was stirred again for 1 h at -78 °C. After consumption of the starting material, the reaction was allowed to warm to -10 °C (ice/NaCl bath) and the excess hydride was quenched by slow addition of anhydrous MeOH (1 mL). K<sub>2</sub>CO<sub>3</sub> (414 mg, 0.3 mmol, 3.0 equiv.), dimethyl-(1-diazo-2-oxopropyl)phosphonate (300 μL, 0.2 mmol, 2.0 equiv.) and anhydrous MeOH (1 mL) were added and the reaction mixture was stirred overnight at RT. A saturated solution of Rochelle's salt was added and after 1 h of stirring at RT, the solution was diluted with water and CH<sub>2</sub>Cl<sub>2</sub>. The aqueous phase was extracted with CH<sub>2</sub>Cl<sub>2</sub>. The combined organic phases were dried over Na<sub>2</sub>SO<sub>4</sub>, filtered and the solvent was removed *in vacuo*. The corresponding alkyne was obtained after flash chromatography.

## B.2 Synthesis of $\alpha$ -Amino Alkynes from Fmoc-protected Weinreb Amides



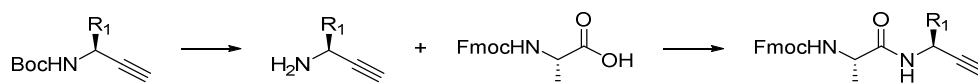
The corresponding Weinreb amide (0.1 mmol) was placed under argon in a flame dried flask and dissolved in anhydrous CH<sub>2</sub>Cl<sub>2</sub> (0.1 M). The solution was cooled to -78 °C (dry ice/diethyl ether bath). 1 M DIBAL-H in toluene (0.3 mL, 0.3 mmol, 3.0 equiv.) was added slowly. After 1 h of stirring, the reaction was checked for completion by TLC. If the reaction was not finished, 1 M DIBAL-H in toluene (0.1 mL, 0.1 mmol, 1.0 equiv.) was added and the reaction was stirred again for 1 h at -78 °C. After consumption of the starting material, the reaction was allowed to warm to -10 °C (ice/NaCl bath) and the excess hydride was quenched by slow addition of anhydrous MeOH (1 mL). K<sub>2</sub>CO<sub>3</sub> (414 mg, 0.3 mmol, 3.0 equiv.), dimethyl-(1-diazo-2-oxopropyl)phosphonate (300 μL, 0.2 mmol, 2.0 equiv.) and MeOH (1 mL) were added and the reaction mixture was stirred overnight at RT. A saturated solution of Rochelle's salt was added and after 1 h of stirring at RT, the solution was diluted with water and CH<sub>2</sub>Cl<sub>2</sub>. The aqueous phase was extracted with CH<sub>2</sub>Cl<sub>2</sub> (3 x 30 mL). The combined organic phases were dried over Na<sub>2</sub>SO<sub>4</sub>, filtered and the solvent was removed *in vacuo*. If cleavage of the Fmoc protective group was observed on TLC, the crude mixture was dissolved in CH<sub>2</sub>Cl<sub>2</sub> (1 mL) and DIPEA (2.5 equiv.) and Fmoc-OSu (2.0 equiv.) were added. The reaction was stirred overnight at RT. The reaction mixture was then diluted with CH<sub>2</sub>Cl<sub>2</sub> and brine. The aqueous phase was extracted with CH<sub>2</sub>Cl<sub>2</sub> (3 x 30 mL). The combined organic



phases were dried over  $\text{Na}_2\text{SO}_4$ , filtered and the solvent was removed *in vacuo*. The corresponding alkyne was obtained after flash chromatography.

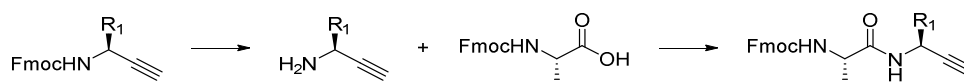
## General Procedure C: Synthesis of Dipeptides from $\alpha$ -Amino Alkynes

### C.1 Synthesis of Dipeptides from Boc-Protected $\alpha$ -Amino Alkynes

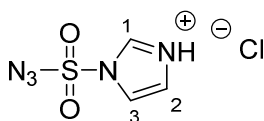


The corresponding  $\alpha$ -amino alkyne (1.0 equiv.) was dissolved in a solution of  $\text{CH}_2\text{Cl}_2/\text{TFA}/\text{H}_2\text{O}$  (75:20:5) (1 M) and the reaction was stirred 15 min-1 h. After completion of the reaction, the solvent was removed under reduced pressure. Residual amounts of water and TFA were removed by co-evaporation with toluene. The residue was dissolved in  $\text{CH}_2\text{Cl}_2$  and Fmoc-Ala-OH (2.0 equiv.), BOP (2.0 equiv.) and DIPEA (5.0 equiv.) were added successively. The reaction was stirred 2 h at RT and monitored with TLC until completion. The solvent was removed from the crude mixture under reduced pressure and flash chromatography yielded the desired product.

### C.2: Synthesis of Dipeptides from Fmoc-Protected $\alpha$ -Amino Alkynes



The corresponding alkyne (0.1 equiv.) was suspended in 25% piperidine in DMF (1 M) and the reaction was stirred for 15 min. Ice-cold  $\text{H}_2\text{O}$  (1 x 1 mL) was added to the reaction mixture and extracted with EtOAc (3 x 10 mL). The combined organic fractions were dried over  $\text{MgSO}_4$ , filtered and the solvent was removed *in vacuo*. The residue was dissolved in  $\text{CH}_2\text{Cl}_2$  (0.1 M) and Fmoc-Ala-OH (2.0 equiv.), BOP (2.0 equiv.) and DIPEA (5.0 equiv.) were added successively. The reaction was monitored with TLC until completion. The solvent was removed from the crude mixture under reduced pressure and flash chromatography yielded the desired product.

**Synthesis of Imidazole-1-sulfonyl Azide Hydrochloride (6)**

MW: 208.98 g/mol

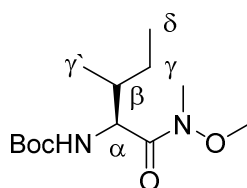
NaN<sub>3</sub> (13.0 g, 0.2 mol, 1.0 equiv.) was suspended under argon in anhydrous MeOH (200 mL). SO<sub>2</sub>Cl<sub>2</sub> (16.1 mL, 0.2 mol, 1.0 equiv.) was slowly added at -10 °C (Ice/NaCl bath). Imidazole (25.9 g, 0.4 mol, 1.9 equiv.) was added to the ice-cold mixture and the reaction was stirred 12 h at RT. The suspension was quenched by addition of water and diluted with EtOAc. After washing of the solution with NaHCO<sub>3</sub> (3 x 300 mL), the organic layer was dried over MgSO<sub>4</sub> and the solvent was removed under reduced pressure. The obtained yellowish oil was dissolved in EtOH (80 mL) and cooled with ice. Ice-cold 1.25 M HCl in EtOH solution (180 mL) was added. A white precipitation was observed. The precipitate was filtered off and washed with EtOAc (3 x 30 mL). Compound **6** was obtained as white crystals (31.4g, 74%).

<sup>1</sup>H-NMR (400 MHz, CDCl<sub>3</sub>): δ=14.60 (bs, 2H, -NH-), 9.12 (s, 1H, H-3), 7.68 (s, 2H, H-1, H-2) ppm

<sup>13</sup>C-NMR (100 MHz, CDCl<sub>3</sub>): δ= 137.7, 134.1, 119.2 ppm

The data was found to be identical as published.<sup>[161]</sup>

**Synthesis of Boc-Ile-(NMe)OMe (26a)**



MW: 214.19 g/mol

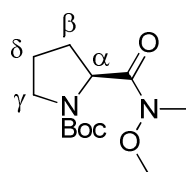
Compound **26a** was obtained following general procedure **A**. Boc-Ile-OH **25a** (1.5 g, 6.5 mmol) was used as starting material. Flash chromatography (MeOH/CH<sub>2</sub>Cl<sub>2</sub>, gradient 5:95 to 10:90) yielded compound **26a** white crystals (1.3 g, 94%).

<sup>1</sup>H-NMR (400 MHz, CDCl<sub>3</sub>): δ= 5.09 (d, <sup>3</sup>J<sub>HH</sub>= 9.6 Hz, 1H, -NH-), 4.60 (m, 1H, H<sub>α</sub>), 3.76 (s, 3H, -OMe), 3.20 (s, 3H, -NMe), 1.71-1.68 (m, 1H, H<sub>β</sub>), 1.57-1.50 (m, 2H, H<sub>γ</sub>), 1.42 (s, 9H, Boc) 0.90 (d, <sup>3</sup>J<sub>HH</sub>= 6.8 Hz, 3H, H<sub>γ'</sub>), 0.81 (t, <sup>3</sup>J<sub>HH</sub>= 6.8 Hz, 3H, H<sub>δ</sub>) ppm

<sup>13</sup>C-NMR (100 MHz, CDCl<sub>3</sub>): δ= 173.3, 155.9, 79.5, 61.7, 54.3, 38.2, 32.0, 28.2, 24.4, 15.6, 11.5 ppm

The data was found to be identical as published.<sup>[116]</sup>

**Synthesis of Boc-Pro-(NMe)OMe (26b)**



MW: 258.16 g/mol

Compound **26b** was synthesized following the general protocol **A**. Boc-Pro-OH **25a** (1.5 g, 6.7 mmol) was used as starting material. Flash chromatography (EtOAc/Hexane, 5:5) yielded compound **26b** as white crystals (0.98 g, 57%). The compound was obtained as a mixture of conformers in a 1:0.9 ratio.

<sup>1</sup>H-NMR (400 MHz, CDCl<sub>3</sub>): δ= Major conformer: 4.57 (m, 1H, H<sub>α</sub>), 3.70 (s, 3H, -NMe), 3.58-3.37 (m, 2H, H<sub>δ</sub>), 3.17 (s, 3H, -OMe), 2.20-1.79 (m, 4H, H<sub>γ</sub>, H<sub>β</sub>), 1.39 (s, 9H, Boc) ppm

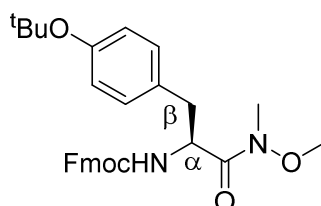
Minor conformer: 4.68 (m, 1H, 1.28, H<sub>α</sub>), 3.75 (s, 3H, N-Me), 1.44 (s, 9H, -<sup>t</sup>Bu) ppm

<sup>13</sup>C-NMR (100 MHz, CDCl<sub>3</sub>): δ= 153.9, 79.7, 61.3, 56.8, 46.6, 32.5, 30.5, 28.44, 23.44 ppm

Minor conformer: 154.5, 79.4, 61.3, 56.6, 46.9, 32.3, 29.6, 28.6, 24.1 ppm

One <sup>13</sup>C signals was not observed due to overlapping signals.

The data was found to be identical as published.<sup>[198]</sup>

**Synthesis of Fmoc-Tyr(<sup>t</sup>Bu)-(NMe)OMe (34c)**

MW: 502.25 g/mol

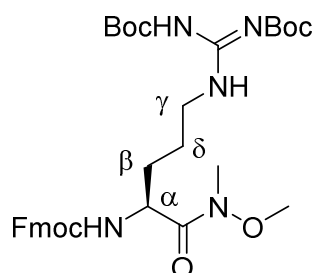
Compound **34c** was synthesized following the general protocol **A**. Fmoc-Tyr(<sup>t</sup>Bu)-OH **33c** (0.5 g, 1.7 mmol) was used as starting material. Flash chromatography (EtOAc/Hexane, 3:7, 4:6, 5:5) yielded compound **34c** as white crystals (0.5 g, 64%).

<sup>1</sup>H-NMR (400 MHz, CDCl<sub>3</sub>): δ= 7.77 (d, <sup>3</sup>J<sub>HH</sub>= 7.4 Hz, 2H, Fmoc), 7.57 (t, <sup>3</sup>J<sub>HH</sub>= 7.5 Hz, 2H, Fmoc), 7.39 (t, <sup>3</sup>J<sub>HH</sub>= 7.4 Hz, 2H, Fmoc), 7.30 (tt, <sup>3</sup>J<sub>HH</sub>= 7.5 Hz, <sup>4</sup>J<sub>HH</sub>= 1.2 Hz, 2H, Fmoc), 7.16 (d, <sup>3</sup>J<sub>HH</sub>= 8.4 Hz, 2H, arom.), 6.83 (d, <sup>3</sup>J<sub>HH</sub>= 8.4 Hz, 2H, arom.), 5.45 (d, <sup>3</sup>J<sub>HH</sub>= 8.8 Hz, 1H, -NH-), 4.98 (dd, <sup>3</sup>J<sub>HH</sub>= 13.6 Hz, <sup>3</sup>J<sub>HH</sub>= 8.8 Hz, 1H, H<sub>α</sub>), 4.53-4.20 (m, 2H, Fmoc), 4.16 (t, <sup>3</sup>J<sub>HH</sub>= 7.2 Hz, 1H, Fmoc), 3.62 (s, 3H, -OMe), 3.15 (s, 3H, -NMe), 3.03 (dd, <sup>2</sup>J<sub>HH</sub>= 13.4 Hz, <sup>3</sup>J<sub>HH</sub>= 6.7 Hz, 1H, H<sub>β</sub>), 2.88 (dd, <sup>2</sup>J<sub>HH</sub>= 13.4 Hz, <sup>3</sup>J<sub>HH</sub>= 6.7 Hz, 1H, H<sub>β</sub>), 1.29 (s, 9H, -<sup>t</sup>Bu) ppm

<sup>13</sup>C-NMR (100 MHz, CDCl<sub>3</sub>): δ= 12.1, 155.9, 154.4, 144.0, 141.4, 131.3, 130.0, 127.8, 127.2, 125.3, 124.3, 120.1, 78.5, 67.1, 61.6, 52.2, 47.3, 38.5, 32.2, 28.9 ppm

The data was found to be identical as published.<sup>[199]</sup>

### Synthesis of Fmoc-Arg(Boc)<sub>2</sub>-(NMe)OMe (34d)



MW: 639.33 g/mol

Fmoc-Arg(Boc)<sub>2</sub>-OH **33d** (400 mg, 0.7 mmol, 1.0 equiv.) was dissolved in CH<sub>2</sub>Cl<sub>2</sub> (3 mL) and HOBt (100 mg, 0.74 mmol, 1.1 equiv.) and EDC (154.1 mg, 0.8 mmol, 1.2 equiv.) were added. The reaction mixture was stirred at 0 °C for 15 min. *N,O*-dimethylhydroxylamine (47.1 mg, 0.74 mmol, 1.1 equiv.) and *N*-methylmorpholine (89 μL, 0.8 mmol, 1.2 equiv.) were added and the reaction was stirred for 12 h. The solvent was then removed under vacuum and the resulting residue was partitioned between EtOAc and 1M HCl (aq.). The organic layer was separated and washed with 1M HCl (aq) (1 x 15 mL), NaHCO<sub>3</sub> (1 x 15 mL) and brine (1 x 15 mL), and then dried over Mg<sub>2</sub>SO<sub>4</sub>. After filtration, the solvent was removed *in vacuo* and the residue was purified *via* flash chromatography (EtOAc/Hexane, 3:7) yielding compound **34d** as white crystals (180 mg, 41%).

$[\alpha]_D^{20} = +3.6$  (c=1.2, CHCl<sub>3</sub>)

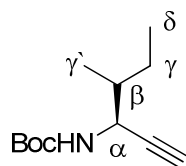
<sup>1</sup>H-NMR (500 MHz, CD<sub>3</sub>CN): δ= 11.65 (s, 1H, -NH-), 8.22 (s, 1H, -NH-), 7.84-7.82 (dd, <sup>3</sup>J<sub>HH</sub>= 7.5 Hz, <sup>4</sup>J<sub>HH</sub>= 1.3 Hz, 2H, Fmoc), 7.69-7.65 (t, <sup>3</sup>J<sub>HH</sub>= 7.5 Hz, 2H, Fmoc), 7.43-7.40 (t, <sup>3</sup>J<sub>HH</sub>= 7.5 Hz, 2H, Fmoc), 7.35-7.31 (tt, <sup>3</sup>J<sub>HH</sub>= 7.5 Hz, <sup>4</sup>J<sub>HH</sub>= 1.3 Hz, 2H, Fmoc), 5.98 (d, <sup>3</sup>J<sub>HH</sub>= 9.0 Hz, 1H, -NH-), 4.58 (m, 1H, H<sub>α</sub>), 4.35-4.29 (m, 1H, Fmoc), 4.23 (t, <sup>3</sup>J<sub>HH</sub>= 7.0 Hz, 2H, Fmoc), 3.73 (s, 3H, -NMe), 3.37-3.31 (m, 2H, H<sub>δ</sub>), 3.13 (s, 3H, -OMe), 1.71-1.54 (m, 4H, H<sub>γ</sub>, H<sub>β</sub>), 1.48 (s, 9H, Boc), 1.42 (s, 9H, Boc) ppm

<sup>13</sup>C-NMR (100 MHz, CDCl<sub>3</sub>): δ= 164.7 (C<sub>q</sub>), 157.2 (C<sub>q</sub>), 153.9 (C<sub>q</sub>), 145.1 (C<sub>q</sub>), 142.1 (C<sub>q</sub>), 128.6 (C<sub>t</sub>, Fmoc), 128.1 (C<sub>t</sub>, Fmoc), 126.2 (C<sub>t</sub>, Fmoc), 120.9 (C<sub>t</sub>, Fmoc), 84.0 (C<sub>q</sub>), 79.4 (C<sub>q</sub>), 67.1 (C<sub>s</sub>, Fmoc), 51.9 (C<sub>α</sub>), 48.0 (C<sub>t</sub>, Fmoc), 40.8 (C<sub>δ</sub>), 29.7 (C<sub>β</sub>), 28.4 (Boc), 26.1 (Boc), 26.1 (C<sub>γ</sub>) ppm

Four <sup>13</sup>C signals were not observed due to overlapping signals.

ESI-HRMS: [M+H]<sup>+</sup> *m/z* calcd for C<sub>33</sub>H<sub>45</sub>N<sub>5</sub>O<sub>8</sub>: 639.3268, found: 640.3344.

### Synthesis of Boc-Ile-alkyne (**28a**)



MW: 211.16 g/mol

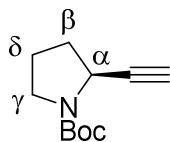
Compound **28a** was synthesized from compound **26b** (100 mg, 0.4 mmol) following the general protocol **B.1**. Flash chromatography (EtOAc/Hexane, 2:98) yielded compound **28a** as white crystals (60 mg, 79%).

$^1\text{H-NMR}$  (400 MHz,  $\text{CDCl}_3$ ):  $\delta$ = 4.76 (m, 1H, -NH-), 4.42 (m, 1H,  $\text{H}_\alpha$ ), 2.23 (d,  $^4J_{\text{HH}} = 2.4$  Hz, 1H, alkyne), 1.68-1.60 (m, 1H,  $\text{H}_\beta$ ), 1.55-1.47 (m, H,  $\text{H}_\gamma$ ), 1.44 (s, 9H, Boc), 1.28-1.17 (m, 1H,  $\text{H}_\gamma$ ) 0.90 (m, 6H,  $\text{H}_\delta$ ,  $\text{H}_\gamma'$ ) ppm

$^{13}\text{C-NMR}$  (100 MHz,  $\text{CDCl}_3$ ):  $\delta$ = 155.00, 81.8, 78.0, 72.0, 47.5, 39.4, 28.5, 26.2, 14.5, 11.7 ppm

The data was found to be identical as published.<sup>[200]</sup>

### Synthesis of Boc-Pro-alkyne (**28b**)



MW: 195.13 g/mol

Compound **28b** was synthesized from compound **26b** (236 mg, 0.9 mmol) following the general protocol **B.1**. Flash chromatography (EtOAc/Hexane, 1:9) yielded compound **28b** as white crystals (117 mg, 66%).

$^1\text{H-NMR}$  (400 MHz,  $\text{CDCl}_3$ ):  $\delta$ = 4.45 (m, 1H,  $\text{H}_\alpha$ ), 3.45-3.30 (m, 2H,  $\text{H}_\delta$ ), 2.20 (bs, 1H, alkyne), 2.06-1.88 (m, 4H,  $\text{H}_\gamma$ ,  $\text{H}_\beta$ ), 1.46 (s, 9H,  $^t\text{Bu}$ ) ppm

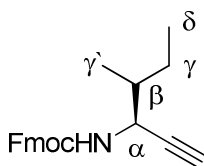
$^{13}\text{C-NMR}$  (100 MHz,  $\text{CDCl}_3$ ):  $\delta$ = 154.0, 79.8, 69.4, 48.0, 45.5, 33.6, 28.5, 23.6 ppm

One  $^{13}\text{C}$  signal was not observed due to overlapping signals.

The data was found to be identical as published.<sup>[172]</sup>



### Synthesis of Fmoc-Ile-alkyne (29a)



MW: 333.17 g/mol

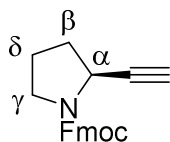
Compound **28a** (10 mg, 0.05 mmol, 1.0 equiv.) was suspended in solution of CH<sub>2</sub>Cl<sub>2</sub>/TFA/H<sub>2</sub>O (75:20:5) (0.5 mL) and was stirred for 1 h at RT. After completion of the reaction, the solvent was removed under reduced pressure and the residue was dissolved several times in toluene, which was then removed *in vacuo*, to remove the residues of H<sub>2</sub>O. The crude was dissolved in CH<sub>2</sub>Cl<sub>2</sub> and Fmoc-OSu (23.8 mg, 0.07 mmol, 1.5 equiv.) and DIPEA (30 μL, 0.09 mmol, 4.0 equiv.) were added. The reaction was stirred for 2 h at RT. After removing the solvent under reduced pressure, the product was purified *via* flash chromatography (EtOAc/Hexane; 5:95). Compound **29a** was obtained as white crystals (15.7 mg, 84%).

<sup>1</sup>H-NMR (500 MHz, CDCl<sub>3</sub>): δ= 7.76 (d, <sup>3</sup>J<sub>HH</sub>= 7.5 Hz, 2H, Fmoc), 7.60 (d, <sup>3</sup>J<sub>HH</sub>= 7.5 Hz, 2H, Fmoc), 7.40 (dd, <sup>3</sup>J<sub>HH</sub>= 7.5 Hz, <sup>4</sup>J<sub>HH</sub>= 0.7 Hz, 2H, Fmoc), 7.76 (td, <sup>3</sup>J<sub>HH</sub>= 7.5 Hz, <sup>4</sup>J<sub>HH</sub>= 0.7 Hz, 2H, Fmoc), 4.99 (d, <sup>3</sup>J<sub>HH</sub>= 7.5 Hz, 1H, -NH-), 4.49 (m, 1H, H<sub>α</sub>), 4.42 (m, 2H, Fmoc), 4.42 (t, <sup>3</sup>J<sub>HH</sub>= 6.5 Hz, 1H, Fmoc), 2.27 (d, <sup>4</sup>J<sub>HH</sub>= 2.5 Hz, 1H, alkyne), 1.70-1.66 (m, 1H, H<sub>β</sub>), 1.57-1.49 (m, 1H, H<sub>γ</sub>), 1.33-1.20 (m, 1H, H<sub>γ</sub>) 0.98 (d, <sup>3</sup>J<sub>HH</sub>= 6.5 Hz, 3H, H<sub>γ</sub>), 0.94 (t, <sup>3</sup>J<sub>HH</sub>= 7.0 Hz, 3H, H<sub>δ</sub>) ppm

<sup>13</sup>C-NMR (100 MHz, CDCl<sub>3</sub>): δ= 143.8, 141.3, 127.7, 127.1, 125.0, 120.00, 119.98, 72.3, 66.9, 47.9, 47.2, 39.1, 26.0, 14.4, 11.5 ppm

One <sup>13</sup>C signal was not observed due to overlapping signals.

The data was found to be identical as published.<sup>[186]</sup>

**Synthesis of Fmoc-Pro-alkyne (29b)**

MW: 317.14 g/mol

Compound **28b** (50 mg, 0.3 mmol, 1.0 equiv.) was suspended in solution of CH<sub>2</sub>Cl<sub>2</sub>/TFA/H<sub>2</sub>O (75:20:5) (0.5 mL) and was stirred for 1 h at RT. After completion of the reaction, the solvent was removed under reduced pressure and the residue was dissolved several times with toluene, which was then removed *in vacuo*, to remove the residues of H<sub>2</sub>O. The deprotected alkyne was dissolved in CH<sub>2</sub>Cl<sub>2</sub> and Fmoc-OSu (129.6 mg, 0.4 mmol, 1.5 equiv.) and DIPEA (85.0  $\mu$ L, 0.5 mmol, 2.0 equiv.) were added. The reaction was stirred for 2 h, at RT. After removing the solvent under reduced pressure, the product was purified *via* flash chromatography (EtOAc:Hexane: 2:8). Compound **29b** was obtained as white crystals (79 mg, 95%).

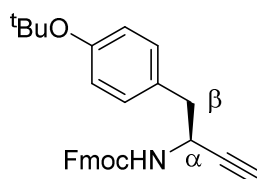
<sup>1</sup>H-NMR (400 MHz, CDCl<sub>3</sub>):  $\delta$ = 7.78 (d, <sup>3</sup>J<sub>HH</sub>= 7.5 Hz, 2H, Fmoc), 7.74-7.60 (m, 2H, Fmoc), 7.40 (td, <sup>3</sup>J<sub>HH</sub>= 7.5 Hz, <sup>4</sup>J<sub>HH</sub>= 1.0 Hz, 2H, Fmoc), 7.31 (td, <sup>3</sup>J<sub>HH</sub>= 7.5 Hz, <sup>4</sup>J<sub>HH</sub>= 1.0 Hz, 2H, Fmoc) 4.58-4.23 (m, 4H, Fmoc, H $\alpha$ ), 3.61-3.40 (m, 2H, H $\delta$ ), 2.28 (bs, 1H, alkyne), 2.16-1.96 (m, 4H, H $\gamma$ , H $\beta$ ) ppm

<sup>13</sup>C-NMR (100 MHz, CDCl<sub>3</sub>):  $\delta$ = 154.7, 144.15, 144.2, 141.5, 127.8, 127.1, 125.3, 120.1, 70.7, 67.5, 48.5, 47.5, 33.1 ppm

Two <sup>13</sup>C signals were not observed due to overlapping signals.

The data was found to be identical as published.<sup>[187]</sup>

Synthesis of Fmoc-Tyr(<sup>t</sup>Bu)-alkyne (**29c**)



MW: 439.21 g/mol

Compound **29c** was synthesized from compound **34c** (140 mg, 0.3 mmol, 1.0 equiv.) following the general protocol **B.2**. Flash chromatography, (EtOAc/Hexane, gradient 5:95 to 8:92) yielded compound **29c** as white crystals (62 mg, 51%).

$[\alpha]_D^{20} = -7.8$  (c=0.6, CHCl<sub>3</sub>)

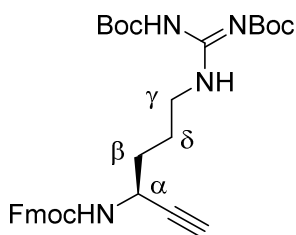
<sup>1</sup>H-NMR (500 MHz, CDCl<sub>3</sub>): δ= 7.77 (dd, <sup>3</sup>J<sub>HH</sub>= 7.5 Hz, <sup>4</sup>J<sub>HH</sub>= 1.0 Hz, 2H, Fmoc), 7.57 (d, <sup>3</sup>J<sub>HH</sub>= 7.5 Hz, 2H, Fmoc), 7.40 (tq, <sup>3</sup>J<sub>HH</sub>= 7.5 Hz, <sup>4</sup>J<sub>HH</sub>= 1.0 Hz, 2H, Fmoc), 7.32 (td, <sup>3</sup>J<sub>HH</sub>= 7.5 Hz, <sup>4</sup>J<sub>HH</sub>= 1.0 Hz, 2H, Fmoc), 7.12 (d, <sup>3</sup>J<sub>HH</sub>= 8.0 Hz, 2H, arom.), 6.92 (dt, <sup>3</sup>J<sub>HH</sub>= 8.0 Hz, <sup>4</sup>J<sub>HH</sub>= 2.5 Hz, 2H, arom.), 4.94 (d, <sup>3</sup>J<sub>HH</sub>= 9.0 Hz, 1H, -NH-), 4.72 (m, 1H, H<sub>α</sub>), 4.47-4.36 (m, 2H, Fmoc), 4.21 (t, <sup>3</sup>J<sub>HH</sub>= 7.5 Hz, 1H, Fmoc), 2.97-2.93 (m, 2H, H<sub>β</sub>), 2.31 (d, <sup>4</sup>J<sub>HH</sub>= 2.0 Hz, 1H, alkyne), 1.33 (s, 9H, -<sup>t</sup>Bu) ppm

<sup>13</sup>C-NMR (100 MHz, CDCl<sub>3</sub>): δ= 154.6 (C<sub>q</sub>), 143.9 (C<sub>q</sub>), 141.5 (C<sub>q</sub>), 130.4 (Fmoc), 127.9 (Fmoc), 127.2 (Fmoc), 125.1 (arom.), 124.1 (Fmoc), 120.1 (arom.), 82.5 (C<sub>q</sub>, alkyne), 78.5 (C<sub>q</sub>), 72.6 (alkyne), 67.0 (Fmoc), 47.3 (Fmoc), 44.4 (C<sub>α</sub>), 40.9 (C<sub>β</sub>), 29.0 (<sup>t</sup>Bu) ppm

Two <sup>13</sup>C signals were not observed due to overlapping signals (confirmed by 2D NMR).

ESI-HRMS: [M+Na]<sup>+</sup> *m/z* calcd for C<sub>29</sub>H<sub>29</sub>NO<sub>3</sub>: 439.2147, found: 462.2037

**Synthesis of Fmoc-Arg(Boc)<sub>2</sub>-alkyne (29d)**



MW: 576.29 g/mol

Compound **29d** was synthesized from compound **34d** (500 mg, 0.8 mmol, 1.0 equiv.) following the general protocol **B.1**. Two flash chromatographies, (EtOAc/Hexane, 3:7) and (MeOH/CH<sub>2</sub>Cl<sub>2</sub>, 0:100 to 5:95) yielded compound **29d** as white crystals (100 mg, 22%).

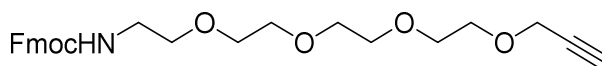
$[\alpha]_D^{20} = -4.1$  (c=0.5, CHCl<sub>3</sub>)

<sup>1</sup>H-NMR (500 MHz, CD<sub>3</sub>CN):  $\delta =$  11.53 (s, 1H, -NH-), 8.21 (m, 1H, -NH-), 7.81 (dq, <sup>3</sup>J<sub>HH</sub> = 7.5 Hz, <sup>4</sup>J<sub>HH</sub> = 1.0 Hz, 2H, Fmoc), 7.63 (t, <sup>3</sup>J<sub>HH</sub> = 8.5 Hz, 2H, Fmoc), 7.40 (tt, <sup>3</sup>J<sub>HH</sub> = 7.5 Hz, <sup>4</sup>J<sub>HH</sub> = 1.0 Hz, 2H, Fmoc), 7.31 (tt, <sup>3</sup>J<sub>HH</sub> = 7.5 Hz, <sup>4</sup>J<sub>HH</sub> = 1.0 Hz, 2H, Fmoc), 6.10 (d, <sup>3</sup>J<sub>HH</sub> = 8.5 Hz, 1H, -NH-), 4.37-4.32 (m, 3H, Fmoc, H $\alpha$ ), 4.21 (t, <sup>3</sup>J<sub>HH</sub> = 7.5 Hz, 1H, Fmoc), 3.32-3.31 (m, 2H, H $\delta$ ), 2.54 (d, <sup>4</sup>J<sub>HH</sub> = 2.0 Hz, 1H, alkyne) 1.65-1.61 (m, 4H, H $\gamma$ , H $\beta$ ), 1.47 (s, 9H, Boc), 1.41 (s, 9H, Boc) ppm

<sup>13</sup>C-NMR (100 MHz, CDCl<sub>3</sub>):  $\delta =$  164.6 (C<sub>q</sub>), 157.2 (C<sub>q</sub>), 153.9 (C<sub>q</sub>), 145.1 (C<sub>q</sub>), 128.6 (C<sub>t</sub>, Fmoc), 128.0 (C<sub>t</sub>, Fmoc), 126.1 (C<sub>t</sub>, Fmoc), 120.9 (C<sub>t</sub>, Fmoc), 83.9 (C<sub>q</sub>, Boc), 79.4 (C<sub>q</sub>, Boc), 67.1 (C<sub>s</sub>, Fmoc), 48.0 (C<sub>t</sub>, Fmoc) 43.5 (C $\alpha$ ), 40.7 (C $\delta$ ), 33.2 (C $\beta$ ), 28.4 (Boc), 28.1 (Boc), 26.3 (C $\gamma$ ) ppm

Four <sup>13</sup>C signals were not observed due to overlapping signals (confirmed by 2D NMR).

ESI-HRMS: [M+H]<sup>+</sup> *m/z* calcd for C<sub>32</sub>H<sub>40</sub>N<sub>4</sub>O<sub>6</sub>: 576.2948, found: 577.3024

**Synthesis of Fmoc-PEG<sub>4</sub>-alkyne (29f)**

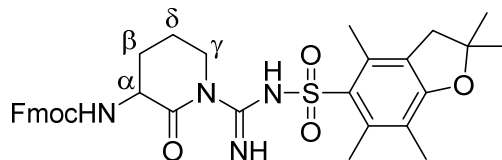
MW: 453.22 g/mol

tert-butyl (2-(2-(2-(2-hydroxyethoxy)ethoxy)ethoxy)ethyl)carbamate (Boc-PEG<sub>3</sub>-ethyl alcohol) (**31**) (500 mg, 1.7 mmol, 1.0 equiv.) was dissolved in anhydrous THF and NaH (27.6 mg, 2.0 mmol, 1.15 equiv.) was added under argon. The mixture was stirred for 45 min. The reaction was cooled to 0 °C, and propargylbromide (280 µL, 2.6 mmol, 1.5 equiv.) was slowly added to the reaction mixture through a dropping funnel. After allowing the reaction stir for 12 h, the THF was removed *in vacuo* and the residue was dissolved in CH<sub>2</sub>Cl<sub>2</sub> and washed with H<sub>2</sub>O (3 x 20 mL) and brine (3 X 20 mL). The combined organic phases were dried over Mg<sub>2</sub>SO<sub>4</sub>, filtered and the solvent was removed under reduced pressure. The resulting residue was dissolved in CH<sub>2</sub>Cl<sub>2</sub> (2 mL) TFA was slowly added (1 mL). The cleavage of the Boc-group was monitored by TLC. After removal of the protective group, the solvent was removed *in vacuo*. The residue was then dissolved in toluene and the solvent was evaporated. The residue was dissolved in CH<sub>2</sub>Cl<sub>2</sub> (3 mL) and DIPEA (350 µL, 3.0 mmol, 2.0 equiv.) and Fmoc-OSu (230 mg, 2.6 mmol, 1.5 equiv.) were added successively. The reaction was allowed to stir for 2 h at RT until completion of the reaction. The solvent of the crude mixture was evaporated *in vacuo* and the residue was purified *via* flash chromatography (EtOAc/Hexane; 4:6), yielding compound **29f** as a colourless oil (231 mg, 50%).

<sup>1</sup>H-NMR (400 MHz, DMSO-d<sub>6</sub>): δ= 7.89 (d, <sup>3</sup>J<sub>HH</sub>= 7.6 Hz, 2H), 7.70 (d, <sup>3</sup>J<sub>HH</sub>= 7.6 Hz, 2H), 7.42 (t, <sup>3</sup>J<sub>HH</sub>= 7.6 Hz, 2H), 7.33 (t, <sup>3</sup>J<sub>HH</sub>= 7.6 Hz, 2H), 4.30 (d, <sup>3</sup>J<sub>HH</sub>= 6.8 Hz, 2H), 4.21 (t, <sup>3</sup>J<sub>HH</sub>= 6.8 Hz, 1H), 4.13 (d, <sup>3</sup>J<sub>HH</sub>= 3.2 Hz, 2H), 3.55-3.50 (m, 10H), 3.45 – 3.40 (m, 4H), 3.14 (dd, <sup>3</sup>J<sub>HH</sub>= 11.6, 5.8 Hz, 2H), 2.55 – 2.46 (m, 1H) ppm

The data was found to be identical as published.<sup>[138]</sup>

**Synthesis of (9H-fluoren-9-yl)methyl (2-oxo-1-(N-((2,2,4,6,7-pentamethyl-2,3-dihydrobenzofuran-5-yl)sulfonyl)carbamimidoyl)piperidin-3-yl)carbamate (39)**



MW: 630.27 g/mol

Compound **39** was synthesized following the general protocol **A**. Fmoc-Arg(Pbf)-OH **37** (1.5 g, 2.3 mmol, 1.0 equiv.) was used as starting material. Flash chromatography (EtOAc/Hexane, 5:5) yielded compound **39** as white crystals (0.86 g, 82%).

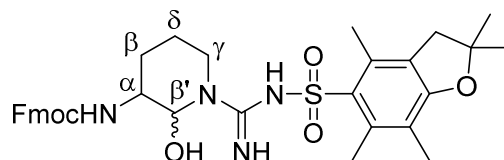
$^1\text{H-NMR}$  (500 MHz,  $\text{CD}_3\text{Cl}_3$ ):  $\delta$ = 9.41 (s, 1H, -NH-), 7.91 (bs, 1H, -NH-), 7.76 (d,  $^3J_{\text{HH}}$ = 7.5 Hz, 2H, Fmoc), 7.59 (t,  $^3J_{\text{HH}}$ = 7.5 Hz, 2H, Fmoc), 7.40 (t,  $^3J_{\text{HH}}$ = 7.5 Hz, 2H, Fmoc), 7.31 (td,  $^3J_{\text{HH}}$ = 7.5 Hz,  $^4J_{\text{HH}}$ = 1.0 Hz, 2H, Fmoc), 5.53 (d,  $^3J_{\text{HH}}$ = 7.0 Hz, 1H, -NH-), 4.58 (d,  $^3J_{\text{HH}}$ = 13.5 Hz, 1H, H $\delta$ ), 4.45-4.38 (m, 3H, Fmoc, H $\alpha$ ), 4.23 (t,  $^3J_{\text{HH}}$ = 6.5 Hz, 1H, Fmoc), 4.41-3.37 (m, 1H, H $\delta$ ), 2.97 (s, 2H, Pbf), 2.58 (s, 3H, Pbf), 2.53 (s, 3H, Pbf), 2.11 (s, 3H, Pbf), 1.90-1.84 (m, 2H, H $\beta$  or H $\gamma$ ), 1.49-1.42 (m, 2H, H $\beta$  or H $\gamma$ ), 1.47 (s, 6H, Pbf) ppm

$^{13}\text{C-NMR}$  (100 MHz,  $\text{CDCl}_3$ ):  $\delta$ = 159.4 ( $\text{C}_q$ ), 154.0 ( $\text{C}_q$ ), 143.9 ( $\text{C}_q$ ), 141.5 ( $\text{C}_q$ ), 139.0 ( $\text{C}_q$ ), 133.0 ( $\text{C}_q$ ), 131.1 ( $\text{C}_q$ ), 127.9 (Fmoc), 127.2 (Fmoc), 125.2 (Fmoc), 120.2 (Fmoc), 117.9 ( $\text{C}_q$ ), 86.8 ( $\text{C}_q$ ), 67.4 (Fmoc), 52.8 ( $\text{C}_\alpha$ ), 47.2 (Fmoc), 43.3 (Pbf), 41.8 (C $\delta$ ), 28.7 (Pbf), 25.0 (C $\beta$  or C $\gamma$ ), 20.0 (C $\beta$ /C $\gamma$ ), 19.4 (Pbf), 18.1 (Pbf), 12.6 (Pbf) ppm

Three  $^{13}\text{C}$  signals were not observed due to overlapping signals.

ESI-MS:  $[\text{M}+\text{H}]^+$   $m/z$  calcd for  $\text{C}_{34}\text{H}_{38}\text{N}_4\text{O}_6\text{S}$ : 630.27, found: 631.5

**Synthesis of cyclic (9H-fluoren-9-yl)methyl (2-hydroxy-1-(N-((2,2,4,6,7-pentamethyl-2,3-dihydrobenzofuran-5-yl)sulfonyl)carbamimidoyl)piperidin-3-yl)carbamate (41)**



MW: 632.27 g/mol

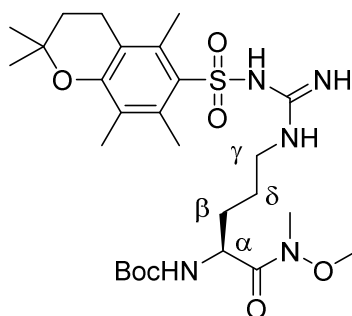
Compound **41** was synthesised from compound **39**, following the general protocol **B.2**. Flash chromatography (EtOAc:Hexane, 8:2) yielded compound **41** as white crystals. Yield was not determined.

$^1\text{H-NMR}$  (500 MHz,  $\text{CD}_3\text{Cl}_3$ ):  $\delta$ = 7.75 (d,  $^3J_{\text{HH}}$ = 7.5 Hz, 2H, Fmoc), 7.58 (d,  $^3J_{\text{HH}}$ = 7.5 Hz, 2H, Fmoc), 7.39 (t,  $^3J_{\text{HH}}$ = 7.5 Hz, 2H, Fmoc), 7.31-7.27 (m, 2H, Fmoc), 6.48 (bs, 2H, -NH-Pbf, -OH), 5.70 (d,  $^3J_{\text{HH}}$ = 6.5 Hz, 1H, H $\beta'$ ), 5.53 (d,  $^3J_{\text{HH}}$ = 9.5 Hz, 1H, -NH-), 4.39-4.36 (m, 2H, Fmoc), 4.20 (t,  $^3J_{\text{HH}}$ = 7.0 Hz, 1H, Fmoc), 3.68-6.63 (m, 1H, H $\alpha$ ), 3.47-3.44 (m, 1H, H $\delta$ ), 3.22-3.17 (m, 1H, H $\delta$ ), 2.95 (s, 2H, Pbf), 2.55 (s, 3H, Pbf), 2.49 (s, 3H, Pbf), 2.10 (s, 3H, Pbf), 1.83-1.79 (m, 2H, H $\beta$ /H $\gamma$ ), 1.67-1.57 (m, 2H, H $\beta$ /H $\gamma$ ), 1.45 (s, 6H, Pbf) ppm

$^{13}\text{C-NMR}$  (100 MHz,  $\text{CDCl}_3$ ):  $\delta$ = 127.7 (Fmoc), 127.1 (Fmoc), 125.1 (Fmoc), 120.0 (Fmoc), 75.5 (C $\beta'$ ) 66.8 (Fmoc), 50.4 (C $\alpha$ ), 47.1 (Fmoc), 43.1 (Pbf), 39.2 (C $\delta$ ), 28.5 (Pbf), 24.7 (C $\beta$  or C $\gamma$ ), 23.7 (C $\beta$ /C $\gamma$ ), 19.1 (Pbf), 17.1 (Pbf), 12.4 (Pbf) ppm

$^{13}\text{C}$  signals were obtained from 2D-NMR data. C $_q$  signals were not visible.

ESI-MS:  $[\text{M}+\text{H}]^+$   $m/z$  calcd for  $\text{C}_{34}\text{H}_{40}\text{N}_4\text{O}_6\text{S}$ : 632.27, found: 633.5

**Synthesis of Fmoc-Arg(Pmc)-O(NMe)OMe (43)**

MW: 583.3 g/mol

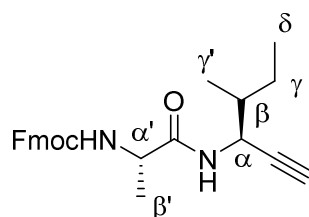
Boc-Arg(Pmc)-OH **42** (2.5 g, 4.6 mmol, 1.0 equiv.) was dissolved in CH<sub>2</sub>Cl<sub>2</sub> (45 mL) and HATU (1.7 g, 4.6 mmol, 1.0 equiv.) was added. The reaction mixture was stirred at RT for 15 min. *N,O*-dimethylhydroxylamine (0.3 g, 5.0 mmol, 1.1 equiv.) and DIPEA (1.7 mL, 0.01 mol, 2.2 equiv.) were added and the reaction was stirred for 12 h. Flash chromatography (MeOH/CH<sub>2</sub>Cl<sub>2</sub>, 2:98) yielded compound **43** as white crystals (0.5 g, 18%).

<sup>1</sup>H-NMR (400 MHz, CD<sub>3</sub>Cl<sub>3</sub>): δ= 6.22 (bs, 1H, -NH-), 6.04 (bs, 2H, -NH-), 5.46 (d, <sup>3</sup>J<sub>HH</sub>= 9.2 Hz, 1H, -NH-), 4.66 (m, 1H, H<sub>α</sub>), 3.73 (s, 3H, Pmc), 3.72-3.70 (m, 1H, H<sub>δ</sub>), 3.20 (s, 3H, N-Me), 3.19-3.15 (m, 1H, H<sub>δ</sub>), 2.62 (t, <sup>3</sup>J<sub>HH</sub>= 6.8 Hz, 2H, Pmc), 2.59 (s, 3H, Pmc), 2.57 (s, 3H, Pmc), 2.10 (s, 3H, -OMe), 1.80 (t, <sup>3</sup>J<sub>HH</sub>= 6.8 Hz, 2H, Pmc), 1.64-1.60 (m, 4H, H<sub>β</sub>/H<sub>γ</sub>), 1.42 (s, 9H, Boc), 1.47 (s, 6H, Pbf) ppm

<sup>13</sup>C-NMR was not recorded.



**Synthesis of Fmoc-Ala-Ile-alkyne (50a)**



MW: 404.21 g/mol

Compound **50a** was synthesized from compound **29a** (10 mg, 0.05 mmol, 1.0 equiv.) following the general procedure **C.1**. Flash chromatography (EtOAc/Hexane, 4:6) yielded compound **50a** as white crystals (18 mg, 90%).

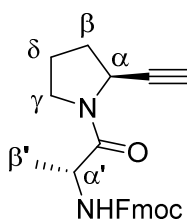
$^1\text{H-NMR}$  (500 MHz,  $\text{CDCl}_3$ ):  $\delta$ = 7.76 (d,  $^3J_{\text{HH}}$  = 7.5 Hz, 2H, Fmoc), 7.58 (m, 2H, Fmoc), 7.40 (t,  $^3J_{\text{HH}}$  = 7.5 Hz, 2H, Fmoc), 7.31 (td,  $^3J_{\text{HH}}$  = 7.5 Hz,  $^4J_{\text{HH}}$  = 1.5 Hz, 2H, Fmoc), 6.43 (d,  $^3J_{\text{HH}}$  = 5.5 Hz, 1H, -NH-Ala), 5.38 (d,  $^3J_{\text{HH}}$  = 6.5 Hz, 1H, -NH-Ile), 4.73 (m, 1H,  $\text{H}_\alpha$ ), 4.9 (m, 2H, Fmoc), 4.25 (m, 1H,  $\text{H}_{\alpha'}$ ), 4.41 (t,  $^3J_{\text{HH}}$  = 7.0 Hz, 1H, Fmoc), 2.17 (d,  $^4J_{\text{HH}}$  = 2.5 Hz, 1H, alkyne), 1.68-1.63 (m, 1H,  $\text{H}_\beta$ ), 1.51-1.47 (m, 1H,  $\text{H}_\gamma$ ), 1.39 (d,  $^3J_{\text{HH}}$  = 6.5 Hz, 3H,  $\text{H}_{\beta'}$ ), 1.26-1.18 (m, 1H,  $\text{H}_\gamma$ ) 0.92 (d,  $^3J_{\text{HH}}$  = 6.5 Hz, 3H,  $\text{H}_{\gamma'}$ ), 0.90 (t,  $^3J_{\text{HH}}$  = 7.5 Hz, 3H,  $\text{H}_\delta$ ) ppm

$^{13}\text{C-NMR}$  (100 MHz,  $\text{CDCl}_3$ ):  $\delta$ = 171.2 ( $\text{C}_q$ ), 143.8 ( $\text{C}_q$ ), 141.4 ( $\text{C}_q$ ), 127.9 (Fmoc), 127.2 (Fmoc), 125.2 (Fmoc), 120.2 (Fmoc), 81.1 ( $\text{C}_q$ ), 72.4 (alkyne), 67.4 (Fmoc), 47.2 (Fmoc), 46.2 ( $\text{C}_\alpha$ ), 39.0 ( $\text{C}_\beta$ ), 26.1 ( $\text{C}_\gamma$ ), 14.5 ( $\text{C}_{\gamma'}$ ), 11.6 ( $\text{C}_\delta$ ) ppm

Three  $^{13}\text{C}$  signals were not observed due to overlapping signals (confirmed with 2D NMR).

ESI-MS:  $[\text{M}+\text{H}]^+$   $m/z$  calcd for  $\text{C}_{25}\text{H}_{28}\text{N}_2\text{O}_3$ : 404.21, found: 405.3

**Synthesis of Fmoc-Ala-Pro-alkyne (50b)**



MW: 388.18 g/mol

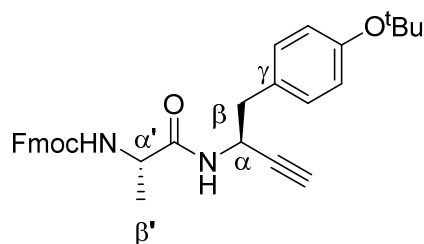
Compound **50b** was synthesized from compound **29b** (20 mg, 0.11 mmol, 1.0 equiv.) following the general procedure **C.1**. Flash chromatography (EtOAc:Hexane, 3:7) yielded compound **50b** as white crystals (13.5 mg, 30%).

$^1\text{H-NMR}$  (500 MHz,  $\text{DMSO-d}_6$ ):  $\delta$ = 7.89 (d,  $^3J_{\text{HH}} = 7.5$  Hz, 2H, Fmoc), 7.73 (d,  $^3J_{\text{HH}} = 7.5$  Hz, 2H, Fmoc), 7.64 (d,  $^3J_{\text{HH}} = 7.5$  Hz, 1H, -NH-), 7.41 (t,  $^3J_{\text{HH}} = 7.5$  Hz, 2H, Fmoc), 7.33 (tt,  $^3J_{\text{HH}} = 7.5$  Hz,  $^4J_{\text{HH}} = 1.0$  Hz, 2H, Fmoc) 4.70-4.68 (m, 0.24  $\text{H}_{\text{cis}}$ ,  $\text{H}\alpha$ ), 4.61-4.58 (m, 0.62  $\text{H}_{\text{trans}}$ ,  $\text{H}\alpha$ ), 4.55-4.58 (m, 0.35  $\text{H}_{\text{cis}}$ ,  $\text{H}\alpha'$ ), 4.28-4.18 (m, 3.45  $\text{H}_{\text{trans}}$ , Fmoc,  $\text{H}\alpha'$ ), 3.57-3.39 (m, 1.6 $\text{H}_{\text{trans}}$ ,  $\text{H}\delta$ ), 3.30-3.25 (m, 0.27 $\text{H}_{\text{cis}}$ ,  $\text{H}\delta$ ), 3.10 (d,  $^4J_{\text{HH}} = 2.0$  Hz, 1H, alkyne), 2.16-1.85 (m, 4H,  $\text{H}\gamma$ ,  $\text{H}\beta$ ), 1.22 (d,  $^3J_{\text{HH}} = 7.0$  Hz, 1.2 $\text{H}_{\text{cis}}$ ,  $\text{H}\beta'$ ), 1.19 (d,  $^3J_{\text{HH}} = 7.0$  Hz, 1.9 $\text{H}_{\text{trans}}$ ,  $\text{H}\beta'$ ) ppm

$^{13}\text{C-NMR}$  (100 MHz,  $\text{DMSO-d}_6$ ):  $\delta$ = 170.4 ( $\text{C}_q$ ), 155.6 ( $\text{C}_q$ ), 143.7 ( $\text{C}_q$ ), 140.6 ( $\text{C}_q$ ), 127.5 (Fmoc), 127.0 (Fmoc), 125.2 (Fmoc), 120.0 (Fmoc), 72.1 (alkyne), 65.5 (Fmoc), 47.8 (Fmoc or  $\text{C}\alpha'$ ), 46.4 (Fmoc or  $\text{C}\alpha'$ ) 45.0 ( $\text{C}\alpha$ ), 45.5 ( $\text{C}\delta$ ), 31.6 ( $\text{C}\beta$ ), 24.5 ( $\text{C}\gamma$ ), 16.7 ( $\text{C}\beta'$ ) ppm

ESI-HRMS:  $[\text{M}+\text{H}]^+$   $m/z$  calcd for  $\text{C}_{24}\text{H}_{24}\text{N}_2\text{O}_3$ : 388.1787, found: 389.1863

### Synthesis of Fmoc-Tyr(<sup>t</sup>Bu)-alkyne (50c)



MW: 510.25 g/mol

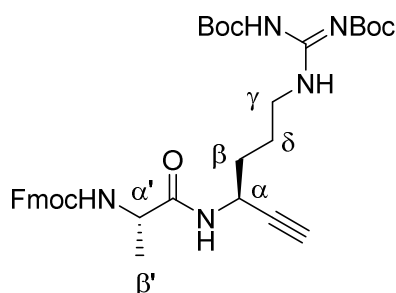
Compound **50c** was synthesized from compound **29c** (20 mg, 0.04 mmol, 1.0 equiv.) following the general procedure **C.2**. Flash chromatography (EtOAc/Hexane; 3:7) yielded compound **50c** as white crystals (13 mg, 65%).

<sup>1</sup>H-NMR (500 MHz, CDCl<sub>3</sub>): δ= 7.77 (dd, <sup>3</sup>J<sub>HH</sub>= 7.5 Hz, <sup>4</sup>J<sub>HH</sub>= 1.0 Hz, 2H, Fmoc), 7.60 (d, <sup>3</sup>J<sub>HH</sub>= 7.5 Hz, 2H, Fmoc), 7.40 (t, <sup>3</sup>J<sub>HH</sub>= 7.5 Hz, 2H, Fmoc), 7.32 (td, <sup>3</sup>J<sub>HH</sub>= 7.5 Hz, <sup>4</sup>J<sub>HH</sub>= 1.0 Hz, 2H, Fmoc), 7.11 (dt, <sup>3</sup>J<sub>HH</sub>= 8.5 Hz, <sup>4</sup>J<sub>HH</sub>= 2.0 Hz, 2H, arom.), 6.88 (dt, <sup>3</sup>J<sub>HH</sub>= 8.5 Hz, <sup>4</sup>J<sub>HH</sub>= 2.0 Hz, 2H, arom.), 5.34 (d, <sup>3</sup>J<sub>HH</sub>= 8.0 Hz, 1H, -NH-Tyr), 4.94 (d, <sup>3</sup>J<sub>HH</sub>= 8.0 Hz, 1H, -NH-Ala), 4.95-4.90 (m, 1H, H<sub>α</sub>-Tyr), 4.43-4.36 (m, 2H, Fmoc), 4.22 (t, <sup>3</sup>J<sub>HH</sub>= 7.0 Hz, 1H, Fmoc), 4.19 (m, 1H, H<sub>α</sub>'), 2.95-2.87 (m, 2H, H<sub>β</sub>), 2.21 (d, <sup>4</sup>J<sub>HH</sub>= 2.5 Hz, 1H, alkyne), 1.34 (d, <sup>3</sup>J<sub>HH</sub>= 7.0 Hz, 3H, H<sub>β</sub>'), 1.31 (s, 9H, -<sup>t</sup>Bu) ppm

<sup>13</sup>C-NMR (100 MHz, CDCl<sub>3</sub>): δ= 171.2 (C<sub>q</sub>), 156.1 (C<sub>q</sub>), 154.1 (C<sub>q</sub>), 143.8 (C<sub>q</sub>), 141.4 (C<sub>q</sub>), 130.3 (arom.), 128.0 (Fmoc), 127.2 (Fmoc), 125.2 (Fmoc), 125.2 (C<sub>q</sub>), 124.1 (arom.), 120.2 (Fmoc), 82.3 (C<sub>q</sub>), 78.5 (C<sub>q</sub>), 72.6 (alkyne), 67.3 (Fmoc), 50.5 (C<sub>α</sub>'), 47.2 (Fmoc), 42.7 (C<sub>α</sub>-Tyr), 40.6 (C<sub>β</sub>), 29.0 (-<sup>t</sup>Bu), 18.6 (-C<sub>β</sub>') ppm

ESI-MS: [M+H]<sup>+</sup> *m/z* calcd for C<sub>32</sub>H<sub>34</sub>N<sub>2</sub>O<sub>4</sub>: 510.3, found: 511.5

**Synthesis of Fmoc-Arg(Boc)<sub>2</sub>-alkyne (50d)**



MW: 647.33 g/mol

Compound **50d** was synthesized from compound **29d** (20 mg, 0.04 mmol, 1.0 equiv.), following the general procedure **C.2**. Flash chromatography (EtOAc/Hexane, 3:7) yielded compound **50d** as white crystals (14.6 mg, 65%).

<sup>1</sup>H-NMR (600 MHz, CD<sub>3</sub>CN): δ= 11.51 (s, 1H, -NH-), 8.19 (s, 1H, -NH-), 7.82 (d, <sup>3</sup>J<sub>HH</sub>= 7.8 Hz, 2H, Fmoc), 7.65 (d, <sup>3</sup>J<sub>HH</sub>= 7.8 Hz, 2H, Fmoc), 7.41 (t, <sup>3</sup>J<sub>HH</sub>= 7.8 Hz, 2H, Fmoc), 7.33 (tt, <sup>3</sup>J<sub>HH</sub>= 7.8 Hz, <sup>4</sup>J<sub>HH</sub>= 1.2 Hz, 2H, Fmoc), 6.93 (d, <sup>3</sup>J<sub>HH</sub>= 8.4 Hz, 1H, -NH-Arg), 5.94 (d, <sup>3</sup>J<sub>HH</sub>= 7.8 Hz, 1H, -NH-Ala), 4.65-4.61 (m, 1H, H<sub>α</sub>), 4.33-4.31 (m, 2H, Fmoc), 4.22 (t, <sup>3</sup>J<sub>HH</sub>= 6.9 Hz, 1H, Fmoc), 4.05-4.01 (m, 1H, H<sub>α'</sub>), 3.31-3.29 (m, 2H, H<sub>δ</sub>), 2.51 (d, <sup>4</sup>J<sub>HH</sub>= 2.4 Hz, 1H, alkyne), 1.68-1.60 (m, 4H, H<sub>γ</sub>, H<sub>β</sub>), 1.44 (s, 9H, Boc), 1.41 (s, 9H, Boc), 1.26 (d, (d, <sup>3</sup>J<sub>HH</sub>= 7.2 Hz, 3H, H<sub>β'</sub>) ppm

<sup>13</sup>C-NMR (100 MHz, CDCl<sub>3</sub>): δ= 173.1 (C<sub>q</sub>), 165.1 (C<sub>q</sub>), 157.7 (C<sub>q</sub>), 157.3 (C<sub>q</sub>), 154.4 (C<sub>q</sub>), 145.6 (C<sub>q</sub>), 142.6 (C<sub>q</sub>), 129.2 (Fmoc), 128.6 (Fmoc), 126.7 (Fmoc), 121.5 (Fmoc), 84.62 (alkyne), 84.4 (C<sub>q</sub>, Boc), 79.9 (C<sub>q</sub>, Boc), 72.6 (C<sub>q</sub>), 67.7 (C<sub>s</sub>, Fmoc), 52.0 (C<sub>α'</sub>), 48.5 (Fmoc), 41.9 (C<sub>α</sub>), 41.3 (C<sub>δ</sub>), 33.7 (C<sub>β</sub>), 28.9 (<sup>t</sup>Bu, Boc), 28.6 (<sup>t</sup>Bu, Boc), 26.6 (C<sub>γ</sub>), 18.3 (C<sub>β'</sub>) ppm

ESI-HRMS: [M+H]<sup>+</sup> *m/z* calcd for C<sub>35</sub>H<sub>45</sub>N<sub>5</sub>O<sub>7</sub>: 647.3319, found: 648.3319

## 5.3 Synthesis of Peptides

### 5.3.1 General Procedures

#### General Procedure D: Manual Solid Phase Peptide Synthesis

Resin (Leu-preloaded PEG-PS or rink amide MBHA resin LL) (0.03 mmol) was swollen in DMF (3 x 3 mL) in a syringe fitted with a polypropylene frit and a teflon tap. The Fmoc-protected amino acid (0.06 mmol, 2.0 equiv.), HATU (0.06 mmol, 2.0 equiv.) and DIPEA (0.15 mmol, 5.0 equiv.) were added to the resin and the suspension was shaken for 1.5 h at RT. The solvent was removed by filtration, and the resin was repeatedly washed with DMF and CH<sub>2</sub>Cl<sub>2</sub>. Completion of the reaction was checked by Kaiser test and repeated if necessary. Coupling of the spacers Fmoc-PEG<sub>4</sub>-OH and Fmoc-Ahx-OH and the chelator DOTA-(*tris*-<sup>t</sup>Bu) was performed with the same reaction conditions.

#### General Procedure E: Fmoc Deprotection on the Resin

20% piperidine in DMF was added to the resin and was left to react for 3 min. The deprotection agent was then filtered off and this process was repeated three times. The resin was then washed thoroughly with DMF and CH<sub>2</sub>Cl<sub>2</sub>.

#### General Procedure F: Introduction of the Azido Functionality on the *N*-Terminus of the Peptide on the Resin

After Fmoc-cleavage to obtain the free *N*-terminal amine, imidazole-1-sulfonyl azide hydrochloride (**6**) (5.0 equiv.) and DIPEA (6.0 equiv.) were added in DMF to the resin. The suspension was shaken for 1 h at RT. The solvent was filtered off and the resin was washed with DMF and CH<sub>2</sub>Cl<sub>2</sub>. Completion of the reaction was checked with a Kaiser test and by the colorimetric test for solid-support azides developed by Punna and Finn.<sup>[185]</sup>

#### General Procedure G: Solid Phase Copper Catalysed Cycloaddition (CuAAC)

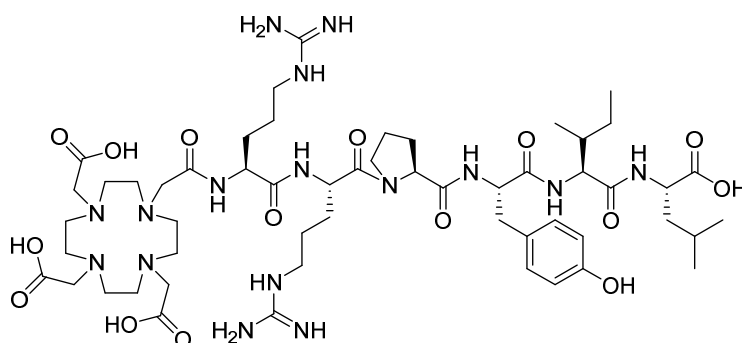
The resin functionalized *N*-terminally with an azide was swollen with anhydrous DMF. The corresponding Fmoc-protected  $\alpha$ -amino alkyne (2.0 equiv.), DIPEA (1.0 equiv.), tetrakis(acetonitrile)copper(I) hexafluorophosphate (0.5 equiv.) and TBTA (0.5 equiv.) were added in anhydrous DMF. The suspension was shaken for 12-15 h at RT. The resin was then washed repeatedly with a solution of 0.5% diethyldithiocarbamate in DMF. Washing steps were repeated with DMF and CH<sub>2</sub>Cl<sub>2</sub>. Kaiser test and azide test were performed to check the completion of the reaction.

### **General Procedure H: Cleavage and Purification of the Peptide Conjugates**

After completion of the elongation of the amino acid sequence and the attachment of the spacer and the chelator, the conjugates were cleaved and deprotected by a standard treatment of 6 h with TFA/ H<sub>2</sub>O/TIS/ PhOH (87.5:5:2.5:2.5). The resin was filtered off and the cleavage mixture was removed by evaporation with a stream of argon. The crude peptide conjugate was then precipitated by addition of ice-cold diethyl ether (15 mL). After centrifugation and two washing steps with diethyl ether, the peptide conjugate was dissolved in H<sub>2</sub>O and MeCN and purified by preparative HPLC, using 0.1% TFA in H<sub>2</sub>O as solvent A and 0.1% TFA in MeCN as solvent B.

### 5.3.3 Synthesis of Peptide Conjugates

#### Synthesis of DOTA-Arg-Arg-Pro-Tyr-Ile-Leu (AM-NT 1)

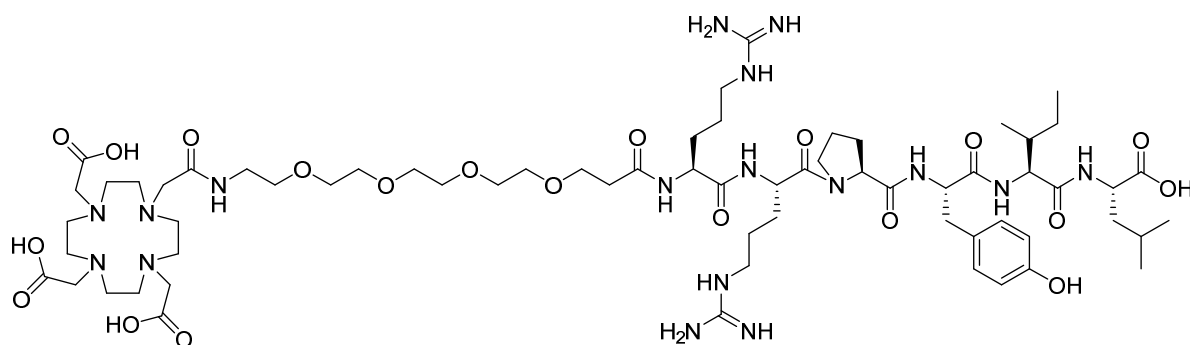


MW: 1202.7 g/mol

Peptide conjugate **AM-NT 1** was prepared following procedures **D**, **E** and **H** using a Leu-preloaded PEG-PS resin (0.03 mmol) and commercial DOTA-(*tris*-<sup>t</sup>Bu), Fmoc-Arg(Pbf)-OH, Fmoc-Pro-OH, Fmoc-Tyr(<sup>t</sup>Bu)-OH and Fmoc-Ile-OH. Preparative HPLC (80-70% A in B in 15 min) yielded peptide conjugate **AM-NT 1** in a high purity (>98%) as a white powder (25.3 mg, 70%).

Analytical HPLC: (90-50% A in B in 20 min),  $t_r = 8.47$  min.

ESI-HRMS  $m/z$   $[M+2H^+]^{2+}$  calcd for  $C_{54}H_{90}N_{16}O_{15}$ : 1202.6772, theor.  $[M+2H^+]^{2+}$ : 602.3386, found: 602.3468

**Synthesis of DOTA-PEG<sub>4</sub>-Arg-Arg-Pro-Tyr-Ile-Leu (AM-NT 2)**

MW: 1449.8 g/mol

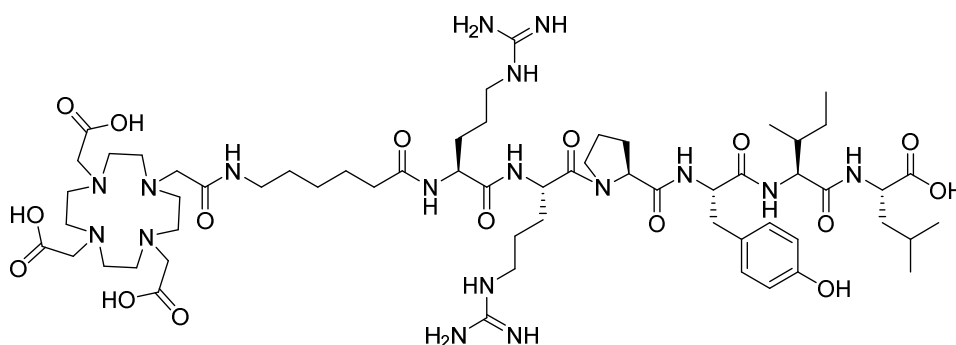
Peptide conjugate **AM-NT 2** was prepared following procedures **D**, **E** and **H** using a Leu-preloaded PEG-PS resin (0.03 mmol) and commercial DOTA-(*tris*-*t*Bu), Fmoc-PEG<sub>4</sub>-COOH, Fmoc-Arg(Pbf)-OH, Fmoc-Pro-OH, Fmoc-Tyr(*t*Bu)-OH and Fmoc-Ile-OH. Purification of the by preparative HPLC (80-70% A in B in 15 min) yielded peptide conjugate **AM-NT 2** in high purity (>98%), as a white powder (1 mg, 2%).

Analytical HPLC: (90-50% A in B in 20 min),  $t_r = 8.69$  min.

ESI-HRMS  $m/z$   $[M+2H^+]^{2+}$  calcd for C<sub>65</sub>H<sub>111</sub>N<sub>17</sub>O<sub>20</sub>: 1449.8191, theor.  $[M+2H^+]^{2+}$ : 725.9095, found: 725.9174



**Synthesis of DOTA-Ahx-Arg-Arg-Pro-Tyr-Ile-Leu (AM-NT 3)**

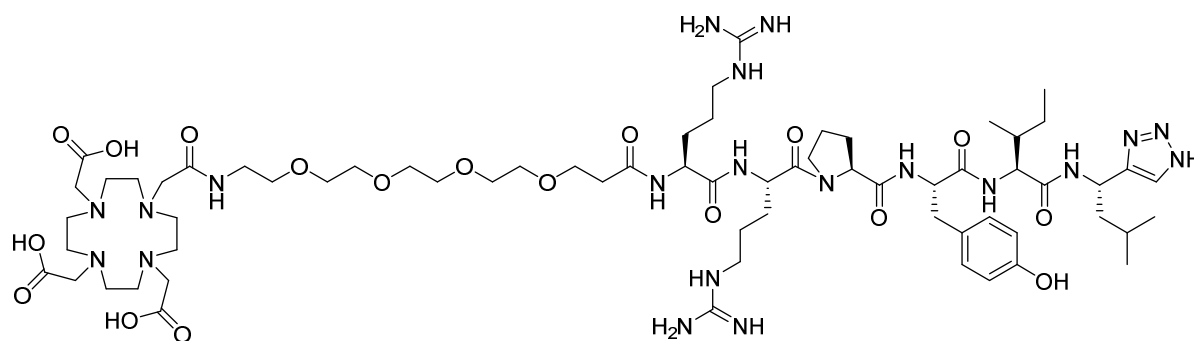


MW: 1315.8 g/mol

Peptide conjugate **AM-NT 3** was prepared following procedures **D**, **E** and **H** using a Leu-preloaded PEG-PS resin (0.03 mmol) and commercial DOTA-(*tris*-<sup>t</sup>Bu), Fmoc-Ahx-OH, Fmoc-Arg(Pbf)-OH, Fmoc-Pro-OH, Fmoc-Tyr(<sup>t</sup>Bu)-OH and Fmoc-Ile-OH. Purification by preparative HPLC (80-70% A in B in 15 min) and lyophilisation (74%), peptide conjugate **AM-NT 3** was obtained in high purity (> 98%) as a white powder (9.6 mg, 30%).

Analytical HPLC: (90-50% A in B in 20 min),  $t_r = 8.83$  min.

ESI- HRMS  $m/z$   $[M+3H]^3+$  calcd for  $C_{60}H_{101}N_{17}O_{15}$ : 1315.7612, theor.  $[M+3H]^3+$ : 439.5870, found: 439.5941

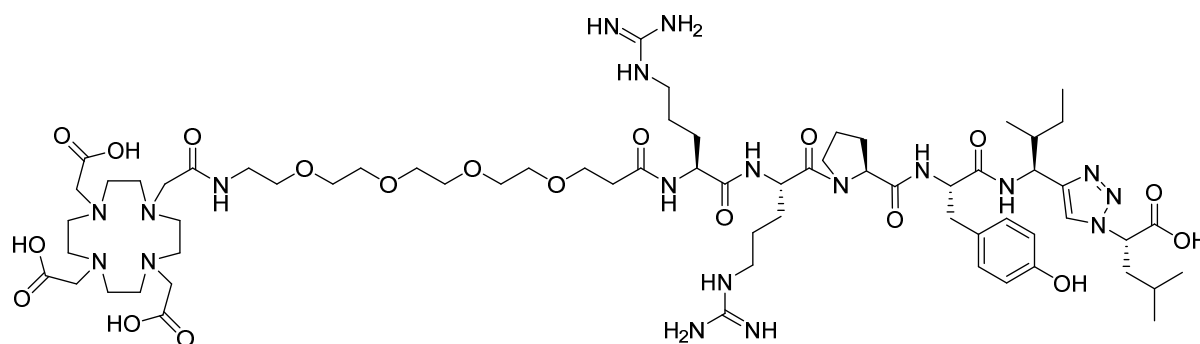
**Synthesis of DOTA-PEG<sub>4</sub>-Arg-Arg-Pro-Tyr-Ile-Leu-Ψ[Tz]-H (AM-NT 4)**

MW: 1472.8 g/mol

Peptide conjugate **AM-NT 4** was prepared following procedures **D**, **E** and **H** using a rink amide MBHA resin LL (100-200 mesh) (0.03 mmol). After deprotection, the C-terminal triazole was formed following general procedures **F** and **G**, using Fmoc-Leu-alkyne **29e** (kindly provided by Dr. I. Valverde). Commercially available Fmoc-Ile-OH, Fmoc-Tyr(<sup>t</sup>Bu)-OH, Fmoc-Pro-OH, Fmoc-Arg(Pbf)-OH, Fmoc-PEG<sub>4</sub>-COOH and DOTA-(*tris*-<sup>t</sup>Bu) were then coupled following general procedure **D**. Peptide conjugate **AM-NT 4** was obtained in high purity (>99%) as a white powder after purification by preparative HPLC (80-60% A in B in 20 min) (5.0 mg, 11%).

Analytical HPLC: (90-50% A in B in 15 min),  $t_r$  = 9.10 min.

ESI-HRMS  $m/z$   $[M+3H]^3+$  calcd for C<sub>66</sub>H<sub>112</sub>N<sub>20</sub>O<sub>18</sub>: 1472.8463, theor.  $[M+3H]^3+$ : 491.9487  
found: 492.2848

**Synthesis of DOTA-PEG<sub>4</sub>-Arg-Arg-Pro-Tyr-Ile-Ψ[Tz]-Leu (AM-NT 5)**

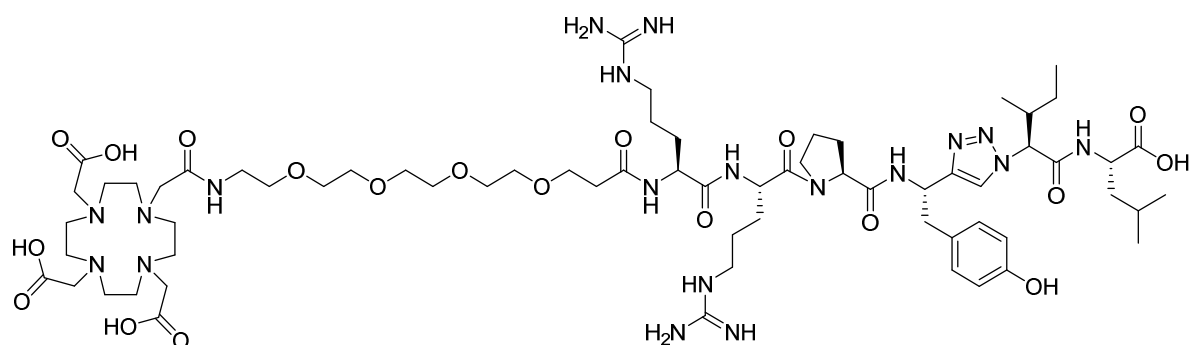
MW: 1473.8 g/mol

Peptide conjugate **AM-NT 5** was prepared following procedures **D**, **E**, **F**, **G** and **H** using a Leu-preloaded PEG-PS resin (0.03 mmol) and commercial available Fmoc-Tyr(<sup>t</sup>Bu)-OH, Fmoc-Pro-OH, Fmoc-Arg(Pbf)-OH, Fmoc-PEG<sub>4</sub>-COOH and DOTA-(*tris*-<sup>t</sup>Bu). Alkyne **29a** was used as triazole precursor. The peptide conjugate was **AM-NT 5** obtained as a white powder in high purity (> 99%) after purification by preparative HPLC (70-65% A in B in 20 min) (2.0 mg, 5%).

Analytical HPLC: (90-50% A in B in 15 min),  $t_r$  = 10.14 min.

ESI-MS  $m/z$   $[M+2H]^+^{2+}$  calcd for C<sub>66</sub>H<sub>111</sub>N<sub>19</sub>O<sub>19</sub>: 1473.8304, theor.  $[M+2H]^+^{2+}$ : 737.9, found: 738.3

**Synthesis of DOTA-PEG<sub>4</sub>-Arg-Arg-Pro-Tyr-Ψ[Tz]-Ile-Leu (AM-NT 6)**

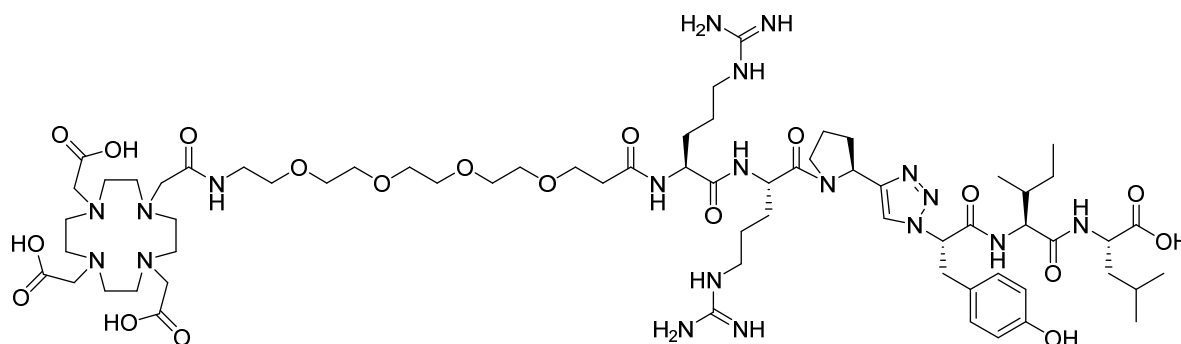


MW: 1473.8 g/mol

Peptide conjugate **AM-NT 6** was prepared following procedures **D**, **E**, **F**, **G** and **H** using a Leu-preloaded PEG-PS resin (0.03 mmol) and commercial available Fmoc-Ile-OH, Fmoc-Pro-OH, Fmoc-Arg(Pbf)-OH, Fmoc-PEG<sub>4</sub>-COOH and DOTA-(*tris*-<sup>t</sup>Bu). Alkyne **29c** was used as triazole precursor. Purification by preparative HPLC (80-70% A in B in 20 min) and yielded peptide conjugate **AM-NT 6** in high purity (> 99%) as a white powder (14.0 mg, 32%).

Analytical HPLC: (90-50% A in B in 15 min),  $t_r = 9.46$  min.

ESI-HRMS  $m/z$   $[M+2H^+]^{2+}$  calcd for C<sub>66</sub>H<sub>111</sub>N<sub>19</sub>O<sub>19</sub>: 1473.8304, theor.  $[M+2H^+]^{2+}$ : 737.9152, found: 737.9226

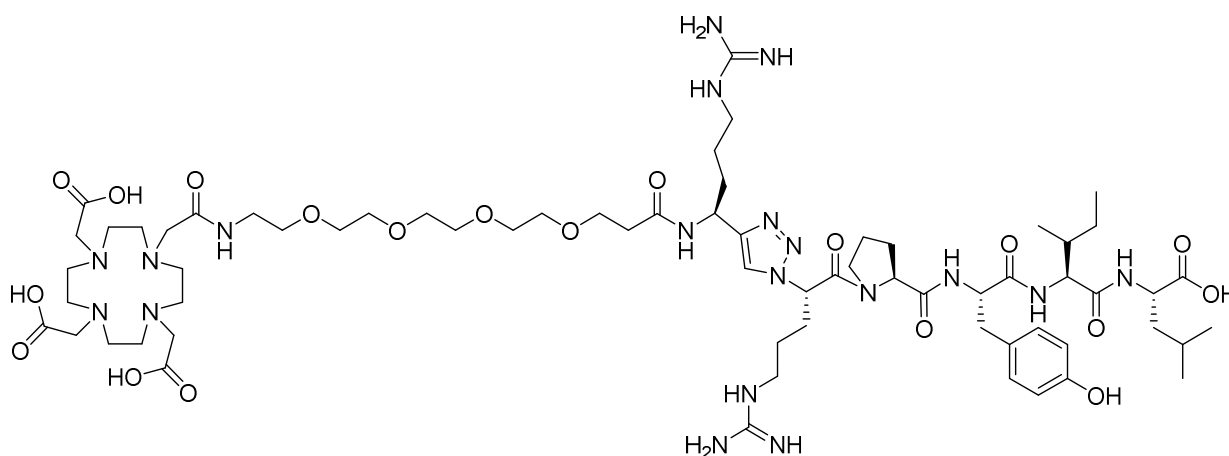
**Synthesis of DOTA-PEG<sub>4</sub>-Arg-Arg-Pro-ψ[Tz]-Tyr-Ile-Leu (AM-NT 7)**

MW: 1473.8 g/mol

Peptide conjugate **AM-NT 7** was prepared following procedures **D**, **E**, **F**, **G** and **H** using a Leu-preloaded PEG-PS resin (0.03 mmol) and commercial available Fmoc-Ile-OH, Fmoc-Tyr(<sup>t</sup>Bu)-OH, Fmoc-Arg(Pbf)-OH, Fmoc-PEG<sub>4</sub>-COOH and DOTA-(*tris*-<sup>t</sup>Bu). Alkyne **29b** was used as triazole precursor. After purification by preparative HPLC (75-70% A in B in 16 min) peptide conjugate **AM-NT 7** was obtained in high purity (> 98%) as a white powder (2.7 mg, 27%).

Analytical HPLC: (90-50% A in B in 15 min),  $t_r$  = 9.73 min.

ESI-HRMS  $m/z$   $[M+2H^+]^{2+}$  calcd for C<sub>66</sub>H<sub>111</sub>N<sub>19</sub>O<sub>19</sub>: 1473.8304, theor.  $[M+2H^+]^{2+}$ : 737.9152, found: 737.9232

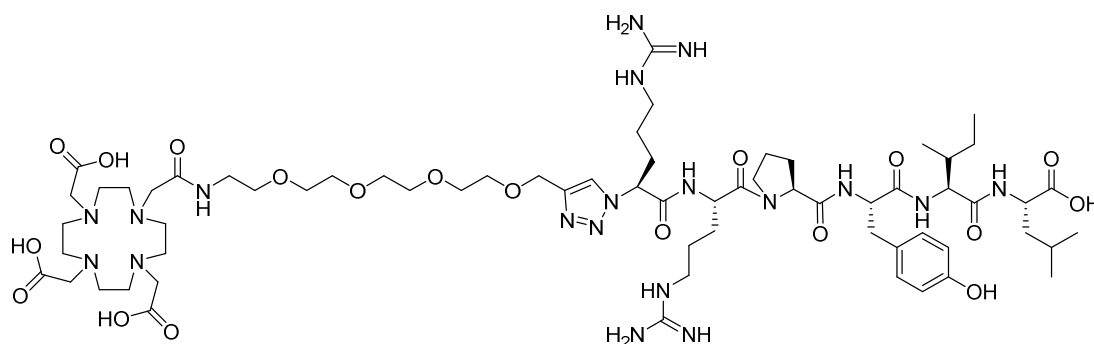
**Synthesis of DOTA-PEG<sub>4</sub>-Arg-ψ[Tz]-Arg-Pro-Tyr-Ile-Leu (AM-NT 8)**

MW: 1473.8 g/mol

Peptide conjugate **AM-NT 8** was prepared following procedures **D**, **E**, **F**, **G** and **H** using a Leu-preloaded PEG-PS resin (0.03 mmol) and commercial available Fmoc-Ile-OH, Fmoc-Tyr(<sup>t</sup>Bu)-OH, Fmoc-Pro-OH, Fmoc-Arg(Pbf)-OH, Fmoc-PEG<sub>4</sub>-COOH and DOTA-(*tris*-<sup>t</sup>Bu). Alkyne **29d** was used as triazole precursor. After purification by preparative HPLC (80-60% A in B in 20 min) peptide conjugate **AM-NT 8** was obtained in high purity (> 99%) as a white powder (6.1 mg, 14%).

Analytical HPLC: (90-50% A in B in 15 min),  $t_r$  = 9.25 min.

ESI-HRMS  $m/z$   $[M+2H^+]^{2+}$  calcd for C<sub>66</sub>H<sub>111</sub>N<sub>19</sub>O<sub>19</sub>: 1473.8304, theor.  $[M+2H^+]^{2+}$ : 737.9152, found: 737.9226

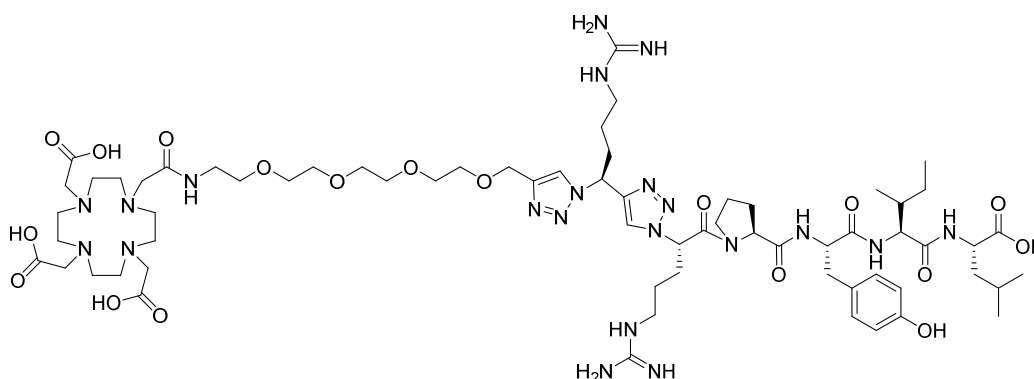
**Synthesis of DOTA-PEG<sub>4</sub>-ψ[Tz]-Arg-Arg-Pro-Tyr-Ile-Leu (AM-NT 9)**

MW: 1459.8 g/mol

Peptide conjugate **AM-NT 9** was prepared following procedures **D**, **E**, **F**, **G** and **H** using a Leu-preloaded PEG-PS resin (0.03 mmol) and commercial available Fmoc-Ile-OH, Fmoc-Tyr(<sup>t</sup>Bu)-OH, Fmoc-Pro-OH, Fmoc-Arg(Pbf)-OH, and DOTA-(*tris*-<sup>t</sup>Bu). Alkyne **29f** was used as triazole precursor. Peptide conjugate **AM-NT 9** was obtained as a highly pure (> 98%) white powder after purification by preparative HPLC (80-60% A in B in 20 min) (2.0 mg, 5%).

Analytical HPLC: (90-50% A in B in 15 min),  $t_r = 9.23$  min.

ESI-HRMS  $m/z$   $[M+2H^+]^{2+}$  calcd for C<sub>66</sub>H<sub>111</sub>N<sub>19</sub>O<sub>19</sub>: 1459.8147, theor.  $[M+2H^+]^{2+}$ : 730.9073, found: 730.9152

**Synthesis of DOTA-PEG<sub>4</sub>- $\Psi$ [Tz]-Arg- $\Psi$ [Tz]-Arg-Pro-Tyr-Ile-Leu (AM-NT 10)**

MW: 1483.8 g/mol

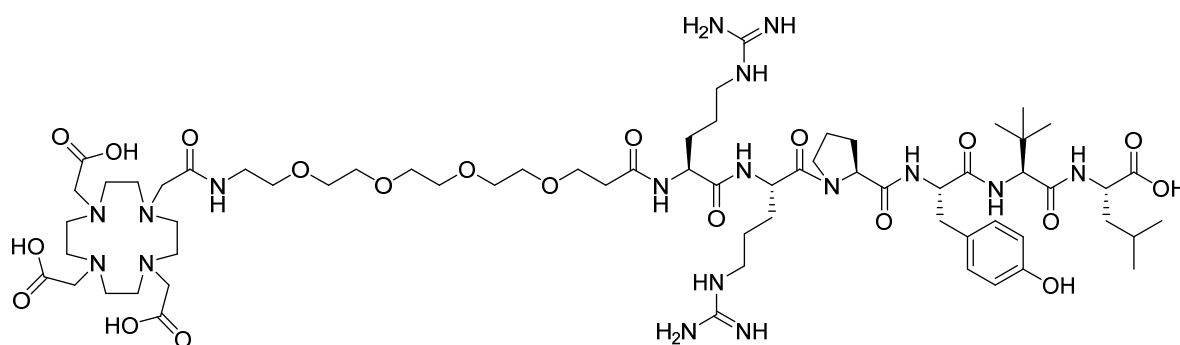
Peptide conjugate **AM-NT 10** was prepared following procedures **D**, **E**, **F**, **G** and **H** using a Leu-preloaded PEG-PS resin (0.03 mmol) and commercial available Fmoc-Ile-OH, Fmoc-Tyr(<sup>t</sup>Bu)-OH, Fmoc-Pro-OH, Fmoc-Arg(Pbf)-OH, Fmoc-PEG<sub>4</sub>-COOH and DOTA-(*tris*-<sup>t</sup>Bu). Alkyne **29d** and **29f** were used as triazole precursors. After purification by preparative HPLC (80-60% A in B in 20 min) peptide conjugate **AM-NT 10** was obtained in high purity (> 95%) as a white powder (1 mg, 2%).

Analytical HPLC: (90-50% A in B in 15 min),  $t_r$  = 9.38 min.

ESI-HRMS  $m/z$   $[M+2H^+]^{2+}$  calcd for C<sub>66</sub>H<sub>109</sub>N<sub>21</sub>O<sub>18</sub>: 1483.8259, theor.  $[M+2H^+]^{2+}$ : 742.9130, found: 742.9211



**Synthesis of DOTA-PEG<sub>4</sub>-Arg-Arg-Pro-Tyr-Tle-Leu (AM-NT 11)**

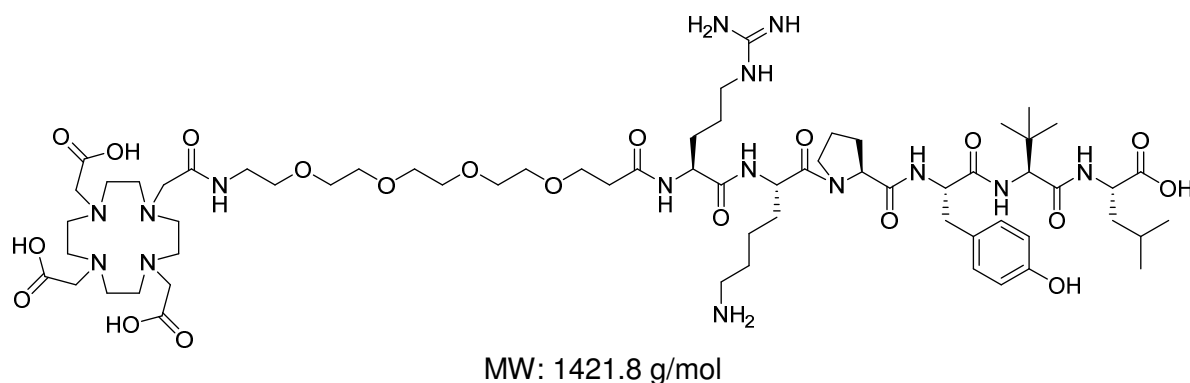


MW: 1449.8 g/mol

Peptide conjugate **AM-NT 11** was prepared following procedures **D**, **E**, and **H** using a Leu-preloaded PEG-PS resin (0.03 mmol) and commercial available Fmoc-Tle-OH, Fmoc-Tyr(<sup>t</sup>Bu)-OH, Fmoc-Pro-OH, Fmoc-Arg(Pbf)-OH, Fmoc-PEG<sub>4</sub>-COOH and DOTA-(*tris*-<sup>t</sup>Bu). Peptide conjugate **AM-NT 11** was obtained as a highly pure (> 99%) white powder after purification by preparative HPLC (80-60% A in B in 20 min) (13.0 mg, 30%).

Analytical HPLC: (90-50% A in B in 15 min),  $t_r = 9.00$  min.

ESI-HRMS  $m/z$   $[M+2H^+]^{2+}$  calcd for C<sub>65</sub>H<sub>111</sub>N<sub>17</sub>O<sub>20</sub>: 1449.8191, theor.  $[M+2H^+]^{2+}$ : 725.9096, found: 725.9172

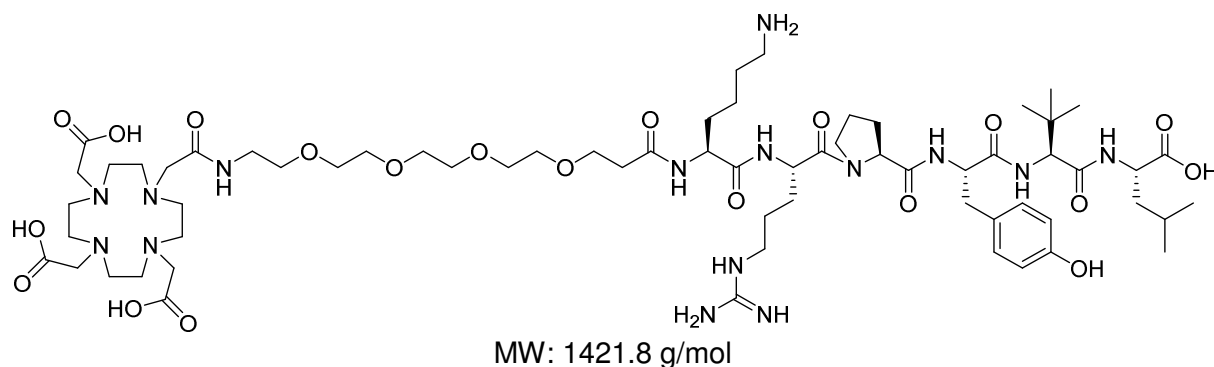
**Synthesis of DOTA-PEG<sub>4</sub>-Arg-Lys-Pro-Tyr-Tle-Leu (AM-NT 12)**

Peptide conjugate **AM-NT 12** was prepared following procedures **D**, **E**, and **H** using a Leu-preloaded PEG-PS resin (0.03 mmol) and commercial available Fmoc-Tle-OH, Fmoc-Tyr(<sup>t</sup>Bu)-OH, Fmoc-Pro-OH, Fmoc-Lys(Boc)-OH, Fmoc-Arg(Pbf)-OH, Fmoc-PEG<sub>4</sub>-COOH and DOTA-(*tris*-<sup>t</sup>Bu). Peptide conjugate **AM-NT 12** was obtained in high purity (> 98%) as a white powder after purification by preparative HPLC (80-60% A in B in 20 min) (21.8 mg, 52%).

Analytical HPLC: (90-50% A in B in 15 min),  $t_r$  = 8.76 min.

ESI-HRMS  $m/z$  [ $M+2H^+$ ]<sup>2+</sup> calcd for C<sub>65</sub>H<sub>111</sub>N<sub>15</sub>O<sub>20</sub>: 1421.8130, found: 711.9138

**Synthesis of DOTA-PEG<sub>4</sub>-Lys-Arg-Pro-Tyr-Tle-Leu (AM-NT 13)**

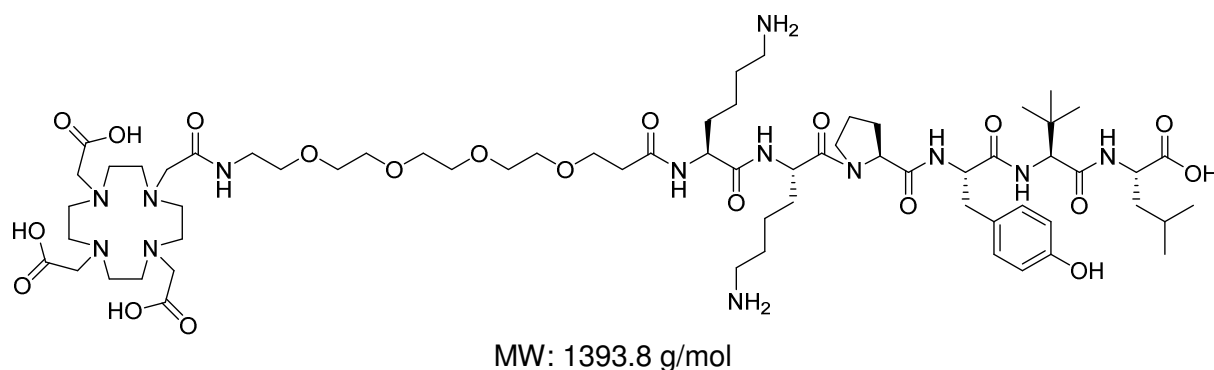


Peptide **AM-NT 13** was prepared following procedures **D**, **E**, and **H** using a Leu-preloaded PEG-PS resin (0.03 mmol) and commercial available Fmoc-Tle-OH, Fmoc-Tyr(<sup>t</sup>Bu)-OH, Fmoc-Pro-OH, Fmoc-Lys(Boc)-OH, Fmoc-Arg(Pbf)-OH, Fmoc-PEG<sub>4</sub>-COOH and DOTA-(*tris*-<sup>t</sup>Bu). Peptide conjugate **AM-NT 13** was obtained in high purity (> 98%) as a white powder after purification by preparative HPLC (80-60% A in B in 20 min) (24.7 mg, 58%).

Analytical HPLC: (90-50% A in B in 15 min),  $t_r = 8.76$  min.

ESI-HRMS  $m/z$   $[M+2H]^+^{2+}$  calcd for C<sub>65</sub>H<sub>111</sub>N<sub>15</sub>O<sub>20</sub>: 1421.8130, found: 711.9138

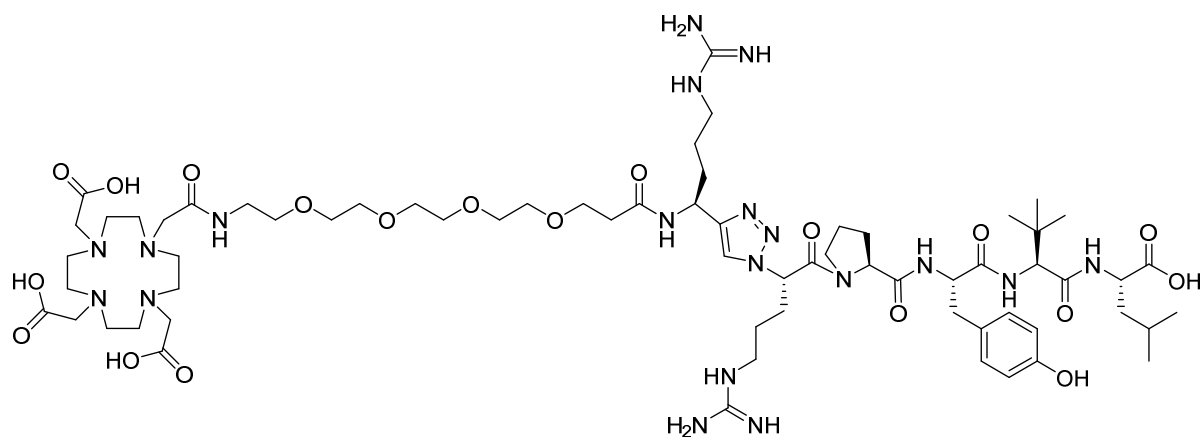
**Synthesis of DOTA-PEG<sub>4</sub>-Lys-Lys-Pro-Tyr-Tle-Leu (AM-NT 14)**



Peptide conjugate **AM-NT 14** was prepared following procedures **D**, **E**, and **H** using a Leu-preloaded PEG-PS resin (0.03 mmol) and commercial available Fmoc-Tle-OH, Fmoc-Tyr(<sup>t</sup>Bu)-OH, Fmoc-Pro-OH, Fmoc-Lys(Boc)-OH, Fmoc-PEG<sub>4</sub>-COOH and DOTA-(*tris*-<sup>t</sup>Bu). Peptide conjugate **AM-NT 14** was obtained as a highly pure (> 99%) white powder after purification by preparative HPLC (80-60% A in B in 20 min) (29.8 mg, 71%).

Analytical HPLC: (90-50% A in B in 15 min),  $t_r$  = 8.50 min.

ESI-HRMS  $m/z$  [ $M+2H^{+}$ ]<sup>2+</sup> calcd for C<sub>65</sub>H<sub>111</sub>N<sub>13</sub>O<sub>20</sub>: 1393.8068, found: 697.9115

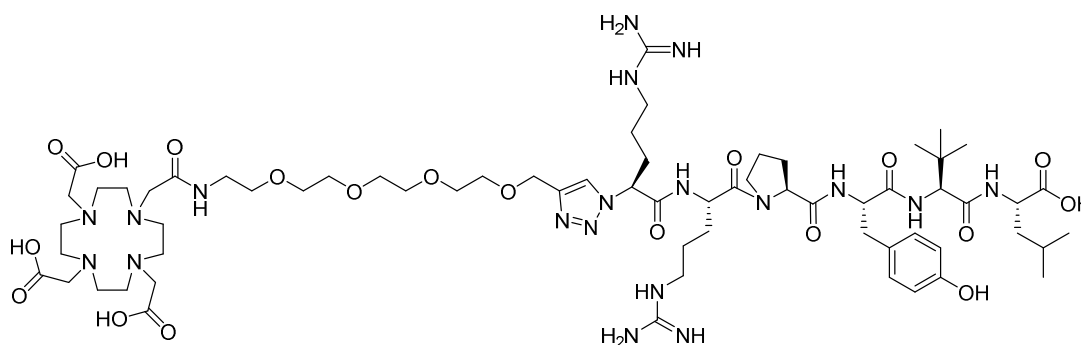
**Synthesis of DOTA-PEG<sub>4</sub>-Arg-ψ[Tz]-Arg-Pro-Tyr-Tle-Leu (AM-NT 15)**

MW: 1473.8 g/mol

Peptide conjugate **AM-NT 15** was prepared following procedures **D**, **E**, **F**, **G** and **H** using a Leu-preloaded PEG-PS resin (0.03 mmol) and commercial available Fmoc-Tle-OH, Fmoc-Tyr(<sup>t</sup>Bu)-OH, Fmoc-Pro-OH, Fmoc-Arg(Pbf)-OH, Fmoc-PEG<sub>4</sub>-COOH and DOTA-(*tris*-<sup>t</sup>Bu). Alkyne **29d** was used as triazole precursor. Peptide conjugate **AM-NT 15** was obtained in high purity (> 99%) as a white powder after purification by preparative HPLC (80-60% A in B in 20 min) (7.0 mg, 16%).

Analytical HPLC: (90-50% H<sub>2</sub>O with 0.1% TFA in 15 min), *t<sub>r</sub>*= 10.13 min.

ESI-HRMS *m/z* [M+2H<sup>+</sup>]<sup>2+</sup> calcd for C<sub>65</sub>H<sub>111</sub>N<sub>17</sub>O<sub>20</sub>: 1473.8304, theor. [M+2H<sup>+</sup>]<sup>2+</sup>: 737.9152, found: 737.9232

**Synthesis of DOTA-PEG<sub>4</sub>- $\psi$ [Tz]-Arg-Arg-Pro-Tyr-Tle-Leu (AM-NT 16)**

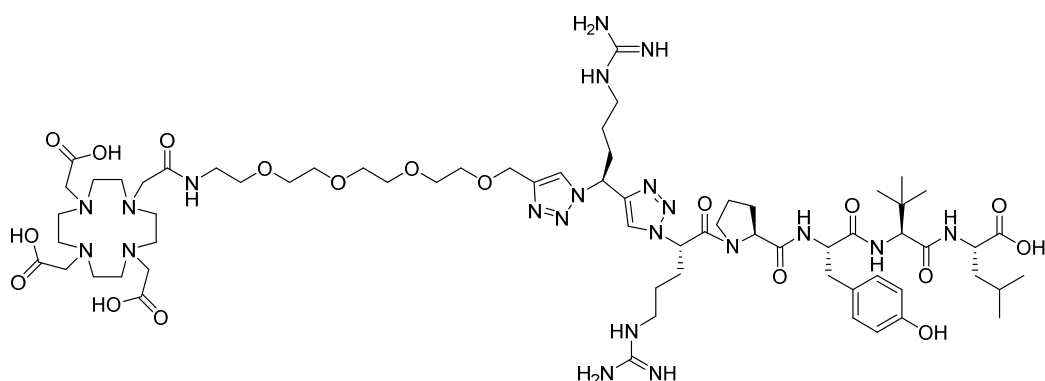
MW: 1459.8 g/mol

Peptide conjugate **AM-NT 16** was prepared following procedures **D**, **E**, **F**, **G** and **H** using a Leu-preloaded PEG-PS resin (0.03 mmol) and commercial available Fmoc-Tle-OH, Fmoc-Tyr(<sup>t</sup>Bu)-OH, Fmoc-Pro-OH, Fmoc-Arg(Pbf)-OH, and DOTA-(*tris*-<sup>t</sup>Bu). Alkyne **29f** was used as triazole precursor. Peptide conjugate **AM-NT 16** was obtained in high purity (> 98%) as a white powder after purification by preparative HPLC (80-60% A in B in 20 min) (6.9 mg, 16%).

Analytical HPLC: (90-50% A in B in 15 min),  $t_r$  = 10.18 min.

ESI-HRMS  $m/z$   $[M+2H^+]^{2+}$  calcd for C<sub>65</sub>H<sub>111</sub>N<sub>17</sub>O<sub>20</sub>: 1459.8147, theor.  $[M+2H^+]^{2+}$ : 730.9074, found: 730.9145

**Synthesis of DOTA-PEG<sub>4</sub>-Ψ[Tz]-Arg-Ψ[Tz]-Arg-Pro-Tyr-Tle-Leu (AM-NT 17)**



MW: 1483.8 g/mol

Peptide conjugate **AM-NT 17** was prepared following procedures **D**, **E**, **F**, **G** and **H** using a Leu-preloaded PEG-PS resin (0.03 mmol) and commercial available Fmoc-Tle-OH, Fmoc-Tyr(<sup>t</sup>Bu)-OH, Fmoc-Pro-OH, Fmoc-Arg(Pbf)-COOH, and DOTA-(*tris*-<sup>t</sup>Bu). Alkynes **29d** and **29f** were used as triazole precursors. After purification by preparative HPLC (80-60% A in B in 20 min) peptide conjugate **AM-NT 17** was obtained in high purity (> 98%) as a white powder (3.8 mg, 9%).

Analytical HPLC: (90-50% A in B in 15 min),  $t_r = 10.47$  min.

ESI-HRMS  $m/z$   $[M+2H^+]^{2+}$  calcd for C<sub>66</sub>H<sub>109</sub>N<sub>21</sub>O<sub>18</sub>: 1483.8259, theor.  $[M+2H^+]^{2+}$ : 742.9130, found: 742.9207

## 5.4 Radiolabelling

NT (8-13) derivatives **1-18** were radiolabelled with different specific activities depending on the experiment. Peptide conjugates were used as stock solutions of 1 mg/ mL in H<sub>2</sub>O.

**In Vitro Studies.** 10 µg (6.9 nmol conjugate in 10 µL H<sub>2</sub>O) of analogues [<sup>177</sup>Lu]AM-NT **1-17** were added to 150 µL NH<sub>4</sub>OAc buffer (0.4 M, pH 5.0). 37 MBq of [<sup>177</sup>Lu]LuCl<sub>3</sub> were added and the mixture was heated for 30 min at 100 °C. After the quality control *via* γ-HPLC, 2 µL of a 0.3 mM <sup>nat</sup>LuCl<sub>3</sub> solution in H<sub>2</sub>O (6 nmol) were added and the mixture was heated again for 30 min at 100 °C. The reaction solution was then diluted with a 0.9% NaCl solution giving a solution **A** with a final concentration of 1 nmol radiopeptide per mL. For cell internalisation experiments, a second solution **B** was prepared from solution **A**, by diluting 200 µL in 8 mL of saline solution, obtaining a final concentration of 2.5 pmol of radiopeptide per 100 µL. For receptor saturation experiments, solution **A** was used as stock solution for the preparation of the dilutions of different concentration.

**In Vivo Biodistribution Studies.** 10 µg (6.9 nmol in 10 µL H<sub>2</sub>O) of analogues [<sup>177</sup>Lu]AM-NT **2, 8, 9, 10, 11** and **15** were added to 150 µL NH<sub>4</sub>OAc buffer (0.4 M, pH 5.0). 150 MBq of [<sup>177</sup>Lu]LuCl<sub>3</sub> was added and the mixture was heated for 30 min at 100 °C. Radiolabelling yields and purities were determined *via* γ-HPLC. For injection, the solution was diluted twice. In the first dilution **C**, 1% HSA in NaCl was added till reaching a final volume of 1 mL. Then 0.9% NaCl in H<sub>2</sub>O was added reaching a final concentration of 1 nmol radiopeptide per mL. For the second dilution **D**, 200 µL of the first dilution **C** were added to 1.8 mL 0.9% NaCl in H<sub>2</sub>O (reaching a final volume of 2 mL) and 10 µL of Ca-DTPA were added. Each animal received 100 µL of this solution **D** (10 pmol radiolabelled radiopeptide, approx. 0.2 MBq). For the blocking solution **E**, 200 µL of the first dilution **C**, a 200 µL solution of NT (1-13) (1.2 nmol in 200 µL) and 10 µL of Ca-DTPA were diluted with 0.9% NaCl in H<sub>2</sub>O (reaching a final volume of 2 mL). For blocking experiments, each animal received 100 µL of solution **E** (10 pmol radiolabelled radiopeptide, 60 nmol NT (1-13), approx. 0.2 MBq).

**In Vivo Imaging Studies.** 1 µg (6.9 nmol conjugate in 1 µL H<sub>2</sub>O) of analogues **8** and **11** were added to 100 µL NH<sub>4</sub>OAc buffer (0.4 M, pH 5.0). 150 MBq of a [<sup>177</sup>Lu]LuCl<sub>3</sub> was added and the mixture was heated for 30 min at 100 °C. Radiolabelling yields and purities were determined *via* γ-HPLC. For injection, the solution was diluted twice. In the first dilution **F**, 70 µL 1% HSA was added and 0.9% NaCl in H<sub>2</sub>O was added reaching a final volume of 690 µL (1 nmol/mL). For the second dilution **G**, 600 µL of the first dilution were added to 400 mL 0.9% NaCl in H<sub>2</sub>O (reaching a final volume of 1 mL) and 10 µL of Ca-DTPA were added.



Each animal received 100  $\mu\text{L}$  of this solution **D** (60 pmol peptide conjugate, approx. 13.0 MBq).

**Serum Stabilities.** 5  $\mu\text{g}$  (3.5 nmol in 5  $\mu\text{L}$   $\text{H}_2\text{O}$ ) of analogues [ $^{177}\text{Lu}$ ]AM-NT 1-17 were added to 150  $\mu\text{L}$   $\text{NH}_4\text{OAc}$  buffer (0.4 M, pH 5.0). 150 MBq of [ $^{177}\text{Lu}$ ]LuCl<sub>3</sub> was added and the mixture was heated for 30 min at 100 °C. Radiolabelling yields and purities were determined *via*  $\gamma$ -HPLC. The reacting solution was diluted with 0.9% NaCl in  $\text{H}_2\text{O}$  to a concentration of 1 nmol radiopeptide per mL. This solution was the directly applied to 1 mL serum.

All NT (8-13) analogues [ $^{177}\text{Lu}$ ]AM-NT 1-17 were obtained in radiochemical yields and purities of >95%.

## 5.5 *In Vitro* Evaluation

### Stability Studies

The radiolabelled peptide conjugates (30 pmol, 1nM in PBS, approx. 0.7 MBq) were incubated in fresh blood serum (1 mL) at 37 °C. At different time points (1, 5, 10, 20, 30, 40, 60, 120, 240, 360 min, 24 h) aliquots (100  $\mu\text{L}$ ) were taken and the proteins were precipitated in 200  $\mu\text{L}$  EtOH and centrifuged (5 min, 5000 rpm). The supernatant was again precipitated with 100  $\mu\text{L}$  EtOH and centrifuged. The supernatant was diluted with  $\text{H}_2\text{O}$  (1:2) and analysed with  $\gamma$ -HPLC.

### Log D Determination

The lipophilicity of the radiolabelled conjugated was determined by the 'shake-flask method'. The radiolabelled peptides (30 pmol, 1nM in PBS, approx. 0.2 MBq) were added to 1 mL of a mixture of *n*-octanol/PBS (1:1) and shaken vigorously for 1 min by vortex. After centrifugation, aliquots (100  $\mu\text{L}$ ) of both *n*-octanol and PBS phases were taken and analysed with a gamma-counter (n=5).

### Cell Culture

Human colorectal adenocarcinoma (HT-29) cells were cultured at 37 °C and 5%  $\text{CO}_2$  in Dulbecco's modified Eagle's medium (DMEM, high glucose) containing 10% (v/v) fetal bovine serum, L-glutamine (200 mM), 100 IU mL<sup>-1</sup> penicillin and 100  $\mu\text{g}$  mL<sup>-1</sup> streptomycin. The cells were subcultured weekly after detaching them with a commercial solution of

trypsin-EDTA (1:250) in PBS. For experiments,  $8 \cdot 10^5$  cells/well were seeded out the night before, reaching a concentration of  $1 \cdot 10^6$  cells/well on the day of the experiment.

### Cell Internalisation Experiments

On the day prior to the experiment, HT-29 cells ( $1 \cdot 10^6$  cells/well) were placed in six-well plates with cell culture medium (1% FBS) and incubated overnight at 37 °C and 5% CO<sub>2</sub> for allowing the cells to attach. On the day of the experiment, the medium was removed and fresh medium (1% FBS, 1.3 mL) was added. Radiolabelled conjugates [<sup>177</sup>Lu]-AM-NT 1-17 (2.5 pmol per well, 2.5 pM solution in PBS, approx. 0.01 MBq) were added and the cells were incubated for different time points (30, 60, 120, 240 min) in triplicates to allow binding and internalisation. Nonspecific receptor binding and internalisation was determined by blocking experiments in the presence of a 1000-fold excess of NT (8-13) as a blocking agent (2.5 nmol per well, 2.5 nM solution in H<sub>2</sub>O). After each time point, the supernatant was removed and the cells were washed twice with PBS (1 mL). The combined supernatants represent the free, unbound fraction of radioactivity. Receptor-bound radioactivity was determined by incubating the cells on ice twice for 5 min with an acidic glycine solution (1 mL; 100 nM NaCl, 50 nM glycine, pH 2.8). The internalized fraction was isolated by lysis of the cells with 1M NaOH (1 mL) for 10 min at 37 °C and 5% CO<sub>2</sub>. The wells of the lysed cells were washed twice with 1 mL 1M NaOH. The radioactivity of the fractions were measured quantitatively in a gamma counter and calculated as a percentage of applied dosage. Data was fitted by non-linear regression with GraphPad Prism 5.0 (n=2-3 in triplicate).

### Receptor Saturation Studies

HT-29 cells in six-well plates were prepared as described above. In order to reach receptor saturation, the cells were incubated with increasing concentrations of the peptide conjugates [<sup>177</sup>Lu]-AM-NT 1-17 (0.1, 0.5, 1, 5, 10, 20, 50, 75, 100, 200, 400, 600, 800, 1600, 3200 nM). Non-specific binding was determined by blocking experiments using a 1000 fold excess of NT (8-13) solution (2.5 nmol/1 mL per well, corresponding to 2.5 μM). After incubation of 1 h at 37 °C and 5% CO<sub>2</sub>, the supernatant was removed and the cells were washed twice with PBS (1 mL per well). The combined supernatants represent the free, unbound radiopeptide fraction. In order to determine the receptor bound and internalized fraction, the cells were treated with 1 M NaOH (1 mL per well) for 10 min at 37 °C and washed twice with 1 M NaOH (1 mL per well). The free and the receptor bound fractions were measured in a gamma counter for quantification. Dissociation constants (K<sub>D</sub>) were calculated from the specific binding data by performing a non-linear regression using GraphPad Prism5 (n=2-3 in triplicate).

## 5.6 *In Vivo* Evaluation

### Biodistributions

Biodistributions of compounds [<sup>177</sup>Lu]AM-NT **2, 8, 9, 10, 11** and **15** were performed with female nude Foxn 1nu mice (6-8 week old), bearing HT-29 colon carcinoma xenografts. For induction of the xenografts, HT-29 cells in a concentration of 7·10<sup>6</sup> cells/mouse were injected subcutaneously in the right shoulder and allowed to grow for 8 days.

On the day of the experiment, the mouse received the <sup>177</sup>Lu-labelled peptide analogues (10 pmol/mouse, 0.5-0.7 MBq/mouse) into the tail vein. The mice were sacrificed at different times (1, 4, 24 h p.i.), and their organs (blood, heart, lungs, liver, spleen, pancreas, stomach, intestine, colon, adrenal, kidneys, muscle, bone, brain and tumour) were harvested by dissection. The radioactivity in the organs was determined by  $\gamma$ -counting. 3-5 animals were used per time point.

For blocking experiments, a solution of NT (1-13) (60 nmol/mouse) was co-injected with the labelled compound. The animals were sacrificed at 1 h p.i., dissected and their organs were measured with a  $\gamma$ -counter. Tissue distribution data were calculated as percent injected activity per gram of tissue (% ID/g) (n=3-5). Statistical analysis was performed with Graphpad Prism 5.

### *In Vivo* Imaging

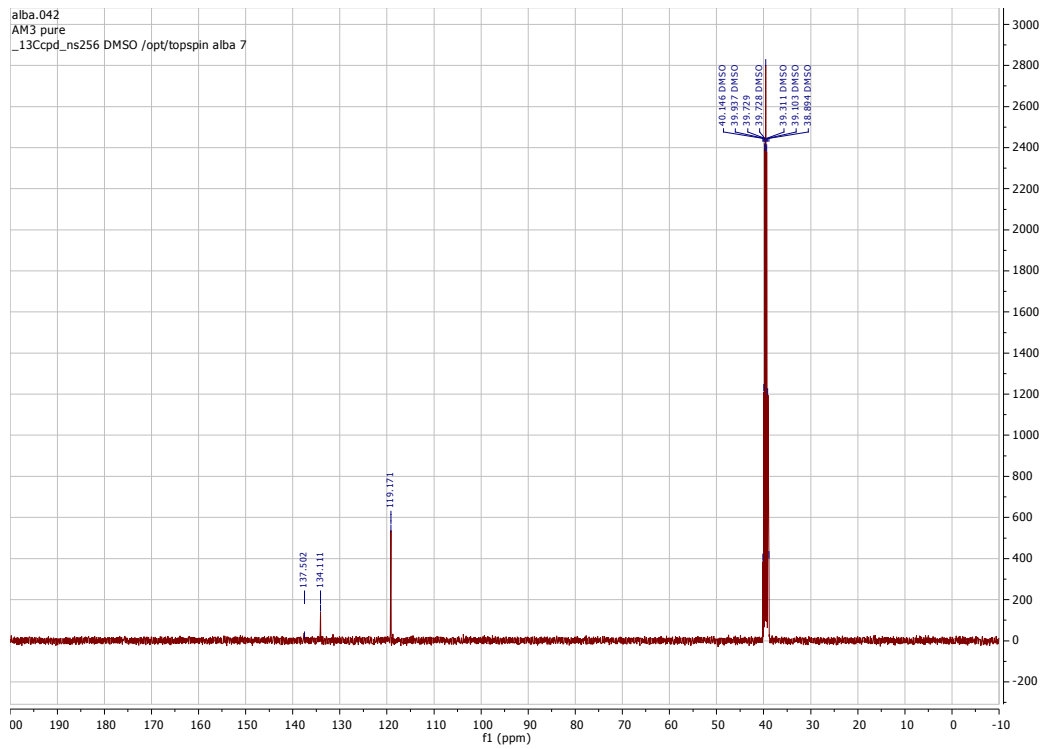
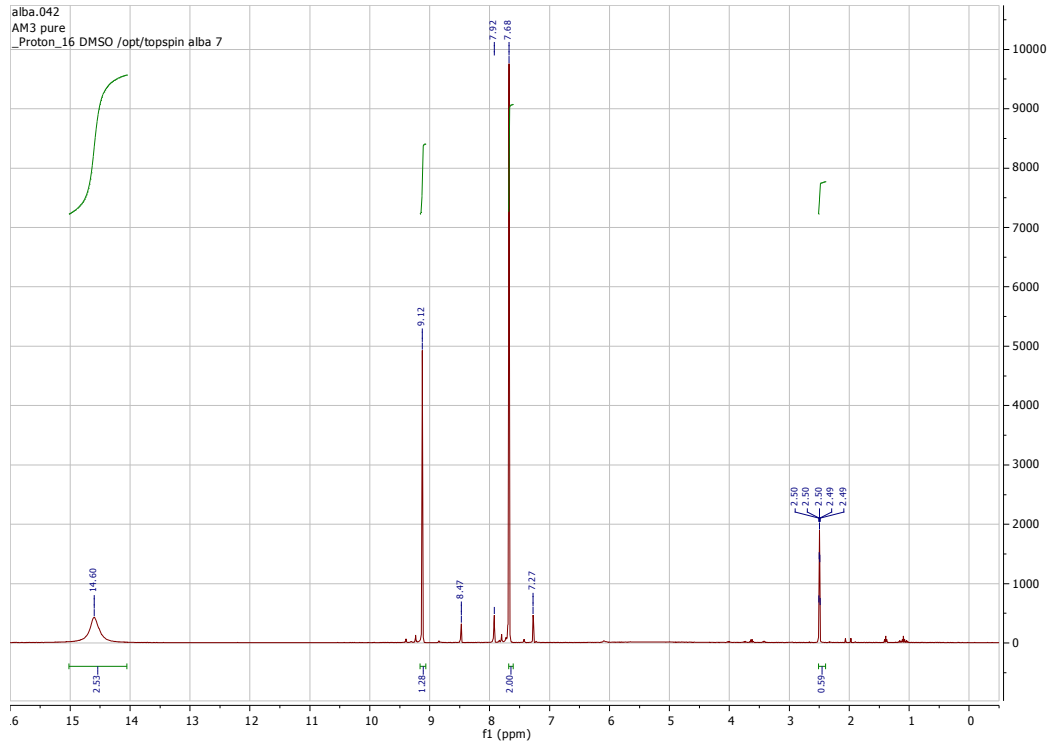
For *in vivo* imaging, female nude Foxn 1nu mice (6-8 week old), bearing HT-29 colon carcinoma xenografts were used. The induction of the xenografts was identical to the described for biodistributions. On the day of the experiment, the mice received the <sup>177</sup>Lu-labelled peptide analogue (60 pmol/mouse, 13 MBq/mouse) into the tail vein. The mice were sacrificed 1 h p.i., and imaged on a SPECT/CT Bioscan imager for 12 h.



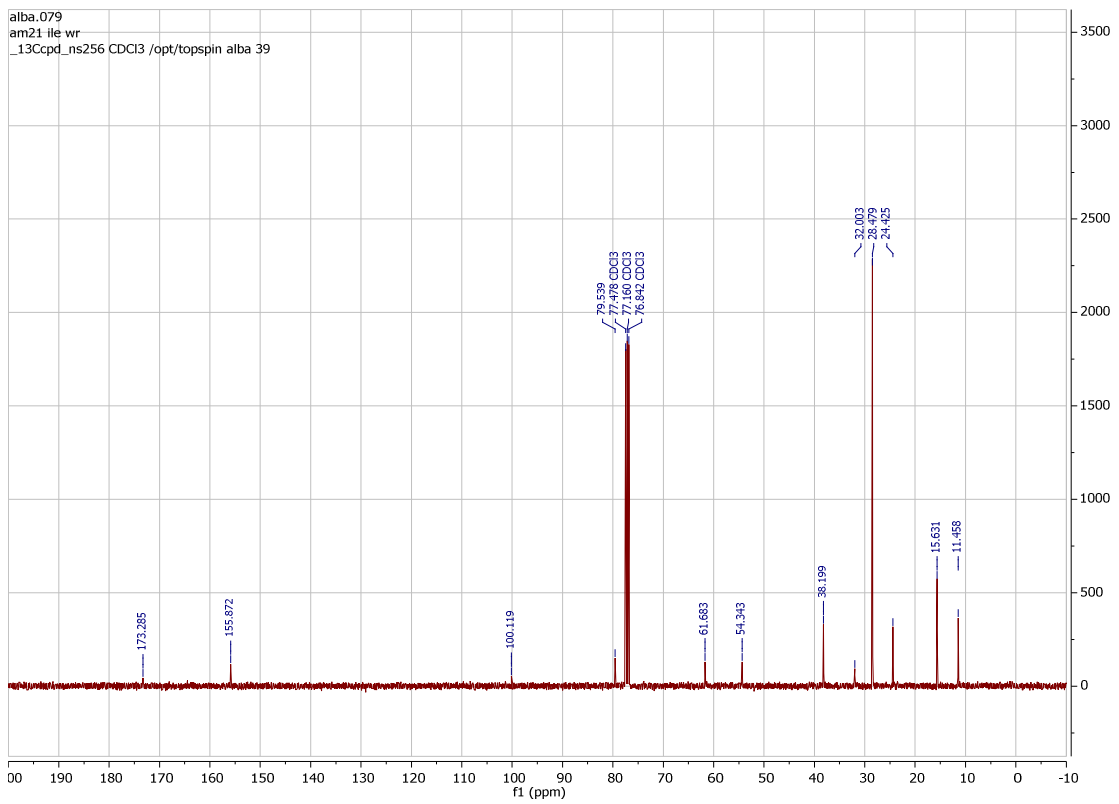
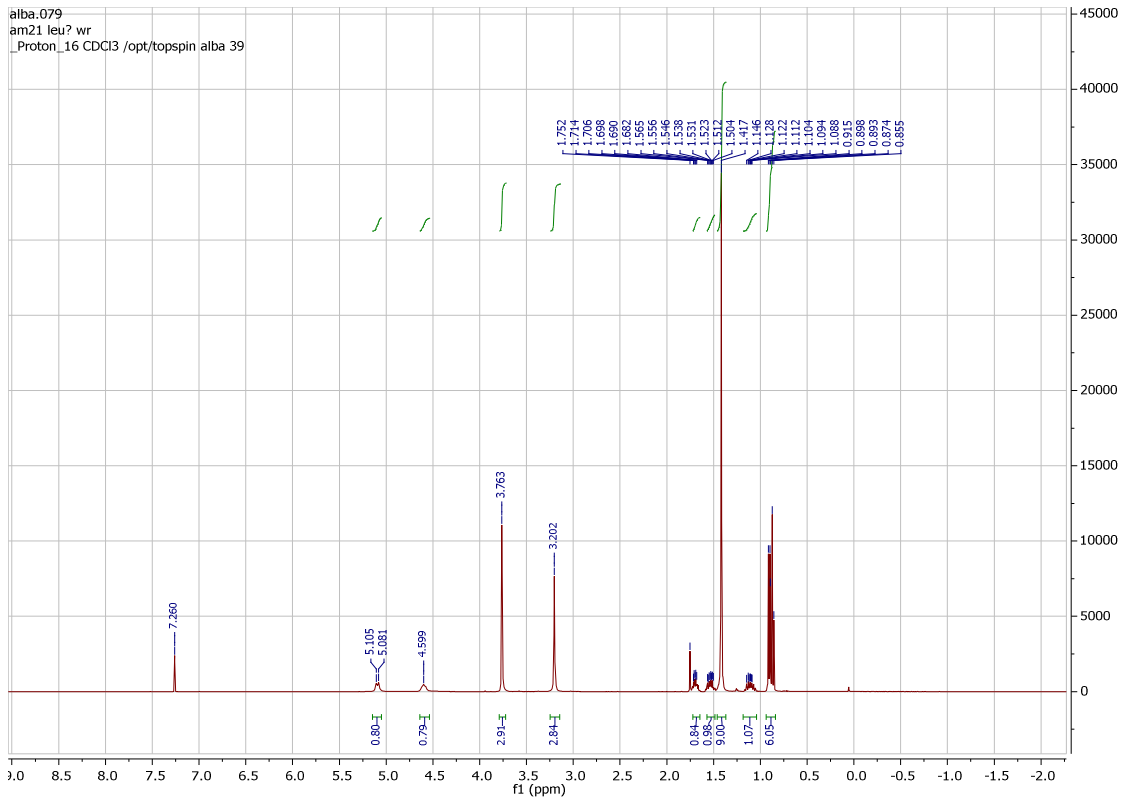
## 6. Appendix

### 6.1 NMR Spectra

#### Imidazole-1-sulfonyl Azide Hydrochloride (6)

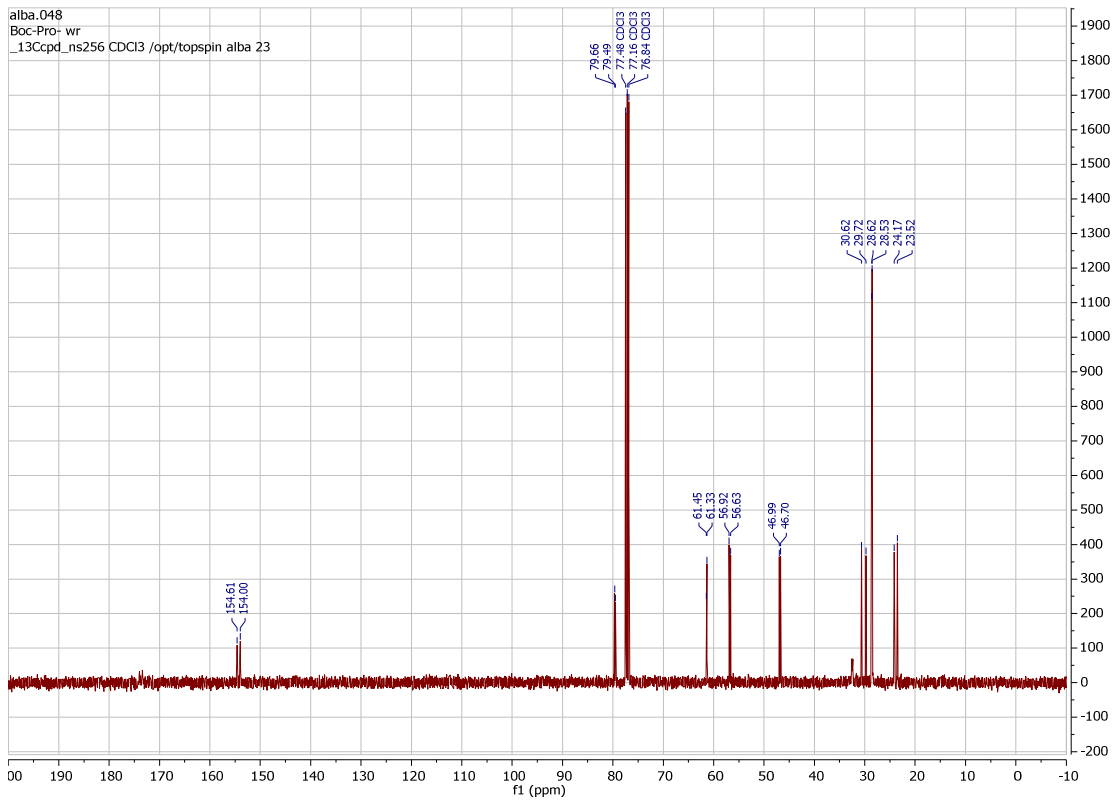
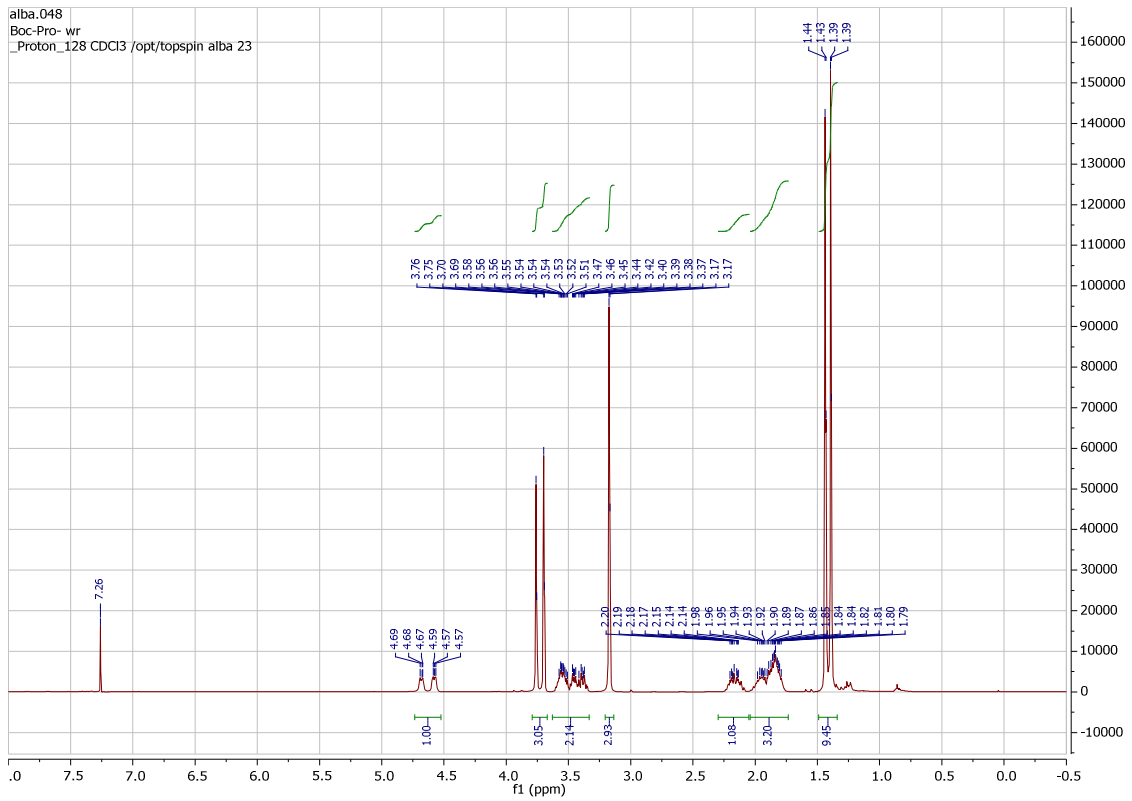


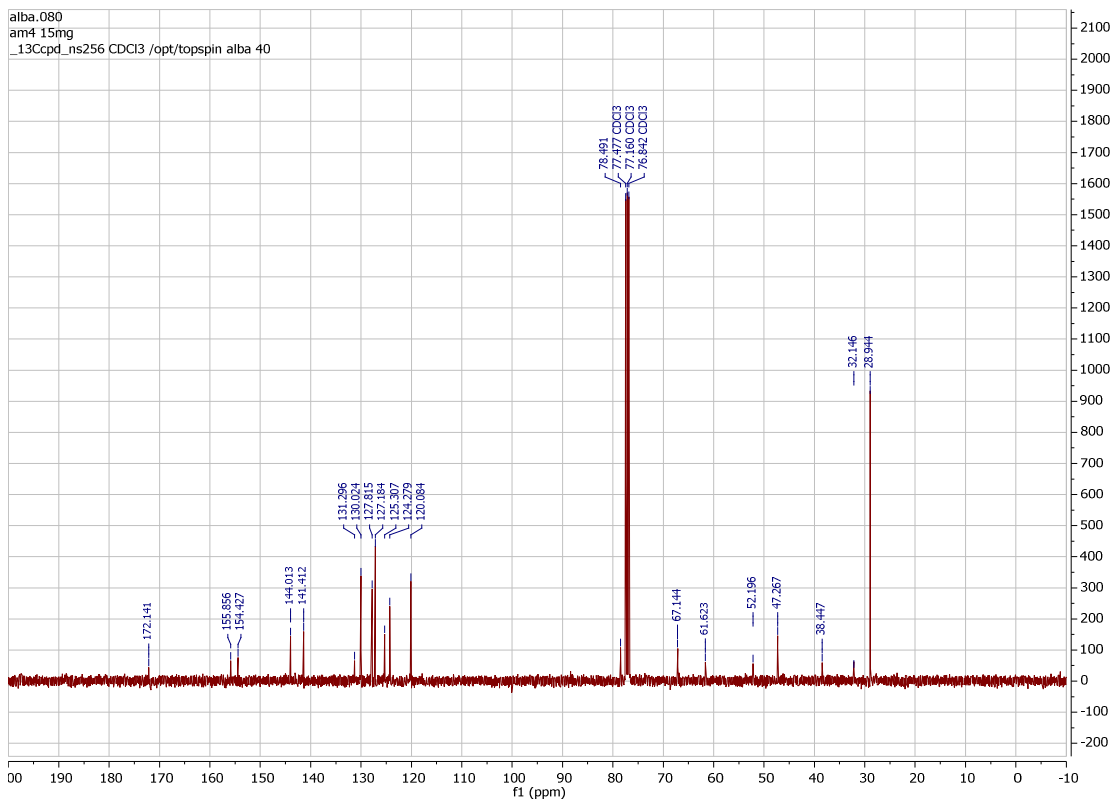
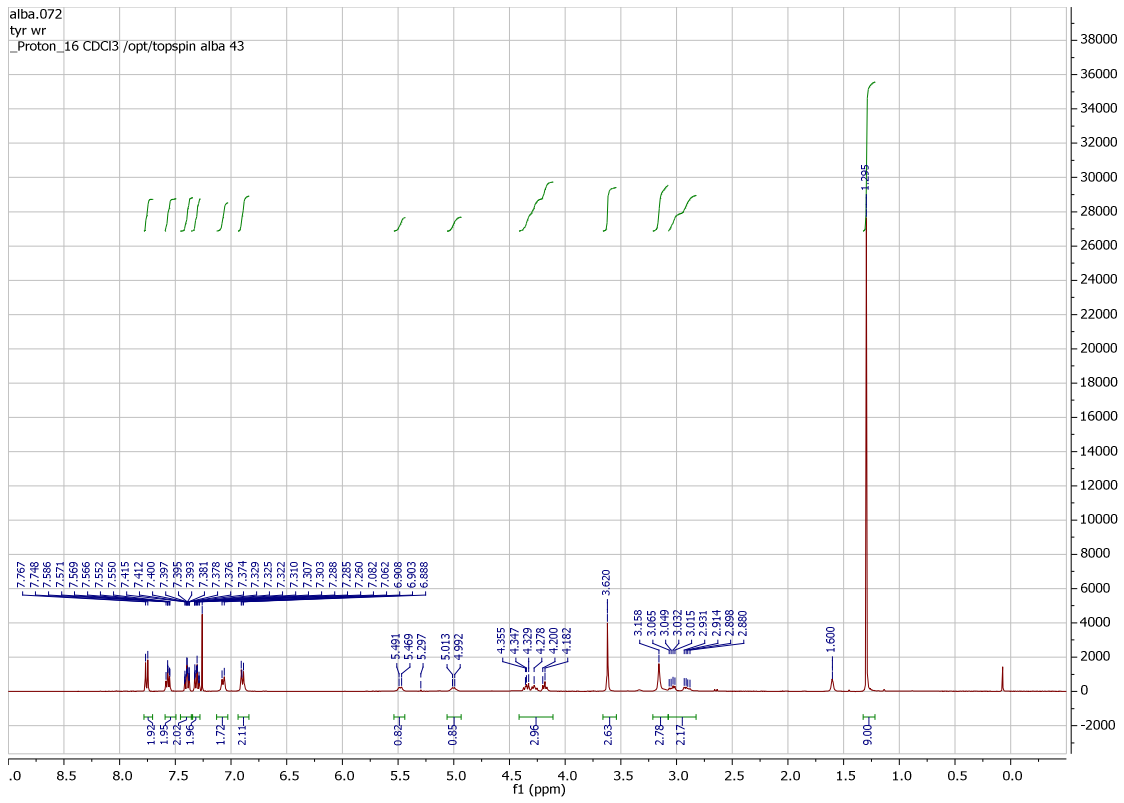
Boc-Ile-N(Me)OMe (26a)



# Appendix

## Boc-Pro-N(Me)OMe (24b)

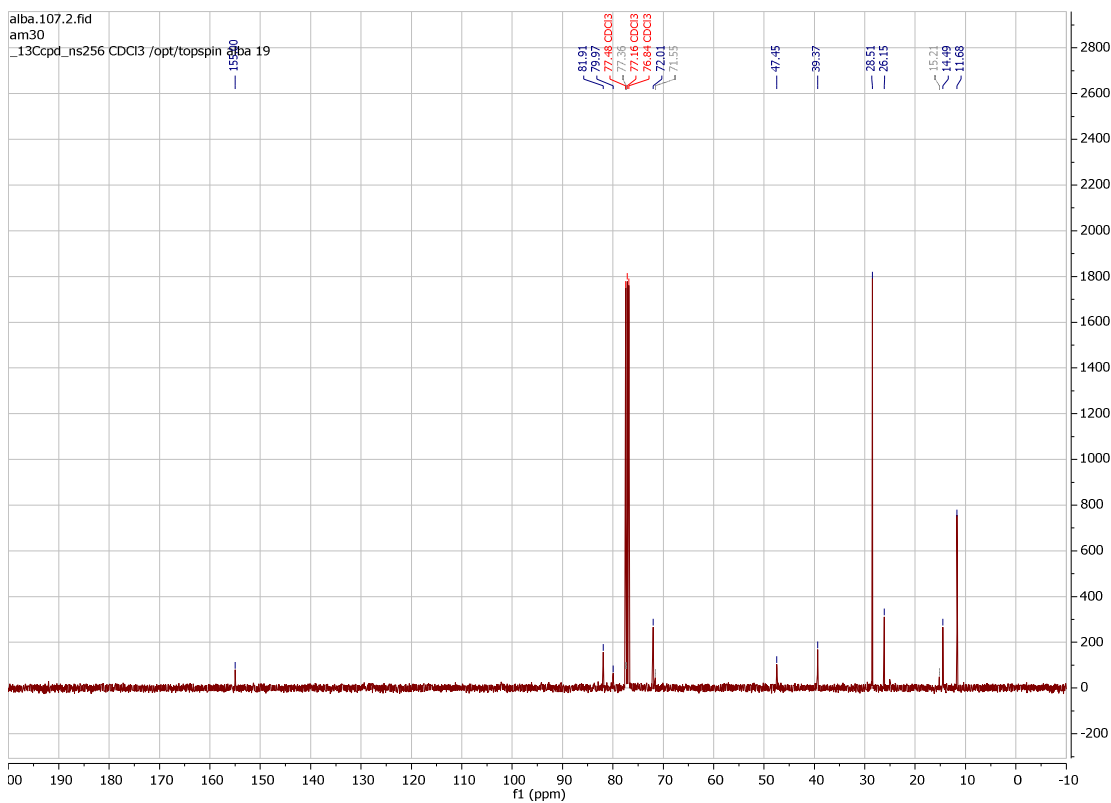
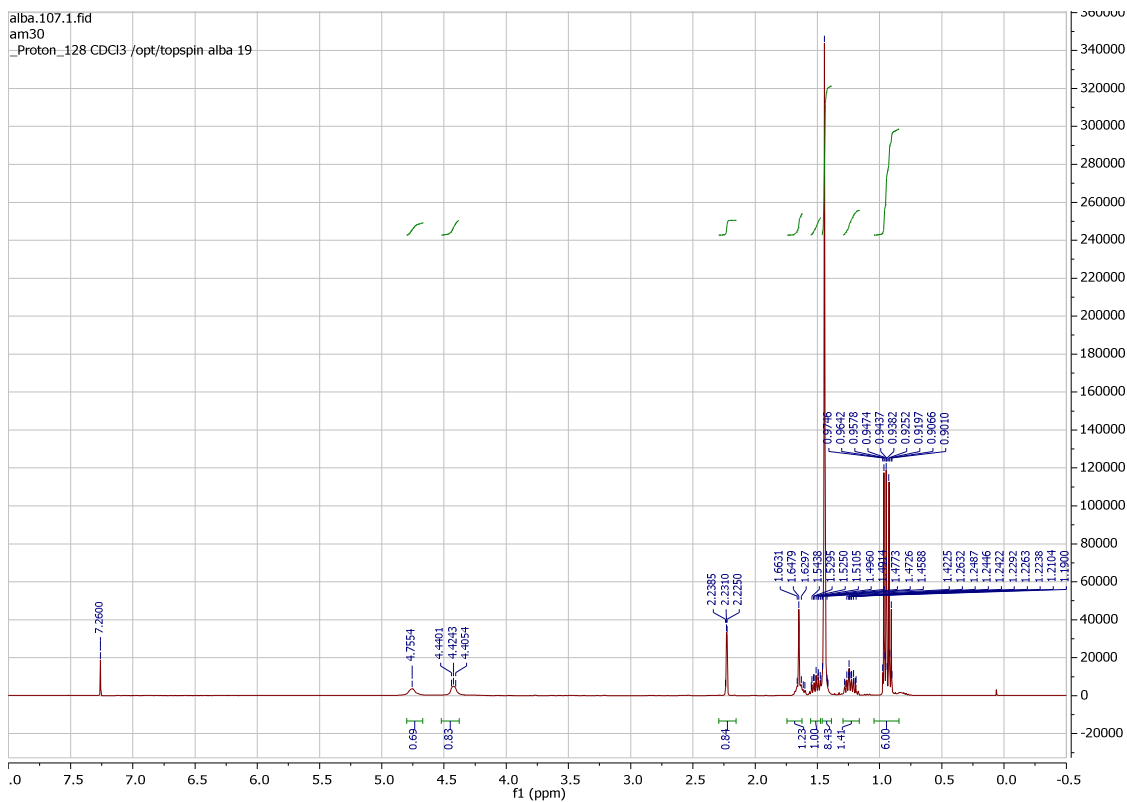


Fmoc-Tyr(<sup>t</sup>Bu)-N(Me)OMe (34c)

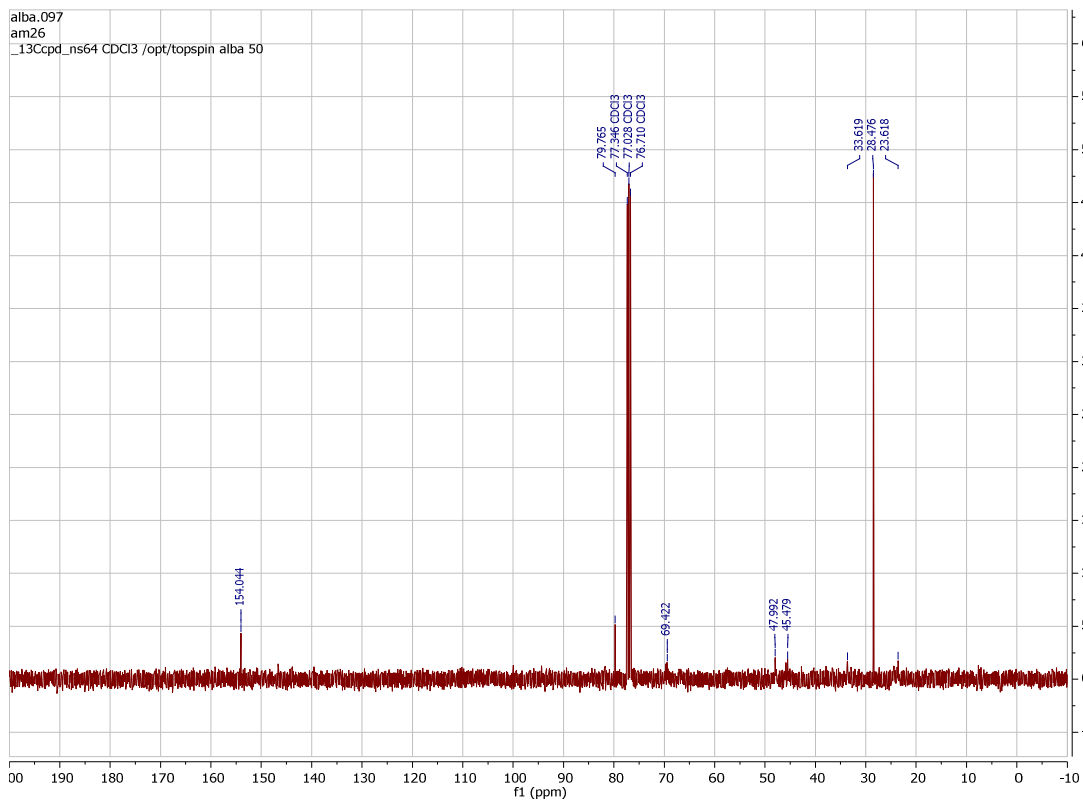
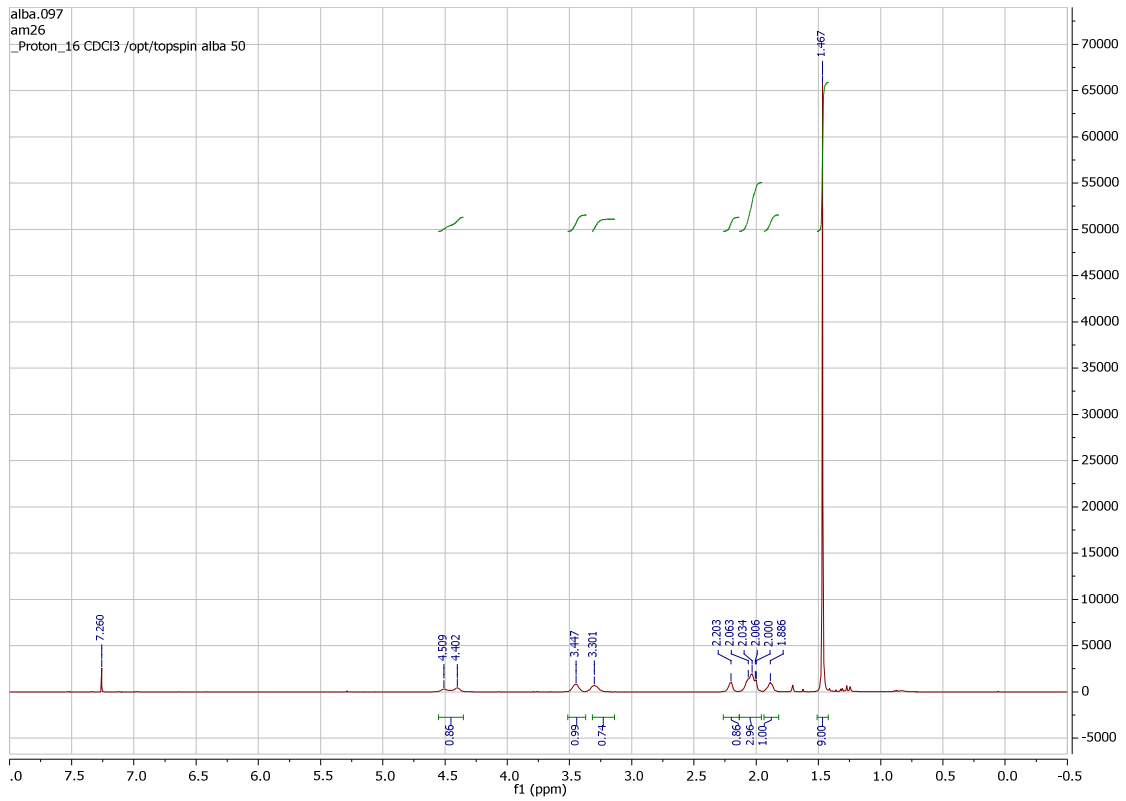




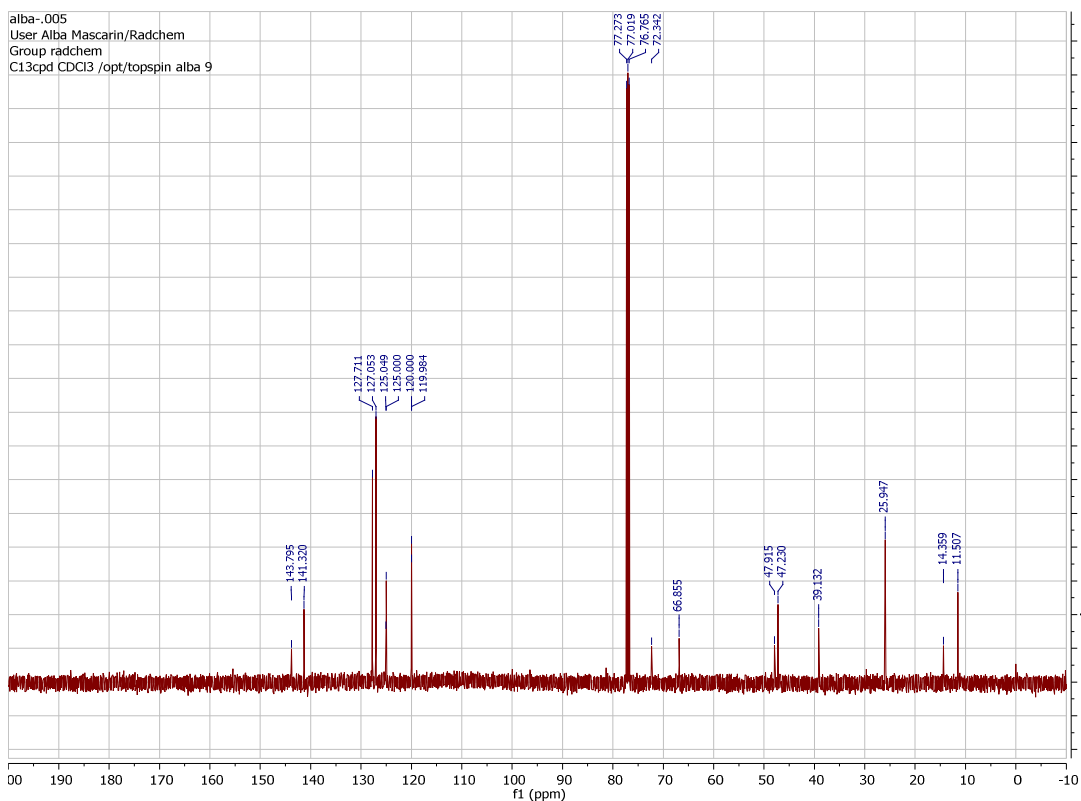
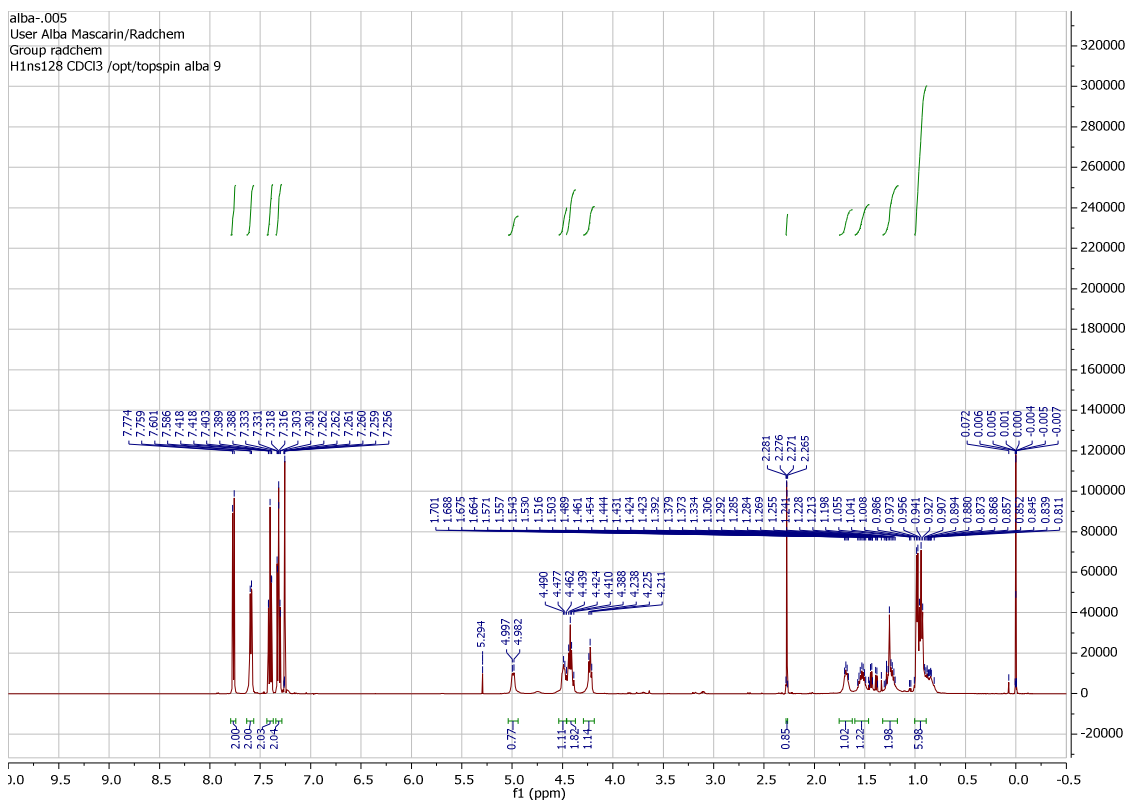
Boc-Ile-alkyne (28a)



## Boc-Pro-alkyne (28b)

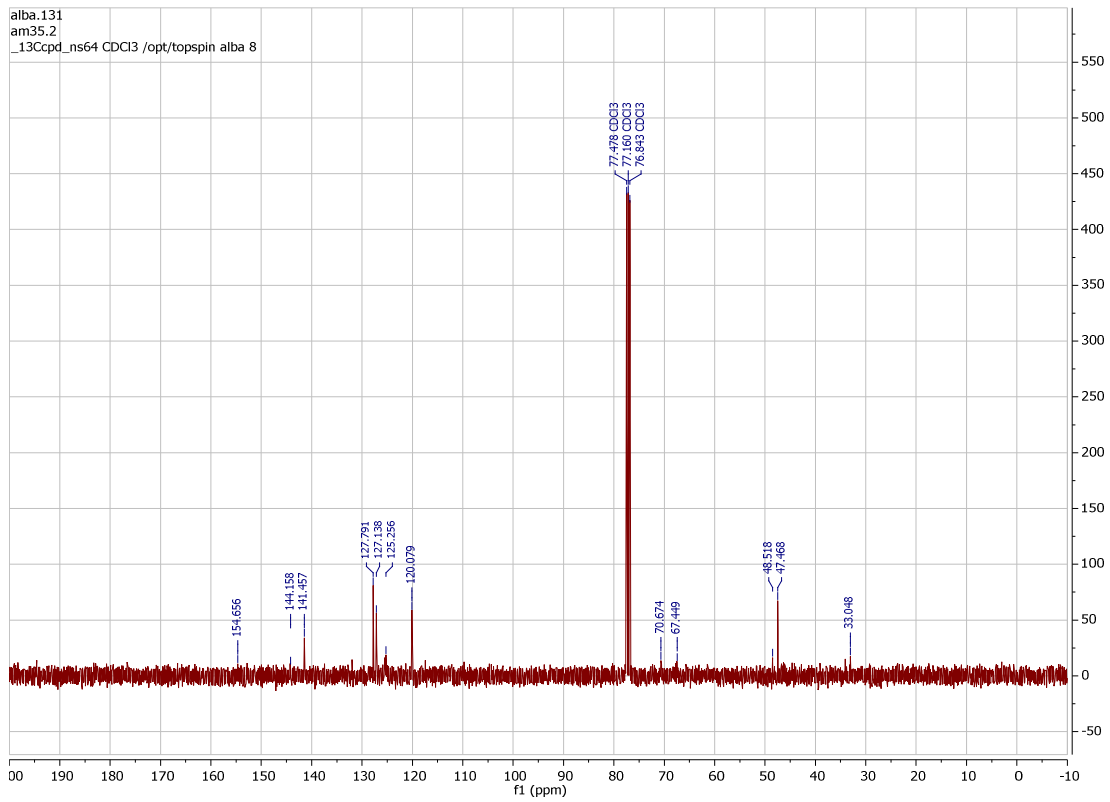
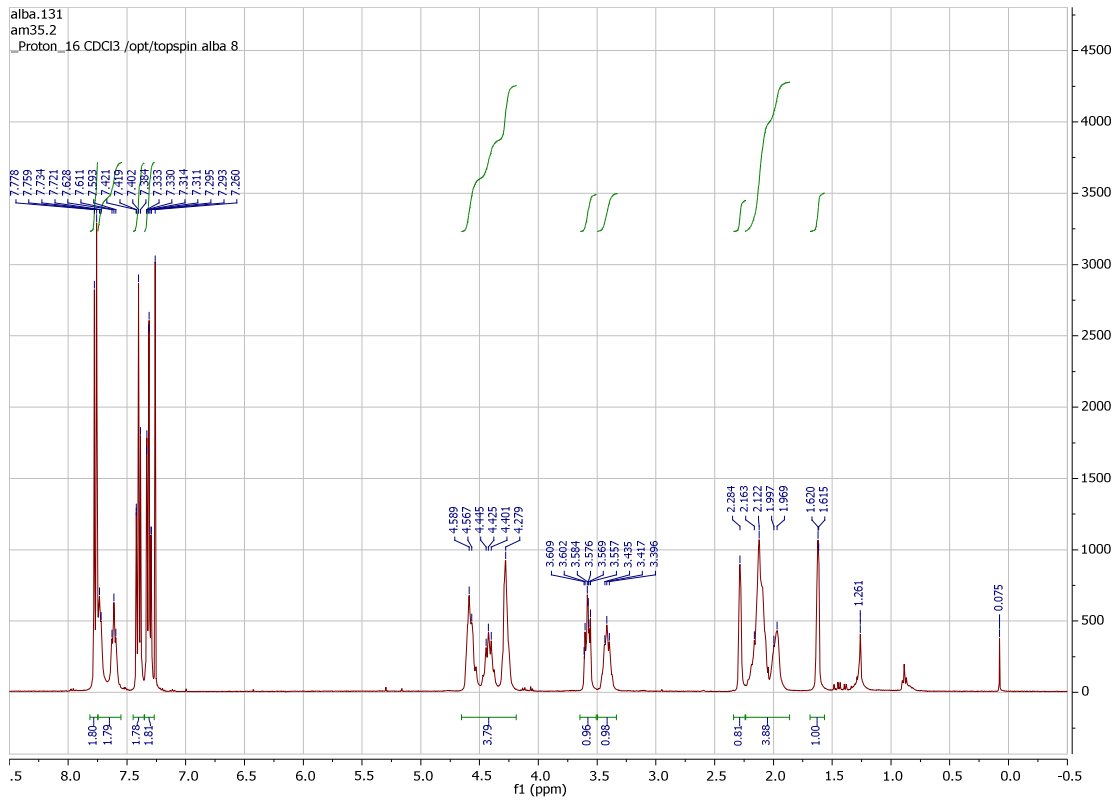


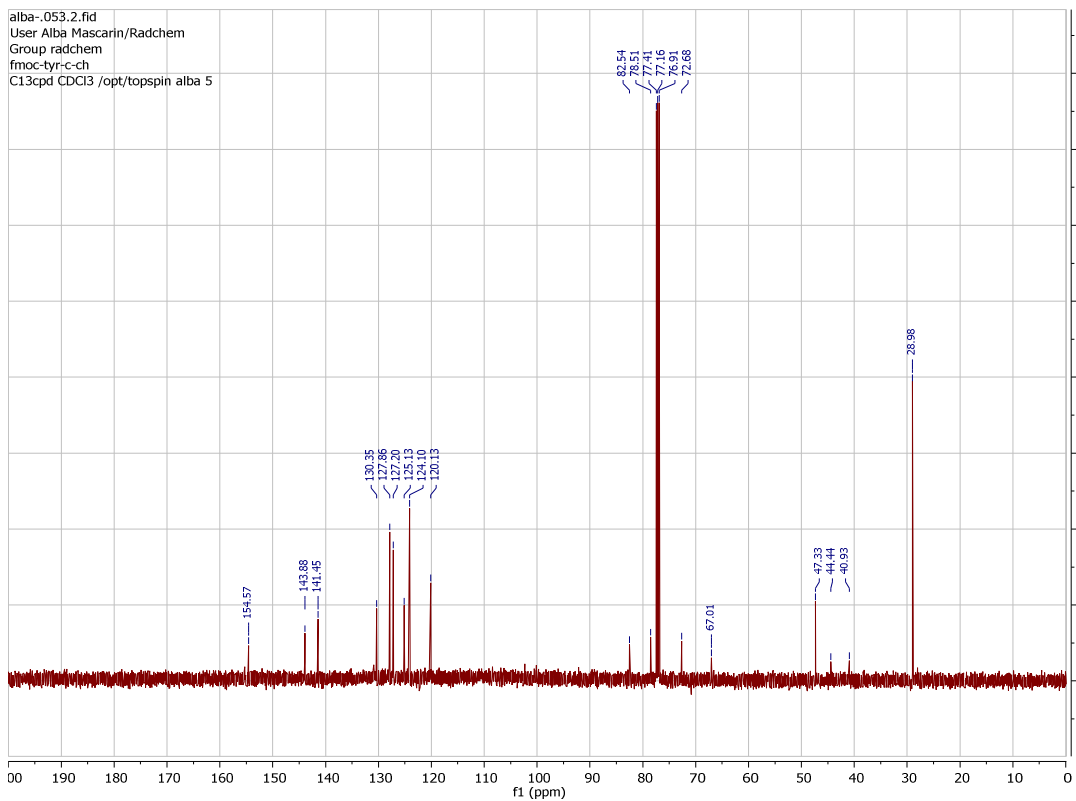
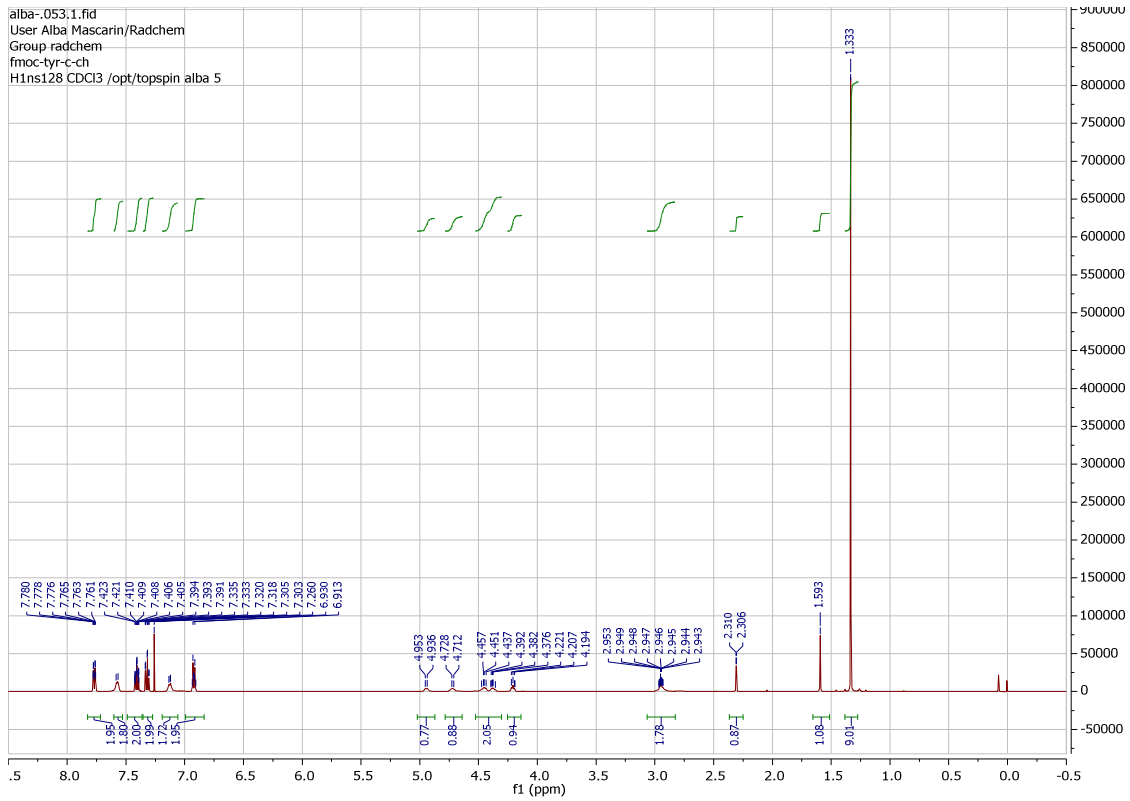
Fmoc-Ile-alkyne (29a)



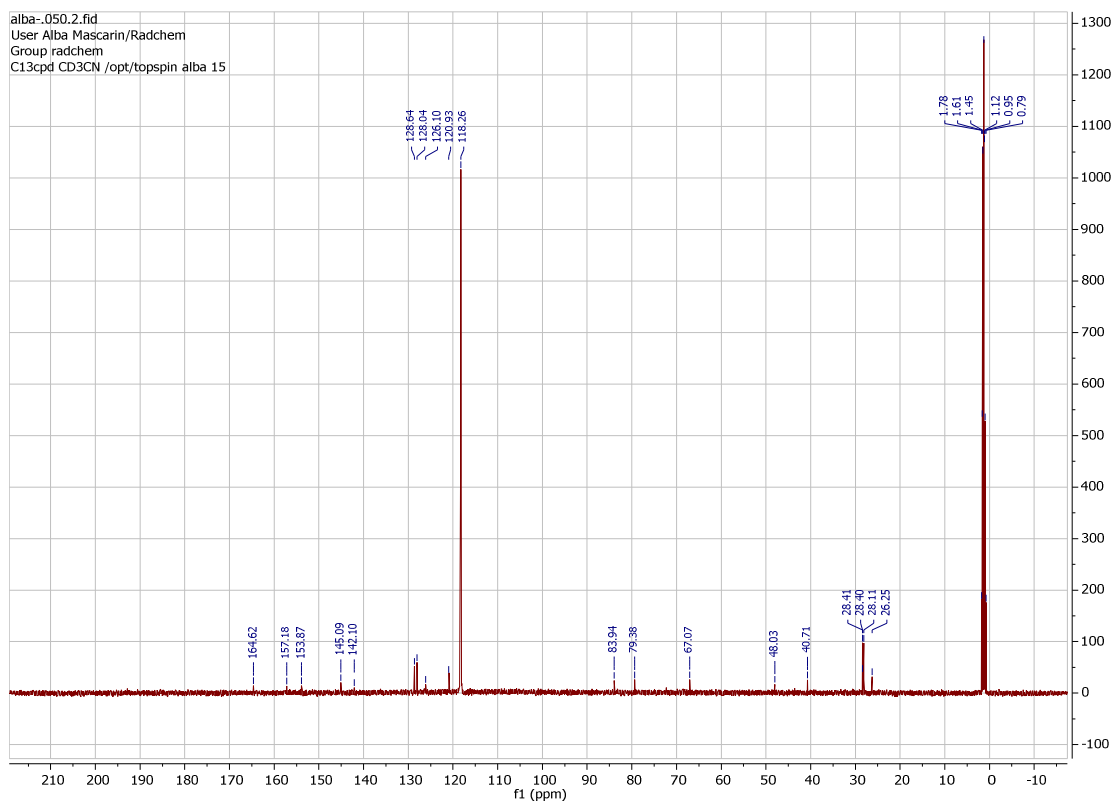
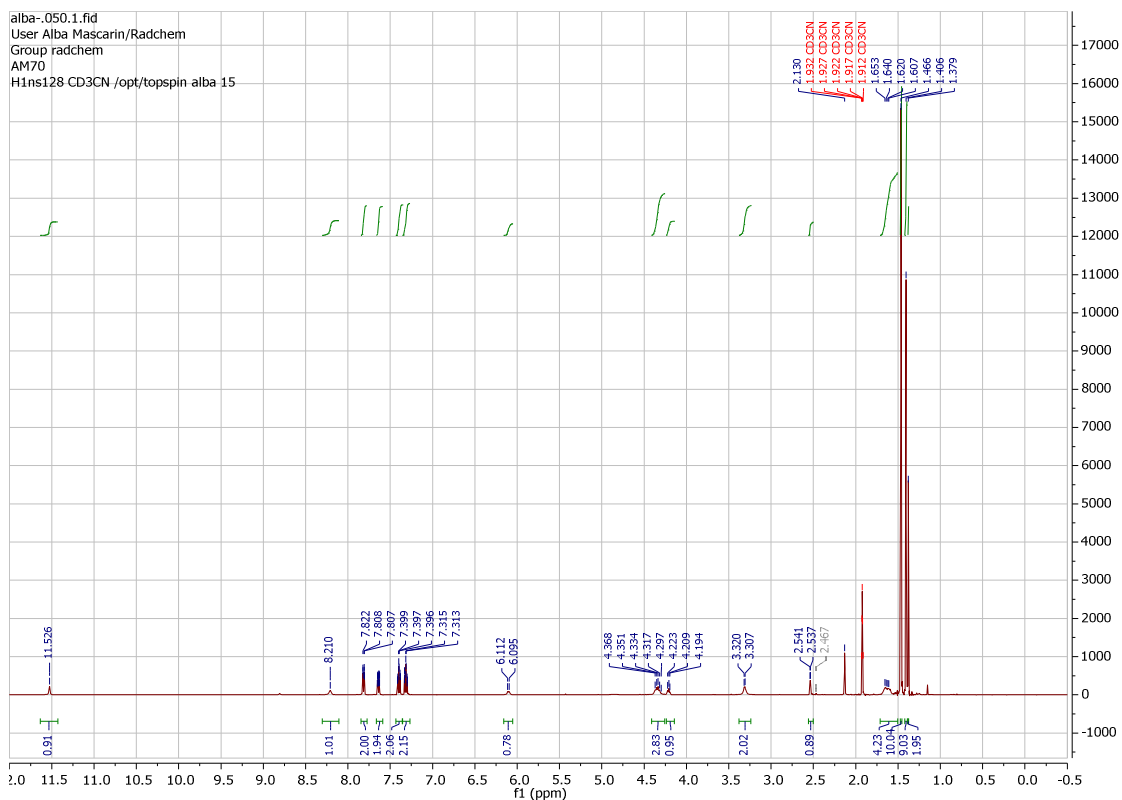
# Appendix

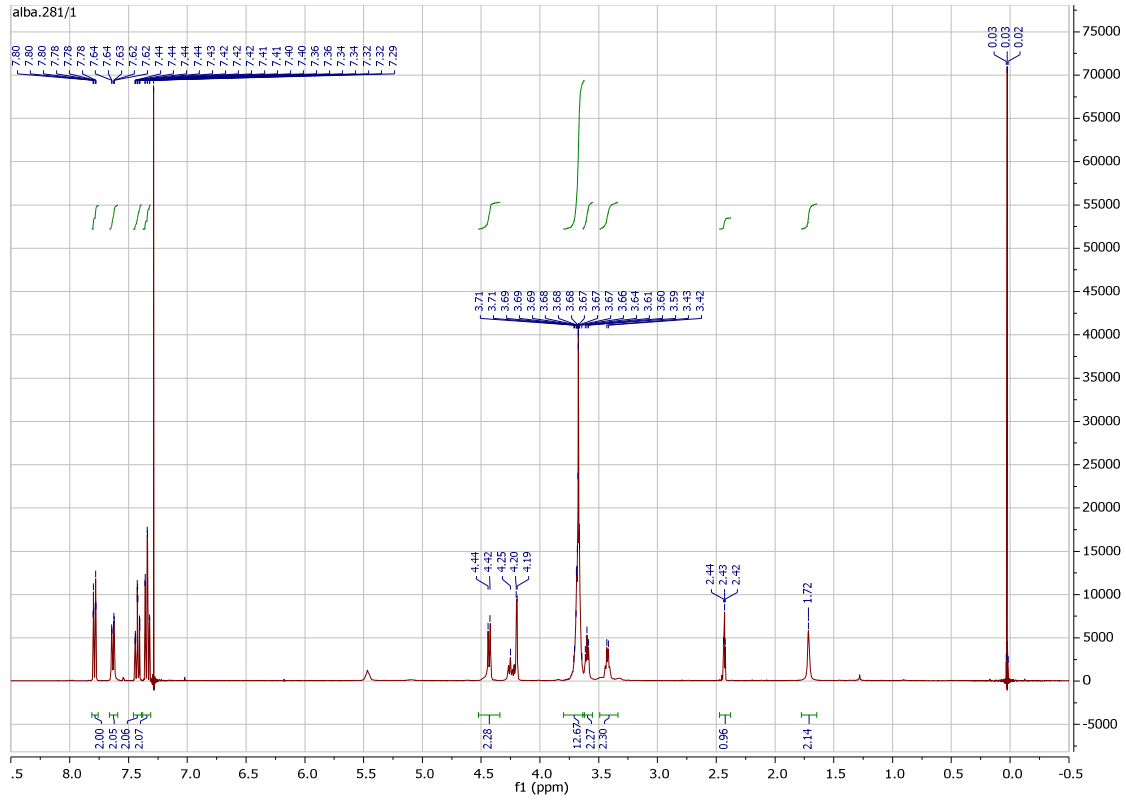
## Fmoc-Pro-alkyne (29b)



Fmoc-Tyr(<sup>t</sup>Bu)-alkyne (29c)

Fmoc-Arg(Boc)<sub>2</sub>-alkyne (29d)

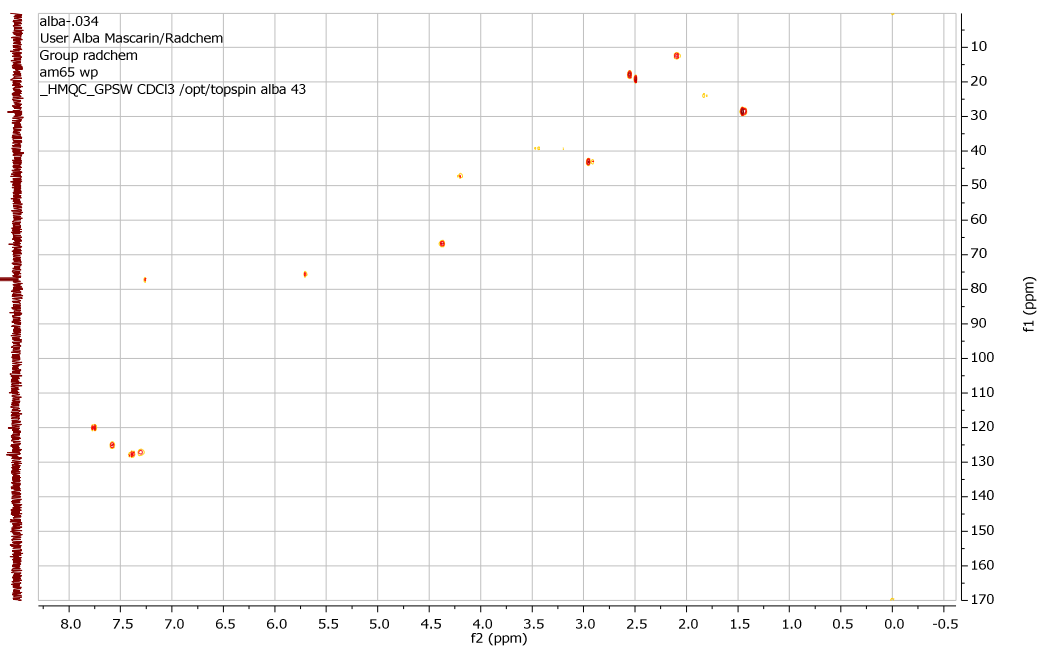
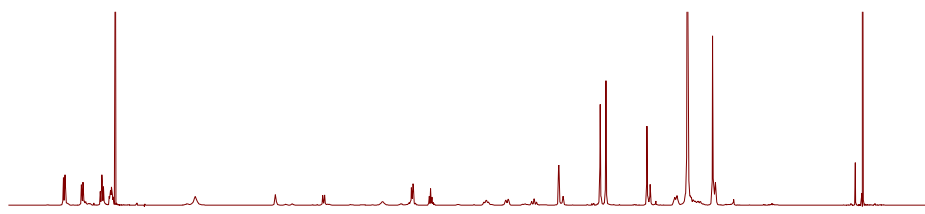
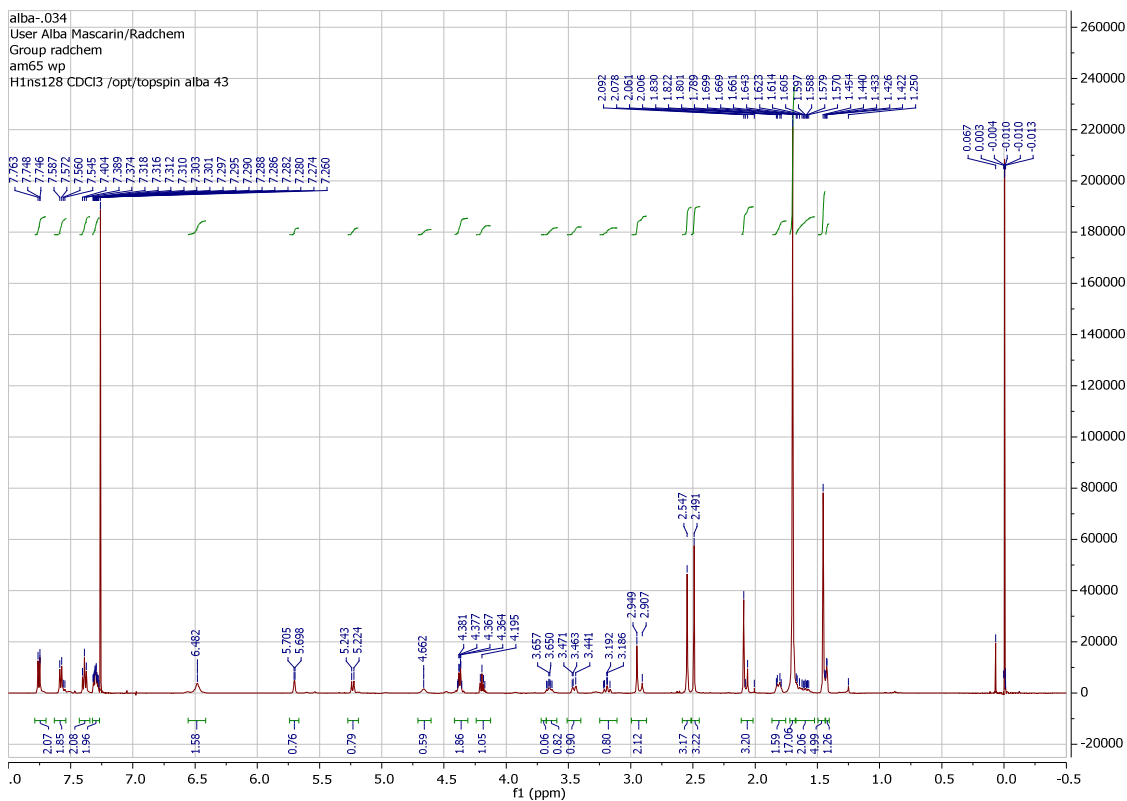


Fmoc-PEG<sub>4</sub>-alkyne (29f)

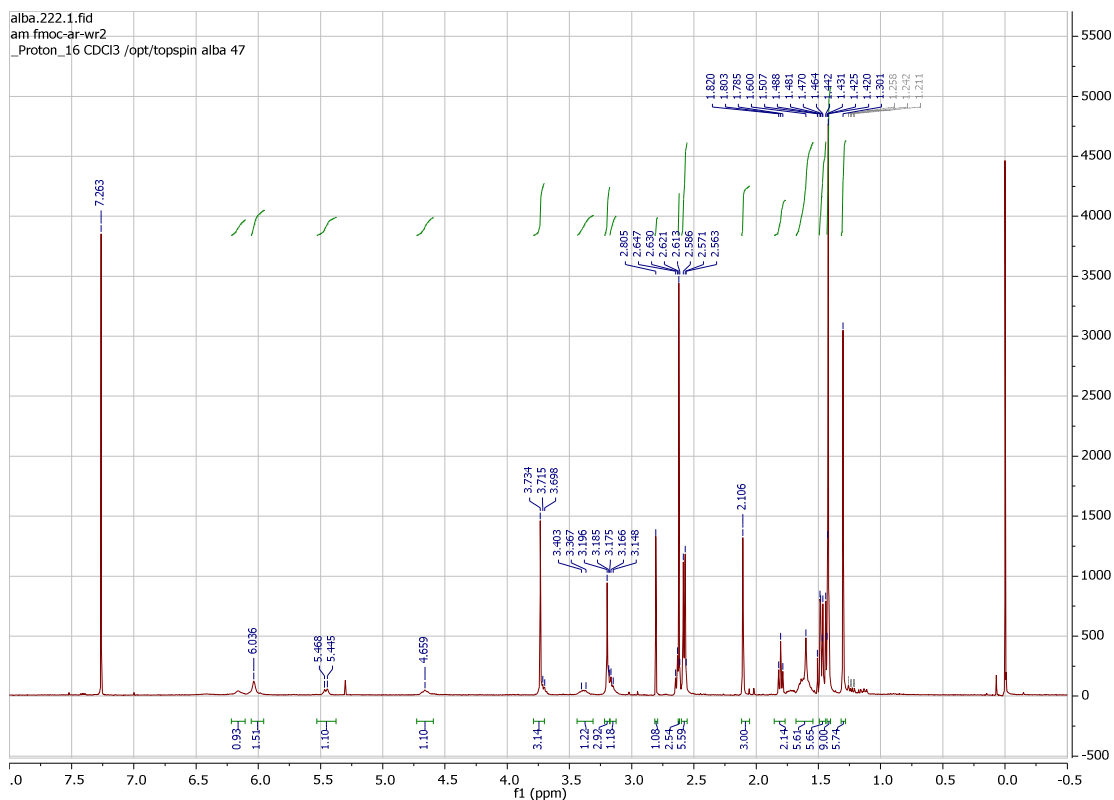




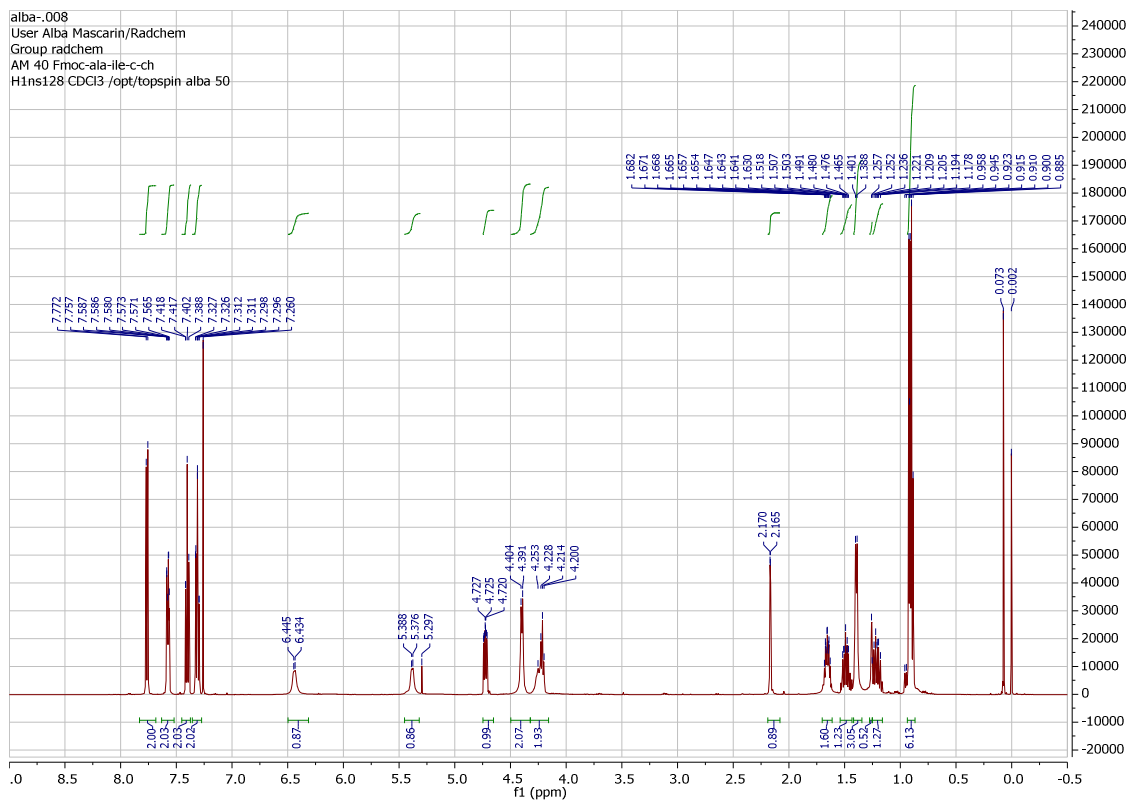
**(9H-fluoren-9-yl)methyl (2-hydroxy-1-(N-((2,2,4,6,7-pentamethyl-2,3-dihydrobenzofuran-5-yl)sulfonyl)carbamimidoyl)piperidin-3-yl)carbamate 41**



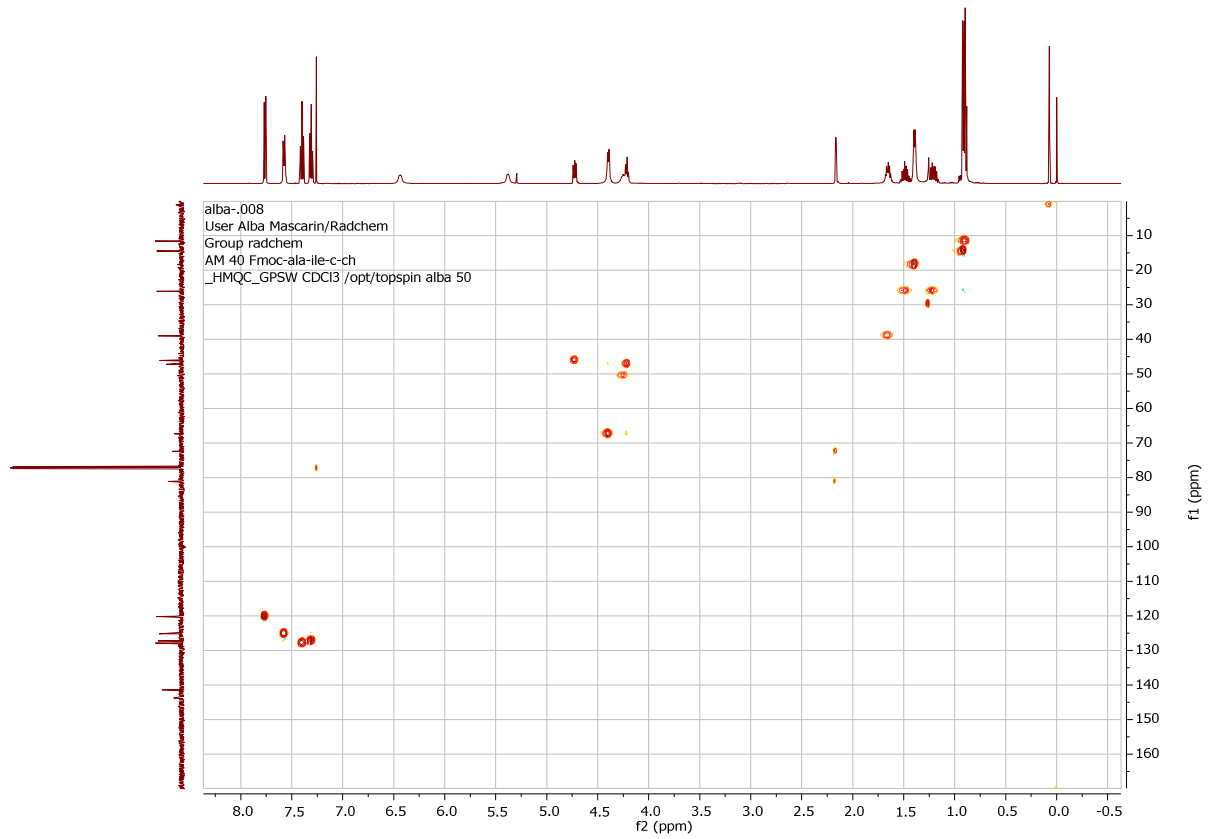
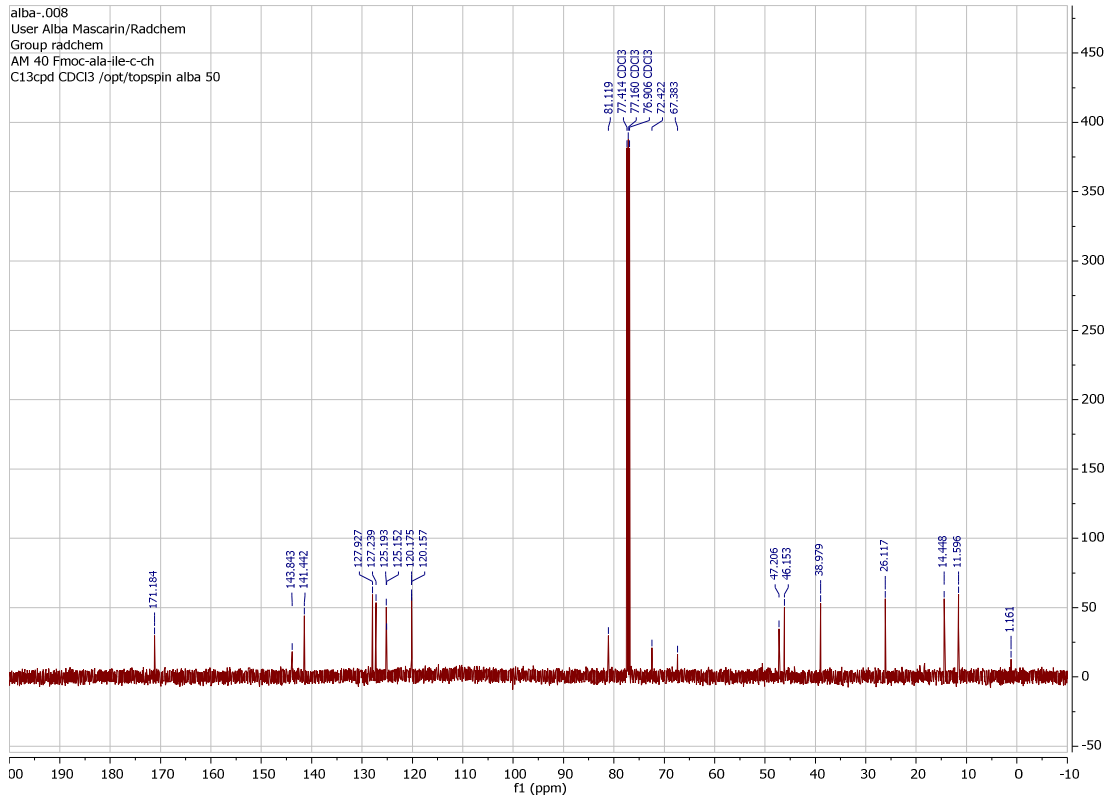
## Fmoc-Arg(Pmc)-N(Me)OMe (43)



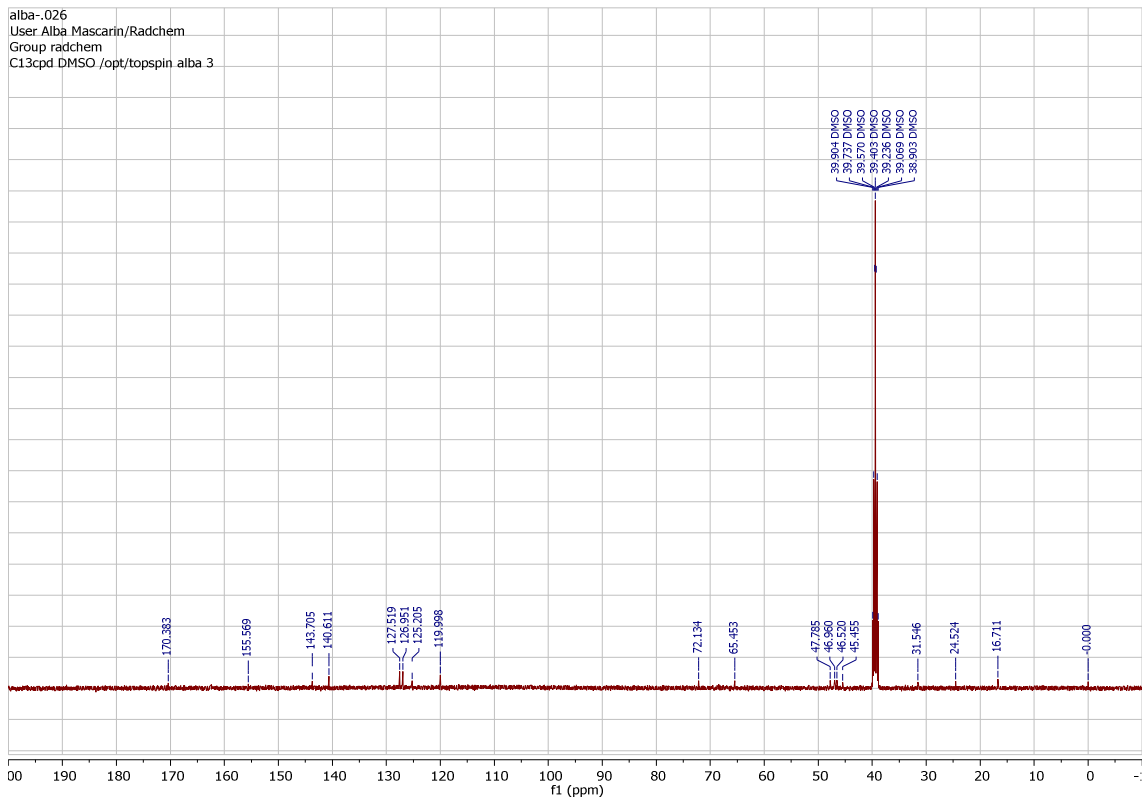
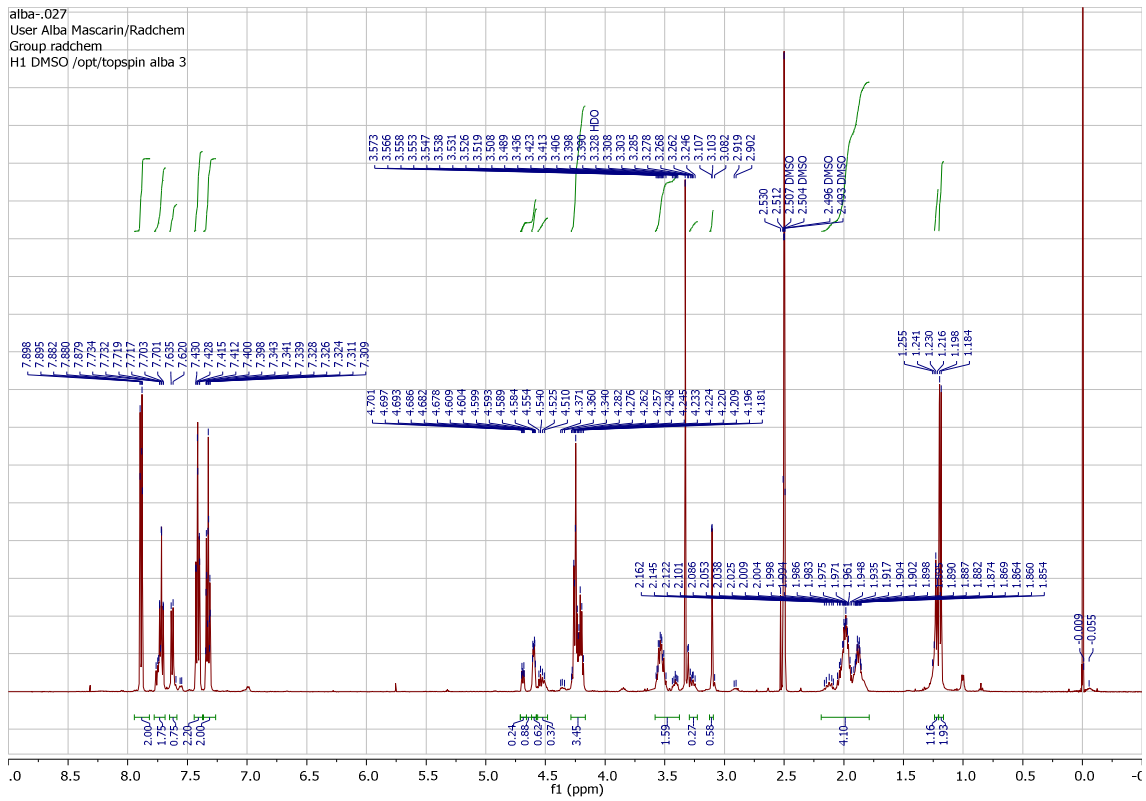
## Fmoc-Ala-Ile-alkyne (50a)



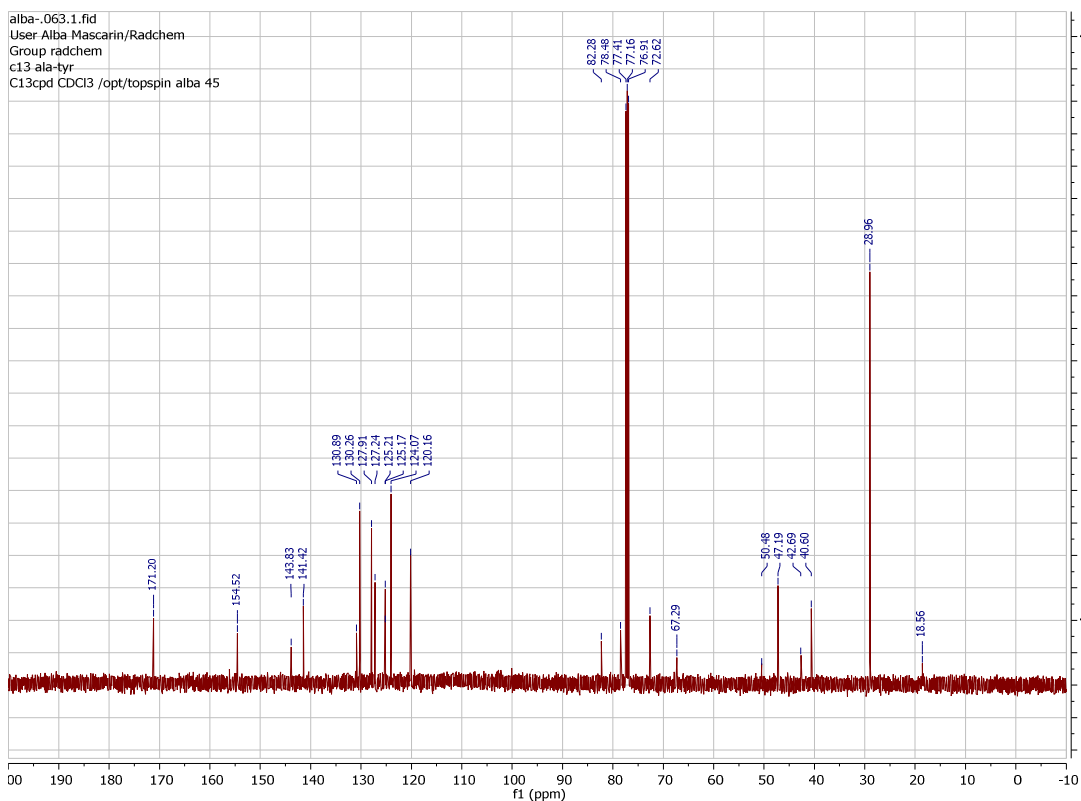
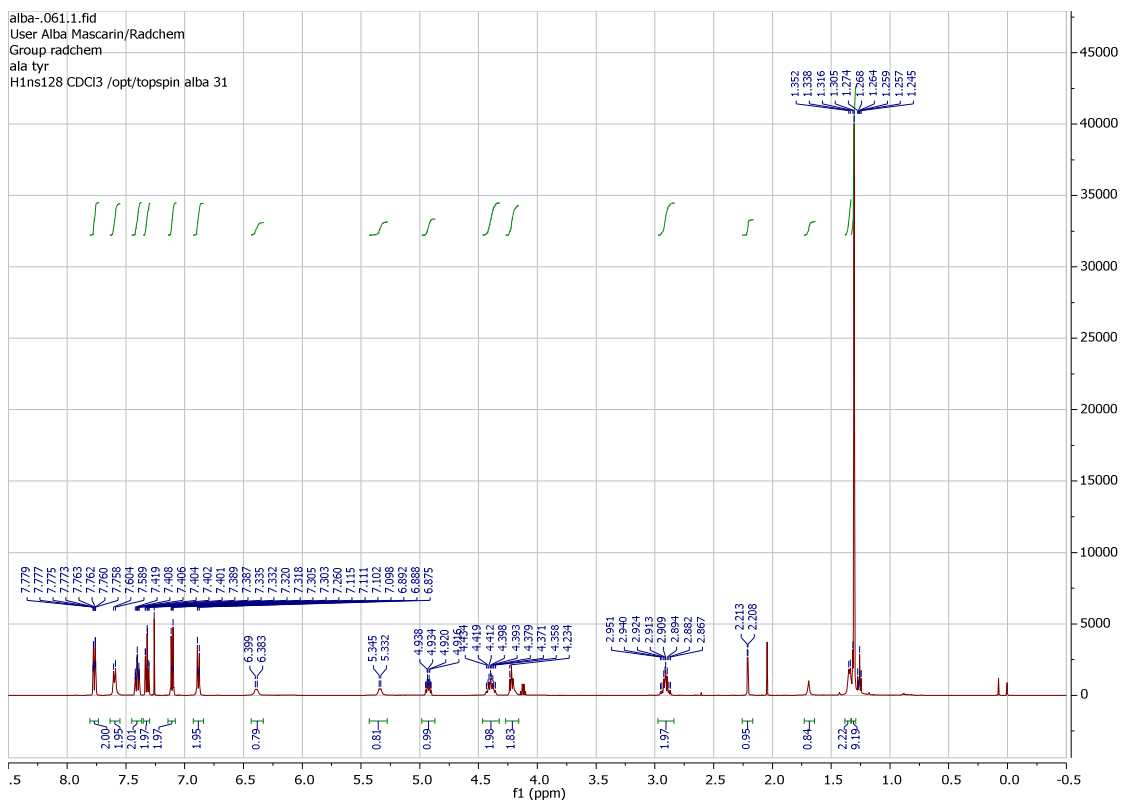
# Appendix

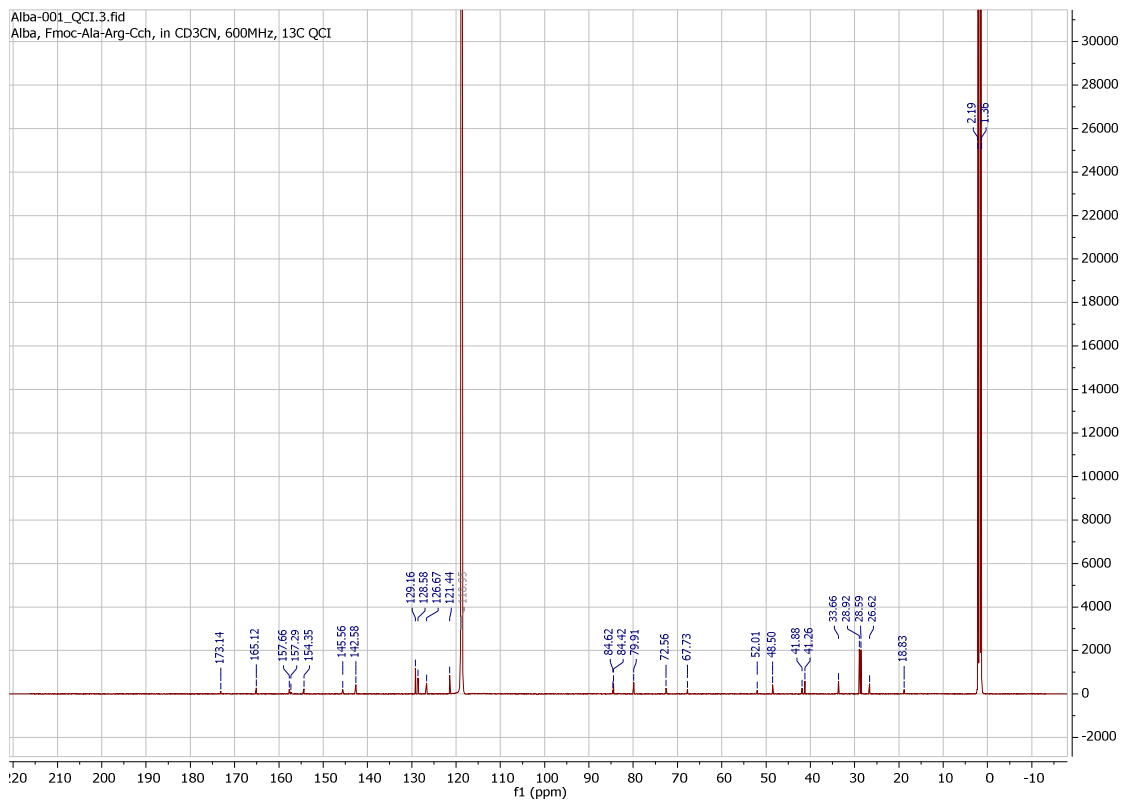
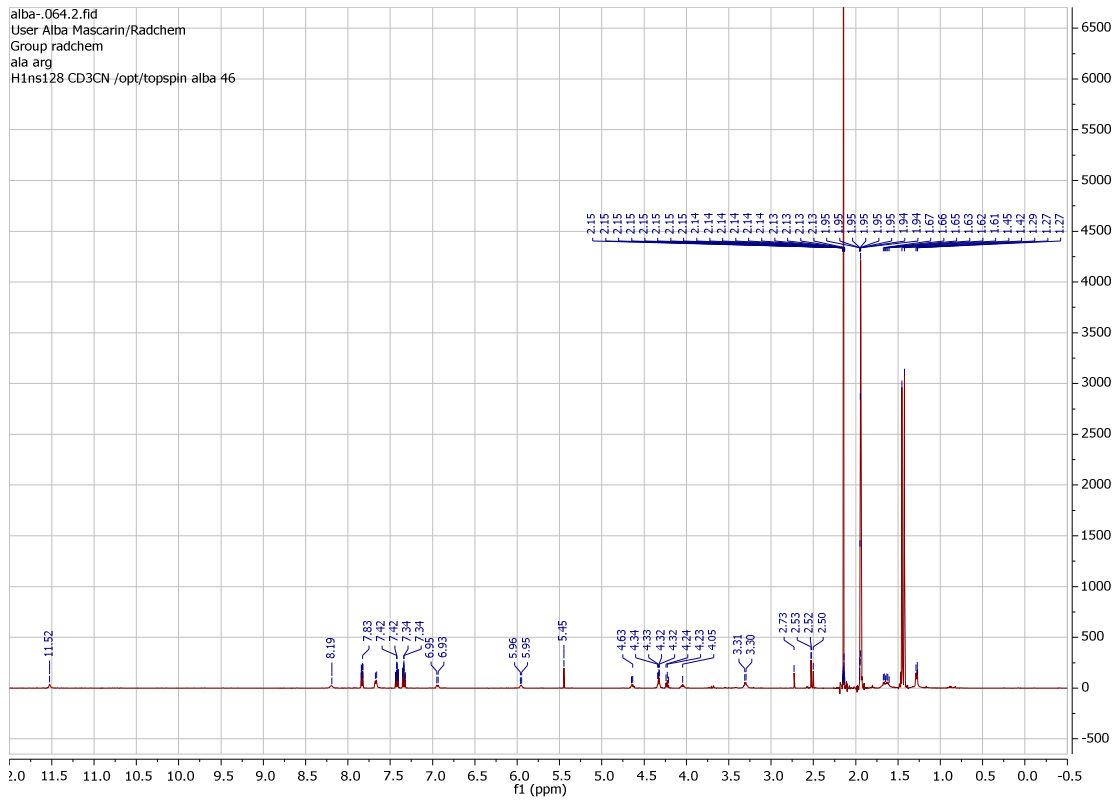


**Fmoc-Ala-Pro-alkyne (50b)**



Fmoc-Ala-Tyr(<sup>t</sup>Bu)-alkyne (50c)



Fmoc-Ala-Arg(Boc)<sub>2</sub>-alkyne (50d)

### 6.3 MS Data

#### Fmoc-Arg(Boc)<sub>2</sub>-N(Me)OMe (34d)

**Analysis Info**

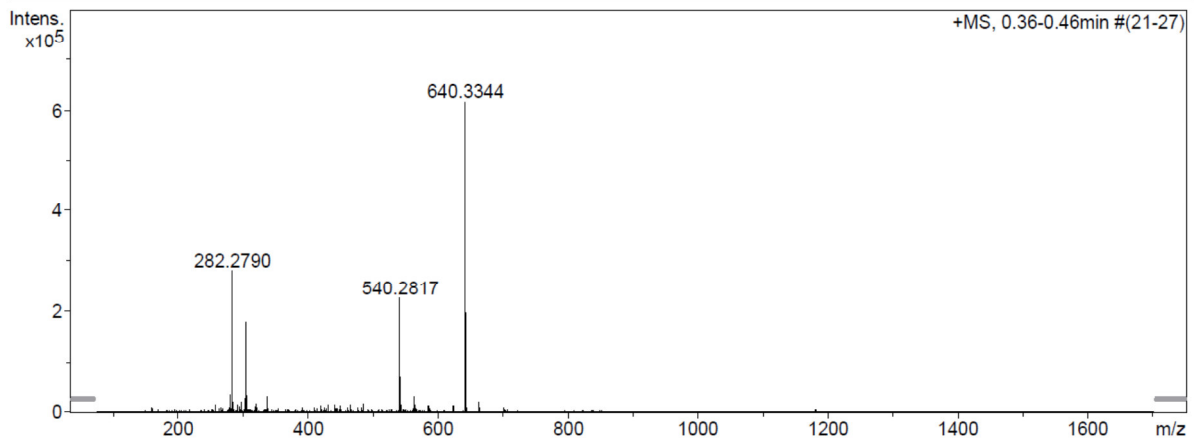
Analysis Name N:\new acq data\AM 28 001.d  
Method hn Direct\_Infusion\_pos mode\_75-1700 mid 4eV.m  
Sample Name Alba Mascarin, AM 28  
Comment AM 28, ? ug/ml MeOH

Acquisition Date 02.12.2014 09:35:19

Operator hn  
Instrument / Ser# maXis 4G 21243

**Acquisition Parameter**

Source Type	ESI	Ion Polarity	Positive	Set Nebulizer	0.4 Bar
Focus	Not active	Set Capillary	3600 V	Set Dry Heater	180 °C
Scan Begin	75 m/z	Set End Plate Offset	-500 V	Set Dry Gas	4.0 l/min
Scan End	1700 m/z	Set Collision Cell RF	500.0 Vpp	Set Ion Energy ( MS only )	4.0 eV



#### Fmoc-Tyr(<sup>t</sup>Bu)-alkyne (29c)

**Analysis Info**

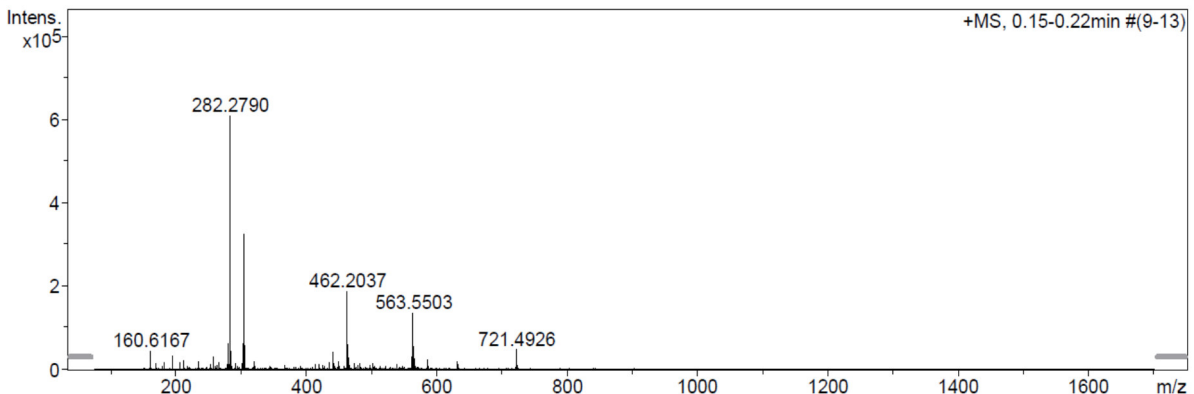
Analysis Name N:\new acq data\AM 24 001.d  
Method hn Direct\_Infusion\_pos mode\_75-1700 mid 4eV.m  
Sample Name Alba Mascarin, AM 24  
Comment AM 24, ? ug/ml MeOH

Acquisition Date 16.12.2014 09:27:50

Operator hn  
Instrument / Ser# maXis 4G 21243

**Acquisition Parameter**

Source Type	ESI	Ion Polarity	Positive	Set Nebulizer	0.4 Bar
Focus	Not active	Set Capillary	3600 V	Set Dry Heater	180 °C
Scan Begin	75 m/z	Set End Plate Offset	-500 V	Set Dry Gas	4.0 l/min
Scan End	1700 m/z	Set Collision Cell RF	500.0 Vpp	Set Ion Energy ( MS only )	4.0 eV





**Fmoc-Arg(Boc)<sub>2</sub>-alkyne (29d)**

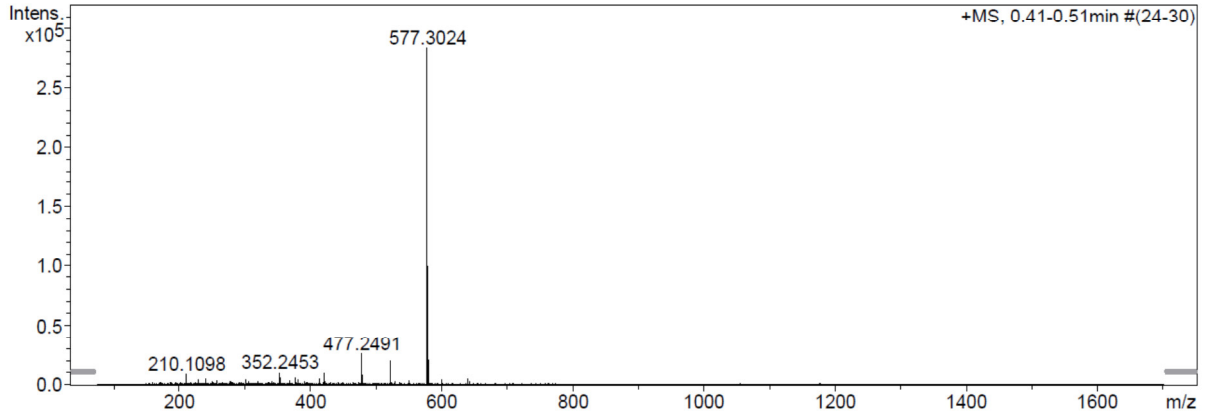
**Analysis Info**

Analysis Name N:\new acq data\AM 70 001.d  
 Method hn Direct\_Infusion\_pos mode\_75-1700 mid 4eV.m  
 Sample Name Alba Mascarin, AM 70  
 Comment AM 70, ? ug/ml MeOH/H2O

Acquisition Date 18.11.2014 09:18:53  
 Operator hn  
 Instrument / Ser# maXis 4G 21243

**Acquisition Parameter**

Source Type	ESI	Ion Polarity	Positive	Set Nebulizer	0.4 Bar
Focus	Not active	Set Capillary	3600 V	Set Dry Heater	180 °C
Scan Begin	75 m/z	Set End Plate Offset	-500 V	Set Dry Gas	4.0 l/min
Scan End	1700 m/z	Set Collision Cell RF	500.0 Vpp	Set Ion Energy ( MS only )	4.0 eV



**(9H-fluoren-9-yl)methyl (2-oxo-1-(N-((2,2,4,6,7-pentamethyl-2,3-dihydrobenzofuran-5-yl)sulfonyl)carbamidoyl)piperidin-3-yl)carbamate 39**

**Display Report**

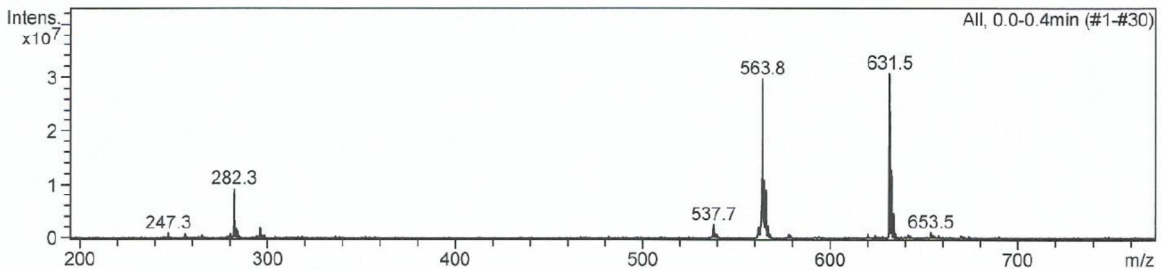
**Analysis Info**

Analysis Name AM-FmocArgPbfWR.d (lactame)  
 Method Copy of DEFAULT.MS  
 Sample Name AM-FmocArgPbfWR  
 Comment

Acquisition Date 02/19/15 11:55:48  
 Operator Administrator  
 Instrument esquire3000plus\_01096

**Acquisition Parameter**

Ion Source Type	ESI	Ion Polarity	Positive	Alternating Ion Polarity	off
Mass Range Mode	Std/Normal	Scan Begin	100 m/z	Scan End	1500 m/z
Capillary Exit	134.3 Volt	Skim 1	40.0 Volt	Trap Drive	61.4
Accumulation Time	22 µs	Averages	5 Spectra	Auto MS/MS	off

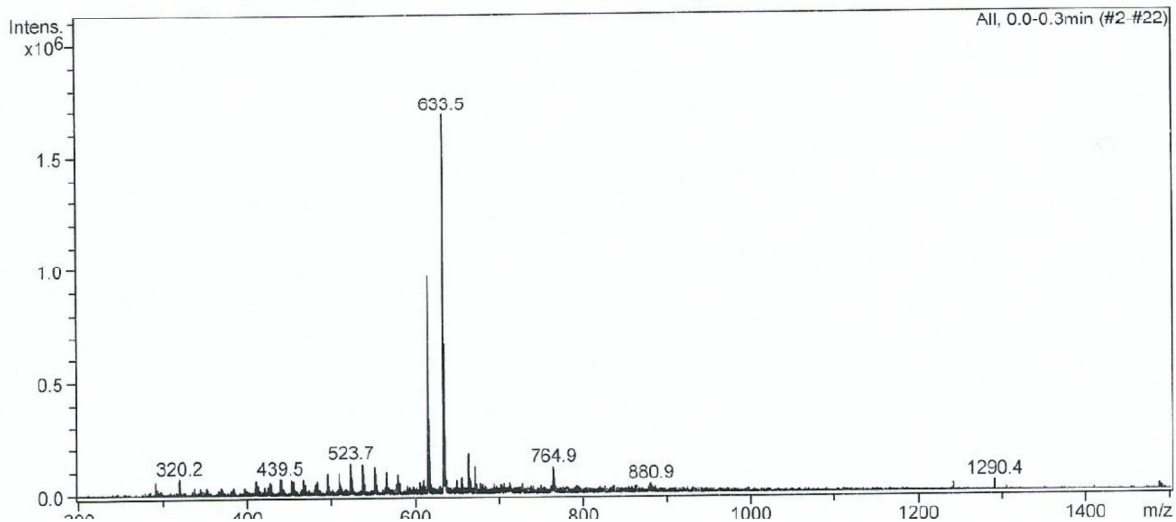


Appendix

**(9H-fluoren-9-yl)methyl (2-hydroxy-1-(N-((2,2,4,6,7-pentamethyl-2,3-dihydrobenzofuran-5-yl)sulfonyl)carbamimidoyl)piperidin-3-yl)carbamate 41**

Analysis Info *A765 Fmoc-Arg(Pbf)-hemiacetal*  
 Analysis Name AM\_WTFsmpl\_4.d Acquisition Date 10/01/13 16:43:04  
 Method Copy(3) of E3Kp Default.ms Operator Administrator  
 Sample Name AM\_WTFsmpl\_4 Instrument esquire3000plus\_01096  
 Comment

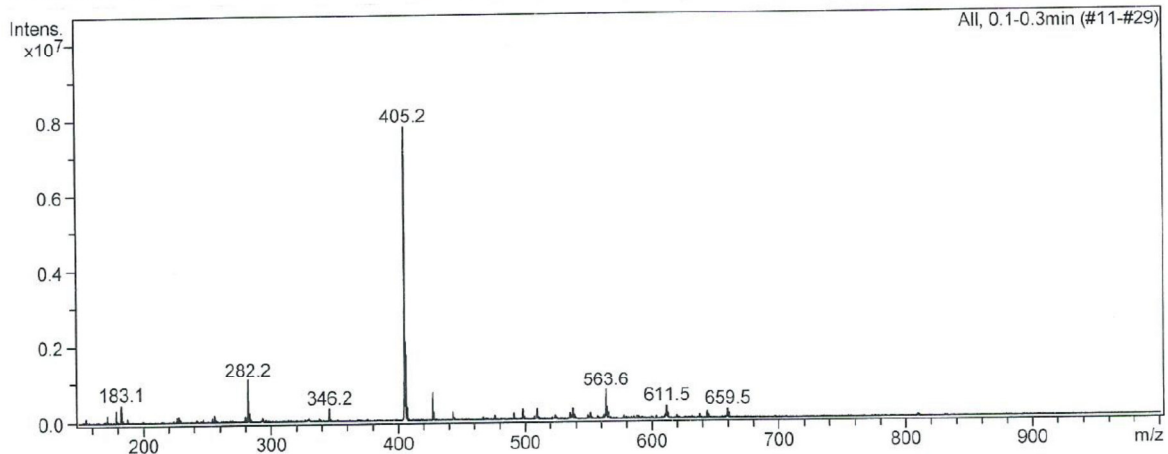
Acquisition Parameter  
 Ion Source Type ESI Ion Polarity Positive Alternating Ion Polarity off  
 Mass Range Mode Std/Normal Scan Begin 200 m/z Scan End 1500 m/z  
 Capillary Exit 95.7 Volt Skim 1 40.0 Volt Trap Drive 65.8  
 Accumulation Time 253 µs Averages 5 Spectra Auto MS/MS off



**Fmoc-Ala-Ile-alkyne (50a)**

Analysis Info *Fmoc-Ala-Ile-alkyne*  
 Analysis Name AM\_XXX\_peakB.d Acquisition Date 03/12/13 13:50:35  
 Method Copy of DEF\_MS.MS Operator Administrator  
 Sample Name AM\_XXX\_peakB Instrument esquire3000plus\_01096  
 Comment MeOH

Acquisition Parameter  
 Ion Source Type ESI Ion Polarity Positive Alternating Ion Polarity off  
 Mass Range Mode Std/Normal Scan Begin 150 m/z Scan End 1000 m/z  
 Capillary Exit 121.4 Volt Skim 1 40.0 Volt Trap Drive 47.9  
 Accumulation Time 207 µs Averages 5 Spectra Auto MS/MS off



**Fmoc-Ala-Pro-alkyne (50b)****Generic Display Report****Analysis Info**

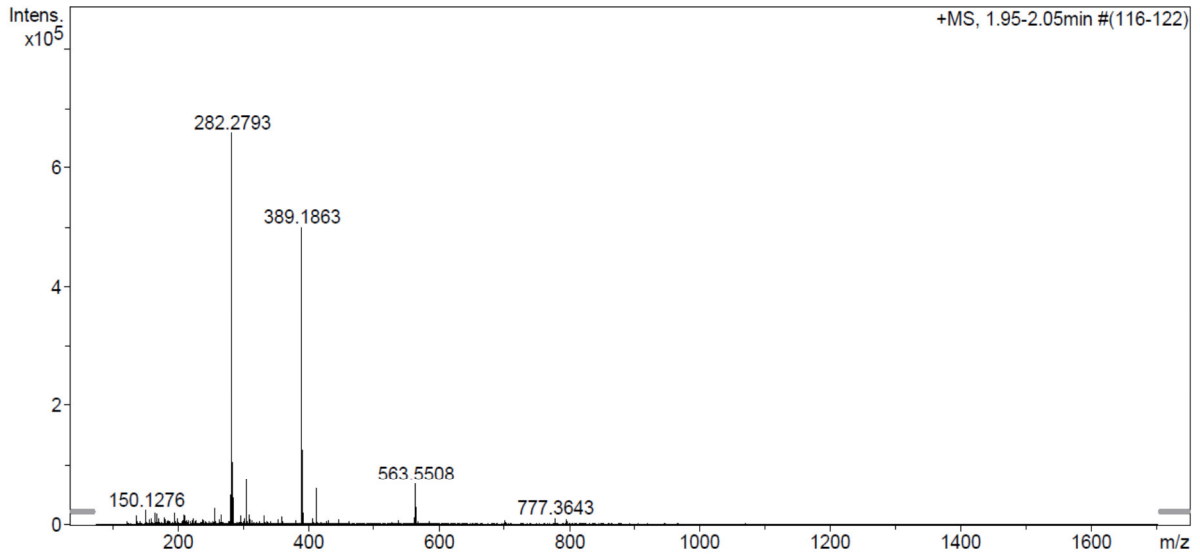
Analysis Name N:\new acq data\AM 29 001.d  
Method hn Direct\_Infusion\_pos mode\_75-1700 mid 4eV.m  
Sample Name Alba Mascarin, AM 29  
Comment AM 29, ? ug/ml MeOH

Acquisition Date 02.12.2014 09:00:49

Operator hn  
Instrument / Ser# maXis 4G 21243

**Acquisition Parameter**

Source Type	ESI	Ion Polarity	Positive	Set Nebulizer	0.4 Bar
Focus	Not active	Set Capillary	3600 V	Set Dry Heater	180 °C
Scan Begin	75 m/z	Set End Plate Offset	-500 V	Set Dry Gas	4.0 l/min
Scan End	1700 m/z	Set Collision Cell RF	500.0 Vpp	Set Ion Energy ( MS only )	4.0 eV



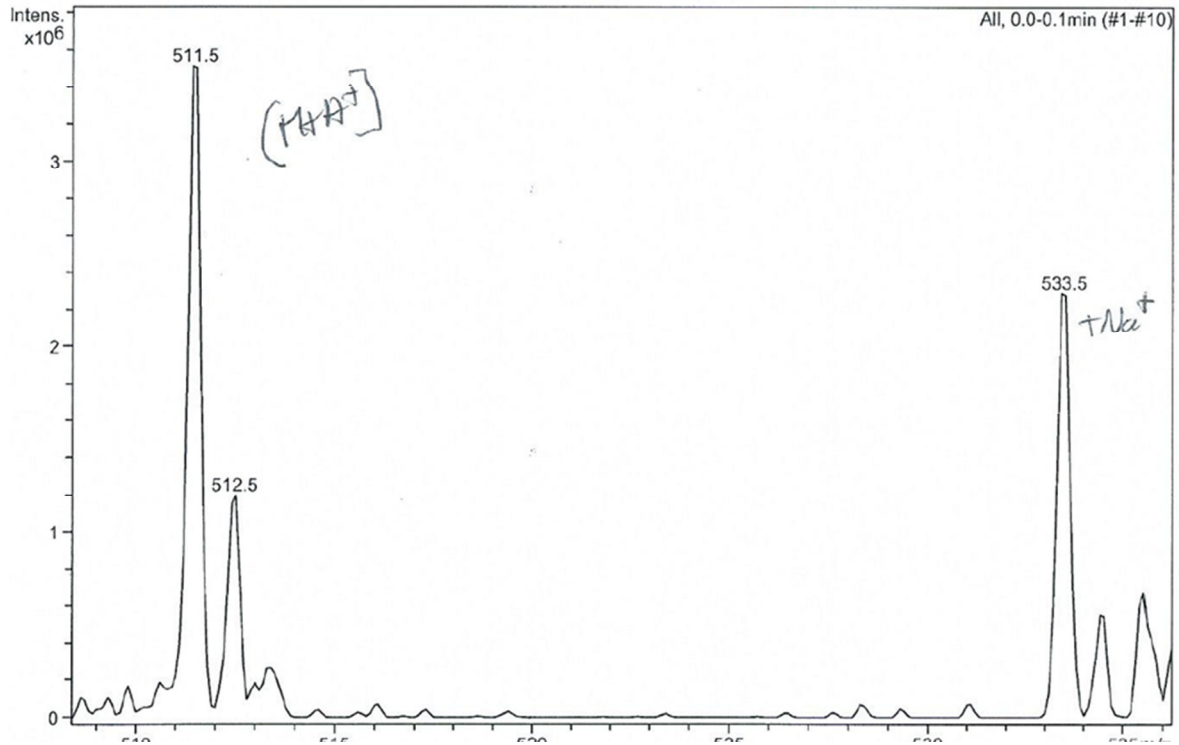
**Fmoc-Ala-Tyr(<sup>t</sup>Bu-alkyne (50c)****Analysis Info**

Analysis Name AM\_FmocAlaTyr\_alk.d  
Method Copy(2) of E3Kp Default.ms  
Sample Name AM\_FmocAlaTyr\_alk  
Comment 1:2

Acquisition Date 12/09/14 10:30:02  
Operator Administrator  
Instrument esquire3000plus\_01096

**Acquisition Parameter**

Ion Source Type	ESI	Ion Polarity	Positive	Alternating Ion Polarity	off
Mass Range Mode	Std/Normal	Scan Begin	150 m/z	Scan End	1500 m/z
Capillary Exit	129.3 Volt	Skim 1	40.0 Volt	Trap Drive	56.1
Accumulation Time	21 $\mu$ s	Averages	5 Spectra	Auto MS/MS	off



**Fmoc-Ala-Arg(Boc)<sub>2</sub>-alkyne (50d)****Analysis Info**

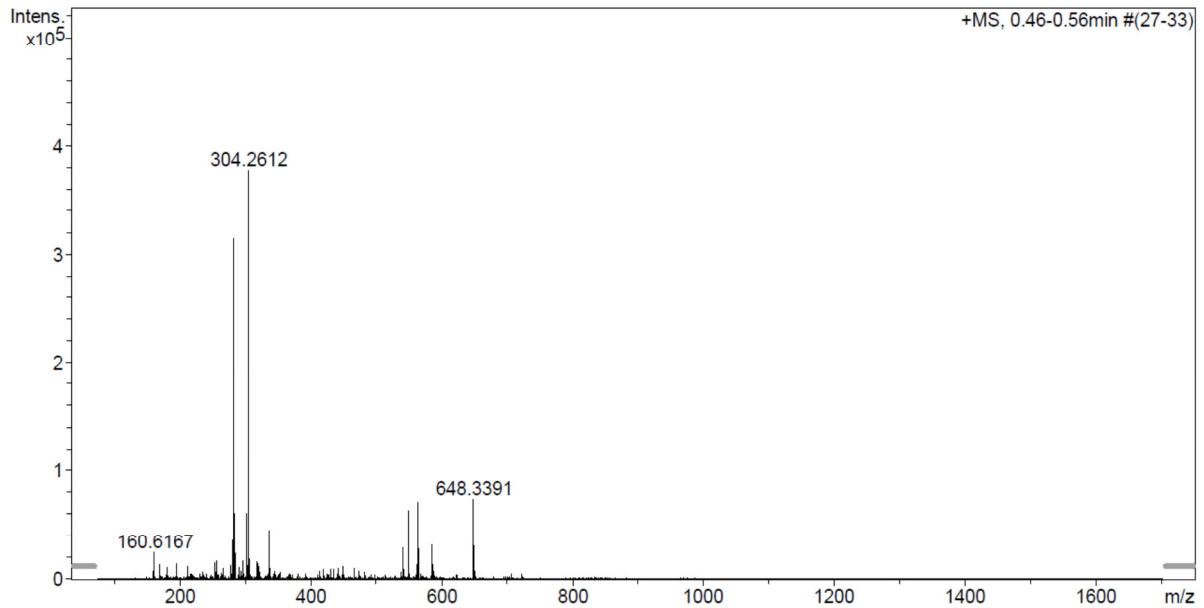
Analysis Name N:\new acq data\AM 26 001.d  
Method hn Direct\_Infusion\_pos mode\_75-1700 mid 4eV.m  
Sample Name Alba Mascarin, AM 26  
Comment AM 26, ? ug/ml MeOH

Acquisition Date 02.12.2014 09:59:51

Operator hn  
Instrument / Ser# maXis 4G 21243

**Acquisition Parameter**

Source Type	ESI	Ion Polarity	Positive	Set Nebulizer	0.4 Bar
Focus	Not active	Set Capillary	3600 V	Set Dry Heater	180 °C
Scan Begin	75 m/z	Set End Plate Offset	-500 V	Set Dry Gas	4.0 l/min
Scan End	1700 m/z	Set Collision Cell RF	500.0 Vpp	Set Ion Energy ( MS only )	4.0 eV

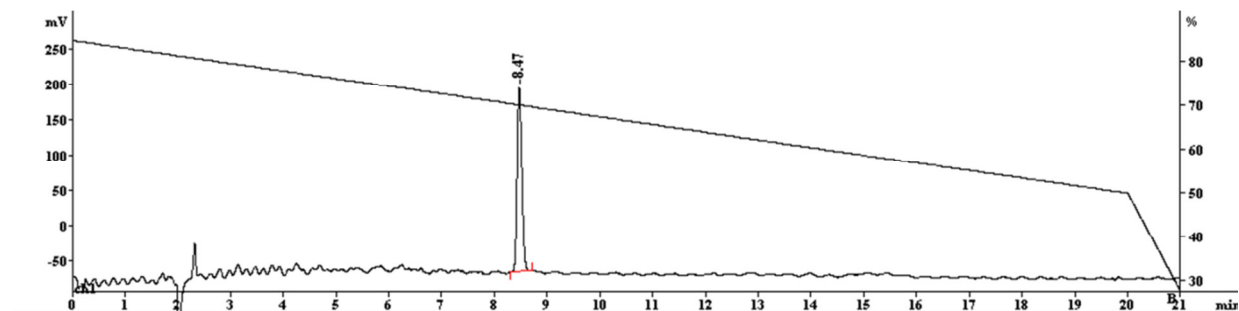


## 6.5 Peptides

### 6.5.1 Analytical UV-chromatograms

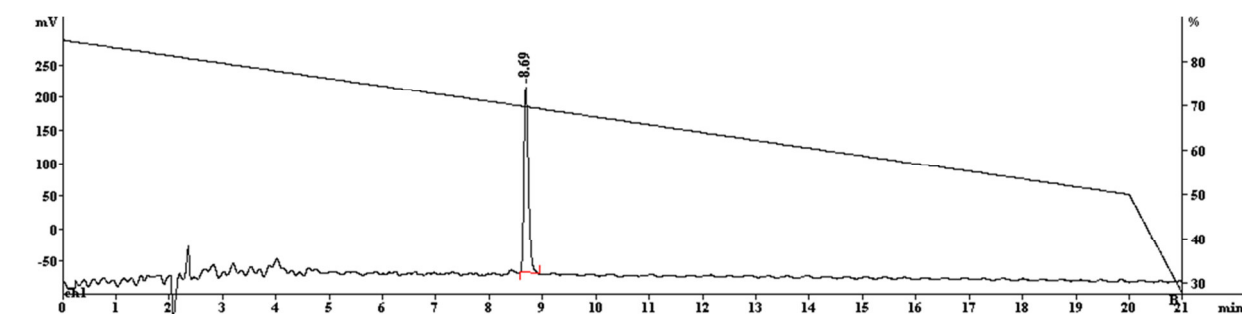
#### AM-NT 1

Analytical HPLC profile: gradient 90-50% A in B in 20 min.



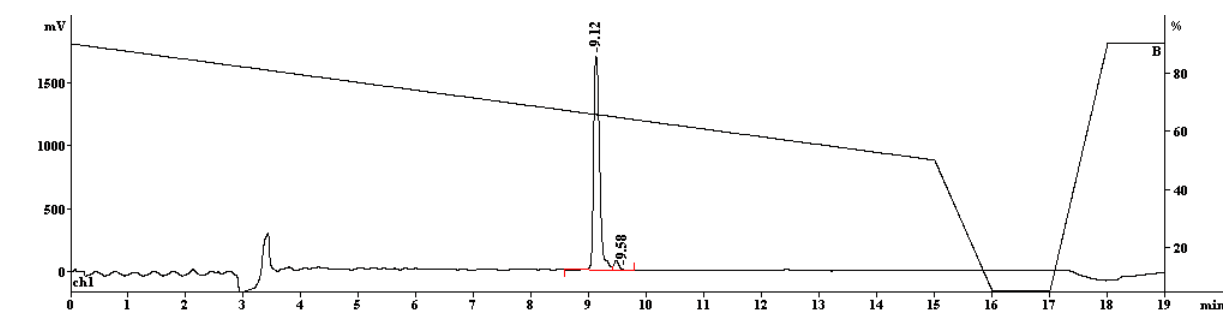
#### AM-NT 2

Analytical HPLC profile: gradient 90-50% A in B in 20 min.



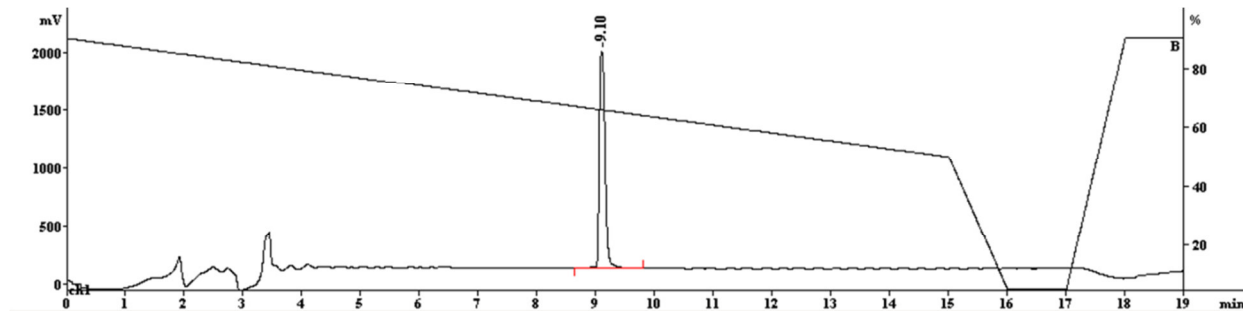
#### AM-NT 3

Analytical HPLC profile: gradient 90-50% A in B in 15 min.



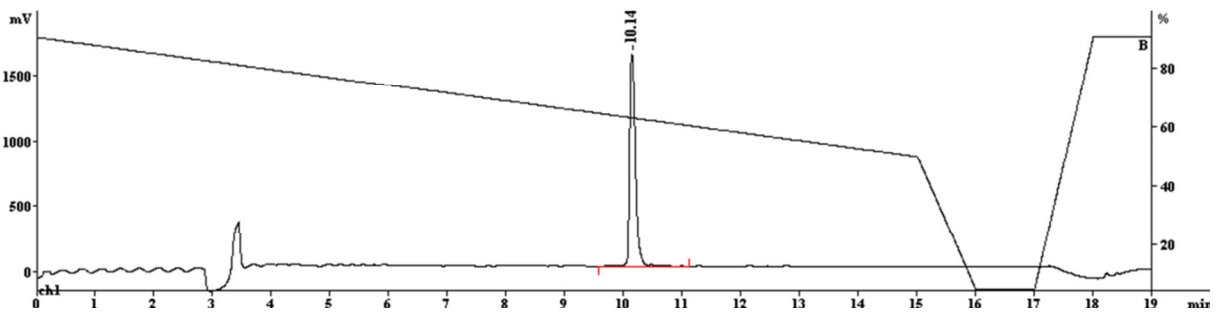
**AM-NT 4**

**Analytical HPLC profile:** gradient 90-50% A in B in 15 min.



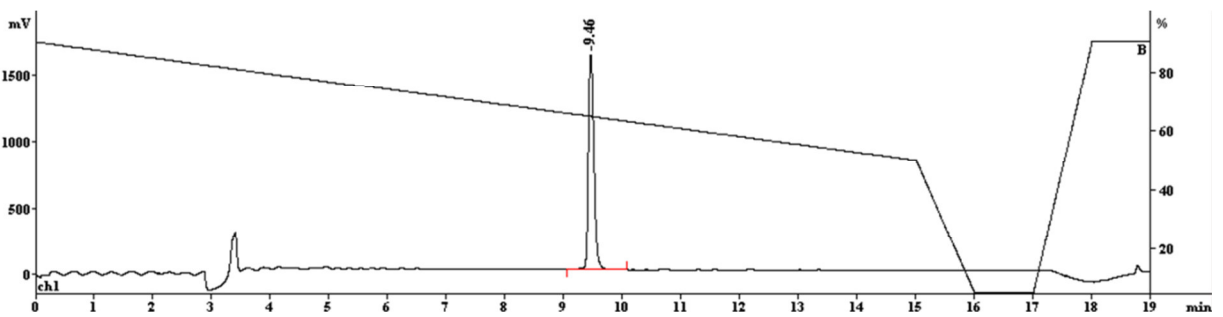
**AM-NT 5**

**Analytical HPLC profile:** gradient 90-50% A in B in 15 min.



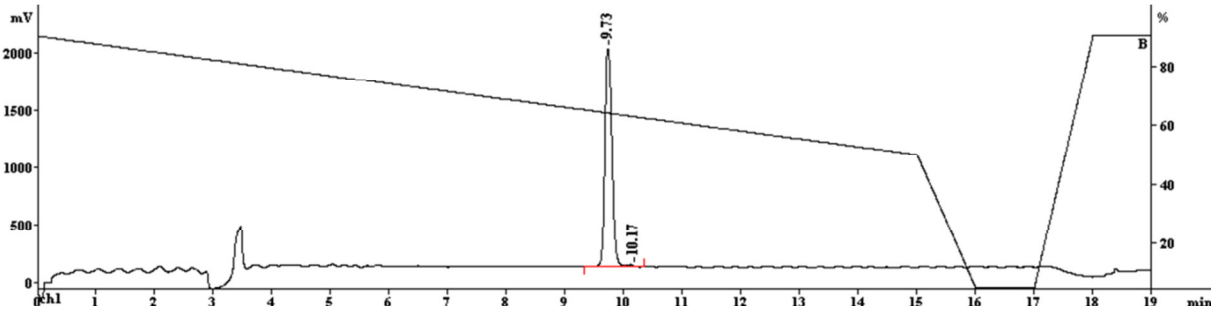
**AM-NT 6**

**Analytical HPLC profile:** gradient 90-50% A in B in 15 min.



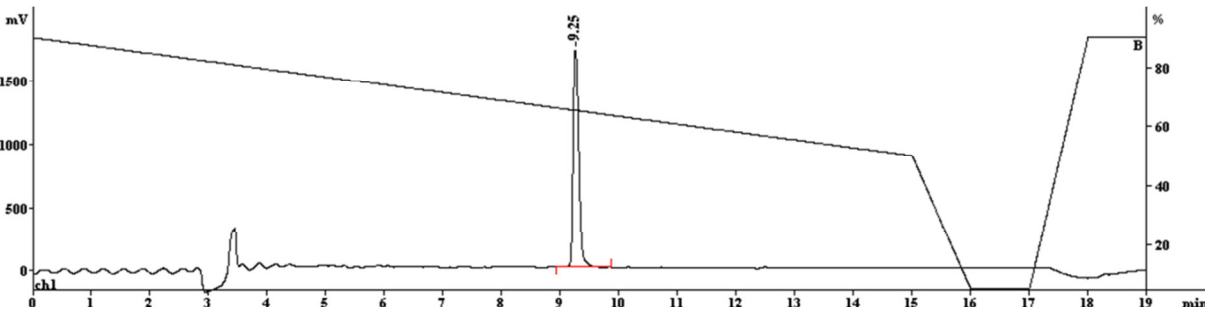
**AM-NT 7**

**Analytical HPLC profile:** gradient 90-50% A in B in 15 min.



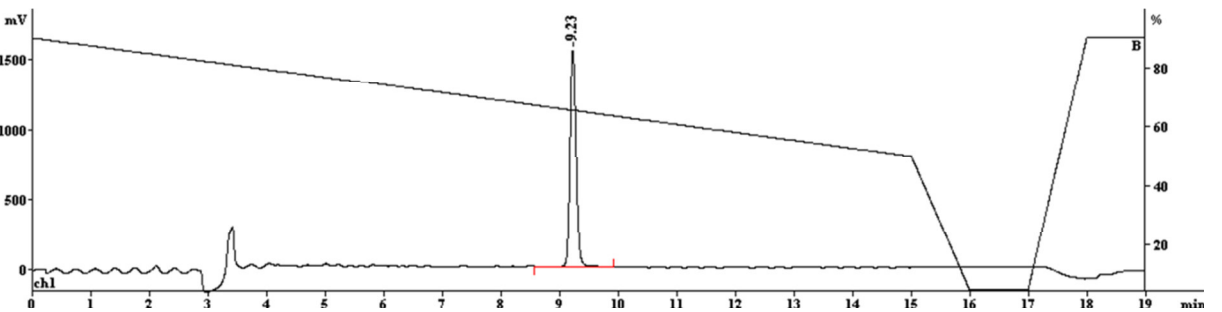
**AM-NT 8**

**Analytical HPLC profile:** gradient 90-50% A in B in 15 min.



**AM-NT 9**

**Analytical HPLC profile:** gradient 90-50% A in B in 15 min.

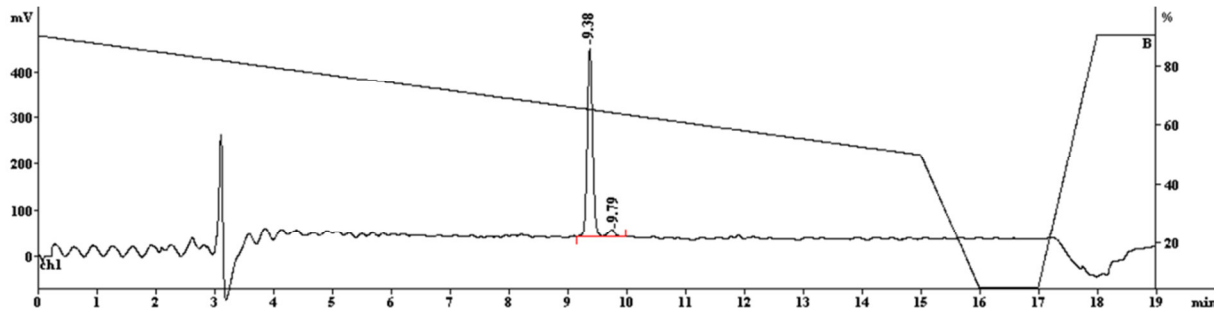


**AM-NT 10**



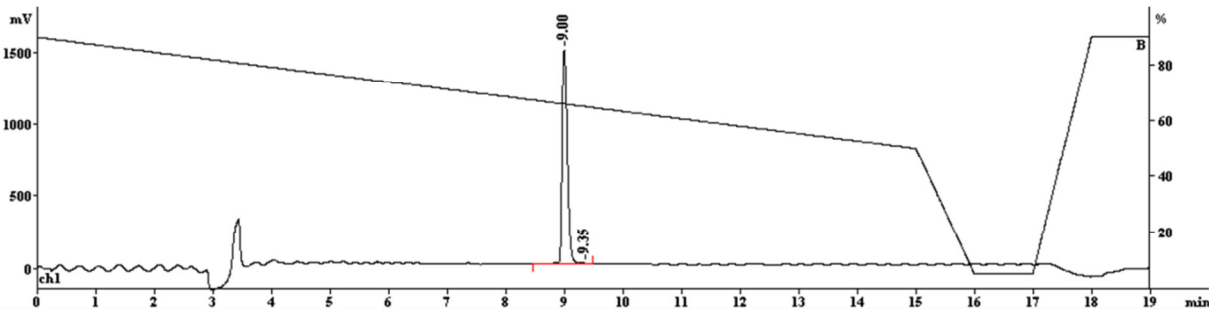
## Appendix

**Analytical HPLC profile:** gradient 90-50% A in B in 15 min.



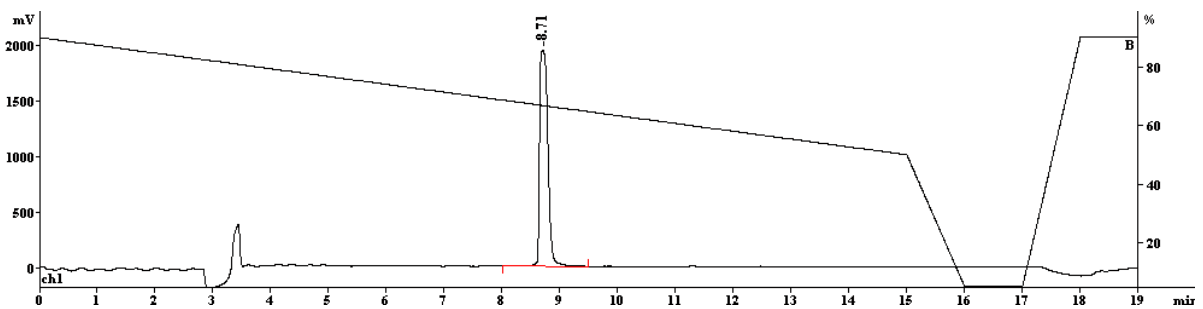
**AM-NT 11**

**Analytical HPLC profile:** gradient 90-50% A in B in 15 min.



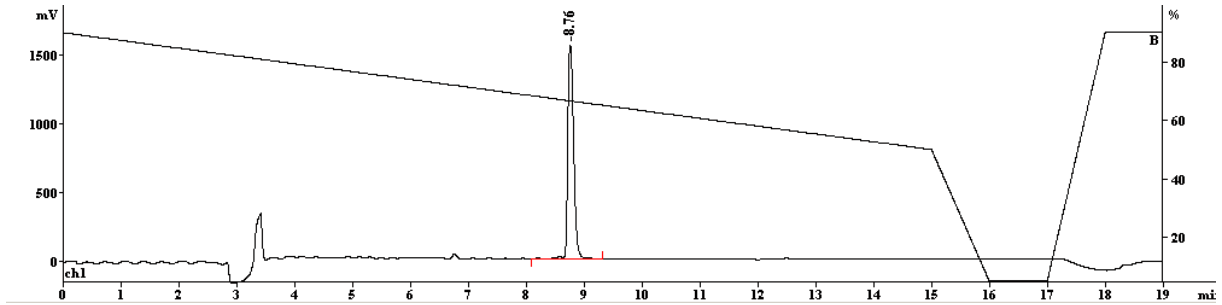
**AM-NT 12**

**Analytical HPLC profile:** gradient 90-50% A in B in 15 min.



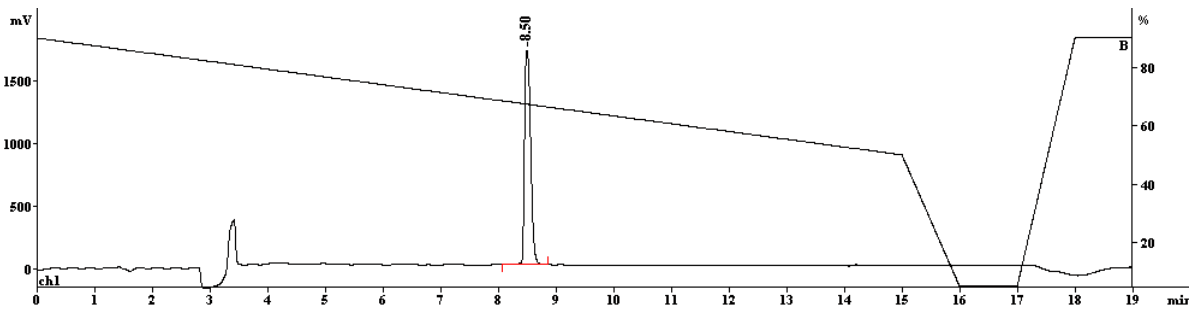
**AM-NT 13**

**Analytical HPLC profile:** gradient 90-50% A in B in 15 min.



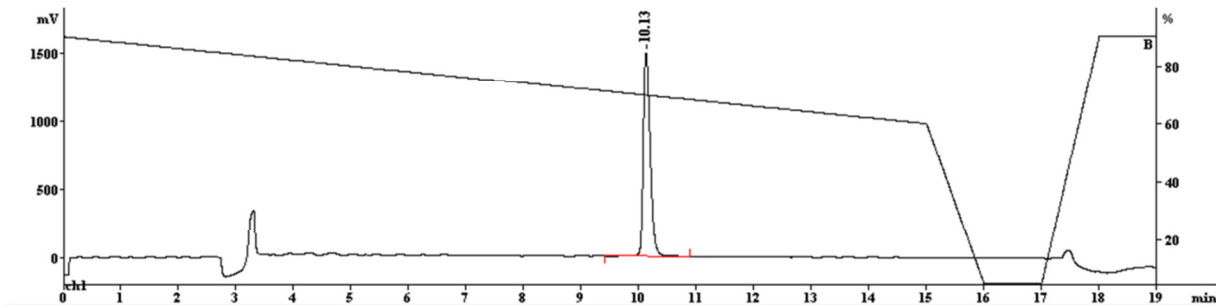
**AM-NT 14**

**Analytical HPLC profile:** gradient 90-50% A in B in 15 min.



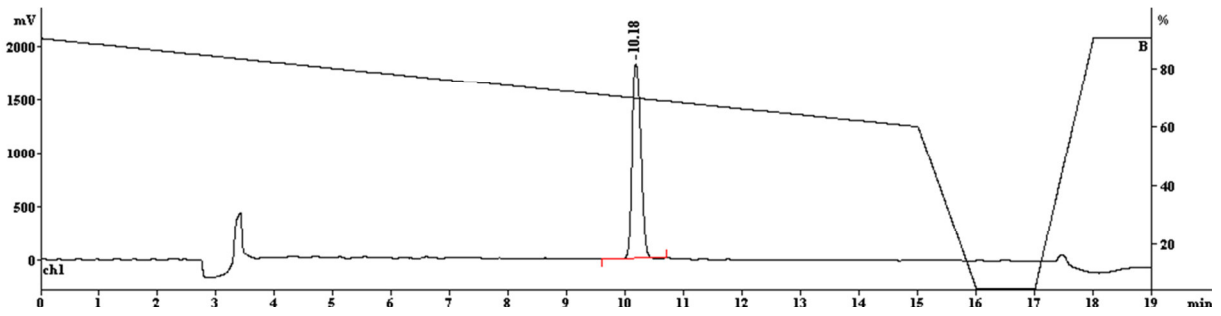
**AM-NT 15**

**Analytical HPLC profile:** gradient 90-60% A in B in 15 min.



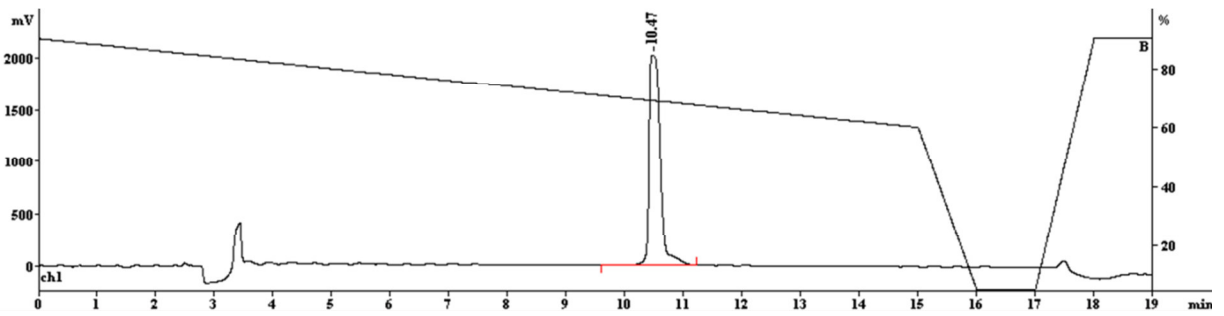
**AM-NT 16**

**Analytical HPLC profile:** gradient 90-60% A in B in 15 min.



**AM-NT 17**

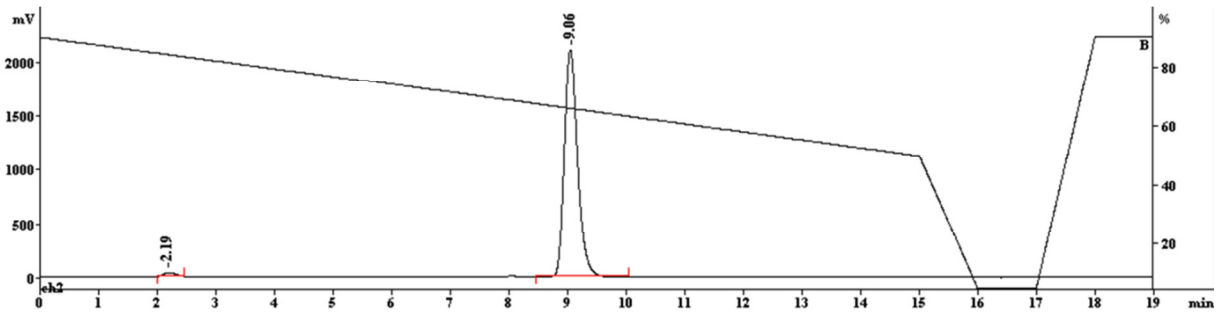
**Analytical HPLC profile:** gradient 90-60% A in B in 15 min.



## 6.5.2 $\gamma$ -HPLC Chromatograms

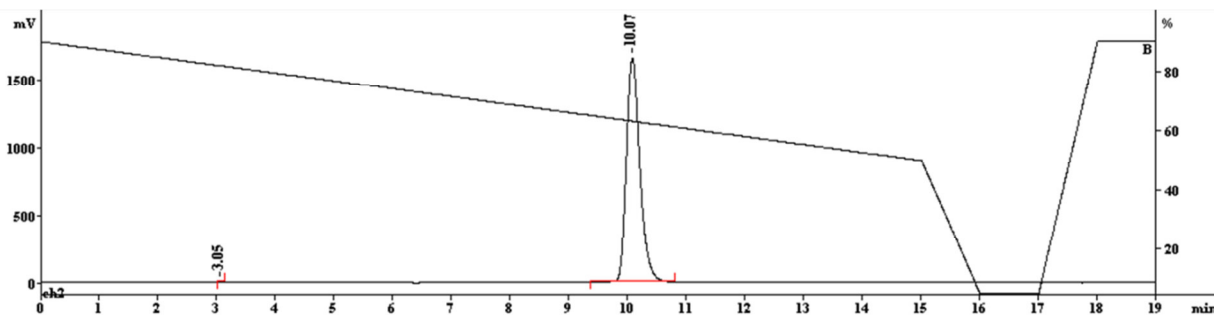
### [<sup>177</sup>Lu]-AM-NT 1

$\gamma$ -HPLC profile: gradient 90-50% A in B in 15 min.



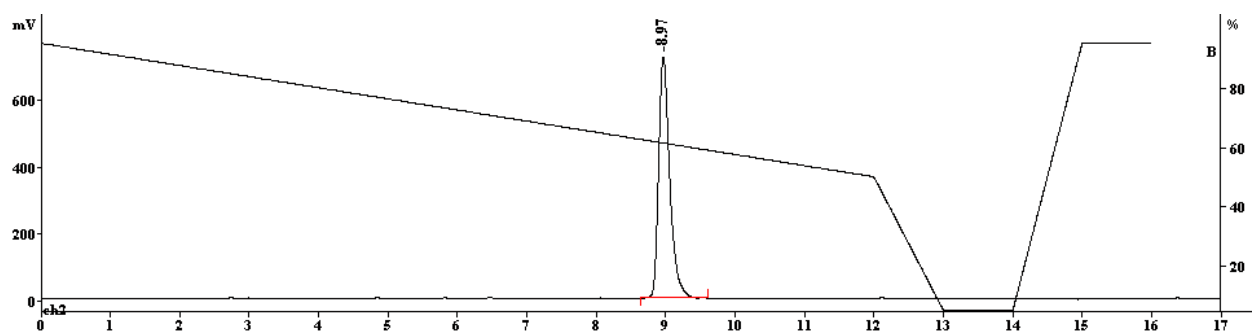
### [<sup>177</sup>Lu]-AM-NT 2

$\gamma$ -HPLC profile: gradient 90-50% A in B in 15 min.



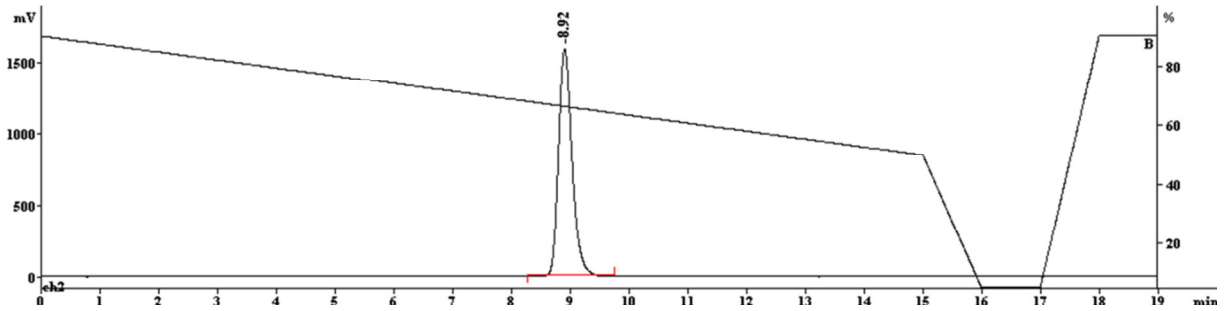
### [<sup>177</sup>Lu]-AM-NT 3

$\gamma$ -HPLC profile: gradient 90-50% A in B in 15 min.



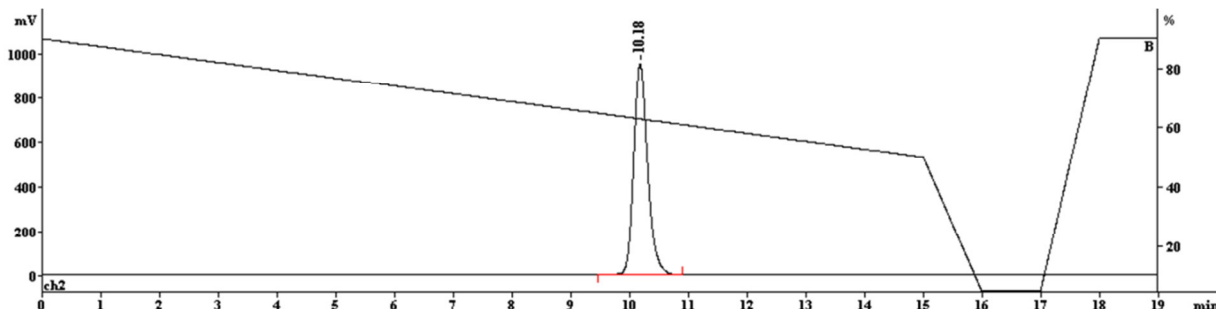
**[<sup>177</sup>Lu]-AM-NT 4**

**γ-HPLC profile:** gradient 90-50% A in B in 15 min.



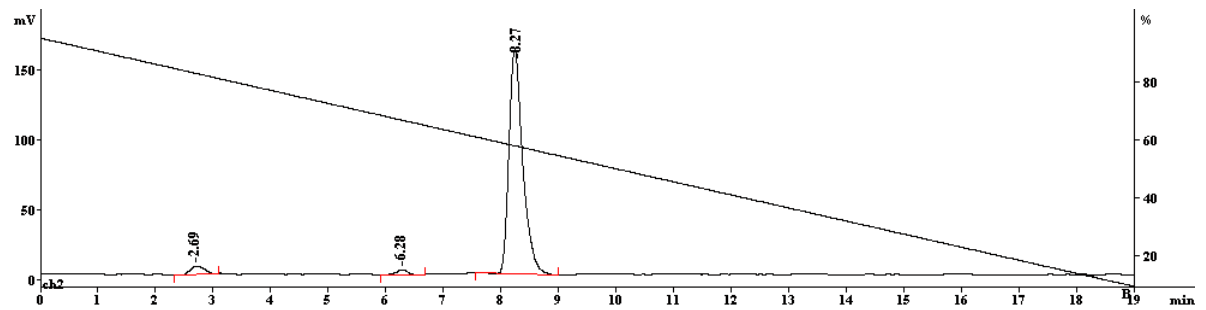
**[<sup>177</sup>Lu]-AM-NT 5**

**γ-HPLC profile:** gradient 90-50% A in B in 15 min.



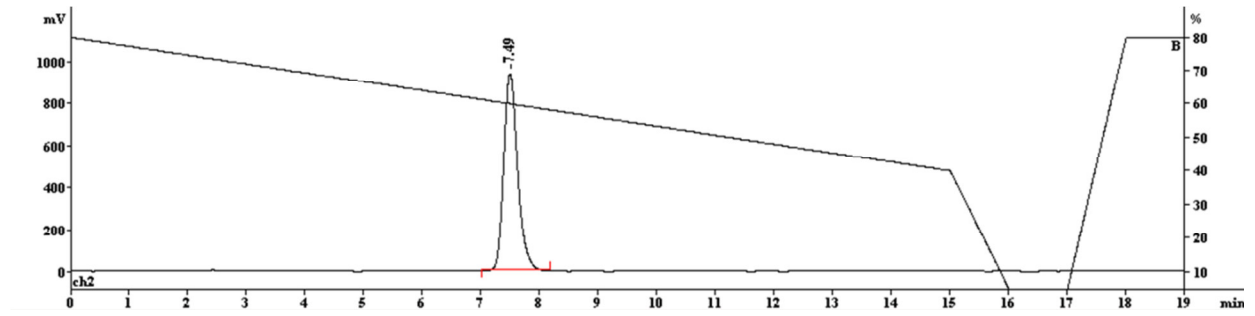
**[<sup>177</sup>Lu]-AM-NT 6**

**γ-HPLC profile:** gradient 90-30% A in B in 19 min.



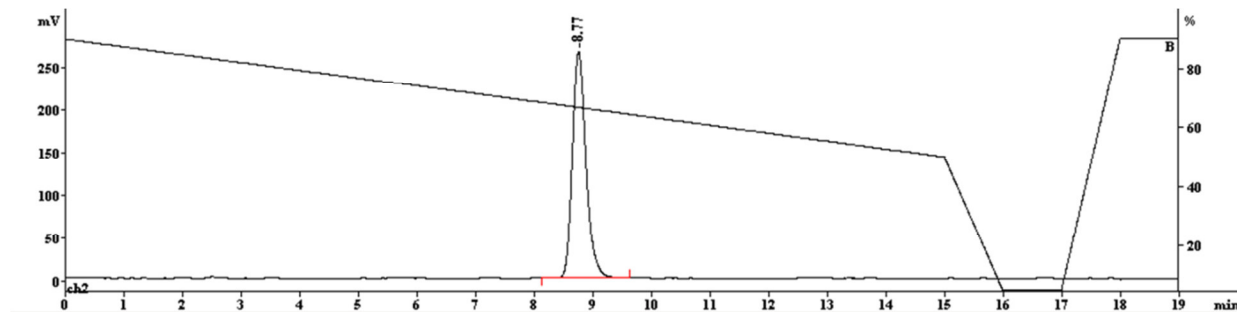
**[<sup>177</sup>Lu]-AM-NT 7**

**γ-HPLC profile: gradient 80-40% A in B in 15 min.**



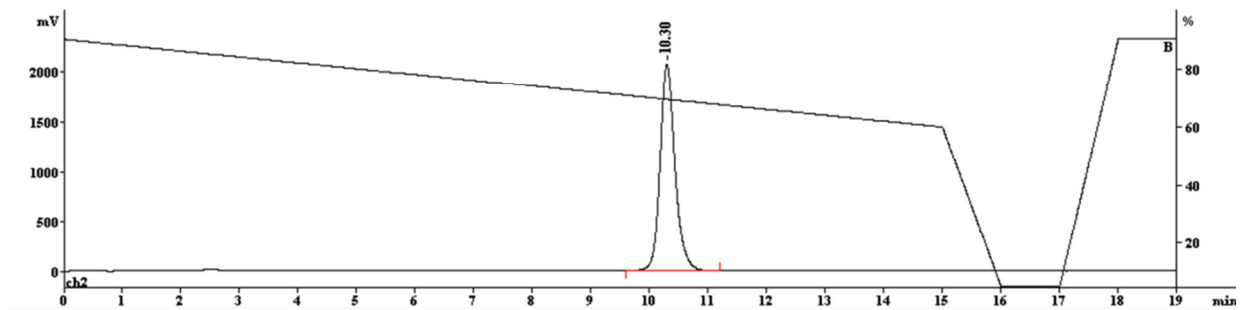
**[<sup>177</sup>Lu]-AM-NT 8**

**γ-HPLC profile: gradient 90-50% A in B in 15 min.**



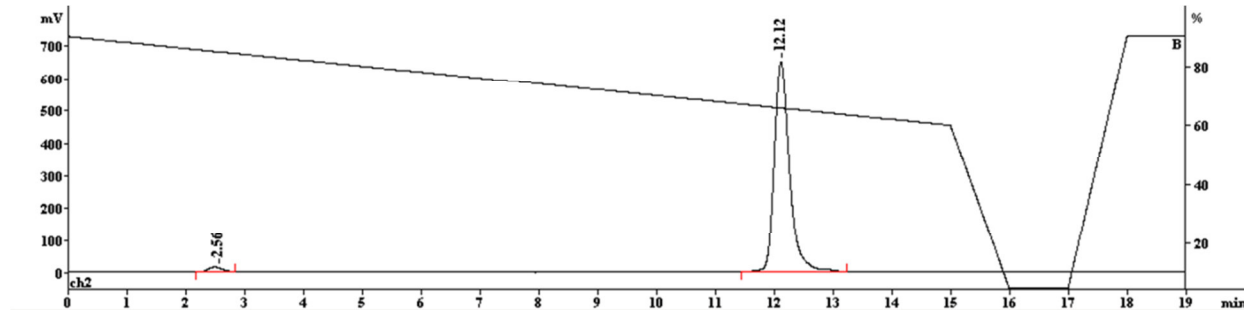
**[<sup>177</sup>Lu]-AM-NT 9**

**γ-HPLC profile: gradient 90-60% A in B in 15 min.**



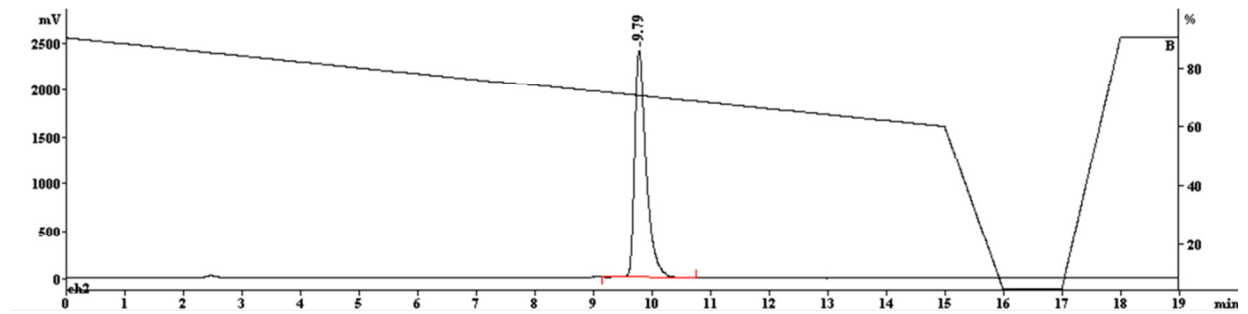
**[<sup>177</sup>Lu]-AM-NT 10**

**γ-HPLC profile:** gradient 90-60% A in B in 15 min.



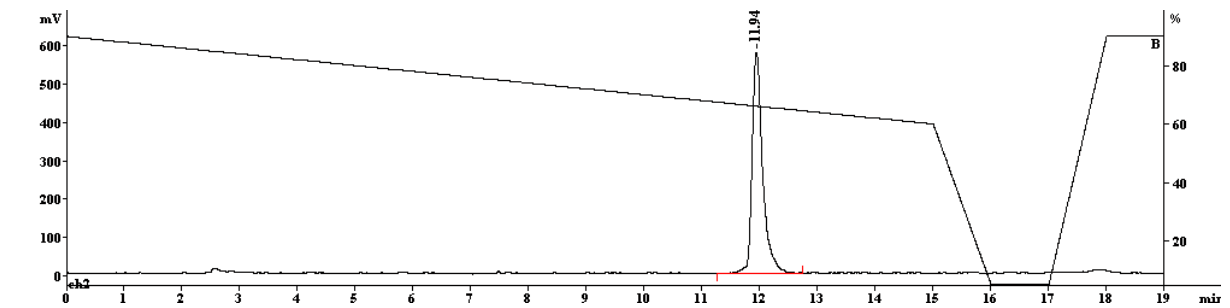
**[<sup>177</sup>Lu]-AM-NT 11**

**γ-HPLC profile:** gradient 90-60% A in B in 15 min.



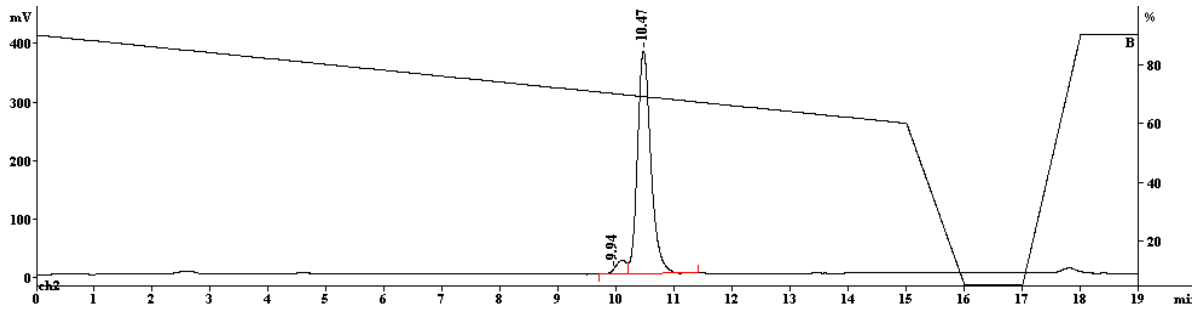
**[<sup>177</sup>Lu]-AM-NT 12**

**γ-HPLC profile:** gradient 90-60% A in B in 15 min.



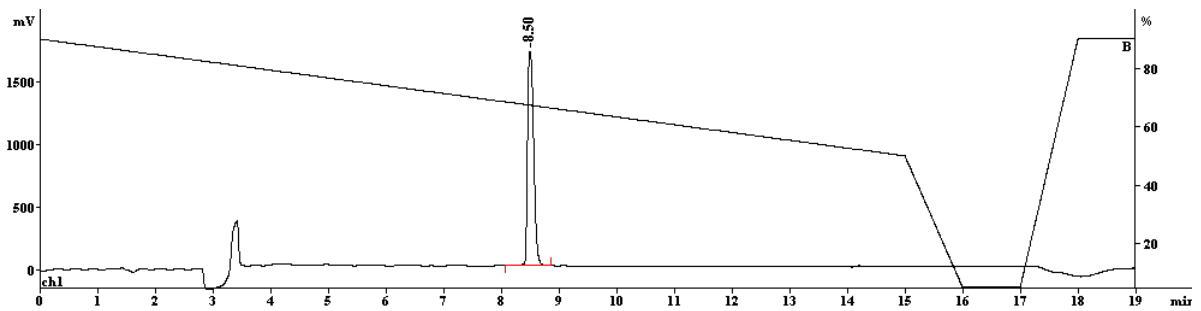
**[<sup>177</sup>Lu]-AM-NT 13**

**γ-HPLC profile: gradient 90-60% A in B in 15 min.**



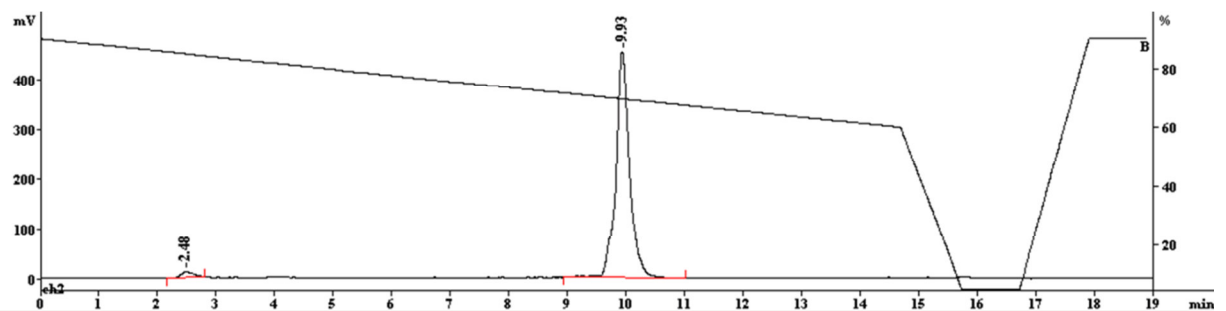
**[<sup>177</sup>Lu]-AM-NT 14**

**γ-HPLC profile: gradient 90-60% A in B in 15 min.**



**[<sup>177</sup>Lu]-AM-NT 15**

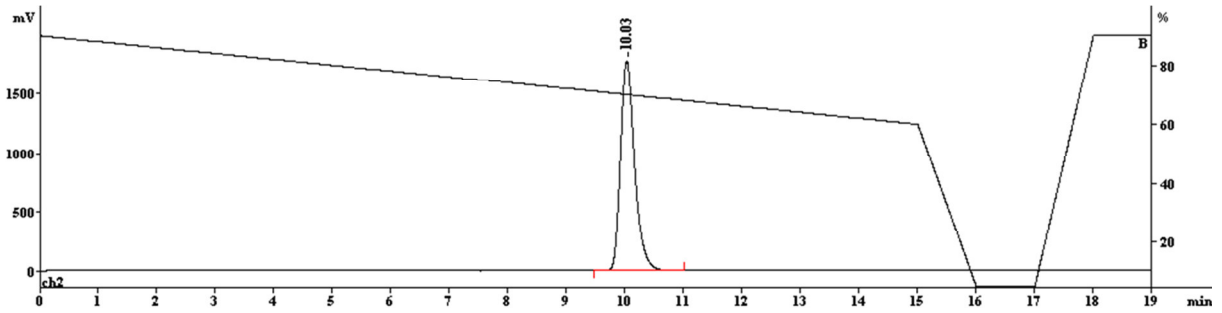
**γ-HPLC profile: gradient 90-60% A in B in 15 min.**





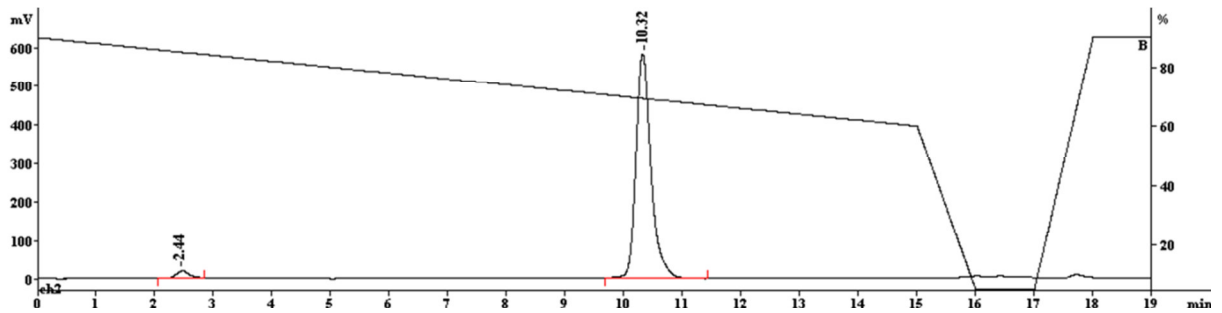
**[<sup>177</sup>Lu]-AM-NT 16**

**γ-HPLC profile:** gradient 90-60% A in B in 15 min



**[<sup>177</sup>Lu]-AM-NT 17**

**γ-HPLC profile:** gradient 90-60% A in B in 15 min



6.5.3 MS Data

AM-NT 1

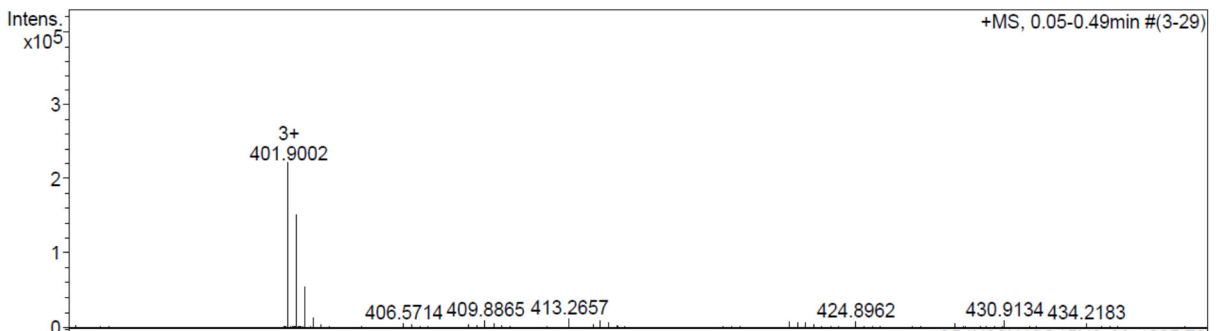
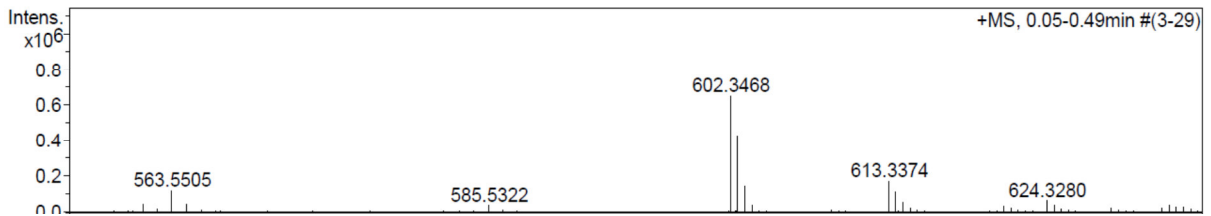
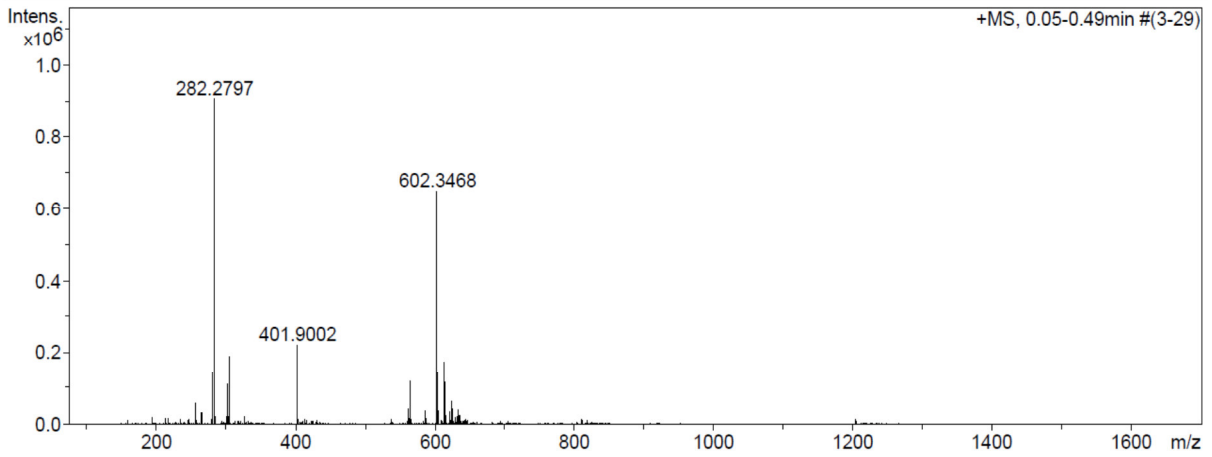
Analysis Info

Analysis Name N:\new acq data\AM 37\_2 001.d  
 Method hn Direct\_Infusion\_pos mode\_75-1700 mid 4eV.m  
 Sample Name Alba Mascarin, AM 37.2  
 Comment AM 37.2, ? ug/ml MeOH

Acquisition Date 02.12.2014 10:24:32  
 Operator hn  
 Instrument / Ser# maXis 4G 21243

Acquisition Parameter

Source Type	ESI	Ion Polarity	Positive	Set Nebulizer	0.4 Bar
Focus	Not active	Set Capillary	3600 V	Set Dry Heater	180 °C
Scan Begin	75 m/z	Set End Plate Offset	-500 V	Set Dry Gas	4.0 l/min
Scan End	1700 m/z	Set Collision Cell RF	500.0 Vpp	Set Ion Energy ( MS only )	4.0 eV



Appendix

AM-NT 2

Analysis Info

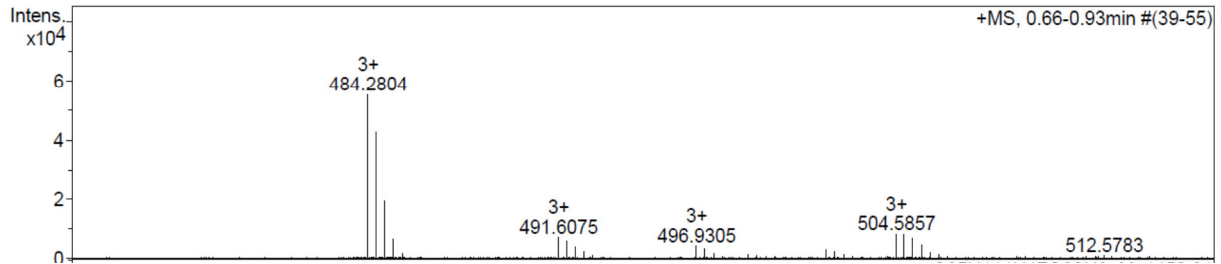
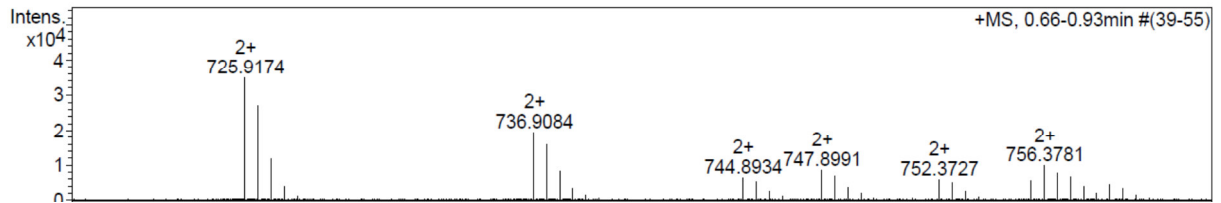
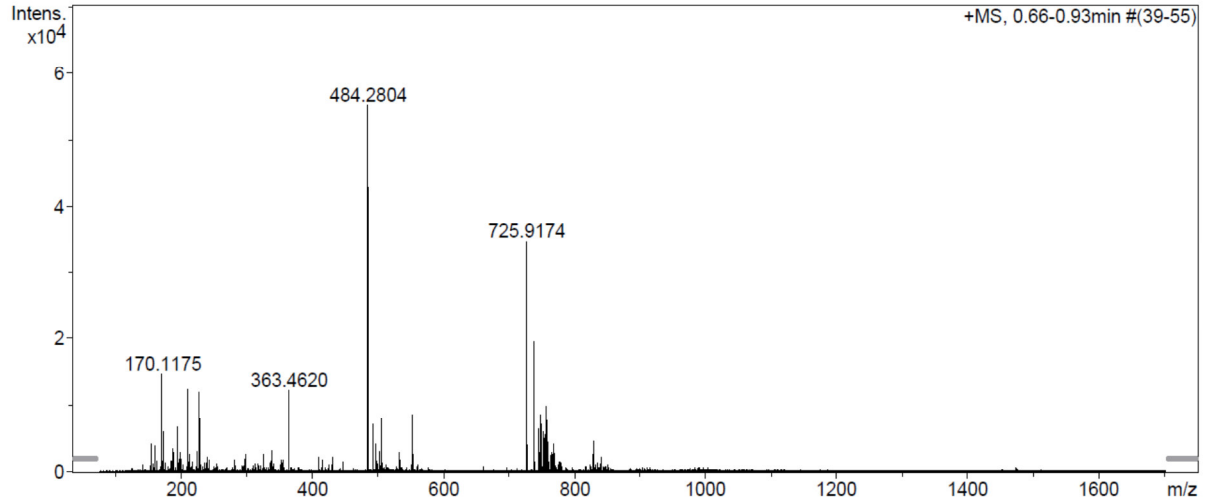
Analysis Name N:\new acq data\AM 37.1 004.d  
Method hn Direct\_Infusion\_pos mode\_75-1700 mid 4eV.m  
Sample Name Alba Mascarin, AM 37.1  
Comment AM 37.1, ? ug/ml MeOH

Acquisition Date 17.10.2014 11:05:59

Operator hn  
Instrument / Ser# maXis 4G 21243

Acquisition Parameter

Source Type	ESI	Ion Polarity	Positive	Set Nebulizer	0.4 Bar
Focus	Not active	Set Capillary	3600 V	Set Dry Heater	180 °C
Scan Begin	75 m/z	Set End Plate Offset	-500 V	Set Dry Gas	4.0 l/min
Scan End	1700 m/z	Set Collision Cell RF	500.0 Vpp	Set Ion Energy ( MS only )	4.0 eV



Appendix

AM-NT 3

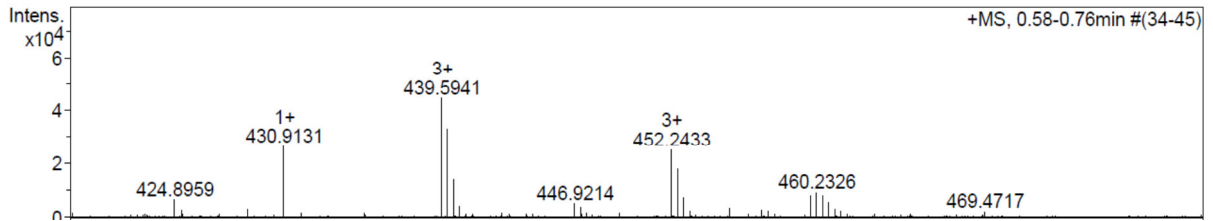
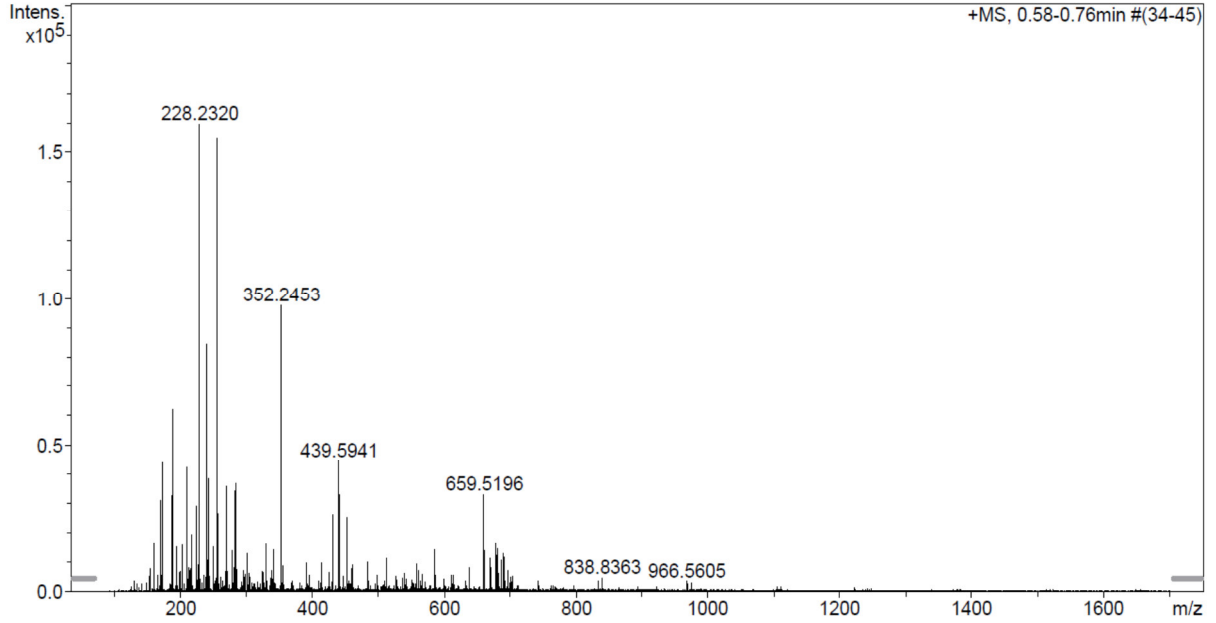
Analysis Info

Analysis Name N:\new acq data\AM 37\_3 002.d  
Method hn Direct\_Infusion\_pos mode\_75-1700 mid 4eV.m  
Sample Name Alba Mascarin, AM 37.3  
Comment AM 37.3, ? ug/ml MeOH

Acquisition Date 02.12.2014 11:29:31  
Operator hn  
Instrument / Ser# maXis 4G 21243

Acquisition Parameter

Source Type	ESI	Ion Polarity	Positive	Set Nebulizer	0.4 Bar
Focus	Not active	Set Capillary	3600 V	Set Dry Heater	180 °C
Scan Begin	75 m/z	Set End Plate Offset	-500 V	Set Dry Gas	4.0 l/min
Scan End	1700 m/z	Set Collision Cell RF	500.0 Vpp	Set Ion Energy ( MS only )	4.0 eV



Appendix

AM-NT 4

Analysis Info

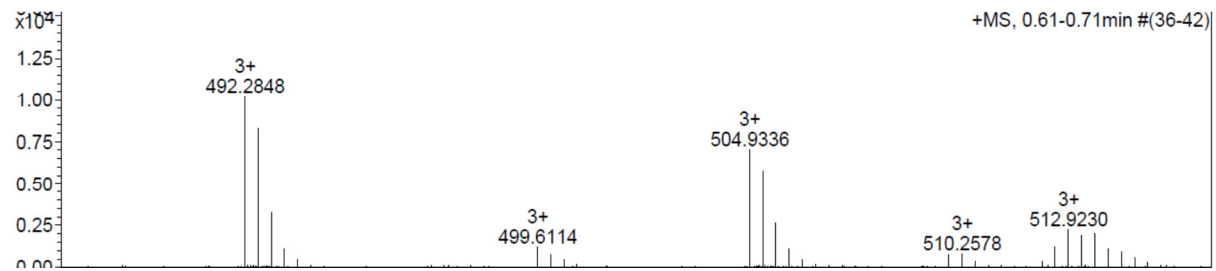
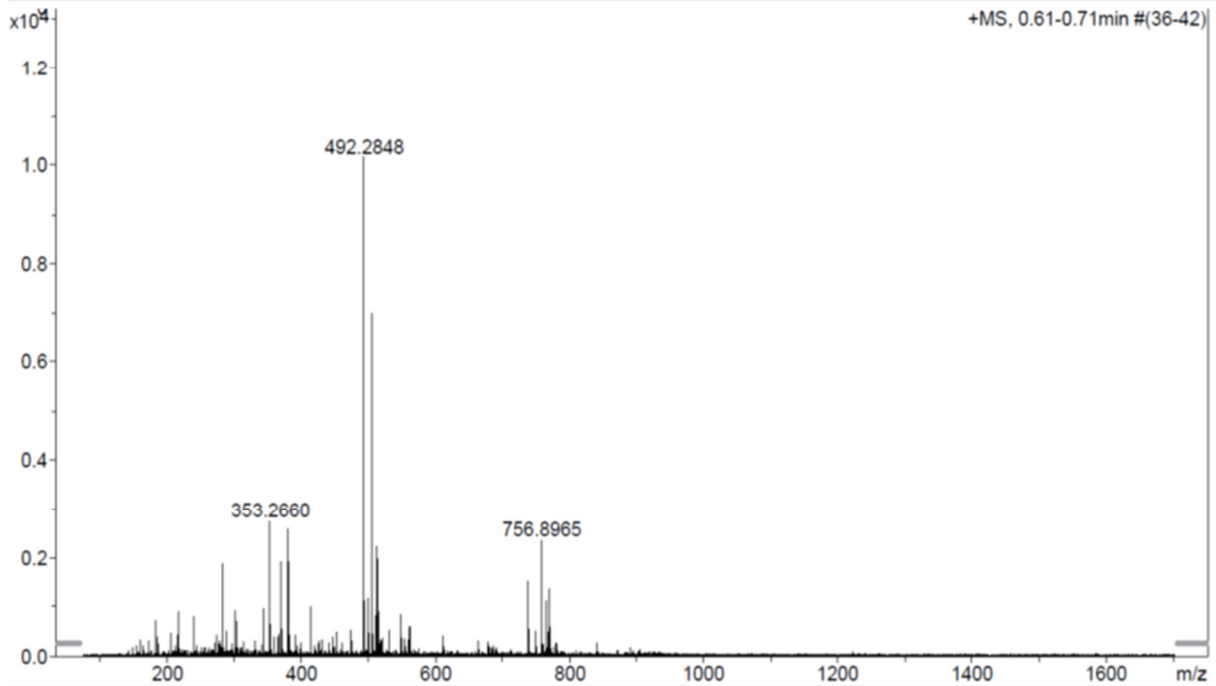
Analysis Name N:\new acq data\AM NT6 001.d  
Method hn Direct\_Infusion\_pos mode\_75-1700 mid 4eV.m  
Sample Name Alba Mascarin, AM NT6  
Comment AM NT6, ? ug/ml MeOH

Acquisition Date 02.12.2014 14:37:23

Operator hn  
Instrument / Ser# maXis 4G 21243

Acquisition Parameter

Source Type	ESI	Ion Polarity	Positive	Set Nebulizer	0.4 Bar
Focus	Not active	Set Capillary	3600 V	Set Dry Heater	180 °C
Scan Begin	75 m/z	Set End Plate Offset	-500 V	Set Dry Gas	4.0 l/min
Scan End	1700 m/z	Set Collision Cell RF	500.0 Vpp	Set Ion Energy ( MS only )	4.0 eV



# Appendix

## AM-NT 5

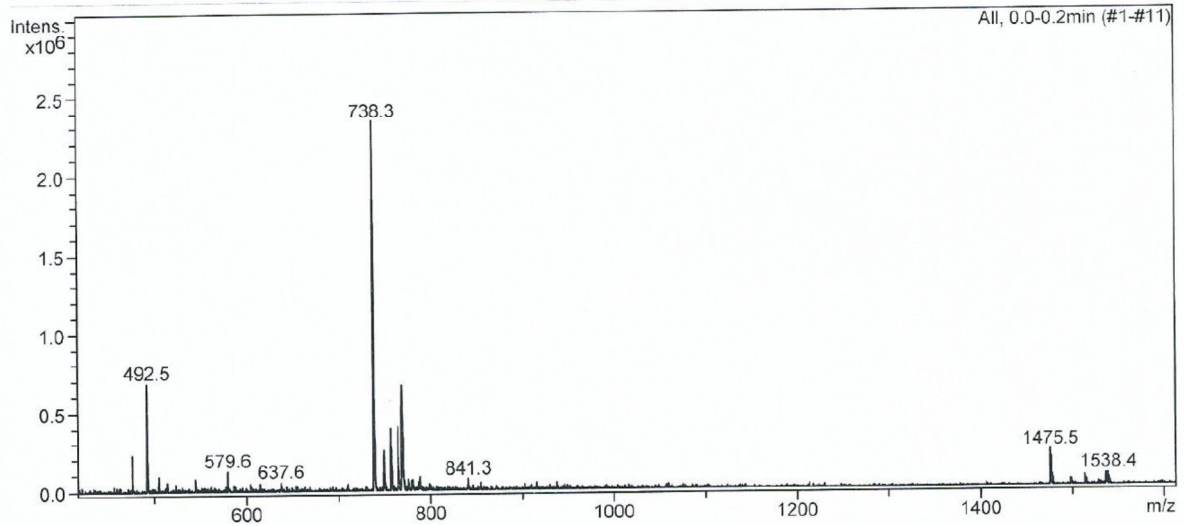
### Analysis Info

Analysis Name AM-NT5.3-2\_2.d  
Method Copy(2) of E3Kp Default.ms  
Sample Name AM-NT5.3-2\_2  
Comment H2O/MeCN

Acquisition Date 06/12/13 11:33:53  
Operator Administrator  
Instrument esquire3000plus\_01096

### Acquisition Parameter

Ion Source Type	ESI	Ion Polarity	Positive	Alternating Ion Polarity	off
Mass Range Mode	Std/Normal	Scan Begin	100 m/z	Scan End	2000 m/z
Capillary Exit	201.6 Volt	Skim 1	40.0 Volt	Trap Drive	132.2
Accumulation Time	209 $\mu$ s	Averages	5 Spectra	Auto MS/MS	off



Appendix

AM-NT 6

Analysis Info

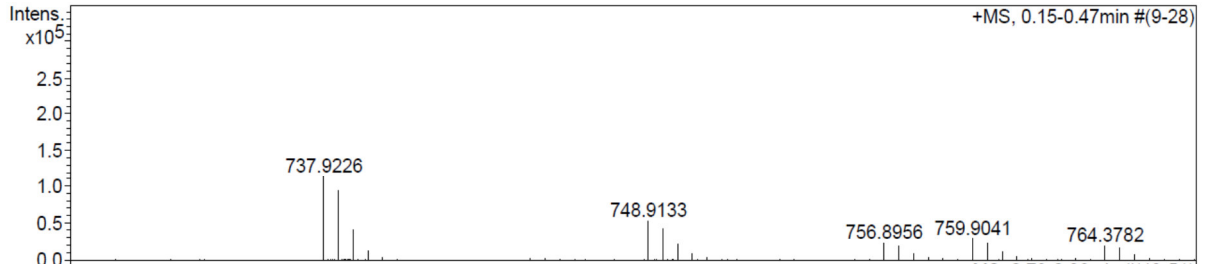
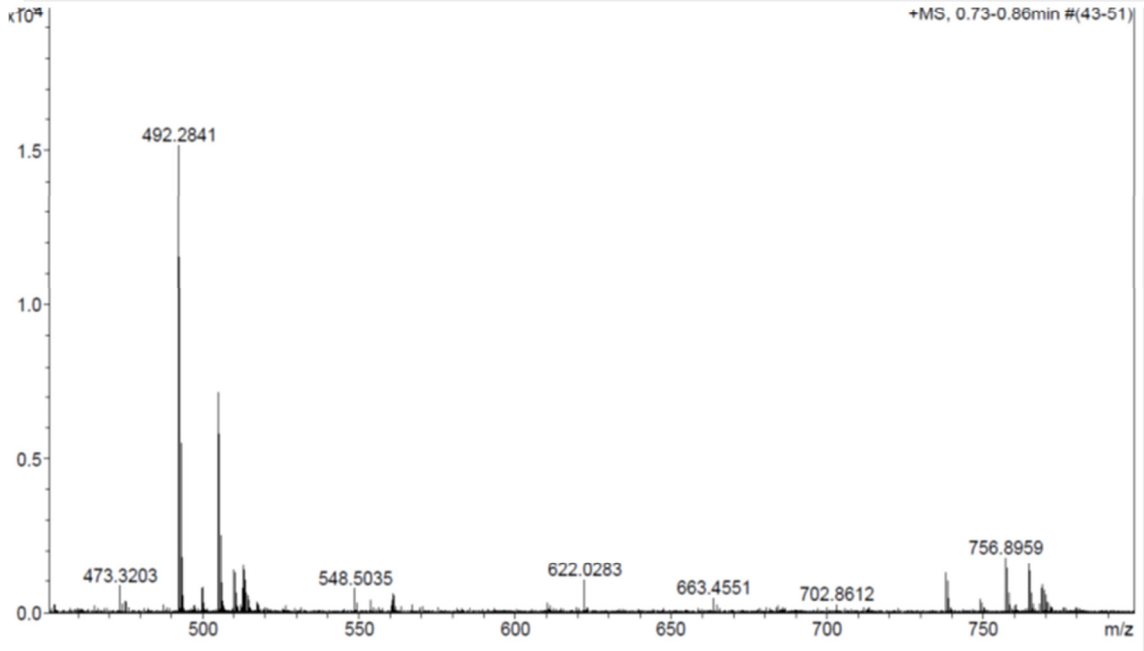
Analysis Name N:\new acq data\AM NT3 001.d  
Method hn Direct\_Infusion\_pos mode\_75-1700 mid 4eV.m  
Sample Name Alba Mascarin, AM NT3  
Comment AM NT3, ? ug/ml MeOH

Acquisition Date 02.12.2014 15:25:49

Operator hn  
Instrument / Ser# maXis 4G 21243

Acquisition Parameter

Source Type	ESI	Ion Polarity	Positive	Set Nebulizer	0.4 Bar
Focus	Not active	Set Capillary	3600 V	Set Dry Heater	180 °C
Scan Begin	75 m/z	Set End Plate Offset	-500 V	Set Dry Gas	4.0 l/min
Scan End	1700 m/z	Set Collision Cell RF	500.0 Vpp	Set Ion Energy ( MS only )	4.0 eV



Appendix

AM-NT 7

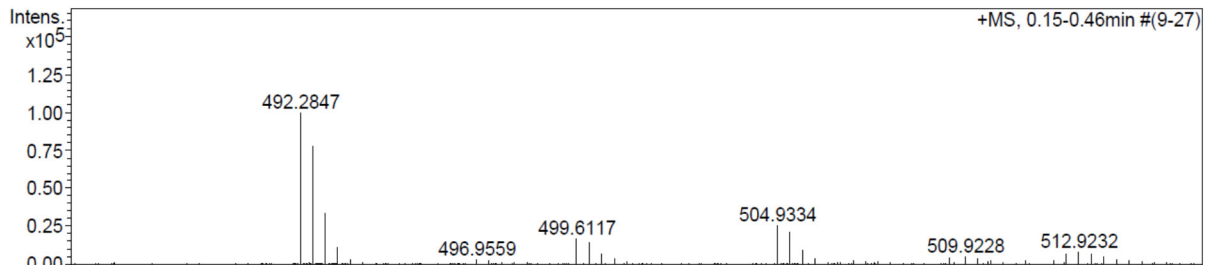
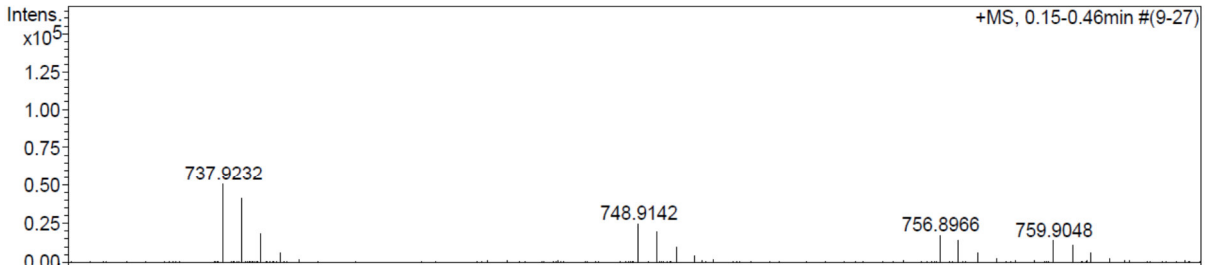
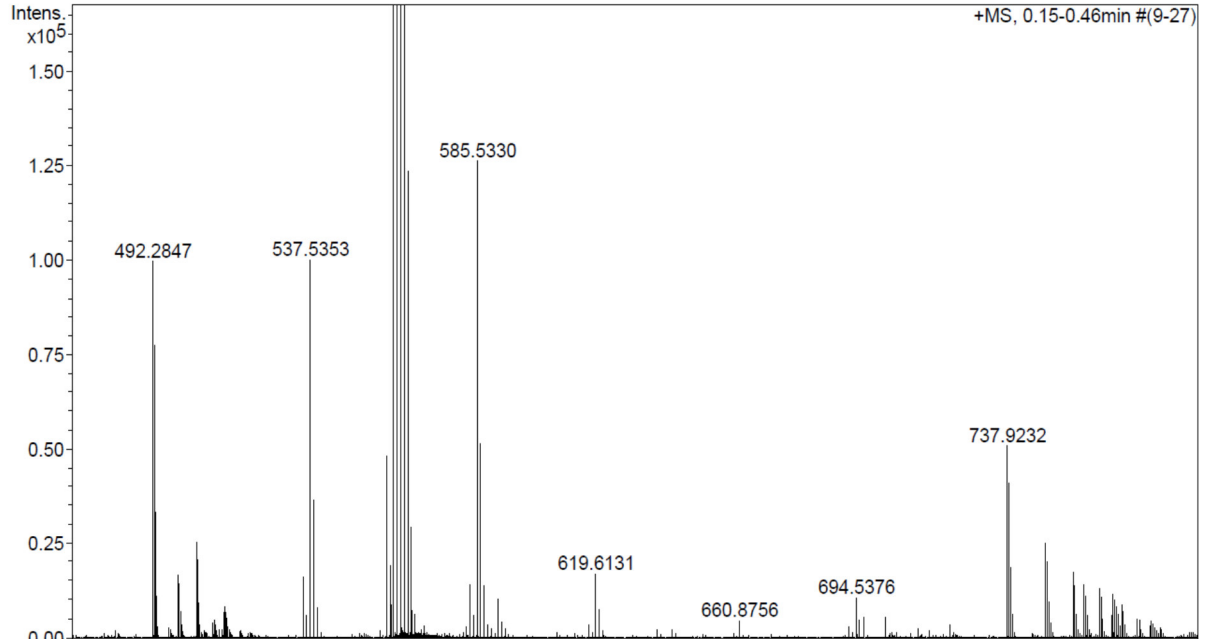
Analysis Info

Analysis Name N:\new acq data\AM NT2 001.d  
Method hn Direct\_Infusion\_pos mode\_75-1700 mid 4eV.m  
Sample Name Alba Mascarin, AM NT2  
Comment AM NT2, ? ug/ml MeOH

Acquisition Date 02.12.2014 16:29:57  
Operator hn  
Instrument / Ser# maXis 4G 21243

Acquisition Parameter

Source Type	ESI	Ion Polarity	Positive	Set Nebulizer	0.4 Bar
Focus	Not active	Set Capillary	3600 V	Set Dry Heater	180 °C
Scan Begin	75 m/z	Set End Plate Offset	-500 V	Set Dry Gas	4.0 l/min
Scan End	1700 m/z	Set Collision Cell RF	500.0 Vpp	Set Ion Energy ( MS only )	4.0 eV





Appendix

AM-NT 8

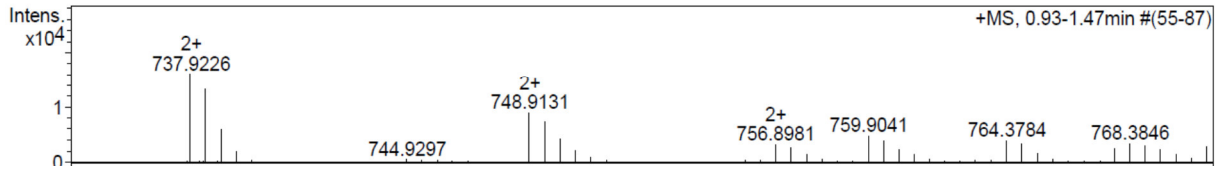
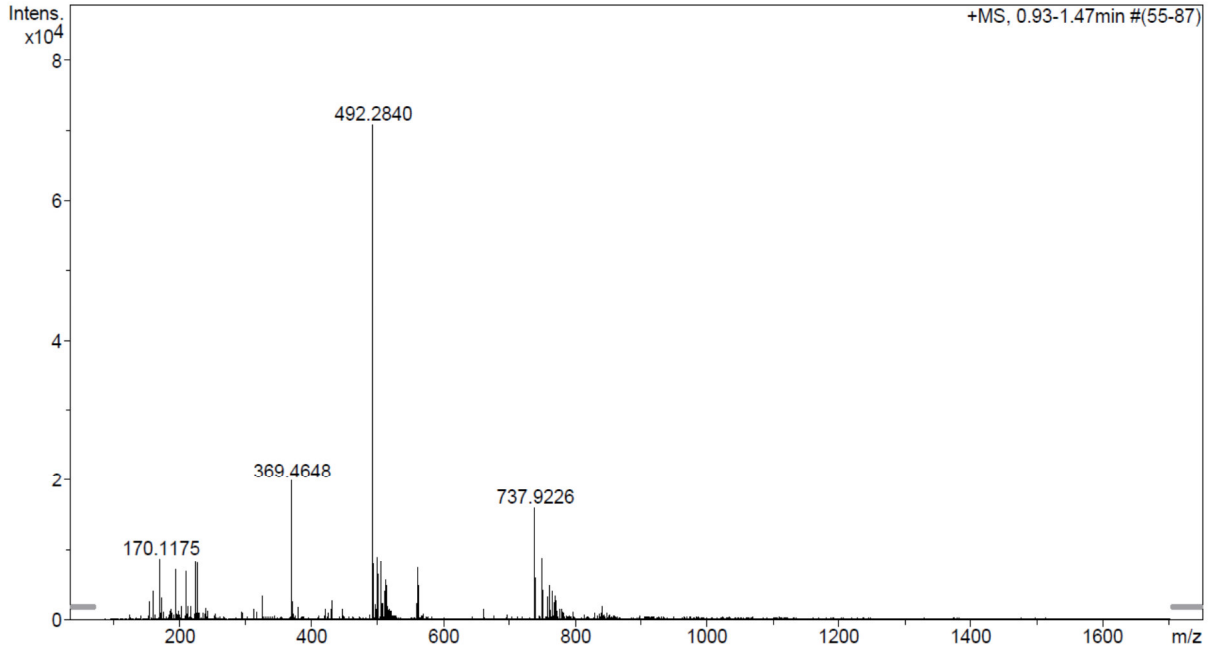
Analysis Info

Analysis Name N:\new acq data\AM NT8 001.d  
Method hn Direct\_Infusion\_pos mode\_75-1700 mid 4eV.m  
Sample Name Alba Mascarin, AM NT8  
Comment AM NT8, ? ug/ml MeOH

Acquisition Date 17.10.2014 16:33:30  
Operator hn  
Instrument / Ser# maXis 4G 21243

Acquisition Parameter

Source Type	ESI	Ion Polarity	Positive	Set Nebulizer	0.4 Bar
Focus	Not active	Set Capillary	3600 V	Set Dry Heater	180 °C
Scan Begin	75 m/z	Set End Plate Offset	-500 V	Set Dry Gas	4.0 l/min
Scan End	1700 m/z	Set Collision Cell RF	500.0 Vpp	Set Ion Energy ( MS only )	4.0 eV



# Appendix

## AM-NT 9

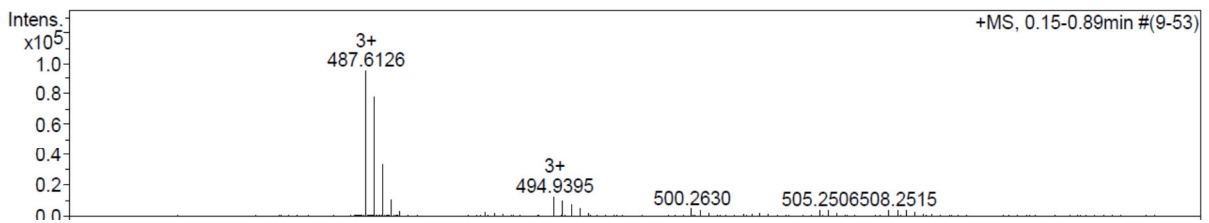
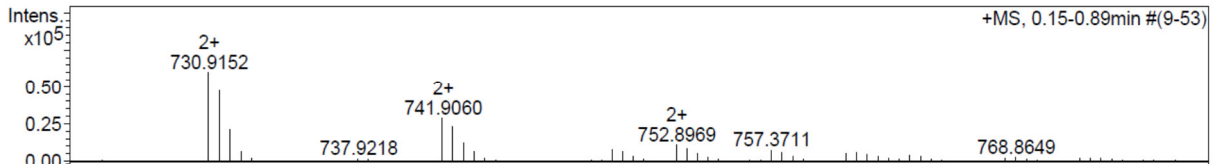
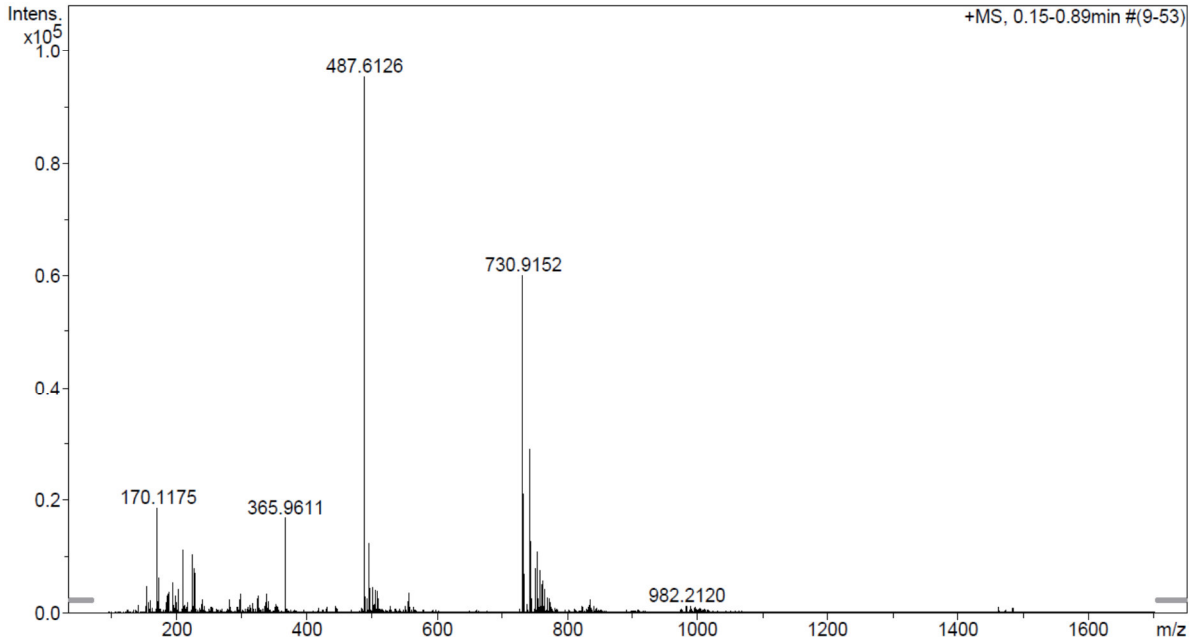
### Analysis Info

Analysis Name N:\new acq data\AM NT7 001.d  
Method hn Direct\_Infusion\_pos mode\_75-1700 mid 4eV.m  
Sample Name Alba Mascarin, AM NT7  
Comment AM NT7, ? ug/ml MeOH

Acquisition Date 17.10.2014 15:27:39  
Operator hn  
Instrument / Ser# maxis 4G 21243

### Acquisition Parameter

Source Type	ESI	Ion Polarity	Positive	Set Nebulizer	0.4 Bar
Focus	Not active	Set Capillary	3600 V	Set Dry Heater	180 °C
Scan Begin	75 m/z	Set End Plate Offset	-500 V	Set Dry Gas	4.0 l/min
Scan End	1700 m/z	Set Collision Cell RF	500.0 Vpp	Set Ion Energy ( MS only )	4.0 eV



Appendix

AM-NT 10

Analysis Info

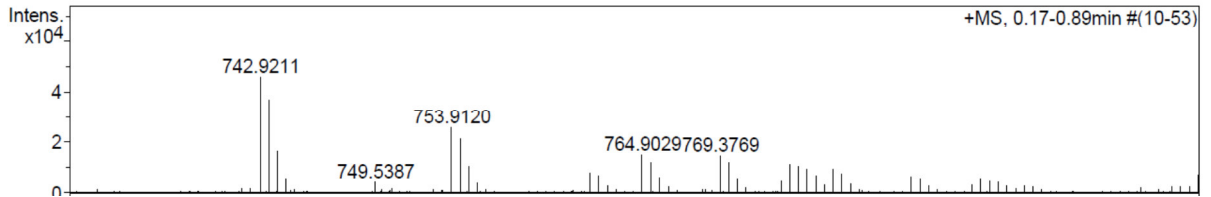
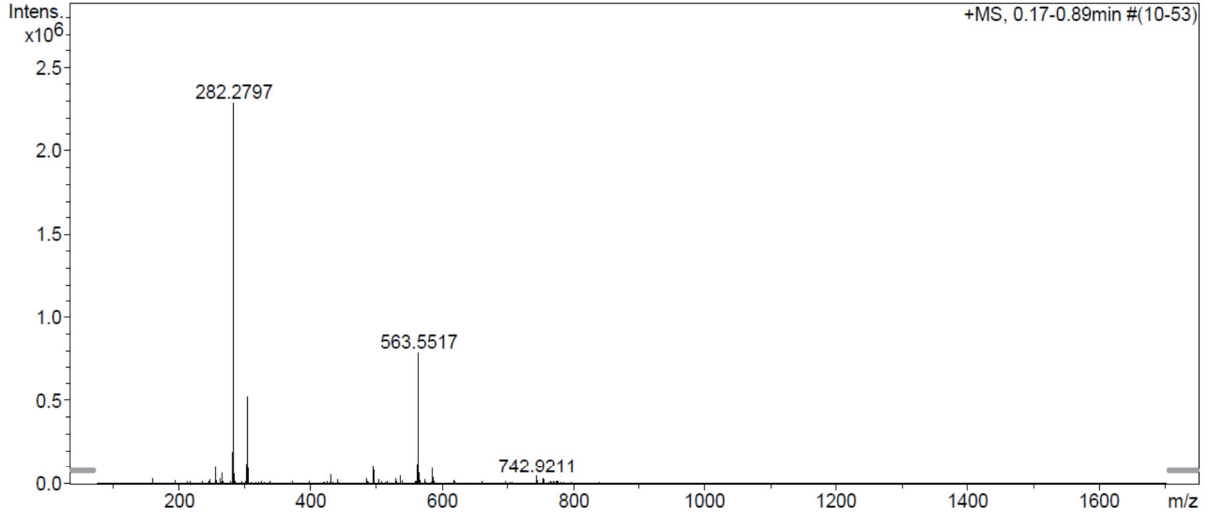
Analysis Name N:\new acq data\AM NT 17 001.d  
Method hn Direct\_Infusion\_pos mode\_75-1700 mid 4eV.m  
Sample Name Alba Mascarin, AM NT 17  
Comment AM NT 17, ? ug/ml MeOH

Acquisition Date 16.12.2014 14:20:01

Operator hn  
Instrument / Ser# maXis 4G 21243

Acquisition Parameter

Source Type	ESI	Ion Polarity	Positive	Set Nebulizer	0.4 Bar
Focus	Not active	Set Capillary	3600 V	Set Dry Heater	180 °C
Scan Begin	75 m/z	Set End Plate Offset	-500 V	Set Dry Gas	4.0 l/min
Scan End	1700 m/z	Set Collision Cell RF	500.0 Vpp	Set Ion Energy ( MS only )	4.0 eV



Appendix

AM-NT 11

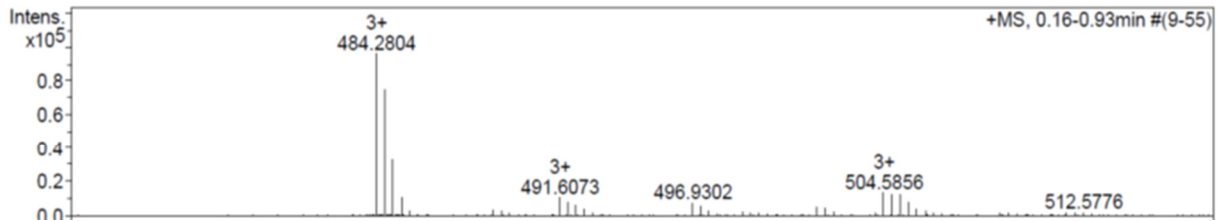
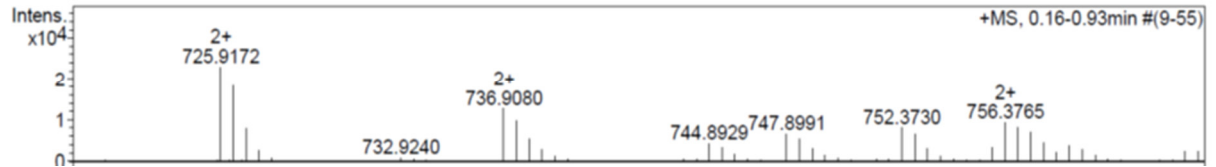
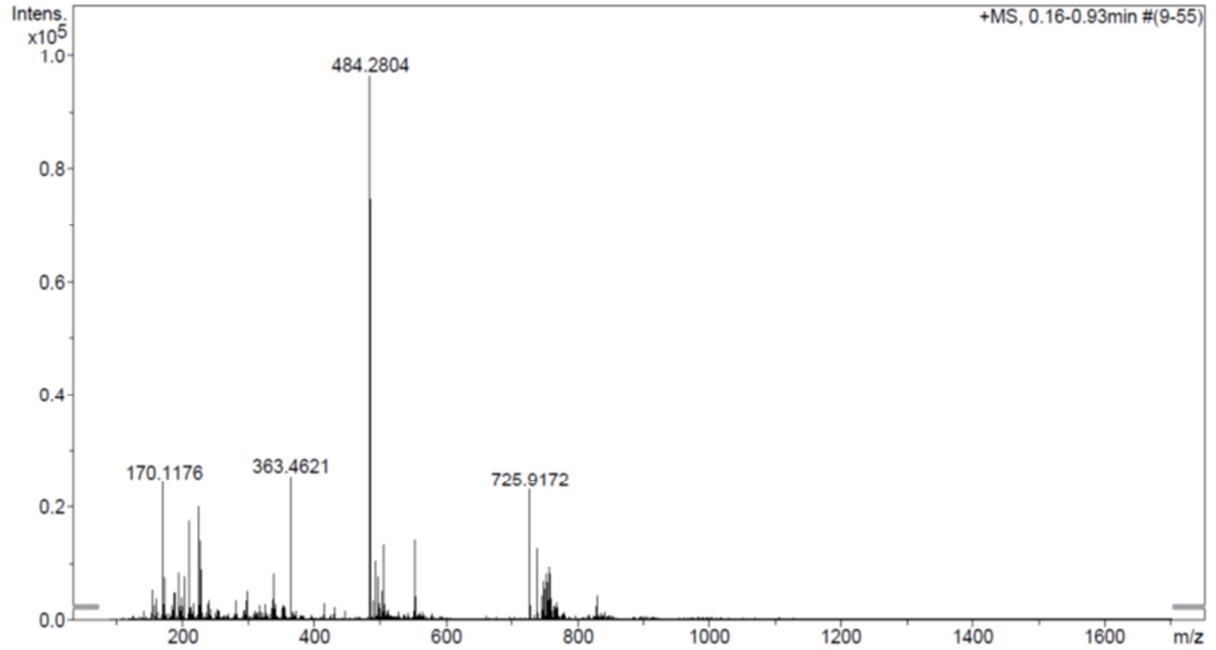
Analysis Info

Analysis Name N:\new acq data\AM NT9 001.d  
Method hn Direct\_Infusion\_pos mode\_75-1700 mid 4eV.m  
Sample Name Alba Mascarin, AM NT9  
Comment AM NT9, ? ug/ml MeOH

Acquisition Date 17.10.2014 14:52:10  
Operator hn  
Instrument / Ser# maXis 4G 21243

Acquisition Parameter

Source Type	ESI	Ion Polarity	Positive	Set Nebulizer	0.4 Bar
Focus	Not active	Set Capillary	3600 V	Set Dry Heater	180 °C
Scan Begin	75 m/z	Set End Plate Offset	-500 V	Set Dry Gas	4.0 l/min
Scan End	1700 m/z	Set Collision Cell RF	500.0 Vpp	Set Ion Energy ( MS only )	4.0 eV



# Appendix

## AM-NT 12

### Analysis Info

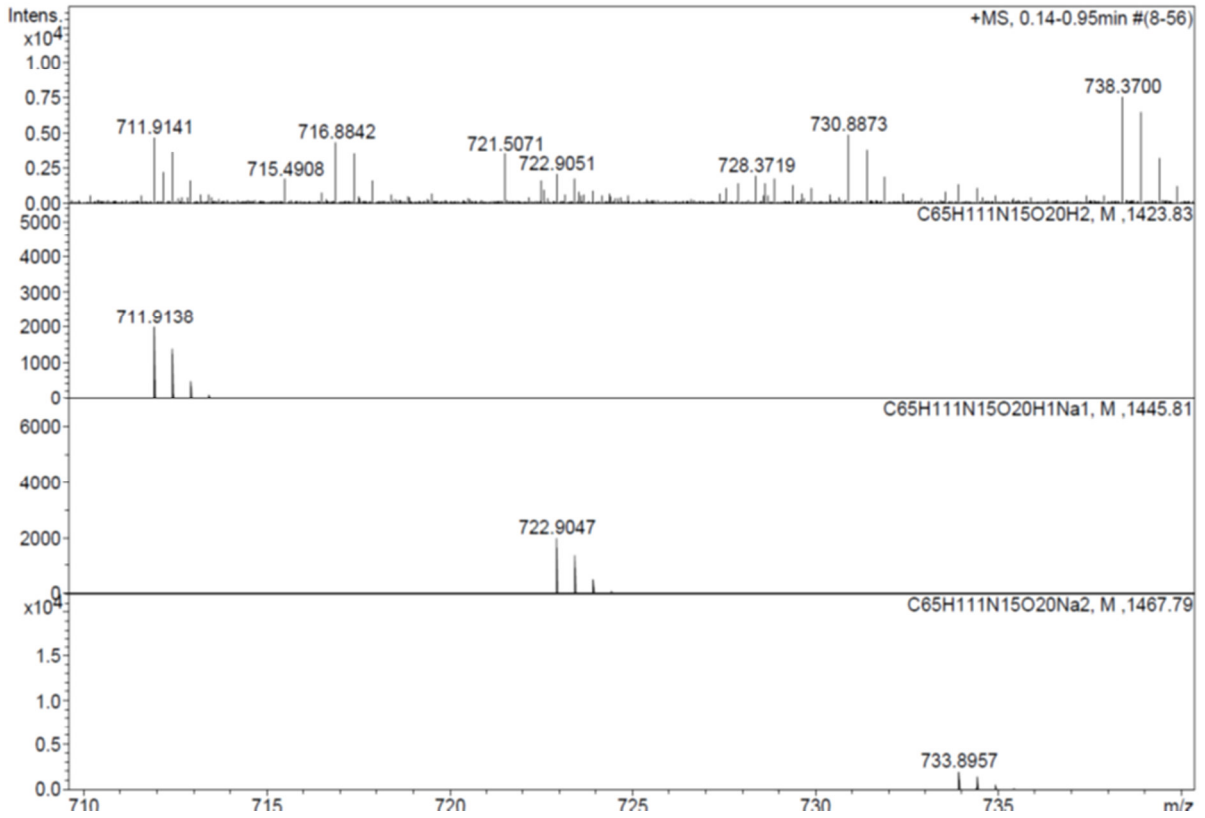
Analysis Name N:\new acq data\AM NT 16 001.d  
 Method hn Direct\_Infusion\_pos mode\_75-1700 mid 4eV.m  
 Sample Name Alba Mascarin, AM NT 16  
 Comment AM NT 16, ? ug/ml MeOH

Acquisition Date 16.12.2014 11:23:54

Operator hn  
 Instrument / Ser# maXis 4G 21243

### Acquisition Parameter

Source Type	ESI	Ion Polarity	Positive	Set Nebulizer	0.4 Bar
Focus	Not active	Set Capillary	3600 V	Set Dry Heater	180 °C
Scan Begin	75 m/z	Set End Plate Offset	-500 V	Set Dry Gas	4.0 l/min
Scan End	1700 m/z	Set Collision Cell RF	500.0 Vpp	Set Ion Energy ( MS only )	4.0 eV



# Appendix

## AM-NT 13

### Analysis Info

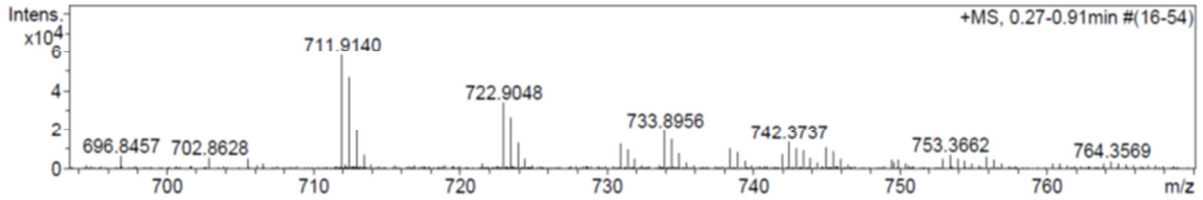
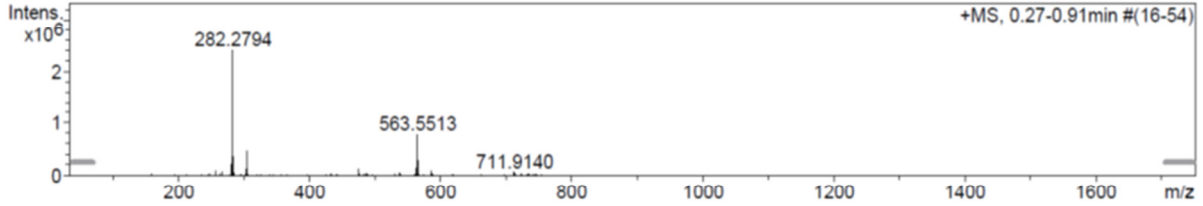
Analysis Name N:\new acq data\AM NT 15 001.d  
 Method hn Direct\_Infusion\_pos mode\_75-1700 mid 4eV.m  
 Sample Name Alba Mascarin, AM NT 15  
 Comment AM NT 15, ? ug/ml MeOH

Acquisition Date 16.12.2014 11:50:14

Operator hn  
 Instrument / Ser# maXis 4G 21243

### Acquisition Parameter

Source Type	ESI	Ion Polarity	Positive	Set Nebulizer	0.4 Bar
Focus	Not active	Set Capillary	3600 V	Set Dry Heater	180 °C
Scan Begin	75 m/z	Set End Plate Offset	-500 V	Set Dry Gas	4.0 l/min
Scan End	1700 m/z	Set Collision Cell RF	500.0 Vpp	Set Ion Energy ( MS only )	4.0 eV



## AM-NT 14

### Analysis Info

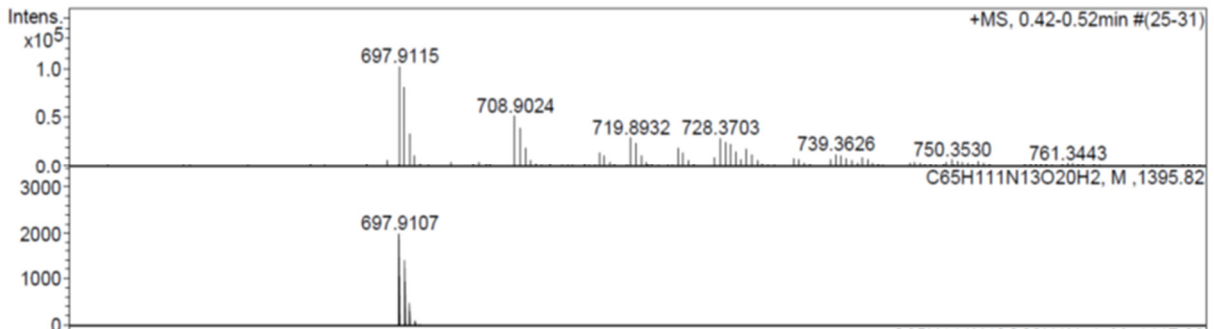
Analysis Name N:\new acq data\AM NT 13 001.d  
 Method hn Direct\_Infusion\_pos mode\_75-1700 mid 4eV.m  
 Sample Name Alba Mascarin, AM NT 13  
 Comment AM NT 13, ? ug/ml MeOH

Acquisition Date 16.12.2014 10:36:43

Operator hn  
 Instrument / Ser# maXis 4G 21243

### Acquisition Parameter

Source Type	ESI	Ion Polarity	Positive	Set Nebulizer	0.4 Bar
Focus	Not active	Set Capillary	3600 V	Set Dry Heater	180 °C
Scan Begin	75 m/z	Set End Plate Offset	-500 V	Set Dry Gas	4.0 l/min
Scan End	1700 m/z	Set Collision Cell RF	500.0 Vpp	Set Ion Energy ( MS only )	4.0 eV



Appendix

AM-NT 15

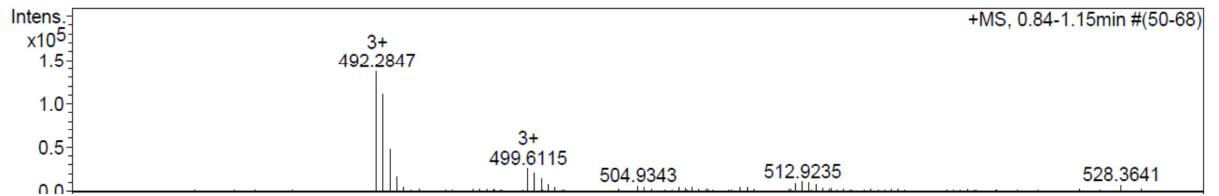
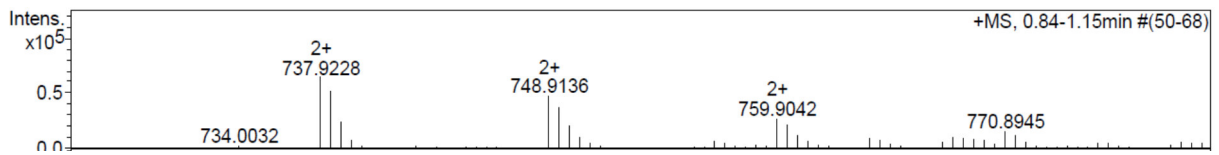
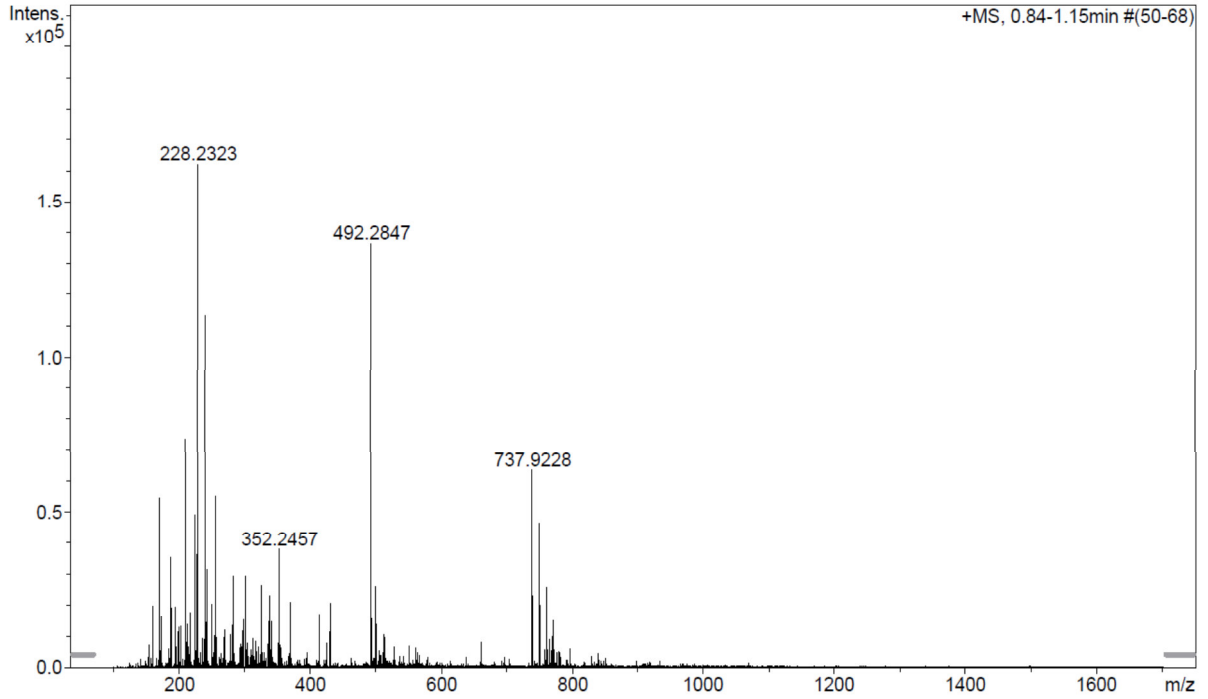
Analysis Info

Analysis Name N:\new acq data\AM NT 10 001.d  
Method hn Direct\_Infusion\_pos mode\_75-1700 mid 4eV.m  
Sample Name Alba Mascarin, AM NT 10  
Comment AM NT 10, ? ug/ml MeOH

Acquisition Date 17.11.2014 17:37:35  
Operator hn  
Instrument / Ser# maXis 4G 21243

Acquisition Parameter

Source Type	ESI	Ion Polarity	Positive	Set Nebulizer	0.4 Bar
Focus	Not active	Set Capillary	3600 V	Set Dry Heater	180 °C
Scan Begin	75 m/z	Set End Plate Offset	-500 V	Set Dry Gas	4.0 l/min
Scan End	1700 m/z	Set Collision Cell RF	500.0 Vpp	Set Ion Energy ( MS only )	4.0 eV



Appendix

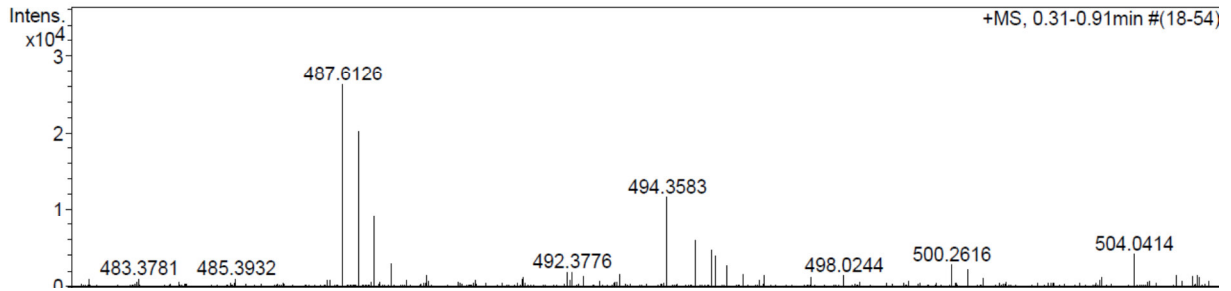
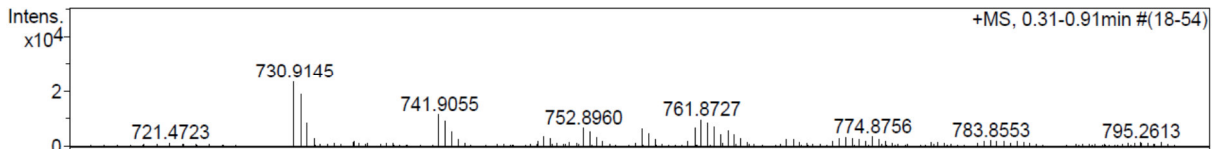
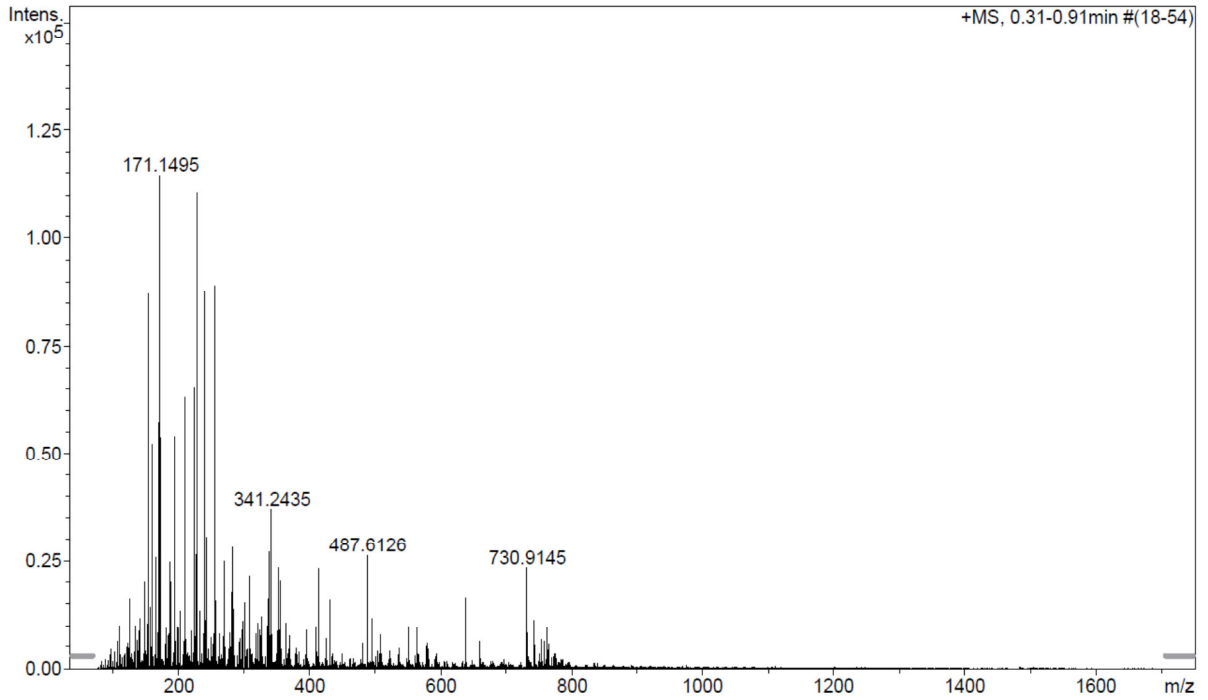
AM-NT 16

Analysis Info

Analysis Name N:\new acq data\AM NT 11 001.d Acquisition Date 17.11.2014 18:04:41  
Method hn Direct\_Infusion\_pos mode\_75-1600 sensitive Komplex.m Operator hn  
Sample Name Alba Mascarin, AM NT 11 Instrument / Ser# maXis 4G 21243  
Comment AM NT 11, ? ug/ml MeOH

Acquisition Parameter

Source Type	ESI	Ion Polarity	Positive	Set Nebulizer	0.4 Bar
Focus	Not active	Set Capillary	4500 V	Set Dry Heater	180 °C
Scan Begin	75 m/z	Set End Plate Offset	-500 V	Set Dry Gas	4.0 l/min
Scan End	1700 m/z	Set Collision Cell RF	300.0 Vpp	Set Ion Energy ( MS only )	30.0 eV





# Appendix

## AM-NT 17

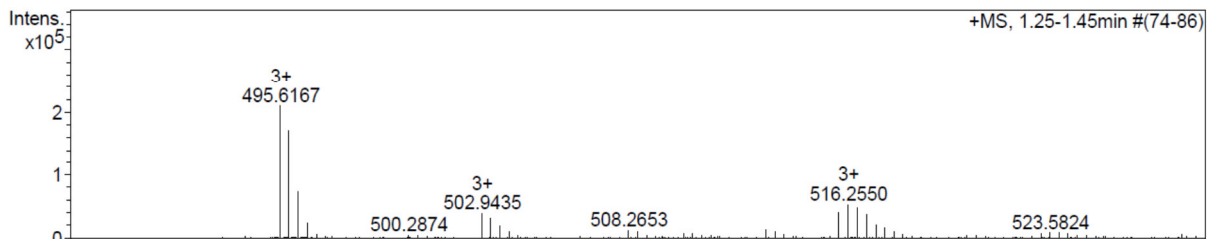
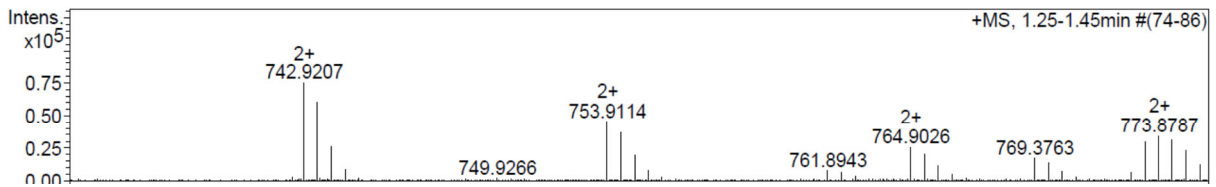
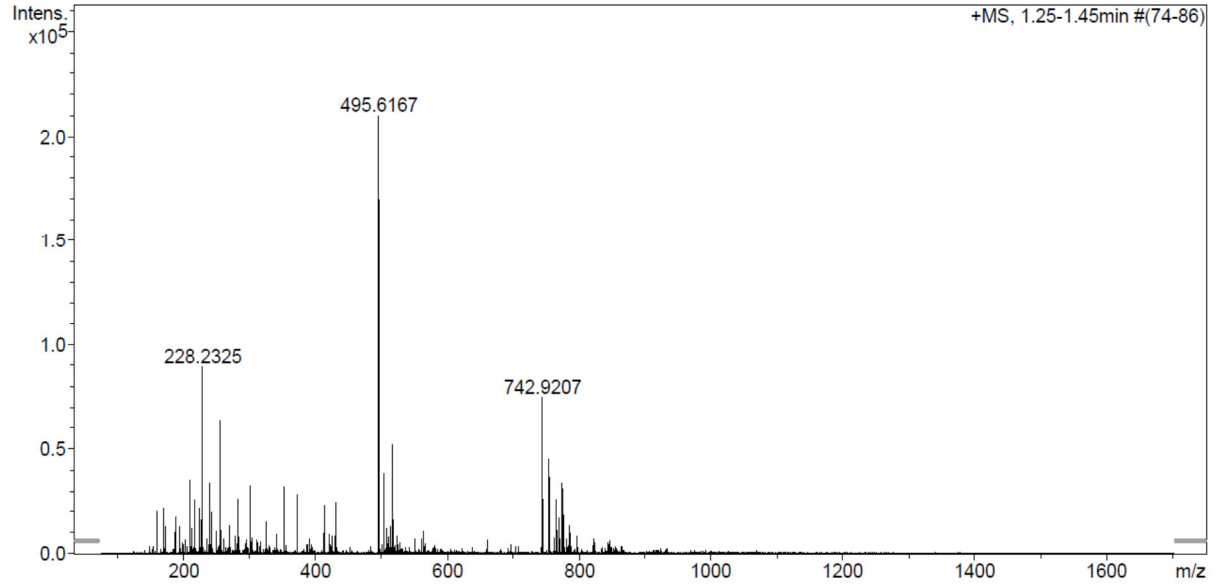
### Analysis Info

Analysis Name N:\new acq data\AM NT 12 001.d  
Method hn Direct\_Infusion\_pos mode\_75-1700 mid 4eV.m  
Sample Name Alba Mascarin, AM NT 12  
Comment AM NT 12, ? ug/ml MeOH

Acquisition Date 17.11.2014 16:34:14  
Operator hn  
Instrument / Ser# maXis 4G 21243

### Acquisition Parameter

Source Type	ESI	Ion Polarity	Positive	Set Nebulizer	0.4 Bar
Focus	Not active	Set Capillary	3600 V	Set Dry Heater	180 °C
Scan Begin	75 m/z	Set End Plate Offset	-500 V	Set Dry Gas	4.0 l/min
Scan End	1700 m/z	Set Collision Cell RF	500.0 Vpp	Set Ion Energy ( MS only )	4.0 eV



## 6.7 Biodistribution Data

### Biodistribution of [<sup>177</sup>Lu]-AM-NT 2

<b>Organ</b>	<b>1h</b>	<b>4h</b>	<b>24h</b>	<b>Blocking</b>
<b>blood</b>	0.03 ± 0.01	0.004 ± 0.001	0.009 ± 0.006	0.02 ± 0.02
<b>heart</b>	0.03 ± 0.01	0.02 ± 0.02	0.013 ± 0.008	0.022 ± 0.007
<b>Liver</b>	0.07 ± 0.02	0.05 ± 0.03	0.027 ± 0.005	0.10 ± 0.03
<b>spleen</b>	0.03 ± 0.02	0.037 ± 0.008	0.024 ± 0.008	0.05 ± 0.03
<b>lung</b>	0.12 ± 0.05	0.040 ± 0.004	0.04 ± 0.02	0.07 ± 0.04
<b>kidney</b>	1.2 ± 0.4	1.2 ± 0.1	0.6 ± 0.2	1.21 ± 0.04
<b>stomach</b>	0.13 ± 0.04	0.11 ± 0.01	0.07 ± 0.02	0.04 ± 0.02
<b>intestine</b>	0.9 ± 0.2	0.48 ± 0.02	0.5 ± 0.1	0.09 ± 0.07
<b>colon</b>	0.4 ± 0.2	0.30 ± 0.03	0.2 ± 0.1	0.04 ± 0.02
<b>adrenal</b>	0.11 ± 0.08	0.22 ± 0.05	0.3 ± 0.1	0.005 ± 0.008
<b>pancreas</b>	0.10 ± 0.07	0.05 ± 0.02	0.3 ± 0.2	0.009 ± 0.006
<b>brain</b>	0.010 ± 0.004	0.004 ± 0.002	0.005 ± 0.003	0.007 ± 0.003
<b>muscle</b>	0.03 ± 0.02	0.02 ± 0.02	0.05 ± 0.02	0.007 ± 0.007
<b>bone</b>	0.03 ± 0.01	0.02 ± 0.02	0.044 ± 0.008	0.021 ± 0.003
<b>HT-29 tumour</b>	1.2 ± 0.2	0.7 ± 0.2	0.4 ± 0.1	0.2 ± 0.1

Biodistribution of [<sup>177</sup>Lu]-AM-NT 8

<b>Organ</b>	<b>1h</b>	<b>4h</b>	<b>24h</b>	<b>Blocking</b>
<b>blood</b>	0.10 ± 0.04	0.005 ± 0.006	0.008 ± 0.003	0.2 ± 0.08
<b>heart</b>	0.07 ± 0.02	0.02 ± 0.01	0.03 ± 0.01	0.08 ± 0.03
<b>Liver</b>	0.11 ± 0.01	0.12 ± 0.03	0.07 ± 0.01	0.15 ± 0.03
<b>spleen</b>	0.07 ± 0.02	0.06 ± 0.02	0.055 ± 0.007	0.10 ± 0.03
<b>lung</b>	0.19 ± 0.05	0.05 ± 0.01	0.06 ± 0.01	0.28 ± 0.07
<b>kidney</b>	1.8 ± 0.4	1.9 ± 0.2	1.1 ± 0.2	2.1 ± 0.4
<b>stomach</b>	0.28 ± 0.07	0.16 ± 0.03	0.12 ± 0.02	0.168 ± 0.008
<b>intestine</b>	1.1 ± 0.2	1.1 ± 0.2	0.7 ± 0.1	0.11 ± 0.07
<b>colon</b>	0.4 ± 0.1	0.5 ± 0.1	0.28 ± 0.05	0.11 ± 0.05
<b>adrenal</b>	0.2 ± 0.1	0.1 ± 0.1	0.2 ± 0.1	0.2 ± 0.2
<b>pancreas</b>	0.2 ± 0.2	0 ± 0	0.14 ± 0.05	0.09 ± 0.05
<b>brain</b>	0.013 ± 0.004	0.005 ± 0.002	0.004 ± 0.002	0.016 ± 0.007
<b>muscle</b>	0.02 ± 0.01	0.1 ± 0.1	0.04 ± 0.03	0.05 ± 0.04
<b>bone</b>	0.09 ± 0.04	0.07 ± 0.08	0.10 ± 0.03	0.07 ± 0.04
<b>HT-29 tumour</b>	2.0 ± 0.3	1.5 ± 0.5	1.0 ± 0.3	0.4 ± 0.1

Biodistribution of [<sup>177</sup>Lu]-AM-NT 9

<b>Organ</b>	<b>1h</b>	<b>4h</b>	<b>24h</b>	<b>Blocking</b>
<b>blood</b>	0.02 ± 0.01	0 ± 0	0 ± 0	0.11 ± 0.03
<b>heart</b>	0.012 ± 0.006	0 ± 0	0.008 ± 0.004	0.06 ± 0.02
<b>Liver</b>	0.035 ± 0.008	0.032 ± 0.004	0.03 ± 0.01	0.10 ± 0.03
<b>spleen</b>	0.017 ± 0.009	0.017 ± 0.006	0.021 ± 0.007	0.07 ± 0.01
<b>lung</b>	0.05 ± 0.04	0.02 ± 0.02	0.01 ± 0.01	0.18 ± 0.04
<b>kidney</b>	0.5 ± 0.1	0.55 ± 0.03	0.4 ± 0.1	1.6 ± 0.3
<b>stomach</b>	0.10 ± 0.03	0.05 ± 0.02	0.038 ± 0.007	0.2 ± 0.1
<b>intestine</b>	0.30 ± 0.06	0.3 ± 0.1	0.22 ± 0.04	0.10 ± 0.01
<b>colon</b>	0.17 ± 0.03	0.17 ± 0.06	0.06 ± 0.04	0.15 ± 0.03
<b>adrenal</b>	0.10 ± 0.08	0.04 ± 0.13	0.07 ± 0.05	0.2 ± 0.4
<b>pancreas</b>	0 ± 0	0.02 ± 0.07	0 ± 0	0.01 ± 0.06
<b>brain</b>	0.003 ± 0.004	0.0032 ± 0.0008	0.002 ± 0.002	0.012 ± 0.001
<b>muscle</b>	0.006 ± 0.009	0 ± 0	0.007 ± 0.019	0.03 ± 0.02
<b>bone</b>	0.05 ± 0.09	0.01 ± 0.01	0.01 ± 0.01	0.04 ± 0.03
<b>HT-29 tumour</b>	1.1 ± 0.3	0.7 ± 0.1	0.45 ± 0.07	0.31 ± 0.04

Biodistribution of [<sup>177</sup>Lu]-AM-NT 10

<b>Organ</b>	<b>1h</b>	<b>4h</b>	<b>24h</b>	<b>Blocking</b>
<b>blood</b>	0.11 ± 0.03	0.0001 ± 0.0003	0.0007 ± 0.0012	0.11 ± 0.04
<b>heart</b>	0.06 ± 0.02	0.015 ± 0.001	0.009 ± 0.006	0.05 ± 0.02
<b>Liver</b>	0.28 ± 0.05	0.17 ± 0.01	0.120 ± 0.007	0.28 ± 0.03
<b>spleen</b>	0.078 ± 0.008	0.05 ± 0.01	0.05 ± 0.01	0.06 ± 0.01
<b>lung</b>	0.21 ± 0.04	0.034 ± 0.008	0.03 ± 0.01	0.20 ± 0.01
<b>kidney</b>	2.0 ± 0.2	1.7 ± 0.2	1.2 ± 0.1	1.8 ± 0.2
<b>stomach</b>	0.5 ± 0.4	0.16 ± 0.02	0.11 ± 0.02	0.10 ± 0.01
<b>intestine</b>	1.0 ± 0.2	1.1 ± 0.2	0.75 ± 0.08	0.04 ± 0.05
<b>colon</b>	0.36 ± 0.07	0.3 ± 0.1	0.2 ± 0.1	0.07 ± 0.07
<b>adrenal</b>	0.05 ± 0.06	0	0.01 ± 0.02	0
<b>pancreas</b>	0.01 ± 0.01	0	0	0
<b>brain</b>	0.011 ± 0.002	0.004 ± 0.003	0.002 ± 0.002	0.012 ± 0.008
<b>muscle</b>	0.04 ± 0.04	0.02 ± 0.04	0.02 ± 0.02	0.03 ± 0.03
<b>bone</b>	0.05 ± 0.03	0.01 ± 0.01	0.03 ± 0.03	0.02 ± 0.01
<b>HT-29 tumour</b>	1.9 ± 0.4	1.29 ± 0.09	0.9 ± 0.1	0.40 ± 0.03

---

**Biodistribution of [<sup>177</sup>Lu]-AM-NT 11**

<b>Organ</b>	<b>1h</b>	<b>4h</b>	<b>24h</b>	<b>Blocking</b>
<b>blood</b>	0.05 ± 0.03	0 ± 0	0 ± 0	0.10 ± 0.08
<b>heart</b>	0.02 ± 0.02	0 ± 0	0 ± 0	0.03 ± 0.02
<b>Liver</b>	0.08 ± 0.01	0.05 ± 0.01	0.018 ± 0.006	0.11 ± 0.05
<b>spleen</b>	0.03 ± 0.01	0.024 ± 0.009	0 ± 0	0.05 ± 0.02
<b>lung</b>	0.06 ± 0.03	0.03 ± 0.02	0.009 ± 0.014	0.13 ± 0.06
<b>kidney</b>	1.3 ± 0.2	1.3 ± 0.4	0.5 ± 0.1	1.7 ± 0.6
<b>stomach</b>	0.05 ± 0.02	0.01 ± 0.01	0 ± 0	0.06 ± 0.05
<b>intestine</b>	0.26 ± 0.08	0.15 ± 0.08	0.05 ± 0.05	0.01 ± 0.06
<b>colon</b>	0.2 ± 0.2	0.10 ± 0.07	0.0008 ± 0.0177	0 ± 0
<b>adrenal</b>	0 ± 0	0 ± 0	0 ± 0	0 ± 0
<b>pancreas</b>	0 ± 0	0 ± 0	0 ± 0	0 ± 0
<b>brain</b>	0.002 ± 0.004	0.002 ± 0.004	0 ± 0	0.003 ± 0.008
<b>muscle</b>	0 ± 0	0 ± 0	0 ± 0	0 ± 0
<b>bone</b>	0 ± 0	0 ± 0	0 ± 0	0 ± 0
<b>HT-29 tumour</b>	1.0 ± 0.3	0.7 ± 0.2	0.2 ± 0.1	0.33 ± 0.08

Biodistribution of [<sup>177</sup>Lu]-AM-NT 15

<b>Organ</b>	<b>1h</b>	<b>4h</b>	<b>24h</b>	<b>Blocking</b>
<b>blood</b>	0.08 ± 0.02	0.006 ± 0.003	0.005 ± 0.001	0.04 ± 0.02
<b>heart</b>	0.05 ± 0.01	0.012 ± 0.007	0.026 ± 0.005	0.03 ± 0.01
<b>Liver</b>	0.12 ± 0.03	0.11 ± 0.02	0.10 ± 0.02	0.13 ± 0.03
<b>spleen</b>	0.08 ± 0.02	0.056 ± 0.005	0.08 ± 0.02	0.076 ± 0.009
<b>lung</b>	0.18 ± 0.04	0.04 ± 0.02	0.06 ± 0.01	0.144 ± 0.007
<b>kidney</b>	1.6 ± 0.4	1.3 ± 0.2	1.2 ± 0.1	2.1 ± 0.7
<b>stomach</b>	0.146 ± 0.009	0.08 ± 0.02	0.09 ± 0.01	0.1 ± 0.1
<b>intestine</b>	1.2 ± 0.1	0.9 ± 0.2	1.1 ± 0.1	0.1 ± 0.1
<b>colon</b>	0.33 ± 0.08	0.23 ± 0.05	0.22 ± 0.06	0.15 ± 0.02
<b>adrenal</b>	0.2 ± 0.2	0.17 ± 0.04	0.3 ± 0.2	0.08 ± 0.16
<b>pancreas</b>	0.13 ± 0.03	0.03 ± 0.32	0.24 ± 0.09	0.001 ± 0.018
<b>brain</b>	0.012 ± 0.003	0.007 ± 0.003	0.005 ± 0.001	0.009 ± 0.003
<b>muscle</b>	0.04 ± 0.02	0.04 ± 0.03	0.07 ± 0.01	0.035 ± 0.003
<b>bone</b>	0.14 ± 0.04	0.07 ± 0.04	0.06 ± 0.02	0.5 ± 0.3
<b>HT-29 tumour</b>	2.2 ± 0.6	1.1 ± 0.1	1.1 ± 0.1	0.60 ± 0.05





## 7. Bibliography

- [1] J. C. Reubi, B. Waser, H. Friess, M. Buchler, J. Laissue, *Gut*, **1998**, *42*, 546-550.
- [2] J. C. Reubi, B. Waser, J. C. Schaer, J. A. Laissue, *Int J Cancer*, **1999**, *82*, 213-218.
- [3] F. Souaze, S. Dupouy, V. Viardot-Foucault, E. Bruyneel, S. Attoub, C. Gespach, A. Gompel, P. Forgez, *Cancer Research*, **2006**, *66*, 6243-6249.
- [4] A. Heppeler, S. Froidevaux, A. N. Eberle, H. R. Maecke, *Curr Med Chem*, **2000**, *7*, 971-994.
- [5] J. C. Reubi, *Endocr Rev*, **2003**, *24*, 389-427.
- [6] M. Bruehlmeier, E. G. Garayoa, A. Blanc, B. Holzer, S. Gergely, D. Tourwe, P. A. Schubiger, P. Blauenstein, *Nucl Med Biol*, **2002**, *29*, 321-327.
- [7] F. Buchegger, F. Bonvin, M. Kosinski, A. O. Schaffland, J. Prior, J. C. Reubi, P. Blauenstein, D. Tourwe, E. Garcia Garayoa, A. Bischof Delaloye, *J Nucl Med*, **2003**, *44*, 1649-1654.
- [8] I. E. Valverde, A. Bauman, C. A. Kluba, S. Vomstein, M. A. Walter, T. L. Mindt, *Angew Chem Int Ed Engl*, **2013**, *52*, 8957-8960.
- [9] D. Lugin, F. Vecchini, S. Doulut, M. Rodriguez, J. Martinez, P. Kitabgi, *European Journal of Pharmacology*, **1991**, *205*, 191-198.
- [10] J. Einsiedel, H. Hübner, M. Hervet, S. Härterich, S. Koschatzky, P. Gmeiner, *Bioorganic & Medicinal Chemistry Letters*, **2008**, *18*, 2013-2018.
- [11] B. W. Stewart, C. P. Wild; *World Cancer Report 2014*, **2014**
- [12] Anonymous; *WHO methods and data sources for country-level causes of death 2000-2012*, **2014**
- [13] G. Danaei, S. Vander Hoorn, A. D. Lopez, C. J. L. Murray, M. Ezzati, *The Lancet*, *366*, 1784-1793.
- [14] Lodish, Berk, Kaiser, Krieger, Scott, Bretscher, Ploegh, Matsudaira, *Molecular Cell Biology*, Sixth Edition ed., **2008**.
- [15] S. Seeber, J. Schütte, *Therapiekonzepte Onkologie*, 5. Auflage ed., Springer Medizin Verlag, **2007**.
- [16] H. S. Schicha, Otmar, *Nuklearmedizin*, 6. Auflage ed., Schattauer, **2007**.
- [17] U. S. Büll, H. Biersack, H.J.; Knapp, W.H.; Reiners, C.; Schober, O., *Nuklearmedizin*, 3. Auflage ed., Thieme, **1999**.
- [18] A. I. Kassis, S. J. Adelstein, *J Nucl Med*, **2005**, *46 Suppl 1*, 4S-12S.
- [19] S. V. Smith, *J Inorg Biochem*, **2004**, *98*, 1874-1901.
- [20] S. A. del Sordo, Leonardo; Caroli, Ezio; Mancini, Anna Maria; Zappettini, Andrea; Upertini, Pietro, *Sensors-Basel*, **2009**, *9*, 3491-3526.
- [21] Anonymous, <http://www.cellsighttech.com/technology/pet.html>.
- [22] R. Weissleder, M. J. Pittet, *Nature*, **2008**, *452*, 580-589.
- [23] A. Otte, E. Jermann, M. Behe, M. Goetze, H. C. Bucher, H. W. Roser, A. Heppeler, J. MuellerBrand, H. R. Maecke, *Eur J Nucl Med*, **1997**, *24*, 792-795.
- [24] B. Lab, [http://isotopes.lbl.gov/education/parent/Cu\\_iso.htm](http://isotopes.lbl.gov/education/parent/Cu_iso.htm).
- [25] S. M. Qaim, *Radiochim Acta*, **2001**, *89*, 297-302.
- [26] C. H. Yeong, M. H. Cheng, K. H. Ng, *J Zhejiang Univ-Sc B*, **2014**, *15*, 845-863.
- [27] S. J. Adelstein, A. I. Kassis, *Nucl Med Biol*, **1987**, *14*, 165-169.
- [28] C. Hoefnagel, *Eur J Nucl Med*, **1991**, *18*, 408-431.
- [29] L. Lahiry, B. Saha, J. Chakraborty, S. Bhattacharyya, S. Chattopadhyay, S. Banerjee, T. Choudhuri, D. Mandal, A. Bhattacharyya, G. Sa, T. Das, *Apoptosis*, **2008**, *13*, 771-781.
- [30] S. Chattopadhyay, K. V. Vimalnath, S. Saha, A. Korde, H. D. Sarma, S. Pal, M. K. Das, *Appl Radiat Isotopes*, **2008**, *66*, 334-339.
- [31] J. F. Eary, *Nucl Med Biol*, **1991**, *18*, 105-108.
- [32] C. Z. Barkhausen, Konstantin <http://www.rcm.tum.de/index.php?id=54&L=1>.
- [33] A. Mascarin, I. E. Valverde, T. L. Mindt, *Radiochim Acta*, **2013**, *101*, 733-737.
- [34] E. W. Price, C. Orvig, *Chemical Society Reviews*, **2014**, *43*, 260-290.

## Bibliography

---

- [35] J. Quinones, Mizejews.G, Beierwal.Wh, *J Nucl Med*, **1971**, *12*, 69-&.
- [36] O. W. Press, J. F. Eary, F. R. Appelbaum, P. J. Martin, W. B. Nelp, S. Glenn, D. R. Fisher, B. Porter, D. C. Matthews, T. Gooley, I. D. Bernstein, *Lancet*, **1995**, *346*, 336-340.
- [37] T. Stigbrand, A. Ullén, P. Sandström, H. Mirzaie-Joniani, B. Sundström, B. Nilsson, L. Ärlestig, R. R. Norrlund, K. R. Åhlström, S.-O. Hietala, *Acta Oncol*, **1996**, *35*, 259-265.
- [38] E. D. G. Fleuren, Y. M. H. Versleijen-Jonkers, S. Heskamp, C. M. L. van Herpen, W. J. G. Oyen, W. T. A. van der Graaf, Otto C. Boerman, *Molecular Oncology*, **2014**, *8*, 799-812.
- [39] J. C. Reubi, H. R. Maecke, *J Nucl Med*, **2008**, *49*, 1735-1738.
- [40] E. P. Krenning, W. A. P. Breeman, P. P. M. Kooij, J. S. Lameris, W. H. Bakker, J. W. Koper, L. Ausema, J. C. Reubi, S. W. J. Lamberts, *Lancet*, **1989**, *1*, 242-244.
- [41] M. Fani, H. Maecke, *Eur J Nucl Med Mol I*, **2012**, *39*, 11-30.
- [42] J. C. Reubi, J. C. Schar, B. Waser, S. Wenger, A. Heppeler, J. S. Schmitt, H. R. Macke, *Eur J Nucl Med*, **2000**, *27*, 273-282.
- [43] M. de Jong, W. A. P. Breeman, D. J. Kwekkeboom, R. Valkema, E. P. Krenning, *Accounts Chem Res*, **2009**, *42*, 873-880.
- [44] J. C. Reubi, B. Waser, J. C. Schaer, J. A. Laissue, *Eur J Nucl Med*, **2001**, *28*, 836-846.
- [45] M. Schottelius, H. J. Wester, *Methods*, **2009**, *48*, 161-177.
- [46] J. C. Reubi, S. Wenger, J. Schmuckli-Maurer, J. C. Schaer, M. Gugger, *Clinical Cancer Research*, **2002**, *8*, 1139-1146.
- [47] J. C. Reubi, J. C. Schaer, B. Waser, *Cancer Research*, **1997**, *57*, 1377-1386.
- [48] M. Korner, M. Stockli, B. Waser, J. C. Reubi, *J Nucl Med*, **2007**, *48*, 736-743.
- [49] X. Z. Zhang, Z. M. Xiong, Y. Wu, W. B. Cai, J. R. Tseng, S. S. Gambhir, X. Y. Chen, *J Nucl Med*, **2006**, *47*, 113-121.
- [50] S. Amar, P. Kitabgi, J. P. Vincent, *Febs Lett*, **1986**, *201*, 31-36.
- [51] W. Siegrist, F. Solca, S. Stutz, L. Giuffre, S. Carrel, J. Girard, A. N. Eberle, *Cancer Research*, **1989**, *49*, 6352-6358.
- [52] J. C. Reubi, *J Nucl Med*, **1995**, *36*, 1846-1853.
- [53] P. Volker, C. Grundker, O. Schmidt, K. D. Schulz, G. Emons, *American Journal of Obstetrics and Gynecology*, **2002**, *186*, 171-179.
- [54] R. Alberto, *Eur J Inorg Chem*, **2009**, *2009*, 21-31.
- [55] T. L. Mindt, H. Struthers, L. Brans, T. Anguelov, C. Schweinsberg, V. Maes, D. Tourwe, R. Schibli, *J Am Chem Soc*, **2006**, *128*, 15096-15097.
- [56] A. Ando, I. Ando, T. Hiraki, K. Hisada, *Nucl Med Biol*, **1989**, *16*, 57-80.
- [57] I. Iakovidis, I. Delimaris, S. M. Piperakis, *Molecular Biology International*, **2011**, *2011*.
- [58] J. Moreau, E. Guillon, J. C. Pierrard, J. Rimbault, M. Port, M. Aplincourt, *Chem-Eur J*, **2004**, *10*, 5218-5232.
- [59] S. Aime, A. Barge, M. Botta, M. Fasano, J. Danilo Ayala, G. Bombieri, *Inorganica Chimica Acta*, **1996**, *246*, 423-429.
- [60] R. Carraway, S. E. Leeman, *Journal of Biological Chemistry*, **1973**, *248*, 6854-6861.
- [61] P. Kitabgi, R. Carraway, S. E. Leeman, *Journal of Biological Chemistry*, **1976**, *251*, 7053-7058.
- [62] J. E. Rivier, L. H. Lazarus, M. H. Perrin, M. R. Brown, *J Med Chem*, **1977**, *20*, 1409-1412.
- [63] R. Carraway, S. E. Leeman, *Journal of Biological Chemistry*, **1975**, *250*, 1907-1911.
- [64] C. Granier, J. Vanrietschoten, P. Kitabgi, C. Poustis, P. Freychet, *European Journal of Biochemistry*, **1982**, *124*, 117-124.
- [65] W. C. Mustain, P. G. Rychahou, B. M. Evers, *Curr Opin Endocrinol*, **2011**, *18*, 75-82.
- [66] C. S. Fawaz, P. Martel, D. Leo, L. E. Trudeau, *Bmc Neurosci*, **2009**, *10*.
- [67] E. B. Binder, B. Kinkead, M. J. Owens, C. B. Nemeroff, *Biol Psychiatry*, **2001**, *50*, 856-872.
- [68] E. B. Binder, B. Kinkead, M. J. Owens, C. B. Nemeroff, *Pharmacological reviews*, **2001**, *53*, 453-486.
- [69] G. Roussy, M. A. Dansereau, S. Baudisson, F. Ezzoubaa, K. Belleville, N. Beaudet, J. Martinez, E. Richelson, P. Sarret, *Molecular pain*, **2009**, *5*, 38.
- [70] R. E. Carraway, A. M. Plona, *Peptides*, **2006**, *27*, 2445-2460.
- [71] S. Guha, J. A. Lunn, C. Santiskulvong, E. Rozengurt, *Cancer Research*, **2003**, *63*, 2379-2387.

## Bibliography

---

- [72] G. P. Amorino, P. D. Deeble, S. J. Parsons, *Oncogene*, **2006**, *26*, 745-756.
- [73] U. Olszewski, M. Hlozek, G. Hamilton, *Biochem Bioph Res Co*, **2010**, *393*, 414-419.
- [74] J. H. Li, F. Sicard, M. A. Salam, M. Baek, J. LePrince, H. Vaudry, K. Kim, H. B. Kwon, J. Y. Seong, *J Mol Endocrinol*, **2005**, *34*, 793-807.
- [75] K. Tanaka, M. Masu, S. Nakanishi, *Neuron*, **1990**, *4*, 847-854.
- [76] N. Vita, P. Laurent, S. Lefort, P. Chalon, X. Dumont, M. Kaghad, D. Gully, G. Lefur, P. Ferrara, D. Caput, *Febs Lett*, **1993**, *317*, 139-142.
- [77] L. Seethalakshmi, S. P. Mitra, P. R. Dobner, M. Menon, R. E. Carraway, *Prostate*, **1997**, *31*, 183-192.
- [78] J. J. Maoret, D. Pospai, C. Rouyerfessard, A. Couvineau, C. Laboisie, T. Voisin, M. Laburthe, *Biochem Bioph Res Co*, **1994**, *203*, 465-471.
- [79] J. G. Reeve, M. Goedert, P. C. Emson, N. M. Bleehen, *Recent Res Cancer*, **1985**, *99*, 175-176.
- [80] J. F. White, N. Noinaj, Y. Shibata, J. Love, B. Kloss, F. Xu, J. Gvozdenovic-Jeremic, P. Shah, J. Shiloach, C. G. Tate, R. Grisshammer, *Nature*, **2012**, *490*, 508-513.
- [81] J. P. Vincent, J. Mazella, P. Kitabgi, *Trends Pharmacol Sci*, **1999**, *20*, 302-309.
- [82] P. Kleczkowska, A. W. Lipkowski, *European Journal of Pharmacology*, **2013**, *716*, 54-60.
- [83] P. R. Dobner, *Peptides*, **2006**, *27*, 2405-2414.
- [84] E. Garcia-Garayoa, L. Allemann-Tannahill, P. Blauenstein, M. Willmann, N. Carrel-Remy, D. Tourwe, K. Iterbeke, P. Conrath, P. A. Schubiger, *Nucl Med Biol*, **2001**, *28*, 75-84.
- [85] P. Kitabgi, F. De Nadai, C. Rovere, J. N. Bidard, *Ann N Y Acad Sci*, **1992**, *668*, 30-42.
- [86] M. de Visser, P. J. J. M. Janssen, A. Srinivasan, J. C. Reubi, B. Waser, J. L. Erion, M. A. Schmidt, E. P. Krenning, M. de Jong, *Eur J Nucl Med Mol I*, **2003**, *30*, 1134-1139.
- [87] C. Hultsch, B. Pawelke, R. Bergmann, F. Wuest, *Bioorgan Med Chem*, **2006**, *14*, 5913-5920.
- [88] J. A. Henry, D. C. Horwell, K. G. Meecham, D. C. Rees, *Bioorganic & Medicinal Chemistry Letters*, **1993**, *3*, 949-952.
- [89] Y. P. Pang, B. Cusack, K. Groshan, E. Richelson, *Journal of Biological Chemistry*, **1996**, *271*, 15060-15068.
- [90] C. Held, M. Plomer, H. Hubner, J. Meltretter, M. Pischetsrieder, P. Gmeiner, *Chemmedchem*, **2013**, *8*, 75-81.
- [91] J. Einsiedel, C. Held, M. Hervet, M. Plomer, N. Tschammer, H. Hubner, P. Gmeiner, *J Med Chem*, **2011**, *54*, 2915-2923.
- [92] D. Seebach, A. Lukaszuk, K. Patora-Komisarska, D. Podwysocka, J. Gardiner, M. O. Ebert, J. C. Reubi, R. Cescato, B. Waser, P. Gmeiner, H. Hubner, C. Rougeot, *Chem Biodivers*, **2011**, *8*, 711-739.
- [93] C. Sparr, N. Purkayastha, T. Yoshinari, D. Seebach, S. Maschauer, O. Prante, H. Hübner, P. Gmeiner, B. Kolesinska, R. Cescato, B. Waser, J. C. Reubi, *Chemistry & Biodiversity*, **2013**, *10*, 2101-2121.
- [94] M. Jamous, M. L. Tamma, E. Gourni, B. Waser, J. C. Reubi, H. R. Maecke, R. Mansi, *Nucl Med Biol*, **2014**, *41*, 464-470.
- [95] P. Antunes, M. Ginj, M. A. Walter, J. Chen, J.-C. Reubi, H. R. Maecke, *Bioconjugate Chem*, **2006**, *18*, 84-92.
- [96] E. Garcia-Garayoa, P. Blauenstein, M. Bruehlmeier, A. Blanc, K. Iterbeke, P. Conrath, D. Tourwe, P. A. Schubiger, *J Nucl Med*, **2002**, *43*, 374-383.
- [97] P. Blauenstein, E. G. Garayoa, D. Ruegg, A. Blanc, D. Tourwe, A. Beck-Sickinger, P. A. Schubiger, *Cancer Biother Radiopharm*, **2004**, *19*, 181-188.
- [98] E. Garcia-Garayoa, V. Maes, P. Blauenstein, A. Blanc, A. Hohn, D. Tourwe, P. A. Schubiger, *Nucl Med Biol*, **2006**, *33*, 495-503.
- [99] P. J. J. M. Janssen, M. de Visser, S. M. Verwijnen, B. F. Bernard, A. Srinivasan, J. L. Erion, W. A. P. Breeman, A. G. Vulto, E. P. Krenning, M. de Jong, *Cancer Biother Radio*, **2007**, *22*, 374-381.
- [100] F. Alshoukr, C. Rosant, V. Maes, J. Abdelhak, O. Raguin, S. Burg, L. Sarda, J. Barbet, D. Tourwe, D. Pelaprat, A. Gruaz-Guyon, *Bioconjug Chem*, **2009**, *20*, 1602-1610.
- [101] B. A. Nock, A. Nikolopoulou, J. C. Reubi, V. Maes, P. Conrath, D. Tourwe, T. Maina, *J Med Chem*, **2006**, *49*, 4767-4776.

## Bibliography

---

- [102] F. Alshoukr, A. I. Prignon, L. Brans, A. Jallane, S. Mendes, J.-N. I. Talbot, D. Tourwé, J. Barbet, A. Gruaz-Guyon, *Bioconjugate Chem*, **2011**, *22*, 1374-1385.
- [103] R. Teodoro, B. L. Faintuch, E. G. F. Nunez, R. G. Queiroz, *Nucl Med Biol*, **2011**, *38*, 113-120.
- [104] S. Maschauer, J. Einsiedel, C. Hocke, H. Hubner, T. Kuwert, P. Gmeiner, O. Prante, *ACS Medicinal Chemistry Letters*, **2010**, *1*, 224-228.
- [105] R. Bergmann, M. Scheunemann, C. Heichert, P. Mäding, H. Wittrisch, M. Kretzschmar, H. Rodig, D. Tourwé, K. Iterbeke, K. Chavatte, D. Zips, J. C. Reubi, B. Johannsen, *Nucl Med Biol*, **2002**, *29*, 61-72.
- [106] S. Maschauer, J. Einsiedel, R. Haubner, C. Hocke, M. Ocker, H. Hubner, T. Kuwert, P. Gmeiner, O. Prante, *Angew Chem Int Ed Engl*, **2010**, *49*, 976-979.
- [107] P. Antunes, M. Ginja, H. Zhang, B. Waser, R. P. Baum, J. C. Reubi, H. Maecke, *Eur J Nucl Med Mol Imaging*, **2007**, *34*, 982-993.
- [108] M. Panait, D. Chiper, V. Negoita, V. Lungu, M. Gruia, *Int J Pept Res Ther*, **2013**, *19*, 345-356.
- [109] I. E. Valverde, A. Bauman, C. A. Kluba, S. Vomstein, M. A. Walter, T. L. Mindt, *Angewandte Chemie International Edition*, **2013**, *52*, 8957-8960.
- [110] A. Frilling, F. Weber, F. Saner, A. Bockisch, M. Hofmann, J. Mueller-Brand, C. E. Broelsch, *Surgery*, **2006**, *140*, 968-977.
- [111] E. Garcia-Garayoa, P. Blauenstein, A. Blanc, V. Maes, D. Tourwe, P. A. Schubiger, *Eur J Nucl Med Mol Imaging*, **2009**, *36*, 37-47.
- [112] V. Maes, E. Garcia-Garayoa, P. Blauenstein, D. Tourwe, *J Med Chem*, **2006**, *49*, 1833-1836.
- [113] J. Vagner, H. C. Qu, V. J. Hruby, *Current Opinion in Chemical Biology*, **2008**, *12*, 292-296.
- [114] A. S. Ripka, D. H. Rich, *Curr Opin Chem Biol*, **1998**, *2*, 441-452.
- [115] I. R. Baxendale, S. Cheung, M. O. Kitching, S. V. Ley, J. W. Shearman, *Bioorgan Med Chem*, **2013**, *21*, 4378-4387.
- [116] E. W. Ko, K. Burgess, *Organic Letters*, **2011**, *13*, 980-983.
- [117] E. Ko, J. Liu, L. M. Perez, G. Lu, A. Schaefer, K. Burgess, *J Am Chem Soc*, **2011**, *133*, 462-477.
- [118] H. An, P. D. Cook, *Chem Rev*, **2000**, *100*, 3311-3340.
- [119] D. Boeglin, W. D. Lubell, *J Comb Chem*, **2005**, *7*, 864-878.
- [120] I. Avan, C. D. Hall, A. R. Katritzky, *Chemical Society Reviews*, **2014**, *43*, 3575-3594.
- [121] A. Negri, E. Marco, V. Garcia-Hernandez, A. Domingo, A. L. Llamas-Saiz, S. Porto-Sanda, R. Riguera, W. Laine, M. H. David-Cordonnier, C. Bailly, L. F. Garcia-Fernandez, J. J. Vaquero, F. Gago, *J Med Chem*, **2007**, *50*, 3322-3333.
- [122] R. C. F. Jones, G. J. Ward, *Tetrahedron Lett*, **1988**, *29*, 3853-3856.
- [123] J. Sperry, C. J. Moody, *Tetrahedron*, **2010**, *66*, 6483-6495.
- [124] F. Cohen, M. F. Koehler, P. Bergeron, L. O. Elliott, J. A. Flygare, M. C. Franklin, L. Gazzard, S. F. Keteltas, K. Lau, C. Q. Ly, V. Tsui, W. J. Fairbrother, *Bioorg Med Chem Lett*, **2010**, *20*, 2229-2233.
- [125] I. S. Bennett, G. Brooks, N. J. Broom, S. H. Calvert, K. Coleman, I. Francois, *The Journal of antibiotics*, **1991**, *44*, 969-978.
- [126] M. Kume, T. Kubota, Y. Kimura, H. Nakashimizu, K. Motokawa, *Chem Pharm Bull (Tokyo)*, **1993**, *41*, 758-762.
- [127] G. C. Tron, T. Pirali, R. A. Billington, P. L. Canonico, G. Sorba, A. A. Genazzani, *Medicinal Research Reviews*, **2008**, *28*, 278-308.
- [128] Q. Wang, T. R. Chan, R. Hilgraf, V. V. Fokin, K. B. Sharpless, M. G. Finn, *Journal of the American Chemical Society*, **2003**, *125*, 3192-3193.
- [129] J. M. Kee, B. Villani, L. R. Carpenter, T. W. Muir, *J Am Chem Soc*, **2010**, *132*, 14327-14329.
- [130] M. Kumin, L. S. Sonntag, H. Wennemers, *Journal of the American Chemical Society*, **2007**, *129*, 466-467.
- [131] I. E. Valverde, T. L. Mindt, *Chimia*, **2013**, *67*, 262-266.
- [132] D. S. Pedersen, A. Abell, *Eur J Org Chem*, **2011**, 2399-2411.
- [133] Y. L. Angell, K. Burgess, *Chemical Society Reviews*, **2007**, *36*, 1674-1689.
- [134] M. H. Palmer, R. H. Findlay, A. J. Gaskell, *J Chem Soc Perk T 2*, **1974**, 420-428.
- [135] V. D. Bock, D. Speijer, H. Hiemstra, J. H. van Maarseveen, *Org Biomol Chem*, **2007**, *5*, 971-975.

## Bibliography

---

- [136] W. S. Horne, C. A. Olsen, J. M. Beierle, A. Montero, M. R. Ghadiri, *Angew Chem Int Edit*, **2009**, *48*, 4718-4724.
- [137] M. R. Davis, E. K. Singh, H. Wahyudi, L. D. Alexander, J. B. Kunicki, L. A. Nazarova, K. A. Fairweather, A. M. Giltrap, K. A. Jolliffe, S. R. McAlpine, *Tetrahedron*, **2012**, *68*, 1029-1051.
- [138] I. E. Valverde, A. Bauman, C. A. Kluba, S. Vomstein, M. A. Walter, T. L. Mindt, *Angew Chem Int Edit*, **2013**, *52*, 8957-8960.
- [139] D. C. Horwell, W. Howson, D. Naylor, S. Osborne, R. D. Pinnock, G. S. Ratcliffe, N. Suman-Chauhan, *Int J Pept Protein Res*, **1996**, *48*, 522-531.
- [140] C. W. Tornoe, C. Christensen, M. Meldal, *J Org Chem*, **2002**, *67*, 3057-3064.
- [141] V. V. Rostovtsev, L. G. Green, V. V. Fokin, K. B. Sharpless, *Angew Chem Int Edit*, **2002**, *41*, 2596-+.
- [142] R. Huisgen, *Angew Chem Int Edit*, **1963**, *75*, 742-&.
- [143] R. Huisgen, *Angew Chem Int Edit*, **1963**, *75*, 604-+.
- [144] H. C. Kolb, K. B. Sharpless, *Drug Discov Today*, **2003**, *8*, 1128-1137.
- [145] H. C. Kolb, M. G. Finn, K. B. Sharpless, *Angew Chem Int Ed Engl*, **2001**, *40*, 2004-2021.
- [146] C. D. Hein, X. M. Liu, D. Wang, *Pharm Res*, **2008**, *25*, 2216-2230.
- [147] R. Berg, B. F. Straub, *Beilstein J Org Chem*, **2013**, *9*, 2715-2750.
- [148] T. R. Chan, R. Hilgraf, K. B. Sharpless, V. V. Fokin, *Organic Letters*, **2004**, *6*, 2853-2855.
- [149] B. T. Worrell, J. A. Malik, V. V. Fokin, *Science*, **2013**, *340*, 457-460.
- [150] F. Himo, T. Lovell, R. Hilgraf, V. V. Rostovtsev, L. Noodleman, K. B. Sharpless, V. V. Fokin, *Journal of the American Chemical Society*, **2004**, *127*, 210-216.
- [151] V. O. Rodionov, V. V. Fokin, M. G. Finn, *Angew Chem Int Ed Engl*, **2005**, *44*, 2210-2215.
- [152] V. V. Rostovtsev, L. Green, K. B. Sharpless, *Abstr Pap Am Chem S*, **2002**, *224*, U186-U186.
- [153] H. Staudinger, J. Meyer, *Helv Chim Acta*, **1919**, *2*, 635-646.
- [154] S. Bräse, C. Gil, K. Knepper, V. Zimmermann, *Angewandte Chemie*, **2005**, *117*, 5320-5374.
- [155] W. Stadlbauer, W. Fiala, M. Fischer, G. Hojas, *J Heterocyclic Chem*, **2000**, *37*, 1253-1256.
- [156] Q. Liu, Y. Tor, *Organic Letters*, **2003**, *5*, 2571-2572.
- [157] Y. H. Kim, K. Kim, S. B. Shim, *Tetrahedron Lett*, **1986**, *27*, 4749-4752.
- [158] M. O. Forster, *J Chem Soc*, **1906**, *89*, 222-239.
- [159] C. J. Cavender, V. J. Shiner, *J Org Chem*, **1972**, *37*, 3567-&.
- [160] P. B. Alper, S. C. Hung, C. H. Wong, *Tetrahedron Lett*, **1996**, *37*, 6029-6032.
- [161] E. D. Goddard-Borger, R. V. Stick, *Organic Letters*, **2007**, *9*, 3797-3800.
- [162] M. B. Hansen, T. H. M. van Gorp, J. C. M. van Hest, D. W. P. M. Lowik, *Organic Letters*, **2012**, *14*, 2330-2333.
- [163] A. R. Katritzky, M. El Khatib, O. Bol'shakov, L. Khelashvili, P. J. Steel, *J Org Chem*, **2010**, *75*, 6532-6539.
- [164] M. Kitamura, M. Yano, N. Tashiro, S. Miyagawa, M. Sando, T. Okauchi, *Eur J Org Chem*, **2011**, 458-462.
- [165] A. K. Pandiakumar, S. P. Sarma, A. G. Samuelson, *Tetrahedron Lett*, **2014**, *55*, 2917-2920.
- [166] P. T. Nyffeler, C. H. Liang, K. M. Koeller, C. H. Wong, *J Am Chem Soc*, **2002**, *124*, 10773-10778.
- [167] S. Schoffelen, M. B. van Eldijk, B. Rooijackers, R. Raijmakers, A. J. R. Heck, J. C. M. van Hest, *Chem Sci*, **2011**, *2*, 701-705.
- [168] A. Elangovan, Y. H. Wang, T. I. Ho, *Org Lett*, **2003**, *5*, 1841-1844.
- [169] S. H. Kim, W. J. Zuercher, N. B. Bowden, R. H. Grubbs, *J Org Chem*, **1996**, *61*, 1073-1081.
- [170] E. J. Corey, P. L. Fuchs, *Tetrahedron Lett*, **1972**, 3769-&.
- [171] S. Muller, B. Liepold, G. J. Roth, H. J. Bestmann, *Synlett*, **1996**, 521-&.
- [172] H. D. Dickson, S. C. Smith, K. W. Hinkle, *Tetrahedron Lett*, **2004**, *45*, 5597-5599.
- [173] K. Miwa, T. Aoyama, T. Shioiri, *Synlett*, **1994**, 107-108.
- [174] D. Seyferth, R. S. Marmor, P. Hilbert, *J Org Chem*, **1971**, *36*, 1379-&.
- [175] D. G. Brown, E. J. Velthuisen, J. R. Commerford, R. G. Brisbois, T. R. Hoye, *J Org Chem*, **1996**, *61*, 2540-2541.
- [176] D. Habrant, V. Rauhala, A. M. P. Koskinen, *Chemical Society Reviews*, **2010**, *39*, 2007-2017.

## Bibliography

---

- [177] A. M. Sefler, J. X. He, T. K. Sawyer, K. E. Holub, D. O. Omecinsky, M. D. Reily, V. Thanabal, H. C. Akunne, W. L. Cody, *J Med Chem*, **1995**, *38*, 249-257.
- [178] C. Schweinsberg, V. Maes, L. Brans, P. Blauenstein, D. A. Tourwe, P. A. Schubiger, R. Schibli, E. Garcia Garayoa, *Bioconjug Chem*, **2008**, *19*, 2432-2439.
- [179] R. P. Schroeder, C. Muller, S. Reneman, M. L. Melis, W. A. Breeman, E. de Blois, C. H. Bangma, E. P. Krenning, W. M. van Weerden, M. de Jong, *Eur J Nucl Med Mol Imaging*, **2010**, *37*, 1386-1396.
- [180] D. Wild, M. Frischknecht, H. Zhang, A. Morgenstern, F. Bruchertseifer, J. Boisclair, A. Provencher-Bolliger, J. C. Reubi, H. R. Maecke, *Cancer Res*, **2011**, *71*, 1009-1018.
- [181] R. Mansi, X. Wang, F. Forrer, B. Waser, R. Cescato, K. Graham, S. Borkowski, J. C. Reubi, H. R. Maecke, *Eur J Nucl Med Mol Imaging*, **2011**, *38*, 97-107.
- [182] D. Wild, M. Béhé, A. Wicki, D. Storch, B. Waser, M. Gotthardt, B. Keil, G. Christofori, J. C. Reubi, H. R. Mäcke, *J Nucl Med*, **2006**, *47*, 2025-2033.
- [183] H. W. Zhang, J. Schuhmacher, B. Waser, D. Wild, M. Eisenhut, J. C. Reubi, H. R. Maecke, *Eur J Nucl Med Mol I*, **2007**, *34*, 1198-1208.
- [184] E. D. Goddard-Borger, R. V. Stick, *Organic Letters*, **2011**, *13*, 2514-2514.
- [185] S. Punna, M. G. Finn, *Synlett*, **2004**, 99-100.
- [186] M. Tischler, D. Nasu, M. Empting, S. Schmelz, D. W. Heinz, P. Rottmann, H. Kolmar, G. Buntkowsky, D. Tietze, O. Avrutina, *Angew Chem Int Edit*, **2012**, *51*, 3708-3712.
- [187] M. Tischler, D. Nasu, M. Empting, S. Schmelz, D. W. Heinz, P. Rottmann, H. Kolmar, G. Buntkowsky, D. Tietze, O. Avrutina, *Angew Chem Int Ed Engl*, **2012**, *51*, 3708-3712.
- [188] Lundquist, J. C. Pelletier, *Organic Letters*, **2001**, *3*, 781-783.
- [189] P. T. Ho, K. Y. Ngu, *J Org Chem*, **1993**, *58*, 2313-2316.
- [190] R. N. Hunston, I. P. Gerathanassis, J. Lauterwein, *Journal of the American Chemical Society*, **1985**, *107*, 2654-2661.
- [191] F. Alshoukr, A. Prignon, L. Brans, A. Jallane, S. Mendes, J. N. Talbot, D. Tourwe, J. Barbet, A. Gruaz-Guyon, *Bioconjugate Chem*, **2011**, *22*, 1374-1385.
- [192] B. M. Tyler, C. L. Douglas, A. Fauq, Y. P. Pang, J. A. Stewart, B. Cusack, D. J. McCormick, E. Richelson, *Neuropharmacology*, **1999**, *38*, 1027-1034.
- [193] T. R. Chen, D. Drabkowski, R. J. Hay, M. Macy, W. Peterson Jr, *Cancer Genet Cytogen*, **1987**, *27*, 125-134.
- [194] F. G. Bahar, K. Ohura, T. Ogihara, T. Imai, *J Pharm Sci*, **2012**, *101*, 3979-3988.
- [195] S. Achilefu, A. Srinivasan, M. A. Schmidt, H. N. Jimenez, J. E. Bugaj, J. L. Erion, *J Med Chem*, **2003**, *46*, 3403-3411.
- [196] B. A. Nock, T. Maina, E. P. Krenning, M. de Jong, *J Nucl Med*, **2014**, *55*, 121-127.
- [197] J.-A. Fehrentz, B. Castro, *Synthesis*, **1983**, *1983*, 676,678.
- [198] J. C. S. Woo, E. Fenster, G. R. Dake, *J Org Chem*, **2004**, *69*, 8984-8986.
- [199] D. H. Appella, J. A. Iera, L. M. M. Jenkins, H. Kajiyama, J. B. Kopp, *Bioorganic & Medicinal Chemistry Letters*, **2010**, *20*, 6500-6503.
- [200] G. Reginato, A. Mordini, F. Messina, A. Degl'Innocenti, G. Poli, *Tetrahedron*, **1996**, *52*, 10985-10996.



## Persönliche Daten

Name Alba Mascarin  
Adresse Mörsbergerstrasse 48  
CH-4057 Basel  
E-Mail alba.mascarin@gmail.com  
Geburtsdatum / -ort 30.01.1986, Basel



## Ausbildung

03/2011 – 06/2015 **Promotion in Chemie**  
Universitätsspital Basel, Abteilung Radiopharmazeutische Chemie,  
Basel, Schweiz  
Doktorarbeit bei Prof. Thomas Mindt und Prof. Edwin Constable  
Titel: *'Triazole-based Peptidomimetics: Novel Neurotensin (8-13)  
Analogues with Increased Metabolic stability.'*

08/2009 – 01/2011 **Master of Science in Chemistry**  
Universität Basel, Basel, Schweiz  
Masterarbeit bei Prof. Helma Wennemers  
Titel: *„Cell Penetrating Properties of Functionalized Oligoprolines  
and Synthesis of a Releasable Linker System for Cell Penetrating  
Peptides‘.*

08/2006 – 07/2009 **Bachelor of Science in Chemistry**  
Universität Basel, Basel, Schweiz

08/2004 – 07/2006 **Studium der Chemie**  
Universitat Jaume I, Castellón de la Plana, Spanien

06/2004 **Matura (Selectividad)**  
Castellón de la Plana, Spanien



**Weiterbildungen und  
Lehraufträge**

08/2002 – 07/2004 **Naturwissenschaftliches Gymnasium**  
Instituto de Educación Superior Penyagolosa, Castellón de la Plana,  
Spanien

03/2015 **Assistenz in Lehre**  
Nuklearmedizinisches Praktikum für Mediziner

07/2013 **Labortierkurs Modul 1 (Felasa)**  
Bern, Schweiz

2013 **Assistenz in Lehre**  
Strahlenschutzmodul für Mediziner

2013 **Assistenz in Lehre**  
Strahlenschutzpraktikum für Mediziner

12/2011 **Ausbildung zur eidgenössisch anerkannten  
Strahlenschutzsachverständigen (SafPro)**  
Basel, Schweiz